THE USE OF METABOLOMICS TOOLS TO ASSESS THE THERAPEUTIC NATURAL PRODUCTS OF HONEY AND PROPOLIS FROM MALAYSIA AND NEW ZEALAND

A THESIS PRESENTED FOR THE DEGREE OF DOCTOR OF PHILOSOPHY IN THE FACULTY OF SCIENCE THE UNIVERSITY OF STRATHCLYDE

BY

YUSNAINI MD YUSOFF

BSc. (Honours), MSc.

Strathclyde Institute of Pharmacy and Biomedical Sciences

University of Strathclyde

161 Cathedral Street

Glasgow

G4 0RE

United Kingdom

May 2018

This thesis is the result of the author's original research. It has been composed by the author and has not been previously submitted for examination which has led to the award of a degree.

Signed: *Yusnaini Md Yusoff*

Date: May 29, 2018

Acknowledgement

I would like to express my gratitude to Allah SWT for His blessing for granted my prayer to accomplish my study. I genuinely would like to express my thankfulness to have a supervisor like Dr. RuAngelie Edrada-Ebel for her patience in guiding me to be a good researcher especially for her time and efforts in providing me the knowledge until I can manage my work during my PhD study. Her dedication and overwhelming supervision have helped me to a very great extent to accomplish my study. I also personally want to thanks my second and third supervisors, Dr. David Watson and Mrs Louise Young for their suggestion and ideas, particularly their technical guidance throughout my PhD study.

I would like to thank my Malaysia's Government, Majlis Amanah Rakyat (MARA) for their generosity to fund my PhD study in SIPBS. My sincerely thanks also goes to Miss. Grainne Abbott for her guidance in doing biological assays. I also would like to acknowledge MSc student, Esther who involved in this project. Not to forget to all my colleagues: Dr. Nashwa F. Tawfike, Dr. Chiara Viegelmann, Dr. Noorwini Mazlan, Dr. Halida Kamal, Dr. Lynsey McIntyre, Dr. Ahmed F. Tawfike, Bela, Kirsty, Hanan, Yahia, Bish, Mohamed, Aisya, Rejab and Abdullah for their sharing knowledge, friendship, support and kindness.

I also would like to express my heartfelt gratitude to have a loving families surround me especially to my husband Mohd Khairi, my mother Maimunah, my siblings, nephews, nieces, as well as my family in-law members and friends for their faith, prayer, sacrifices, support and endless love during my study. At this opportunity I also would like to dedicate this achievement to my late father Md Yusoff and lovely sister Yusliza; their presence and memorise have inspired me a lot until I succeed. Thank you very much everyone for making this happened. I wish all the best to those who are still struggling in the same journey, keep on fighting and the success will become yours.

Table of Contents

Abstract

The bee products including honey, propolis, pollen, and bee venom have been reported to have therapeutic benefits in traditional and conventional medicine. Honey is collected from nectar which appeared as caramelised sugar, while propolis is mainly composed of plant resins and exudates that bees gather. Many studies demonstrated anti-inflammatory, anti-bacterial, anti-oxidant and anti-proliferative properties of honey and propolis extract. However the chemical profiling of Malaysian honey and propolis has not been well studied. The composition of honey and propolis depends on its geographical origin and also on its botanical source. Furthermore, the extraction of secondary metabolites from propolis is very crucial because its bioavailability is only 2% in raw form. Metabolomics tools have been applied employing liquid chromatography-high resolution mass spectrometry (LC-HRMS) and nuclear magnetic resonance (NMR) to afford an intensive chemical profile of the propolis samples to target the bioactive metabolites. The obtained HRLCMS data was processed with MZmine 2.10 and was dereplicated using an in-house Excel Macro to couple the MS data with the Dictionary of Natural Products 2016 database. A supervised multivariate analysis was done by orthogonal partial least squares discriminant analysis (OPLS-DA) in SIMCA-P 14.0 to predict and pinpoint the plausible bioactive components against respective cancer cell lines. The chemical profiling of honey from Malaysia and New Zealand were also obtained using the same metabolomics approach. However, isolation work was only done for propolis due to their potent bioactivities. Ten compounds have been isolated from Malaysia and New Zealand propolis, which consisted mainly of triterpenoid and flavonoid derivatives, respectively. Several compounds revealed anticancer properties on several cancer cell lines (lung, breast and ovary), as well as phenotypic alteration on zebrafish embryo that can be related with activation of Notch signalling for anticancer study.

Abbreviations

Ca.	Circa
CHI	Chalcone isomerise
CoA	Coenzyme A
DCM	Dichloromethane
DEPT	Distortionless Enhancement by Polarization Transfer
DMSO-*d6*	Deuterated dimethyl sulfoxide
DNP	Dictionary of Natural Products
ELSD	Evaporative light scattering detector
ESI-MS	Electrospray ionization mass spectrometry
EtOAc	Ethyl Acetate
FDA	The Food and Drug Administration
H_2O_2	Hydrogen peroxide
HIV	Human immunodeficiency virus
HMBC	Heteronuclear Multiple-Bond Correlation
HMQC	Heteronuclear Multiple-Quantum Correlation
HPLC	High-performance liquid chromatography
HR-LCMS	High Resolution Liquid Chromatography mass spectrometry
MeOH	Methanol
MIC	Minimum inhibitory concentration
MPLC	Medium Pressure Liquid Chromatography
MRSA	Meticillin-resistant *Staphylococcus aureus*
MS	Mass Spectrometry
NMR	Nuclear Magnetic Resonance

OH	Hydroxyl radical
OPLS-DA	Orthogonal Partial Least Square-Discriminant Analysis
PCA	Principal Component Analysis
RT	Retention time
SIDR	Strathclyde Institute for Drug research
SIPBS	Strathclyde Institute of Pharmacy and Biomedical Sciences
TNF-α	Tumour necrosis factor alpha
UK	United Kingdom
UV	Ultra Violet

CHAPTER 1

1 General Introduction

1.1 The history of 'cancer'

Historically the term 'cancer' was first derived from the Greek word 'karkinos' that is referred to crab or crayfish during Hippocrates era (ca. 460 BC – ca. 370 BC) (Hajdu, 2011). The word 'karkinos' described the appearance of the veins on the cross section of solid malignant tumour from breast cancer patient that resembles a moving crab and its feet. During Roman Empire, the Greek physicians were granted the Roman citizenship and there was a physician named Aulus Celsus (ca. 25 BC – 50 AD) who became famous because of his theory about cancer. He started to replace 'karkinos' term into the Latin word 'cancer' which illustrated the crab that adheres to surrounding structures with his claws. Then he also proposed intensive surgery to treat the disease. However, the chances for an advance breast cancer to be reoccurrence at other part of body including lymph nodes and other vital organs are high due to the nature of cancer cell that can metastasis rapidly, which also may lead to mortality. In his book '*De Medicina*' he described several superficial carcinomas and he proposed topical treatment to treat the disease by using boiled cabbage, a salted mixture of honey and egg white. Pliny the Roman (AD 23 – 79) in his manuscript '*Materia Medica*' described the remedies for internal use in advanced cancer during pre- and post-surgery. It was prescribed as a boiled mixture of ash of sea crabs, egg white, honey, and powdered faeces of falcons. Over the time, many scholars have become pioneer in oncology, which creates medical history because of their contribution in cancer detection, diagnosis and treatment. One of them is Avicenna of Persia who also known as Ibnu Sina (980 – 1037) introduced new surgical technique by using wire loop that was made tighter each day until the tumour fell off. It was in 1215, when Pope the 1st banned the surgery that caused bloodshed, but not long after that Theodoric (1205 – 1296) introduced anaesthetic techniques and promoted intensive physical examination before surgery.

1.1.1 Invasive cancer and its mortality rates

Cancer is a leading cause of death worldwide, which represents more than 100 diseases (Trujillo et al., 2017). Different types of cancer share one common feature, where cells in a specific part of body undergo abnormal cell division and reproduce uncontrollably. The cancerous cells divide rapidly in one part of body before it goes into metastasis, invade and destroy the surrounding healthy cells, then spread into other part of vital organs. According to the cancer statistic, it was estimated that approximately 14.1 million new cancer cases have been reported in GLOBOCAN 2012 which led to 8.2 million cancer deaths worldwide (Ferlay et al., 2015). As defined by United Nations, 21 regions all around the world can be categorised into developed countries including United Kingdom and New Zealand, whilst Malaysia, which is part of Asia, was categorised under developing country. Based on cancer statistics in developed countries, lung and pancreas are among the most frequent diagnosed cancer in males, where there were 490,300 and 94,700 new cancer cases reported, which caused 416,700 and 93,100 death, respectively.

Approximately there were an estimated 793,700 and 99,800 new cases for breast and ovary cancer in females from developed countries which also lead to 197,600 and 65,900 cancer death, respectively. On the other side, there were at least 751,300 and 682,000 new lung cancer and mortality cases were reported in males from developing countries, respectively. In addition, breast and ovary cancer are among the most frequent diagnosed cancer in females, which reported 882,900 and 139, 000 new cases, respectively in developing countries. Both cancers were estimated to cause high number of mortality at 324,300 and 86,000 cancer deaths, respectively. Moreover, cancer death caused by pancreas cancer was estimated at 80,700 and 65,300 in males and female from developing countries, respectively. Overall, the incidence rates of lung, breast, pancreas and ovary cancer were relatively higher in developed rather than developing countries. Breast cancer rates are greater in developed countries could be due to some factors including long menstrual history, the use of oral contraceptive and never having children. Risk factors of lung cancer include smoking habit, indoor and outdoor air pollution from poor ventilation of using coal-fuel stove and cooking fumes and the exposure to environmental

carcinogens such as inhalation of asbestos fibers and arsenic. Other cancer risk factors include obesity, the use of menopause hormone pills, unhealthy diet, lack of physical exercise and the habit of taking alcohol. Besides that, cancer risk is also influenced by genetic factor.

1.2 Bee products and their therapeutic properties

Bees are eusocial insects that live in a colony with a single breeding queen, thus the workers and soldiers cooperate in defending and caring for the younger generation. A single bee colony consists of hundreds to thousands of workers responsible for collecting the nectar, resins and pollen from a variety of vegetation. The workers fully utilise the nectar for food in the form of honey, as well as beehive construction using resins. Besides being used to build nests, resins are also modified into chemical substance known as propolis, which can defend the nest from the intruder.

1.2.1 Honey

Honey is a natural product produced by honey bees in a process called regurgitation and evaporation. It has a sweet taste and is yellowish in colour depending on the source of nectar, due to the different dilutions of caramelized sugar (Krell, 1996). Each type of honey may have different properties and composition which are largely influenced by the bee species, source of nectar, geographical area, seasonal condition, storage mode and harvest technique (Kaškonienė and Venskutonis, 2010). Honey is produced as a food source. Meanwhile, in each bee hive, a colony of bees consists of a queen bee, drone, and worker bees (Flottum, 2010). The drone bees are responsible for fertilizing the queen bee in order to produce thousands of eggs (Winston, 1991). Once these eggs are matured, they will turn into a young generation of bees, the majority of which will become worker bees. The worker bees play an important role in honey production. They travel and collect the sugar-rich substance called nectar from different type of flowers, tree trunk and young leaves. They store the nectar in their stomach then return to their hive (Winston, 1991).

The worker bees work together as a group for regurgitation and digestion. At first, the bees ingest and regurgitate the nectar repetitively until the nectar is partially

digested. The bees synthesize an enzyme called invertase in their body, which is used to digest sucrose through acid hydrolysis. This eventually gives a mixture of glucose and fructose (Crane, 2013). After they reach the desired amount of honey in the honeycomb cells, the process continues with the elimination of the water content, thus preventing the fermentation of the sugar in honey (Langstroth, 2004). The bees fan their wings, creating a strong draft across the honeycomb, thus enhancing the evaporation of water and at the same time increasing the sugar concentration in honey, preventing yeast fermentation. The presence of glucose oxidase in honey also plays a role as an antimicrobial agent to avoid spoilage (Crane, 2013). Honey that has been produced is more than enough for a bee colony consumption. Overall, this is a unique characteristic of a bee colony whereas bees have a respective responsibility for honey production, nonetheless the survival of their species.

Although the process for producing honey is the same worldwide, the properties and composition of honey are strictly associated with nectar sources and geographical area, because different soils may produce different nutrients for botanical growth (Castro-Vázquez et al., 2010). Generally, honey can be classified as unifloral, multifloral or non-floral, depending on the source of the nectar collected (Subrahmanyam, 2007). Unifloral honey is comprised of nectar from a single type of flower at a specific area, and so it will have a unique profile such as a distinct flavour, colour and texture that represents the source of the nectar. However, it is very difficult to determine this type of honey due to the short time of flower seasoning and the existence of other types of flowers within the flying range of the honeybee. Multifloral honey consists of an unspecified range of flower, typically across the geographical area and season. Non-floral honey, also known as honeydew, is derived from the secretions of aphids and other insects that feed on plant sap. Louveaux et al. (1978) have developed a technique called melissopalynology to conduct the pollen analysis in order to determine the botanical origin in honey (Louveaux et al., 1978). However, this technique has been described as ‘time consuming, requiring special knowledge and expertise as well as multi-laboratory procedures’ (Kaškonienė and Venskutonis, 2010). It is easier to determine the chemical composition if the botanical origin has been acknowledged at the first

place. Otherwise, it is very crucial to develop a marker for floral detection for unknown nectar sources because there are other factors that contribute to chemical composition in honey including enzyme activity, colour and electrical conductivity (Kaškonienė and Venskutonis, 2010).

In addition, a review paper has summarised the method used for floral phytochemical marker in unifloral honey (Kaškonienė and Venskutonis, 2010). Generally, the analyses were divided according to the presence of volatile compounds, phenolic acids, carbohydrates, amino acids and other constituent compounds. These techniques involve different extraction methods that includes solvent extraction, solid phase extraction, solid phase microextraction or ultrasound-assisted extraction, combined with several characterization methods such as high-performance liquid chromatography (HPLC), gas chromatography-mass spectrometry (GC-MS), thin layer chromatography (TLC), and nuclear magnetic resonance (NMR) (Kaškonienė and Venskutonis, 2010). Subsequently, statistical analysis like multivariate testing is complimentary and supports the evidence obtained from phytochemistry findings which relies on several features including 'acidity, mineral content and degree of freshness' to identify the geographical origin of honey (Sanz et al., 1995).

On top of that, honey is often mentioned in the Bible, the Talmud, the Quran, the sacred books of India, China, Persia, and Egypt which refer to honey as a food, beverage, and curing medicine (Kuropatnicki et al., 2018). For example in the Quran there is an entire chapter (Surah) called "An-Nahl" which mean "The Bee". This sacred book mentions honey as a nutritious and healthy food that offers healing to human disease. In the Quran (chapter 16: verse 68-69) which have been translated into "And your Lord inspired to the bee, saying: Choose for yourself among the mountains, houses, and among the trees and in that which they construct. Then eat from all the fruits and follow the ways of your Lord laid down for you. There emerges from their bellies a drink, varying in colours (referring to honey), in which there is healing for mankind. Indeed in that is a sign for a people who give thought" (Ali, 2011). This translation explains the advantage of honey consumption in human,

particularly in the healing process. This may be one of the first references to honey as a medicine.

According to a book entitled ‘The honey prescription: The amazing power of honey as medicine’ written by Altman (2010) described pre- and probiotics element in honey which contributes to its medicinal resource. It enhances the growth of good bacteria, which is important in maintaining the health in our gastrointestinal tract (Altman, 2010). As an anti-oxidant-rich food, honey helps to prevent cellular damage and delay the aging process, as well as slow down the development of degenerative diseases such as cancers, heart disease and diabetes. Moreover, honey is also effective against bacteria and viruses including *Pseudomonas aeruginosa* and Methicillin-resistant *Staphylococcus aureus* (MRSA) due to its ability to release hydrogen peroxide when honey gets into contact on the wound area. Meanwhile, some other honey contains phytochemicals that can promotes potent anti-bacterial activity. Active Manuka honey, which predominantly made up from *Leptospermum* spp. in different regions of Australia and New Zealand is considered the top medicinal honey for medical creams and wound dressing.

Honey has long tradition not only in Ayurveda medicine but also in traditional Chinese medicine. In Ayurveda, honey also known as ‘madhu’ is used for both internal and external applications including eye diseases, sore throat, cold and cough, stomach ulcers, sleep disturbance, bronchial asthma, arthritis, stress and fatigue, dermatitis, eczema, diabetes mellitus, hypertension, hemiplegia, obesity, leprosy (Ediriweera and Premarathna, 2012). In addition, it also one of the remedy to treat weakness, bad breath, vomiting, dehydration, hiccups, diarrhoea, bed wetting, polyuria, burns, cuts and wounds, allergies, morning sickness, as well as to alleviate teething pain. Whereas, according to Chinese belief, honey consists of the Earth element which has a balance character based on two fundamental theories, Yin and Yang (Lao et al., 2012). Yin-yang theory posts that the universe is a whole composed of two opposites, yin and yang, which are interdependent and can transform into each other. Their equilibrium ensures harmony, for example the harmony in body that can maintain human health. Traditional Chinese Medicine (TCM) has applied honey as

one of the remedy in treating fever, headache, dry and sore throat, brown urine, constipation, reddish eyes and face, burning pain of local tumours, and red tongue with thin yellow tongue coating cause by toxic heat which is one of the major pathologies of paediatric cancer. Moreover, honey also has been used to promote postoperative healing after cancer therapy, which causes side effects such as nausea, and vomiting, fatigue, peripheral neuropathy, hair loss, low white blood cell (WBC) count, anaemia, postoperative pain, and constipation.

Above all, honey has already been used as a medicine for thousands of years, since then the therapeutic properties of honey have well blended with modern medicine which offer cure for wound, gastroenteritis, peptic ulcers and gastritis and ophthalmology (Molan, 1999). Nonetheless, the efficiency of honey for its anti-bacterial activity, boosting immune system, anti-inflammatory action, anti-oxidant activity, stimulation of cell growth and nontoxic side effects are well documented in the literature (Molan, 2001). More recent literature has also documented the clinical responsive of using honey to resolve microbial infections in wound and gastrointestinal tract as well as in diabetes, in addition to increase carbohydrate metabolism and also act as food preservative and prebiotic (Bansal et al., 2005). Nonetheless, honey is also proven to enhance short term memory (Kamarulzaidi et al., 2014), vitiligo disorder (Hussain et al., 2015) and surgical wound (Goharshenasan et al., 2016) treatments.

1.2.2 Propolis

Aside from honey, there is another bee product known as propolis. Propolis or bee glue is built up from a resinous mixture that worker bees collect from plant resins, primarily leaf and tree buds, and enrich with bee secretions (Simone-Finstrom and Spivak, 2010). Propolis is usually sticky at room temperature (25°C) and varies in colour, including green, black, dark brown and yellow depending on botanical sources with a characteristic aromatic odor (Choudhari et al., 2013). This material creates a seal within the open spaces of the beehive that will protect the entrance against insects, parasites, fungal and bacterial growth. Moreover, propolis has the properties to prevent any successful intruders such as small lizards from decaying in

the beehive. The bees will seal the carcass using propolis, essentially mummifying it and making it harmless and odourless (Simone-Finstrom and Spivak, 2010). The chemical composition of propolis varies considerably according to their botanical sources in different regions. **Table 1.1** listed the common propolis types depending on their plant sources and their major constituents (Sforcin and Bankova, 2011). Several constituents from poplar type propolis have shown anti-bacterial, anti-inflammatory, anti-tumour, anti-oxidant, hepatoprotective and allergenic actions (Bankova, 2005). Similar bioactivities were observed with green propolis, which is predominantly found in Brazil (Banskota et al., 2001); the red propolis from Cuba, which yielded prenylated benzophenones and pacific propolis that afforded prenylated flavanones (Bankova, 2005).

Table 1.1: Most widespread propolis types: plant origin and major constituents.

Propolis type	Geographic origin	Plant source	Major constituents	References
Poplar	Europe, North America, non-tropic regions of Asia, New Zealand	*Populus* spp. of section Aigeiros, most often *P. nigra* L.	flavones, flavanones, cinnamic acids and their esters	(Markham et al., 1996) (Bankova et al., 2000)
green (alecrim) Brazilian	Brazil	*Baccharis* spp., predominantly *B. Dracunculifolia* DC.	prenylated p-coumaric acids, diterpenic acids	(Salatino et al., 2005)
Birch	Russia	*Betula verrucosa* Ehrh.	flavones and flavonols (not the same as in Poplar type)	(Popravko and Sokolov, 1980)
red propolis	Cuba, Brazil, Mexico	*Dalbergia* spp.	isoflavonoids (isoflavans, pterocarpans)	(Campo Fernández et al., 2008) (Daugsch et al., 2008) (Lotti et al., 2010)
Mediterranean	Sicily, Greece, Crete, Malta,	*Cupressaceae* (species unidentified)	diterpenes (mainly acids of labdane type)	(Trusheva et al., 2003) (Melliou and Chinou, 2004) (Popova et al., 2010)
"Clusia"	Cuba, Venezuela	*Clusia* spp.	polyprenylated benzophenones	(Cuesta-Rubio et al., 2002) (Trusheva et al., 2004)
"Pacific"	Pacific region (Okinawa, Taiwan, Indonesia)	*Macaranga tanarius*	C-prenyl-flavanones	(Chen et al., 2008) (Kumazawa et al., 2008) (Trusheva et al., 2011)

Over the past few years, more than three hundred compounds have been identified in honey bee propolis (Banskota et al., 2001). A study done by Usman and Mohamed (2015) applied gas chromatography mass spectrometry (GCMS) to identify twelve volatile phytochemical compounds from water extracts of *Trigona itama* Malaysian propolis that included the detection of norolean-12-ene, 2,3-butanediol and 2,6,10,15,19,23 hexamethyl (Usman and Mohamed, 2015). Meanwhile, there were twenty-five phytochemical compounds analysed from ethanol extract and the most predominant were 1,3-benzenediol-5-pentadecyl, cycloartenol and phenol-3-pentadecyl. More volatile compounds were also identified by using less polar solvents in this study. Microwave-assisted extraction (MAE) has also been proven to reduce the solvent used in extraction, while it can increase the yield of identified compounds from *Trigona* spp propolis (Hamzah and Leo, 2015). MAE was optimised at a temperature of 125°C, power supply of 300W, and by mixing 1:5 ratio of sample to solvent (g/ml), the recovery of total flavonoids and phenolics content was improved in just 15 min. However, the optimum condition for MAE is crucial to maintain good results.

Figure 1.1 showed some of the compounds found in propolis. For example, New Zealand honey bee and the Australian stingless bee propolis yielded pinocembrin, galangin, gallic acid, and pimaric acid (Massaro et al., 2011). However, different chemical compositions could be found in other hives, because opportunistic worker bees tend to forage whatever is available around them. Propolis also may contain impurities such as wood, wax, dead bees and pollen (Sforcin and Bankova, 2011). Therefore, it is very important to extract the raw propolis with suitable solvents such as methanol or ethanol in order to determine its major chemical compounds. Interestingly, the propolis has a long history of medicinal use where ancient people used propolis in the removal of abscesses, wound healing and mummification (Bankova et al., 1983). Nowadays, propolis has shown evidence of its effectiveness in treating cold sores, genital herpes and as a mouth wash preparation in surgery (Burdock, 1998). Moreover, in recent years, various biological studies have been done to investigate the potential of propolis and its constituents as anticancer, antioxidant, anti-inflammatory, antibiotic, and antifungal agents (Watanabe et al., 2011). (Oršolić and Bašić, 2003) demonstrated the anti-tumour activities of water-soluble derivatives of Brazilian and Croatian propolis in lung metastases generated by viable tumour cells injected in mice. Subsequently, they proposed the synergistic roles of propolis derivatives such as caffeic acid and its phenethyl ester congener in reducing the incidence of lung metastases in those mice (Orsolic et al., 2003).

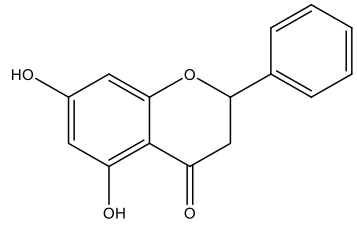

pinocembrin

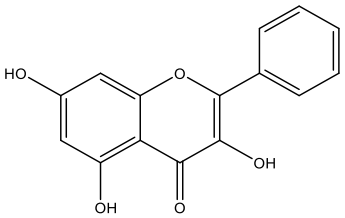

galangin

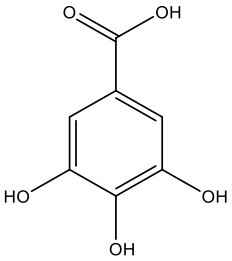

gallic acid

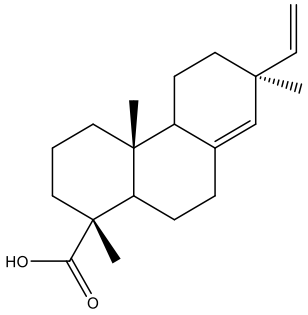

pimaric acid

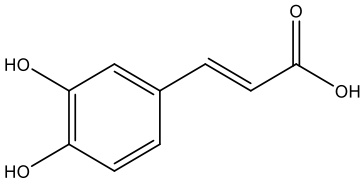

caffeic acid

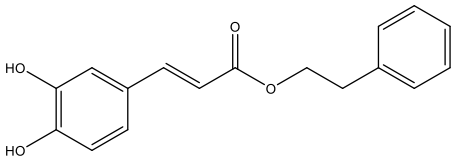

caffeic acid phenethyl ester

Figure 1.1: Some of compound structures found in propolis from New Zealand.

1.2.3 Vegetation in Malaysia and its indigenous bees

In general, according to Saw (2010) that was adapted from Anon (2008), the land use in Peninsular Malaysia is categorised into permanent reserved forests (35.7%), national and state parks (4%), wildlife and bird sanctuaries (2.4%) as well as areas for agriculture and other development purposes (59.3%) (Saw, 2010). Peninsular Malaysia consists of twelve states: Johor, Pahang, Terengganu, Kelantan, Malacca, Negeri Sembilan, Kuala Lumpur, Selangor, Perak, Kedah, Penang and Perlis. It is located at a latitudinal range of between 6°43' N and 1°15' N. It has an annual average rainfall of approximately 2,540 mm, which can exceed 2,750 mm in the wettest area, besides the heaviest rainfall can reach up to 4,000 mm per year on the foothills of Terengganu. The climate in Peninsular Malaysia generally is wet and perhumid throughout the year, with a few months of dry season in certain areas, such as the north-west area including Perlis and Kedah. Meanwhile there is higher rainfall in the north-east (Kelantan and Terengganu) area compared to the south-west (Perak, Selangor and Kuala Lumpur) because of alternate north-east and south-west monsoons every year. In addition, the average annual temperature in the lowlands of Peninsular Malaysia can reach up to 26.7 °C or higher during dry periods, whereas in the highland areas, temperatures are at least within the range of 13 – 14 °C. The forest vegetation, which covers 40.7% of the total land area are closely related to each other across different altitude, except for the alpine vegetation. The varieties of forest that naturally grow wild in Peninsular Malaysia include lowland evergreen, lower and upper mountain rainforests, health forests, vegetation over limestone and quartz, beach vegetation, mangrove and brackish water forests, peat and freshwater swamp forests. The latter all grow in perhumid climates, except for semi-evergreen rainforest formation only grows in dry climate (Saw, 2010).

The most common formation in Peninsular Malaysia is the lowland evergreen rainforest. According to Saw (2010) which was adapted from Wyatt-Smith (1963), this forest consists of three layers of trees, recognised as lowland, hill and upper hill dipterocarp forests (Saw, 2010, Wyatt-Smith, 1963). This tree layers forms based on altitudes ranging respectively from 0 – 300 m, ≤800 m and ≤1200 m above sea level, although each layer may expand into the other layers. The native species that are commonly found in lowland dipterocarp forest are from the family *Dipterocarpaceae*, such as *Dipterocarpus* spp., *Shorea* spp. and *Dryobalanops aromatica*. In addition to these trees, *Shorea curtisi* is also dominant in hill dipterocarp forest. As for upper hill forest, major differences in vegetation are found such as

the predominance of *Shorea platyclados*, *Shorea ciliata*, *Shorea ovate* and *Dipterocarpus retusus* in comparison with the other two tree layers. In some places, non-native plants, such as *Tectona grandis,* are introduced for their crop value. On top of that, other than large trees the seed flora in Peninsular Malaysia is recorded to have 7,834 species from 1,564 genera, which originated from 220 families (Kiew et al., 2010). They are classified into multi-cotyledonous gymnosperms and flowering plants, which are further classified into dicotyledons or monocotyledons. The main families found include *Orchidaceae, Rubiaceae, Leguminosae, Gramineae, Apocynaceae, Palmae, Myrtaceae, Lauraceae, Annonaceae* and *Gesneriaceae* (Kiew et al., 2010). Although a few native families no longer exist, the number of floral families keeps increasing because new families are being recognised over the time. Therefore, Peninsular Malaysia is unique for its diverse nature that is preserved until today.

Preliminary data on stingless bee diversity throughout Peninsular Malaysia has been provided in a study done by Salim et al., (2012), which covers lowland evergreen rainforests, lowland, hill and upper hill rainforests from Negeri Sembilan, Terengganu, Perak and Selangor (Salim et al., 2012). Varieties of 17 stingless bee species were found from six reserve forests in four states. These were *Geniotrigona thoracica* Smith, *Heterotrigona itama* Cockerell, *Homotrigona fimbriata* Smith, *Lepidotrigona nitidiventris* Smith, *Lepidotrigona terminata* Smith, *Lepidotrigona ventralis* Smith, *Lophotrigona canifrons* Smith, *Sundatrigona moorei* Schwarz, *Tetragonillaatripes* Smith, *Tetragonillacollina* Smith, *Tetragonulafuscobalteata* Cameron, *Tetragonulageissleri* Cockerell, *Tetragonulairidipennis* Smith, *Tetragonulalaeviceps* Smith, *Tetragonulamelina* Gribodo, *Tetragonulareepeni* Friese and *Tetrigonaapicalis* Smith. Based on this study, the most abundant stingless bee in Peninsular Malaysia is *Tetragonulalaeviceps* also called *Trigona laeviceps,* is described by Rasmussen and Michener (2010) based on several measurements adopted from the Sakagami (1978) method, such as head width (1.65 mm), wing diagonal length (1.05 mm) and hind tibial length (1.50 mm) (Rasmussen and Michener, 2010). *Trigona* bees are naturally prevalent in Peninsular Malaysia, possibly due to the humidity, variety of local flowers and trees, and a conducive environment that remains spared from human interference, such as logging activities.

1.2.4 Vegetation in New Zealand and its indigenous bees

New Zealand (34ºS – 44ºS/166ºE – 178ºE) is an archipelago located in the southwest Pacific Ocean. Named 'Nieuw Zeeland' by the Dutch explorer Abel Janszoon Tasman in 1642, after an area in the Netherlands, it is separated from Australia by the Tasman Sea. It is made up of two main islands, the North Island and the South Island, as well as a number of smaller islands. New Zealand lies along the Pacific Ring of Fire, and has several volcanoes (both dormant and active) and is prone to earthquakes. Overall, New Zealand experiences a temperate climate and evenly distributed rainfall. Extreme rainfall sometimes occurs due to the location of the mainland in the transition zone of the Westerlies Wind Belt; for this reason, the South Island experiences more rainfall than the North Island. The mountains in the west coast lie on the windward side, and receive less more rainfall than the eastern coastal plain that is sheltered from the wind. Dry periods (up to 2 months of no rain) result from sequences of anticyclone and dry north Westerlies monsoons. The maximum temperature can be up to 40ºC and can drop to -20ºC, with the North Island being generally warmer and drier than the South Island. Plant cover in New Zealand is dominated by grassland (40%), followed by adventives pasture (30%), forest (24%), grass and scrub (19%), forest and scrub (5%), exotic (4.5%), scrub (4%), bare (3%), grass and forest (3%), cropland (1%) and others (1%). Based on the altitude, the forest and its vegetation can be described as warm temperate, cool temperate (or montane), subalpine, alpine or nival (Wardle, 1964).

The warm temperate vegetation is found below 1,500 ft from sea level, where the lowland forest occupies the lowest elevation and a lot of *Araucariaceae* plant family such as *Agathis australis* and *Beilschmiedia tarairi* species can be found. Many smaller trees such as *Melicytus ramiflorus*, *Neopanax arboreum*, and *Myrsine salicina* were identified at a lower stratum of <40 ft. The middle stratum at 40-70 ft contains the larger hardwoods such as *Beilschmiedia tawa*, *Elaeocarpus dentatus* and *Weinmannia racemosa*. *Dacrydium cupressinum*, *Podocarpus spicatus* and *Metrosideros robusta* form the upper stratum at upwards of 80 ft. Moreover, several species also abundant at higher altitudes include *Freycinetia banksii*, *Rhopalostylis sapida*, *Cyathea medullaris*, *Metrosideros robusta*, *Griselina lucida* and *Collospermum hastatum*. The forest at the cool temperate belt (1,500 – 3000 ft) has less diversity in species. Only a few plants are found to be abundant, such as *Weinmannia racemosa* and *Nothofagus* sp. The *Dacrydium cupressinum* and *Podocarpus hallii* are submerged within *Nothofagus* canopy. On the other hand, the small leaf evergreen

beech *Nothofagus menziesii* is frequently abundant in subalpine forest at 3000 – 4000 ft. Some subalpine species such as *Olearia colensoi*, *Secenio bennettii* and *Dracophyllum* genus are frequent at lower altitudes. The lower boundary of the subalpine belt is occupied by the upper cool temperate species including *Wemmannia racemes, Carpodetus serratus*, *Earina orchid* and *Blechnum discolour* ferns. Moreover, the lower alpine belt is dominated by *Chionochloa* species at 4000 – 5000 ft altitude. On the higher alpine belt, vegetation is lesser and more discontinuous. There is permanent snow, which marks the beginning of the nival belt and the only plant life, lichen, which grows on the rocks and is resistant to the extreme temperatures.

The introduced bees in New Zealand, which are predominantly from the *Apidae* family (5 species), in addition to *Halictidae* and *Megachilidae*. The *Apidae* family can be divided into *Apinae* (honeybee) and *Bornbinae* (4 species of bumble bees). In 1839, the first *Apinae* species, *Apis mellifera* L. was introduced in Hokianga, New Zealand. Hence, in 1848 many honeybee hives were observed at the Bay of Island, Auckland, Coromandel, Waikanae and other places. The worker honeybee sizes range from 12 – 13 mm, with a yellow to blackish colour. Similar to the *Halictidae* family, *A. mellifera* species also can forage from different varieties of flower without any preference, depending only on the weather. Notably, *A. mellifera* honeybees also play a role as pollinator for native Manuka (*Leptospermum scoparium*). According to a review paper by Butz (1995), Manuka, a member of the Myrtaceae family, is one of the native plants from New Zealand that are known to provide *A. mellifera* honey bees with surplus honey stores (Butz Huryn, 1995).

1.3 Introduction to metabolomics

Metabolomics is a comprehensive study of all metabolites, which would afford a unique chemical fingerprint during or at end of a cellular process (Kaddurah-Daouk et al., 2008). It is a quantitative study of low molecular weight molecules (<1500 Da) that can be found in cells, tissues, organs and biological fluids. Moreover, several techniques involving high throughput technologies including high resolution nuclear magnetic resonance (NMR) spectroscopy, gas chromatography mass spectrometry (GC-MS) and liquid chromatography mass spectrometry (LC-MS) were used to augment separation, thus to expand the information of selected analytes then to identify their individual chemical structure (Wishart, 2016). In short, a metabolomics tool is a current approach to characterise unique features of complex

biochemical mixtures, commonly applied in drug discovery. There are several reasons for employing NMR as a primary tool for structure elucidation in metabolomics approach. This quantitative analysis is use to determine the structure of known or novel metabolites in crude extract, cell suspension, intact tissue or whole organism via straightforward 1D and 2D NMR experiments. The procedure is not only fully automated, robust, fast and can detect most of organic classes, but also requires no separation and derivatization. In addition, the samples used that have been diluted in solvent can be fully recovered afterwards. Even though the instrument is expensive (>US$ 1 million) and require large space because of it bulky size, it is still cost-effective because it has long lifetime of service up to 20 years.

On the other hand, mass spectrometry (MS) is also an automated quantitative analytical tool to characterise, identify and quantify a large number of compounds. Proper separation can be done via gas chromatography (GS) or liquid chromatography (LC), thus MS can measure the abundance of signals of those compounds based on the retention time and molecular mass. Structural identification of known and unknown compounds are based on mass accuracy, Ion fragmentation along with the software used to do data processing and clean up, thus help provide information on element composition or key sub structure. GCMS provides structural information based on large library database to detect most organic and inorganic molecules in the volatile phase. It also offers robust, good sensitivity to identify most spectral features, excellent separation, reproducibility, and a modest start-up cost (US$150, 000), in spite of some disadvantages including slow analysis (20 – 40 min), sample not recoverable and almost impossible to identify novel compounds. The greatest advantage of using LCMS in metabolomics study is the high sensitivity to detect most of the organic and some inorganic molecules in liquid and solid phase. Moreover, the instrument is very flexible that can be done on extracts without a separation step, thus only require direct injection at minimum sample volume. It is also possible to detect the largest portion of metabolome. The exact compound compositions of many compounds of interest are possible to determine by the combination of high mass accuracy and ion fragmentation with the appropriate software used. Several disadvantages of LCMS including higher start-up cost and less robust instrument than GCMS, slow analysis (15 – 40 min), short instrument lifetime (< 9 year) and quite challenging to obtain consistent quantitative precision. Both NMR and MS have their own advantages and disadvantages, but given the growing importance attached to metabolite identification, there appears to be growing preference for quantitative metabolomics.

The data generated from metabolomics either NMR or MS is further processed using differential expression analysis software which was first introduced to XCMS software that was developed by the Siuzdak laboratory at the Scripps Research Institute in 2006 (Smith et al., 2006). Different software that provides the same purpose has also been introduced such as MZmine, MZmatch, MetAlign and MathDAMP software (Katajamaa et al., 2006, Lommen, 2009, Baran et al., 2006). The softwares could be coupled with online or commercially available database such as Dictionary of Natural Product (DNP), ChemSpider, MarinLit or In-house database to dereplicate the secondary metabolites (Harvey et al., 2015). The processed data is further subjected to multivariate statistical analysis using for example, a SIMCA software either by unsupervised clustering such as principle component analysis (PCA) or supervised clustering such as orthogonal partial least squares discriminant analysis (OPLS-DA) to provide information on the putative bioactive metabolite at the first fractionation step or detect putative biomarkers in a cellular process. Therefore the greatest advantage of implementing metabolomics tools is it could save time and resources, thus provide a guideline in decision making for further isolation work or in determining biomarkers. In details, **Figure 1.2** illustrated a series of metabolomics tool in bioassay-guided fractionation in natural products research (Macintyre et al., 2014). The processed data from multivariate analysis is then plotted in S-plot for recognition pattern of active versus inactive, as well as known versus novel metabolites. The result from multivariate analysis is cross-matched with dereplication database, which provide aid information for the next step of purification. Structural confirmation is obtained via 2D NMR spectroscopy and tandem MS/MS spectrometry.

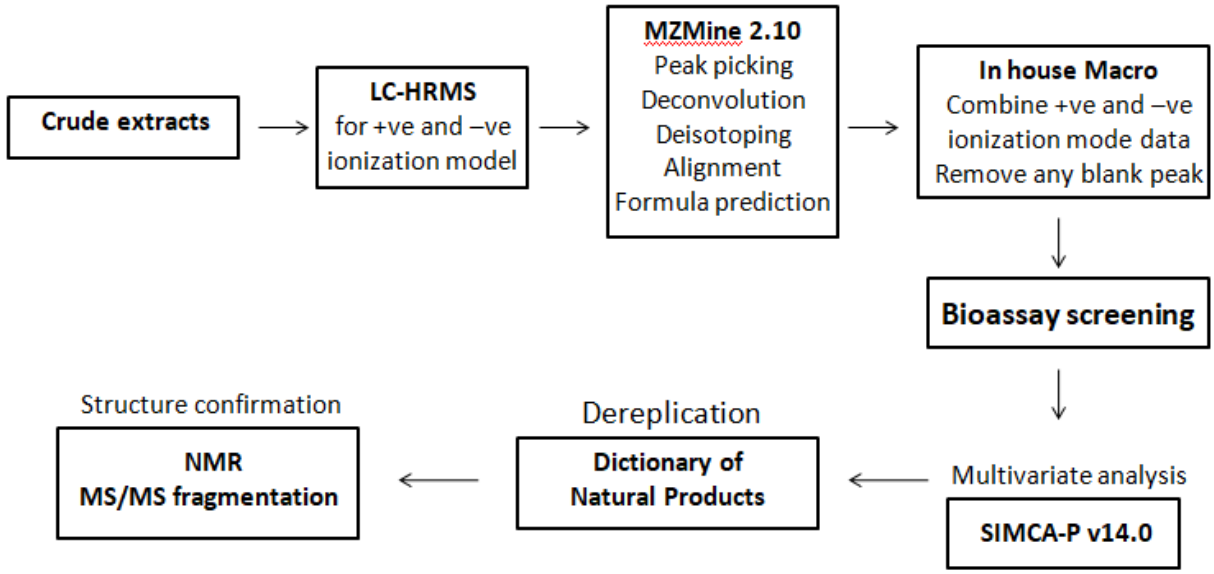

Figure 1.2: Metabolomics work flow in natural product study.

1.3.1 Using metabolomic tools in drug discovery

Metabolomics tools have been widely used in targeting and isolating compounds from a natural product crude extracts (Tawfike et al., 2013). The first report on anti-protozoal activity of *Pulicaria inuloides* was also demonstrated by following a metabolomics approach (Fadel et al., 2018). The plant extract was obtained using three different organic solvents, while the $CHCl_3$ extract was chosen for further fractionation work by silica gel column chromatography based on its activity against two parasite strains, *Leishmania amazonensis* and *Acanthamoeba castellanii* Neff. Nine fractions were obtained from the first stage fractionation and fraction 5 (F5) was chosen for further subfractionation based on its potent activity against *Leishmania amazonensis*, thus yielding five subfractions. The sub fraction (F5D) was obtained as a pure compound by TLC and was identified as 6,4'-dihydroxyl-3,5,7,3'-tetramethoxyflavone and its derivatives 6-acetoxy-4'-hydroxyl-3,5,7,3'-tetramethoxyflavone and 6,4'-diacetoxy-3,5,7,3'-tetramethoxyflavone, using NMR spectrum. This study was performed without implementing multivariate analysis. Meanwhile, a metabolomics-guided study via LCMS and NMR coupled with multivariate analysis using partial least square discriminant analysis (PLS-DA) based on their anti hyperlipidemis activity was demonstrated on the isolation of six bioactive compounds that included hyperoside, myricetin, naringenin, quercetin, kaempferol and ursolic acid from crude crabapple extracts (Wen et al., 2018). The used of metabolomics tools improved the isolation scheme employed on the methanolic extract of *Rhynchosia viscosa* via microfractionation

using semi-preparative LCMS, UHPLC-PDA-TOFMS and quantitative microflow NMR (qNMR) coupled with DNP database dereplication (Bohni et al., 2013). Despite of a high start-up cost on instrumentation, these instruments offer a minimum scale in comparison to the biological and analytical experiments needed in a bioassay-guided isolation work. Metabolomic-guided isolation work can also cut research cost and time, as well as enable the rapid identification of novel compounds, e.g. rhynchoviscin for this particular example along with the bioactive known compounds, genistein and sophoraisoflavone A in the earlier stage of the project. In general, after microfractionation was optimized on UHPLC-PDA-TOFMS, the enriched extract underwent semi-preparative HPLC and was chromatographed at one time yielding 180 microfractions (1.15 ml each). Three aliquots of 115 µl, 11.5 µl and 1.12 ml respectively were used for the zebrafish angiogenesis assay, LCMS and qNMR analysis. Two out of five identified compounds were described to give potent angiogenic activity based on dilution curve performed using GraphPad Prism 6 software. Overall, metabolomics tool with different instrumental approaches were having the same purpose in determining rational bioassay-guided fractionation, most importantly to isolate pure bioactive compound from diverse metabolites present in natural product. Therefore, metabolomic tools have become a current preference in drug discovery from natural product.

1.4 Problem statement

Complementary and alternative treatments have become a great choice for cancer patients because cancer is incurable disease, which is the leading cause of death worldwide, approximately causing 8.2 million cancer deaths in a year. Moreover, the conventional treatment associated with several side effects including sickness, ulcer, diarrhoea, hair loss, rapid weight loss, and vision and hearing problems. Some patients experience worse side effects than others, making it very hard to determine the suitable treatment for each individual. Most cancer patients will experience a reduction in their quality of life. Over the decades, many studies have been done to investigate possible treatments for cancer patients. However, there is a lack of information on the effects of local Malaysian honey and propolis against cancer, particularly on ovarian, lung, breast and pancreas cancer. Due to the different vegetation found in Malaysia and New Zealand, bees from these two countries might produce honey and propolis with a different chemical profiles and might exhibit different biological activities. Therefore the present study will focus on analysing the anti-proliferative effects of

Malaysian and New Zealand honey and propolis on ovarian, lung, breast and pancreas cancer cell line by adapting metabolomics tool for further guided isolation work.

1.5 The aim of this study

The aim of this project is to study the chemistry responsible for the therapeutic effects of Malaysia and New Zealand propolis and honey extracts by applying the tools of metabolomics.

1.6 The objectives of this study

1. To extract and fractionate propolis and honey samples from Malaysia and New Zealand using medium pressure liquid chromatography techniques.
2. To determine cytotoxicity effects of propolis and honey samples from Malaysia and New Zealand on several cell lines including human ovarian cancer (A2780), human lung adenocarcinoma epithelial cell (A549), human breast cancer cell (ZR75), human pancreatic carcinoma (PANC-1), normal human foetal lung fibroblast (HFL-1) and normal prostate epithelial cell (PNT2A).
3. To apply a metabolomic approach to identify the bioactive compounds in propolis and honey extracts from Malaysia and New Zealand.
4. To extract and isolate the active compounds in propolis samples from Malaysia and New Zealand.
5. To generate a metabolites profile for Malaysian and New Zealand honey extracts based on high-resolution liquid chromatography mass spectrometry (HR-LCMS).

CHAPTER 2

2 Materials and General Methods

2.1 Reagents

Absolute acetone, methanol, HPLC grade acetone, methanol (MeOH), acetonitrile (ACN), dichloromethane (DCM), n-hexane, ethyl acetate (EtOAc) and formic acid were purchased from Fisher Scientific (Loughborough, UK). Dimethyl sulphoxide (DMSO), deuterated DMSO-d_6 and deuterated chloroform ($CDCl_3$-d_6) were purchased from Sigma Aldrich Co., (Missouri, USA). HPLC grade water was obtained in-house from a direct Q-3 water purifier system (Millipore, Watford, UK). Celite® S was purchased from Sigma-Aldrich Co., Missouri, USA. Dulbecco's modified Eagle's medium (DMEM), penicillin-streptomycin and L-glutamine were purchased from Gibco BRL (Paisley, UK). RPMI 1640 medium was obtained from the store of Strathclyde Institute Pharmacy and Biomedical Sciences.

2.2 Equipment

2.2.1 General equipment

The rotary evaporator model number R-110 and R-3 were from BÜCHI, Switzerland. The Ultrawave sonicator was from Scientific Laboratory Supplies, Ltd. The UV lamp (UVGL-55 Handheld UV Lamp) was from UVP, Cambridge, UK. The heat gun HL 2010 E Type 3482 was from Steinel, USA. The Stuart® block heater SBH 130D/3 was from Bibby Scientific Ltd., Staffordshire, UK. The freeze dryer, model Christ Alpha 2-4 was from Martin Christ Gefriertrocknunsanlagen GmbH, Germany. The optical rotation was measured on a 341 Polarimeter from PerkinElmer, Inc., USA.

2.2.2 High resolution liquid chromatography mass spectrometry (HR-LCMS)

The High Pressure Liquid Chromatography (UltiMate-3000) was coupled to Mass Spectrometry (Exactive) instrument used was from Thermo Scientific, Germany.

2.2.3 Nuclear Magnetic Resonance spectroscopy

The Nuclear Magnetic Resonance spectroscopy instrument used was a JNM-LA400 model was from JEOL, Japan and the magnet NMR AS400 model EUR0034 came from Oxford Instruments, England. The NMR has a Pulse-Field Gradient "Autotune" TM probe 40TH5AT/FG broadband high sensitivity probe for 5 mm tubes. It has FG coils, 2H lock channel and can operate at various temperatures. Another NMR instrument used was an

AVANCE-III 500/600 instrument with a 14.1 T Bruker UltraShield magnet from the Department of Pure and Applied Chemistry. It has a 24 position autosampler, 3 channel console, is DQD and Waveform-equipped and can use either a BBO-z-ATMA-[31P-183W/1H] probe or a TBI-z-[1H, 13C, 31P-15N] probe. The Wilmad® NMR capillary tubes were purchased from Sigma-Aldrich Inc., USA.

2.2.4 Medium Pressure Liquid Chromatography (MPLC)

The flash chromatography was introduced in 1978 by Still and colleagues where it provide faster technique for routine purification (Still et al., 1978). This system was driven by medium air pressure through short columns. Even though the resolution was moderate with $\Delta R_f \geq 0.05$ on analytical TLC but the cost to operate the system is extremely inexpensive and can reduce the separation times to 1 – 3 hours. Two MPLC instruments were used in this study, one was the Sepacore <<Easy Synthesis>> Purification System BÜCHI, which consisted of two pumps; C-601 pump modules and the C-615 pump manager were from BÜCHI, Switzerland. This system allowed binary solvent gradients with flow rates of 2.5 to 250 mL/min. The column and its loading stand were purchased from VersaFlash/Supelco, Sigma-Aldrich, Germany. The fraction collector (CF2) was from Spectrum Labs and all fractions were collected manually in 100 ml conical flasks (Sigma-Aldrich Inc., USA) per min for a total run of 60 min. Another MPLC instrument used in this study is the Reveleris® Flash Forward system of Grace Davison Discovery Sciences (Illinois, United States) for flash chromatography. This system had two detectors, an evaporative light scattering detector (ELSD) and a UV detector (wavelength range: 200-500 nm). The advantage of this system is to provide greater sensitivity, where it can detect not only the UV-active compounds but also non-UV active compounds. This system allowed binary solvent gradients as well with flow rates from 4 to 200 ml/min that is also equipped with four independent channels where up to four solvents can be used in a single run. In addition, the flow rate was automatically adjusted if the pressure was above 70 bar. The fraction collector was built into the system where the instrument can detect the trays before the fraction had been collected into the test tube. Nonetheless, the instrument is also equipped with USB channel so that the chromatogram could be saved.

2.2.5 Thin Layer Chromatography (TLC)

The normal phase thin layer chromatography plates (TLC silica gel 60 F254) and preparative TLC plates (TLC silica gel 60 F254 on 20x20 cm aluminium sheets) were from Merck KGaA, Germany.

2.3 Software

Thermo Xcalibur 2.2 (Thermo Scientific, Germany) was used to monitor HR-LCMS raw data. The MassConvert file converter was used to convert and separate the raw data into positive and negative ionisation mode files. The MZmine 2.10 was used to process the HR-LCMS database. An in-house EXCEL-Macro was customised to couple the analysis of the mass spectral data with the Dictionary of Natural Products (DNP) 2017 for dereplication work. The MestReNova 10.0 by Mestrelab Research, S.L, (Santiago de Compostela, Spain) was used to process the NMR data. The SIMCA 14 (Umetrics AB, Umeå, Sweden) was used for multivariate data analysis. The GraphPad Prism V 5.0 (Sigma Aldrich, USA) was used to perform the dose response curve. The R version x64 3.0.3(R Foundation for Statistical Computing, Vienna, Austria) was used to generate the heat map.

2.4 General methods

2.4.1 Extraction of crude honey and propolis

Each honey and propolis sample was weighed, crushed, and suspended in 25 mL of 1:1 water and methanol by stirring for a minimum duration of two hours. The supernatant was filtered and collected in a round bottom flask before being concentrated *in vacuo* by using a rotary evaporator, R-110 and R-3 (BŪCHI Labortechnik AG, Switzerland) at a standardised temperature of 40°C. The extraction using a 1:1 ratio of methanol and water was repeated three times, and then the acetone and methanol were repeated three times each as well with the same duration of two hours in each cycle. The acetone and the methanol supernatants were pooled together in a round bottom flask and concentrated using the rotary evaporator. Once dry, all the samples were transferred to 5 mL tared vials by reconstituting the samples in the appropriate solvent such as acetone, methanol, distilled water or a combination of those solvents. Samples that were hard to re-dissolve were sonicated using the Ultrawave sonicator (Scientific Laboratory Supplies, Ltd, Coatbridge, UK). The samples were then further concentrated on heating blocks (STUART Bibby Scientific Limited Stone, Staffordshire, United Kingdom) at 40°C under a stream of nitrogen gas. Aqueous extracts were lyophilized in the Christ Alpha 2-4 freeze dryer (Martin Christ Gefriertrocknungsanlangen GmbH, Germany) at -80°C. All the concentrated samples were weighed, thus yielding organic and

crude extracts as shown in Tables 3.2 and 4.2. All extracts were stored in closed vials at room temperature until further used.

2.4.2 Thin Layer Chromatography (TLC)

The TLC was performed on normal phase silica gel 60 F_{254} aluminium-backed plates (Merck KGaA, Germany). The TLC provided not only simple, inexpensive and direct analytical technique but also highly sensitive to achieve a good resolution for partition of respective compounds (Wall, 2007). Generally, DCM, MeOH, n-hexane and EtOAc were used to perform the normal-phase TLC. The fractions were dissolved in a suitable non-polar solvent and spotted 1 cm above the bottom edge of the TLC plate. The sample volume applied on the starting point should be small to obtain a small spot and also to avoid tailing or double spot formation after the development of the chromatogram (Svendsen and Verpoorte, 2011). The chromatograms were run until it reached 5 cm of length and were observed under short and long wavelengths UVGL-55 Handheld UV light (UVP, Cambridge, UK) at 254 and 365 nm, respectively. Any band that was observed under the UV light was marked using carbon pencil. Anisaldehyde/H_2SO_4 reagent was used to spray TLC plates followed by heating using a heat gun HL 2010 E Type 3482 (Steinel, USA) at 170°C to visualise bands of organic compounds with no UV absorbance. Steroids, terpenes, sugars, phenolic acids, sapogenins and essential oil are examples of compounds that are not UV-active but will react with the spray reagent to be visualised.

Meanwhile, preparative TLC was done to recover compounds from the small volume of fraction and analytical TLC have been performed in advance to obtain the suitable solvent system for good chromatogram separation. The samples were spotted along a line 2 cm above the bottom edge at approximately 10 mg on each of the TLC plate. The TLC chamber that contained mobile phase was allowed to equilibrate for 10 min by placing a tissue or filter paper inside the chamber. This step will make sure that the chamber was saturated or properly equilibrated with the solvent system to develop a good chromatogram separation. The eluted bands were observed under UV light and were marked using a carbon pencil. The respective compound from each eluted band was recovered by cutting the marked bands into several pieces and macerated in 100 ml acetone overnight with stirring for 2 hours. The stirring step was repeated twice and the supernatant was filtered and collected in a tared round bottom

flask to dry using the rotary evaporator. The dried residue was weighed and subjected to further analytical work.

2.4.3 Anisaldehyde/H_2SO_4 reagent preparation

Anisaldehyde/H_2SO_4 spray reagent was prepared with a mixture of 0.5 ml of anisaldehyde, 85 ml of methanol, 10 ml glacial acetic acid and 5 ml of concentrated H_2SO_4 that was added slowly to give a final volume of 100.5 ml reagent. By using anisaldehyde reagent, bands such as triterpenoids and saponins were observed as blue or violet under long UV wavelengths at 365 nm.

2.4.4 High Resolution Liquid Chromatography Mass spectrometry (HR-LCMS)

All crude extracts were prepared to a concentration of 1 mg/ml in methanol (MeOH, HPLC-grade). A blank solvent was also included. The experiment was carried out according to an established standard operating procedure (Macintyre et al., 2014) using the ThermoFinnigan Exactive Orbitrap Mass Spectrometry (Thermofisher Corporation, Hemel Hempstead, United Kingdom) in both positive and negative ionisation on switch mode. Solvents A and B consisted of 0.1% formic acid in water and acetonitrile, respectively. A silica C-18 HPLC column with the size of 75.0 x 3.0 mm^2, particle size of 5µm and pore size of 100 °A (Hichrom Limited, United Kingdom) was used. Each of the samples were eluted at a flow rate of 300 µl/min using a linear gradient of 10% B to 100% B for 30 min, followed by isocratic elution at 100% B for 5 min and a linear gradient of 100% B to 10% B for 1 min, after which the column was further re-equilibrated with the same solvent system for another 9 min. The pressure and temperature were monitored to be within the normal range of 37- 70 bars and 22°C, respectively, for the instrument to operate smoothly. LC-MS data was recorded using Xcalibur version 2.2 (Thermo Scientific, Bremen, Germany). The data were processed using the softwares mentioned in Section 2.3.

2.4.5 LC-MS data analysis using Mzmine 2.10 adapted from Macintyre et al., (2014)

The LC-MS Xcalibur raw data from both positive and negative ionization modes were sliced using the MassConvert file converter to separate both positive and negative masses. The mass files were uploaded separately and processed using Mzmine 2.10 software. The raw data methods were processed using peak detection, started with mass detection by mass detector

was set as centroid, noise level at 1000 and MS level as 1. Followed by chromatogram builder was set at 0.2 min for Min time span, Min height at 10000 and *m/z* tolerance at 0.001 *m/z* or 5 ppm. The analysis continued with peak detection from peak list methods, for the chromatogram deconvolution, where the algorithm was set as local minimum search. The chromatographic threshold was set to 5%, search minimum in RT range at 0.4 min, minimum relative height at 5%, minimum absolute height at 10000, Min ratio of peak top/edge as 3 and peak duration range within 0.2 – 5 min. Meanwhile for deisotope, *m/z* tolerance was set to 0.001 *m/z* or 5 ppm, retention time tolerance at 0.1 min absolute, maximum charge as 2 and representative isotope was set as most intense. For alignment, join aligner was set by following setting, including m/z tolerance at 0.001 *m/z* or 5 ppm, retention time tolerance was set to 5% relative, weight for RT and m/z at 20 because those parameters are given equal importance. Followed by gap filling analysis, peak finder was set as following parameters, *m/z* tolerance at 0.001 *m/z* or 5 ppm, intensity tolerance at least 30% and retention time tolerance at 0.5 min absolute with RT correction. An adduct search for peak identification was analysed for RT tolerance at 0.2 min absolute, adducts for positive mode was set as Na, K, NH4 and ACN + H, *m/z* tolerance at 0.001 *m/z* or 5 ppm and maximum relative adduct peak height at 30%. The complex search was also done by following parameters; ionization was set as M+H for positive mode, retention time tolerance at 0.2 min absolute, *m/z* tolerance at 0.001 *m/z* or 5 ppm and maximum complex peak height at 50%. Lastly, the formula prediction was done by setting the charge at 1, ionization as [M+H]+, *m/z* tolerance at 0.001 *m/z* or 5 ppm and isotope pattern filter was done with all features with isotope peaks. The data were exported as CSV file until further clean-up process. All the Mzmine processing steps were then repeated with negative mode with some modification such as an adduct search was set as formate and ACN + H, complex search ionization was set as M-H and formula prediction ionization was set as [M-H]-.

2.4.6 Data clean up using In-house Macro

An In-house EXCEL Macro was developed by Dr Tong Zhang and was adapted in Macintyre et al., (2014) for both dereplication and metabolomics study. The EXCEL Macro file was coupled with Dictionary of Natural Product (DNP) database for peak identification and dereplication. The positive and negative ionization modes were combined and any blank peaks were removed from the background of individual peak, so that remaining peaks from both ionization modes were overlaid for further statistical analysis. The generated database of

known and unknown metabolites from the Macro was utilised to pinpoint the putative discriminating metabolites from the sample extracts, which provided information of individual peaks including by assigning a feature ID number along with the respective ionization mode, *m/z*, retention time, molecular formula, molecular weight, biological sources and peak intensity. The data were then converted into CSV file and was exported into SIMCA 14.0 (Umetrics, Umeå, Sweden) for multivariate analysis.

2.4.7 Nuclear Magnetic Resonance Spectroscopy

All crude extracts were prepared at a concentration of 5 mg per 600µl deuterated DMSO-d_6 and chloroform-d_6 (Sigma-Aldrich, Dorset, UK) and placed in 5mm NMR tubes (Wilmad, Sigma-Aldrich, Dorset, UK). For small quantity samples, small capillary tubes (Wilmad, Sigma-Aldrich, Dorset, UK) were used by dissolving in 200µl deuterated solvent. The ^{1}H, COSY, ^{13}C, HMBC, NOESY, HSQC and HMQC (400Hz) spectrums were run for one and two dimensional correlation spectroscopy NMR in JEOL-LA400 FT-NMR instrument equipped with a 40TH5AT/FG probe (JEOL, Tokyo, Japan) and also using the Bruker Biospin GmbH-NMR instrument equipped with a 5mm BB-1H/19F/D probe from the Department of Pure and Applied Chemistry, University of Strathclyde. Chemical shifts are given in ppm and coupling constants in Hz. The data obtained were processed with MestReNova (Mnova10.0) software (Mestrelab Research, Santiago de Compostela, Spain) to confirm chemical structures. The ^{1}H spectra were processed under certain conditions which included Whittaker Smoother, manual phase correction and Gaussian was set to 1 for apodization.

2.4.8 Multivariate analysis using SIMCA-P V 14.0

The database generated from the EXCEL Macro was further analysed using SIMCA 14.0 for multivariate analysis. For the mass spectral data, the MZmine feature ID number was merged the with ionization mode to generate a unique primary ID in SIMCA while the other variables like retention time, *m/z*, and molecular weight were considered secondary IDs. While for the NMR data, the chemical shift in ppm is used to generate the unique primary ID and there are no secondary IDs considered for variables. The data were preliminarily analysed with an unsupervised statistical method by using principal component analysis (PCA). A supervised statistical analysis method was done with orthogonal partial least squares discriminant analysis (OPLS-DA) when comparing groups and discriminating metabolites according to the

known variables between groupings. PCA and OPLS-DA analysis were done using Pareto scaling and the models were validated based on multiple correlation coefficients (R^2) and cross-validation (Q^2) as well as permutation tests for the supervised method. The discriminant data was cross-matched with the dereplication database through an in-house EXCEL Macro to pinpoint the putative metabolites for further isolation and purification.

2.4.9 Optical rotation

The optical rotation was performed by Mr. Gavin Bain from Chemistry Department, University of Strathclyde based on standard operating procedure for measuring optical rotation on the Perkin Elmer 341 polarimeter (PerkinElmer Inc, United State). The compound was dissolved in methanol or other appropriate solvents to a concentration of 2 mg/2 ml. The equation to calculate the final optical rotation value was as follows:

$$[\alpha]_{\lambda}^{T} = 100 \times \alpha / l \times C$$

[l = the cell volume in ml (the value of l for the micro test cell is 1), c = the concentration in g per 100ml, α = the average first ten readings of the rotation value]

2.4.10 Bioassay screening

2.4.10.1 Cytotoxicity assay

Several cytotoxicity assays were done using the AlamarBlue™ assay (O'Brien et al., 2000) including human ovarian cancer (A2780), human lung adenocarcinoma epithelial cell (A549), human breast cancer cell (ZR75), human pancreatic carcinoma (PANC-1), normal human foetal lung fibroblast (HFL-1), and normal prostate epithelial cell (PNT2A) under the supervision from Mrs. Louise Young and Mrs. Grainne Abbott from SIDR. All cell lines were obtained from University of Strathclyde that were kept in liquid nitrogen at -80°C. All cell lines were maintained in either DMEM or RPMI 1640 medium supplemented with 1% (v/v) L-glutamine (Invitrogen, Paisley, UK), 100 IU/ml/100 µg/ml penicillin/streptomycin (Invitrogen, Paisley, UK) and 10% (v/v) foetal bovine serum (FBS) (Life Technologies, Carlsbad, CA, USA). The seeding density was dependent on the growth rate of the cell lines. The cells were sub-cultured by trypsinisation every 3 – 4 days and maintained at 37°C in a humidified atmosphere saturated with 5% CO_2 until the cell reached 80% confluent.

The cytotoxicity assays for all cell lines were performed at different cell density in 96-well micro seeding plate (Corning®, Sigma-Aldrich, Poole, UK) and incubated at 37°C in a humidified atmosphere saturated with 5% CO_2 for a duration of 24 hours. For the screening, the cytotoxicity assays for all extract were performed at concentration of 100 µg/ml. Meanwhile for pure compounds, cytotoxicity assays were done in serial dilution from 0.003 – 100 µM. When possible, a serial dilution of sample fractions was performed at the same concentration. After 24 hours drug treatment, the final concentration of 10% (v/v) AlamarBlue™ was added into the seeding plate, the plate was then read at an excitation wavelength of 560 nm and the emission of 590 nm using a Wallac Victor microplate reader (Perkin Elmer, Cambridge, UK) after 5 to 6 hours incubation. All compounds were tested in triplicate and the viability percentages of control were calculated and measured for ≤ 40% for the screening and IC_{50} concentration for the drug testing.

2.4.10.2 Zebrafish assays at Cancer Research Institute Malaysia

The Zebrafish assays including phenotypic and angiogenic tests were done according to the protocol described earlier (Velaithan et al., 2017, Okuda et al., 2016) at Cancer Research Institute Malaysia under supervision from Dr Pei Jean Tan, Dr Kazuhide Shaun Okuda, Mrs Faizah and also special thanks to Dr Vyomesh Patel for providing me the facilities.

2.4.10.2.1 Phenotypic assay

The Riken wild-type zebrafish strain (Riken, Japan) was used for mating and maintained at 28°C. Selection of embryos (~10 embryos/well for 24-well plates) in E3 media were done prior observation under microscope (4 x magnifications) which uniformly divided at ~16-cell stage at ~1.5 hour post fertilisation (hpf). E3 media was prepared as in the literature (5 mM NaCl, 0.17 mM KCl, 0.33 mM $CaCl_2$ and 0.33 mM $MgSO_4$, pH 6.8-6.9). Samples were prepared at 10 mM in DMSO (known compound) as stock and stored at -20°C until further use. DMSO concentration used was 0.5% as vehicle control, DAPT at 50 µM and 20 µM as positive control. Waterborne treatment of samples was carried out from 3 hpf~1000 cells to 72 hpf, which also incubated at 28°C. Any morphological changes were observed every 24 hpf under microscope (OLYMPUS MVX10, CARIF, USA). Any morphological changes were recorded and saved as jpeg at 72 hpf. The phenotypic assay was done in triplicate independent assay (n=3).

2.4.10.2.2 Angiogenic assay

Tg(fli1α:EGFP)y1 transgenic lines were used for mating. Selection of embryos (~10 embryos/well for 24-well plates) in E3 media were done prior observation under microscope (4 x magnifications) which uniformly divided at ~16-cell stage at ~1.5 hpf. E3 media was prepared as in the literature (5 mM NaCl, 0.17 mM KCl, 0.33 mM $CaCl_2$ and 0.33 mM $MgSO_4$, pH 6.8-6.9). Depigmentation solution 0.003% 1-phenyl-2-thiourea (PTU) (Sigma Aldrich, USA) was also added to have transparent visualisation of zebrafish under microscope. Samples were prepared at 10 mM in DMSO (known compound). DMSO concentration used was 0.5% as vehicle control, Sunitinib malate (SM) at 20 μM as positive control. Waterborne treatment of samples is carried out from 3 hpf~1000 cells to 48 hpf, which also incubated at 28°C. Any morphological changes were observed after 48 hpf under microscope. At 48 hpf, 0.4% tricaine (3-amino benzoic acid ethyl ester, pH 7.0) (Sigma Aldrich, USA) solution was added into the wells to stop the zebrafish from moving rapidly. Then the chorion layer of embryos has been removed. The embryos were then organised in lateral position, showing the locations of intersegmental vessel (ISV), subintestinal vessel (SIV) and parachordal lymphangioblast (PL) which were mounted in 1.2% methylcellulose solution, low gelling temperature (Sigma Aldrich, USA). Any morphological changes were recorded as florescent image and saved as jpeg. The angiogenic assay was done in triplicate independent assay (n=3).

2.4.11 Non-linear regression analysis using GraphPad Prism V 5.0

The dose response curve was performed by non-linear regression analysis using GraphPad Prism V 5.0 (GraphPad software, San Diego, USA). The IC_{50} value was determined via cell viability data where the measurement was done in triplicate independent bioassay (n=3).

2.4.12 Heat map generated from programming software R version x64 3.0.3

The heat maps were performed from Macro database generated from HR-LCMS and ^1H NMR. The method was adapted from (Macintyre *et al.*, 2014) using a script utilizing the g-plot package (R Foundation for Statistical Computing, Vienna, Austria).

CHAPTER 3

3 Malaysian propolis secondary metabolites and its bioactivities

3.1 Introduction

The propolis has shown evidence of its effectiveness in various biological studies, including its effectiveness in wound healing (Jacob et al., 2015). Jacob et al., (2015) reported the use of Malaysian propolis from *Trigona* spp. that can inhibit inflammation and trigger the proliferation of fibroblast cells, thus accelerating the wound healing process. The study also claimed that cell proliferation and migration could be triggered by concentrations of 500 µg/ml and 250 µg/ml, respectively, of Malaysian propolis at optimum level of cell proliferation and migration. The bioactivity of propolis depends on its chemical composition, which depends on both the variety of the plant source and on the species of bee. Another study has investigated two sources of Malaysian propolis that were produced by *Heterotrigona itama* (MHI) and *Geniotrigona thoracica* (MGT) stingless bees (Ibrahim et al., 2016). It was shown that MHI and MGT propolis extracts have antioxidant properties, with IC_{50} of 15 µg/ml and 270 µg/ml, respectively. High anti-diabetic activity also was observed in both types of propolis extracts, with IC_{50} 2.5 µg/ml for MIH and 30 µg/ml for MGT. Stronger bioactivity was reported for MHI propolis due to their abundance in terpenoids, flavonoids, saponins, steroids, coumarins, and essential oils. The biological activities of propolis are well-studied in the literature. However, there is still lack information about propolis from Malaysia, particularly the bioactivity of the isolated compounds. Overall, the current study aimed to apply metabolomics tool in order to pinpoint bioactive metabolites from *Trigona* spp. propolis from Peninsular Malaysia. The current study applied metabolomic tools (Macintyre et al., 2014), as a powerful method to distinguish the putative bioactive metabolites prior to the chromatographic separation which can save experimental time and have more economical value in terms of apparatus and materials used.

3.2 Materials and methods

3.2.1 Propolis.

Fresh Malaysian propolis was obtained from Mrs. Cathie from Eco Bee Shop Sdn. Bhd. Johor, Malaysia and Mr. Ong from B-B Town Sdn. Bhd. Malacca, Malaysia. All samples were kept at room temperature until further use (**Table 3.1**). The extractions of crude propolis were conducted as mentioned in *2.4.1* procedure and the **Table 3.2** showed the weights of propolis extracts after solvent partitioning.

Table 3.1: Propolis samples used in the present study.

No.	ID	TYPE OF BEE	COLOUR	GEOGRAPHICAL AREA	DISTRIBUTOR
1	A	*Trigona* spp.	Yellow	Malacca	B-B Town Sdn. Bhd. (Mr.Ong)
2	B		Green		
3	C		Black		
4	D		Black	Johor	Eco Bee Shop SdnBhd (Mrs. Cathie)
5	E		Green		

Table 3.2: The weights of propolis extracts after solvent partitioning.

Sample ID	Initial raw sample weight (g)	Sample ID	MeOH:H_2O (1:1) extract weight (g)	Sample ID	MeOH:Acetone (1:1) extract weight (g)
A	16.0	AO	0.64	AC	12.9
B	1.0	BO	0.01	BC	0.8
C	1.0	CO	0.10	CC	0.6
D	1.0	DO	0.10	DC	0.4
E	20.0	EO	0.20	EC	10.0

3.2.2 Isolation of Malacca crude green propolis extract using MPLC from GRACE

Medium pressure liquid chromatography (MPLC) from GRACE was used to isolate the pure compounds from BC (0.8 g) and AC (12.9 g) extracts. For BC extract, two solvents, Solvent A (MeOH) and Solvent B (DCM), were used in this experiment, eluting at a flow rate of 40 ml/min, which was suitable for a sample load of 40 mg to 8.0g. A silica column from Reveleris (GRACE, USA) was used in MPLC with a particle size of 40 µm and a column volume of 48 ml. The chromatographic run started with elution of 100% B for 5 min for equilibration, followed by a linear gradient elution from 0% to 1% A for 15 min, followed by 5% A for 25 min and then

50% A for another 20 min. The column was washed with 50% A for the last 15 min. The fractions were automatically collected by peak detection to the fraction collector in 20 ml test tubes resulting in 57 fractions. All fractions were subjected to TLC profiling and those with the same chromatogram were pooled together yielding 11 fractions (**Figure 3.1**). For AC extract, Solvents A and B, which are EtoAc and n-hexane, respectively were used to run the MPLC. The chromatographic run started with elution of 100% B for 10 min for equilibration, followed by a linear gradient elution from 0% to 100% A for 60 min. The column was washed with Acetone and MeOH (1:1) for 10 min. The MPLC resulting in 289 fractions, which were pooled together yielding 23 fractions, subjected to TLC profiling (**Figure 3.2**).

3.2.2.1 Isolation and purification of secondary metabolites from BC extract.

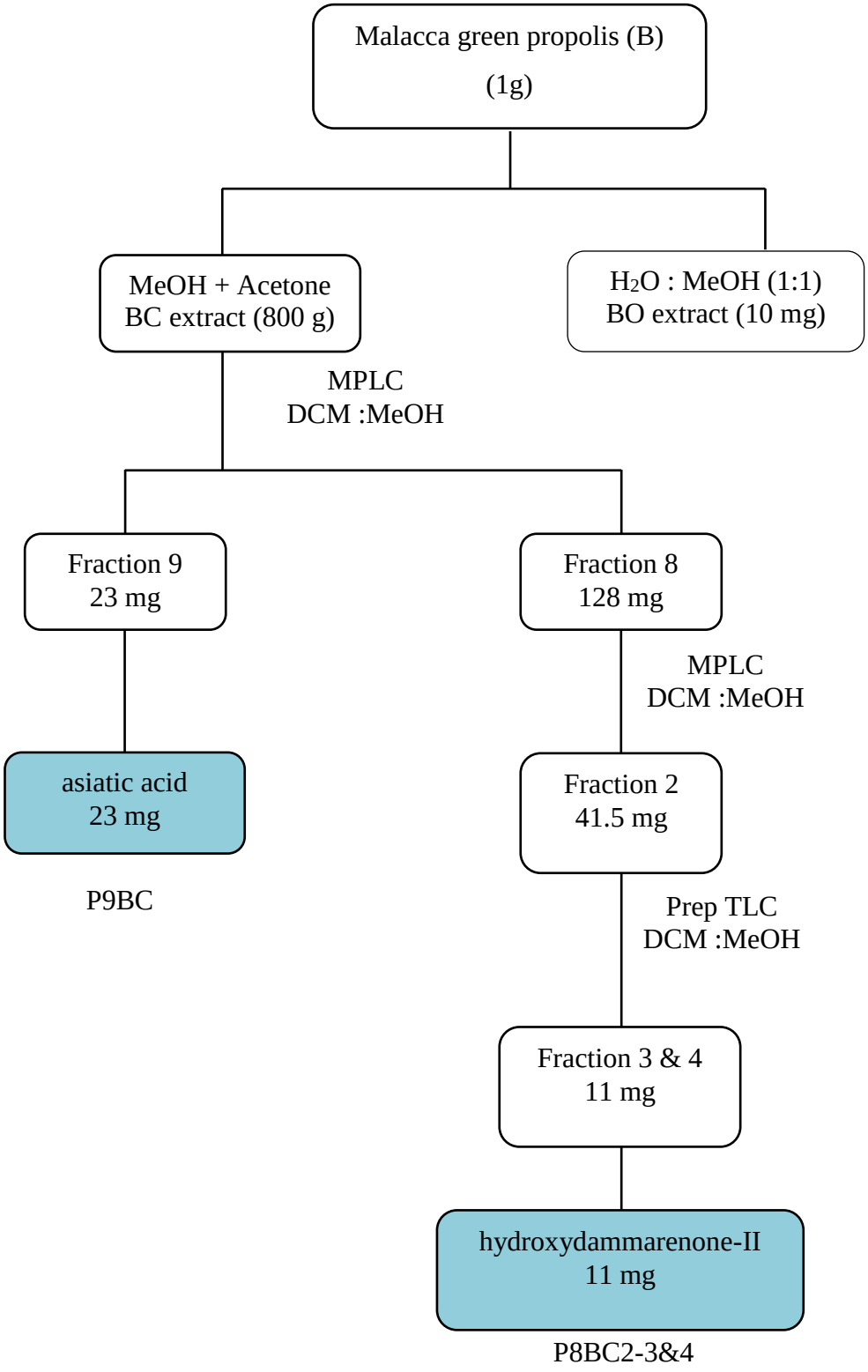

Fig. 3.1: The fractionation of BC extracts afforded asiatic acid and hydroxydammarenone-II.

3.2.2.2 Isolation and purification of secondary metabolites from AC extract.

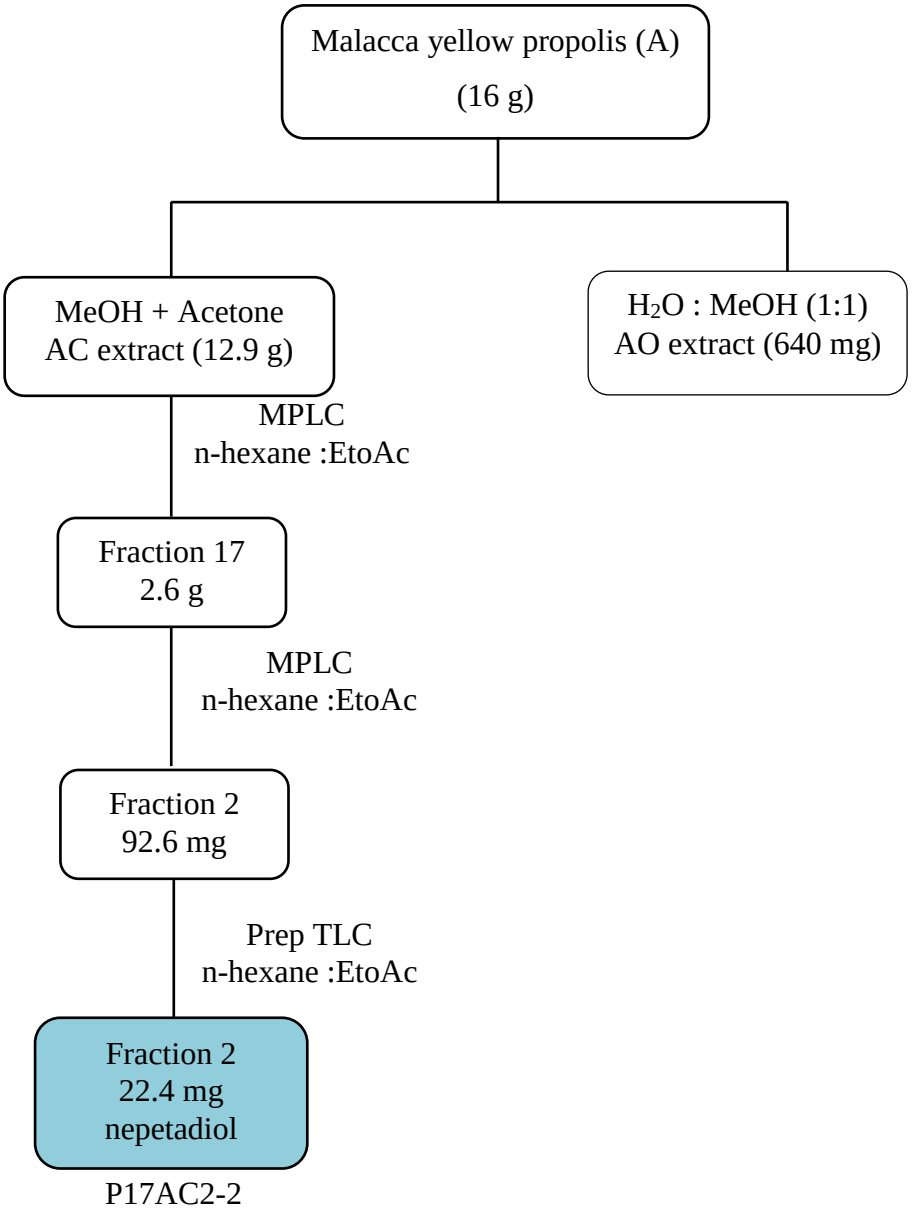

Fig. 3.2: The fractionation of AC extracts afforded nepetadiol.

3.2.3 Isolation of bioactive secondary metabolites from Johor crude green propolis extract (EC) using MPLC from BŪCHI

Flash liquid chromatography set-up from BŪCHI was used to isolate the bioactive compounds from 10g EC extract. Two solvents were used in this system, n-hexane and EtOAc for Solvents A and B, respectively. The run started with equilibration of the system by eluting 100% of A in 1L conical flask for 10 min at a flow rate of 100 ml/min. The chromatography continued with a linear gradient elution from 0% to 100% B for 60 min, followed by a washing step using a 50:50 ratio of Acetone and MeOH for 10 min. All fractions were manually collected in 100 ml conical flasks, which gave 58 fractions, while the waste was collected in a 1L conical flask. All fractions were subjected to TLC profiling and those with the same properties were pooled together yielding 11 fractions (**Figure 3.3**).

3.2.3.1 Isolation and purification of secondary metabolites from EC extract.

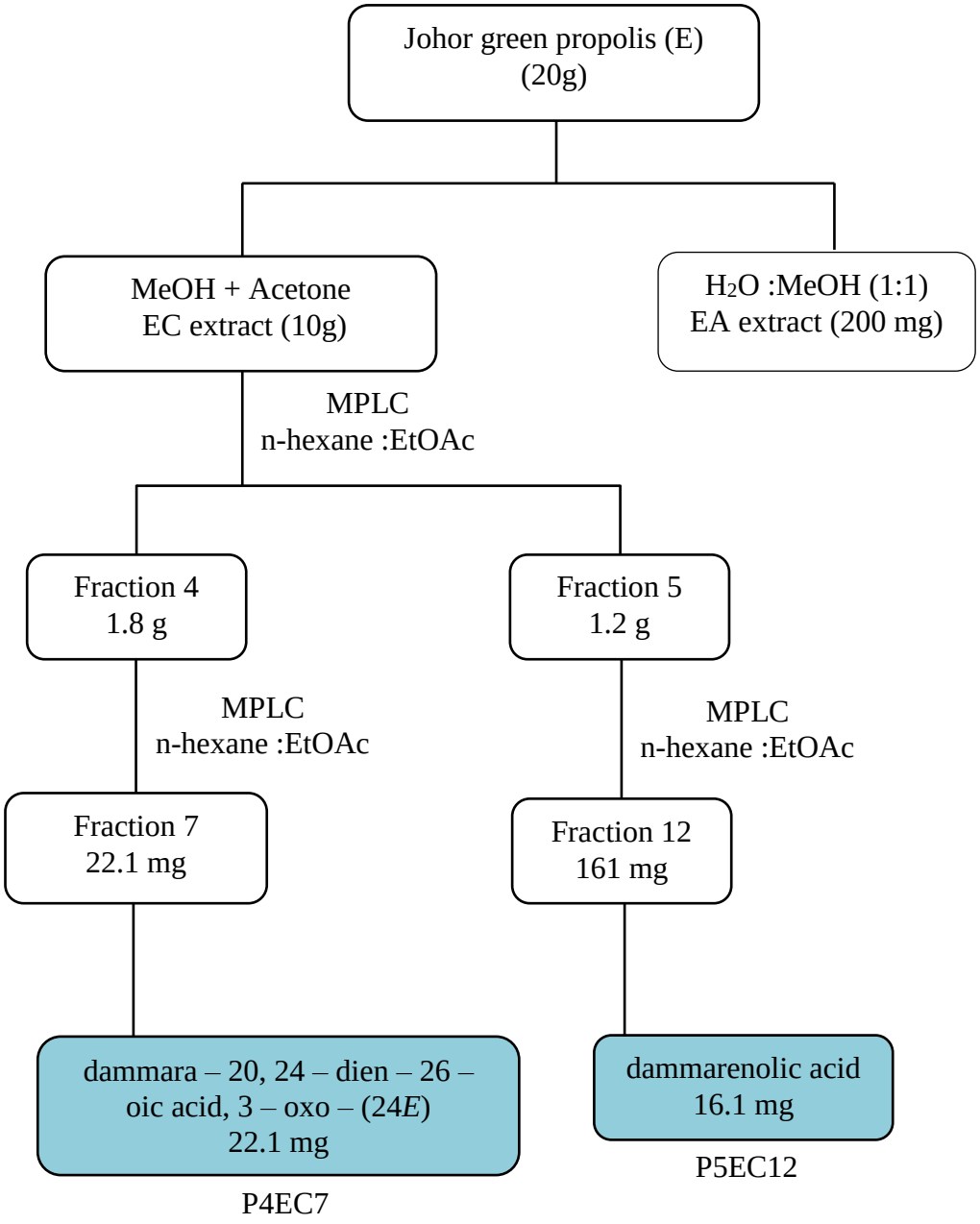

Fig. 3.3: The fractionation of EC extracts afforded dammara-20, 24-dien-26-oic acid, 3-oxo- (24*E*) and dammarenolic acid.

3.3 Results

3.3.1 Metabolomic- and bioassay-guided decision making for further isolation of secondary metabolites from Malaysian propolis.

All five propolis samples were extracted using (1:1) ratio of water and MeOH, followed by using acetone and MeOH to obtain organic and crude extracts, respectively. All extracts were subjected to ^{1}H NMR analysis (**Fig. 3.4** and **Fig. 3.5**). The BC, EC and AC extracts were chosen for further isolation work in accordance to their bioactivity and based on their extract yield (800 mg, 10 g and 12.9 g, respectively). Those extracts were less complex but afforded interesting ^{1}H NMR resonances. Phenolic hydroxyl groups on a 6-membered aromatic ring were indicated by signals at 9 – 13.5ppm. Methyl group signals were also observed at 0.5 – 2.5 ppm, which are possibly related to terpene or steroid type of compounds.

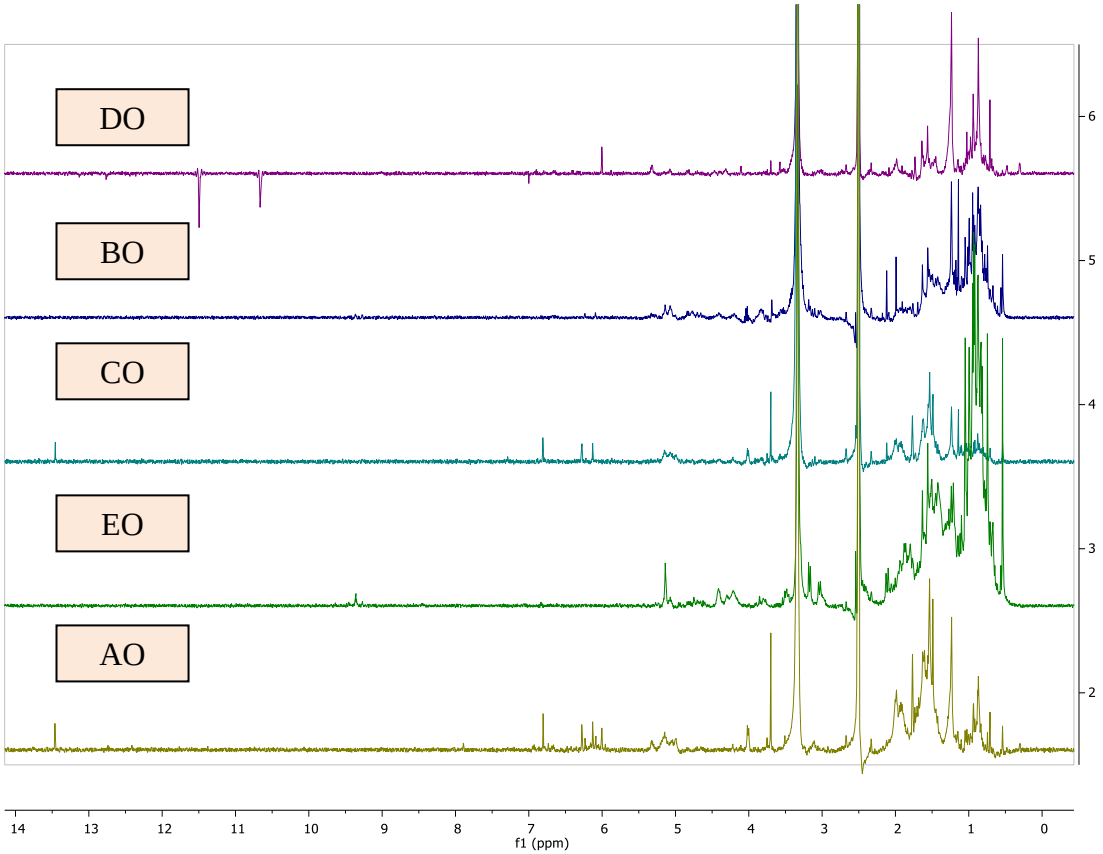

Fig. 3.4: ^{1}H NMR spectra of organic extracts. DMSO-d_6 was used as solvent.

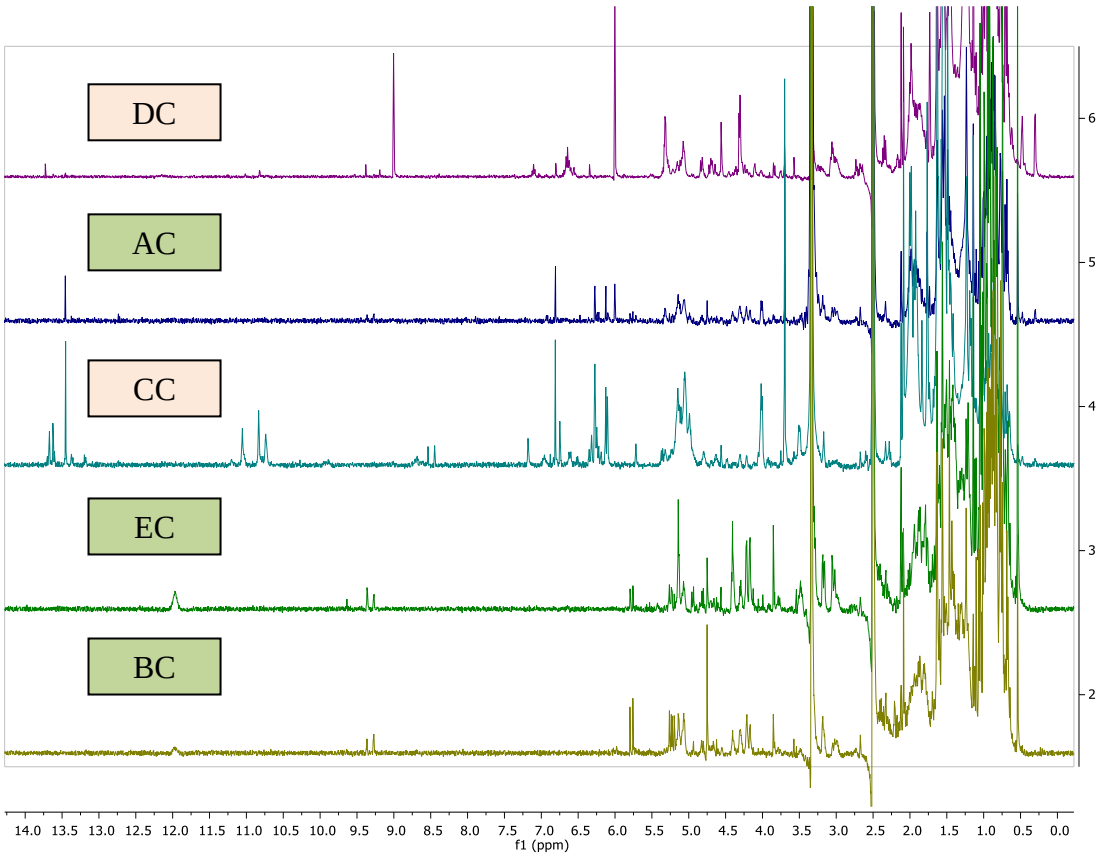

Fig. 3.5: ^{1}H NMR spectra of crude extracts. DMSO-d_6 was used as solvent.

Fig. 3.6 shows the TLC of crude extracts that were eluted using 9:1 DCM : MeOH which further demonstrated the similarity of the extracts particularly those of AC, BC, and EC. The extracts were chosen for further isolation because of their not only high yield and bioactivity but also because their TLC exhibited good separation of the diverse components contained in these extracts. Those compounds in AC, BC, and EC extracts were not UV active, which indicated the occurrence of non-aromatic compounds as supported by the ^{1}H NMR spectrums.

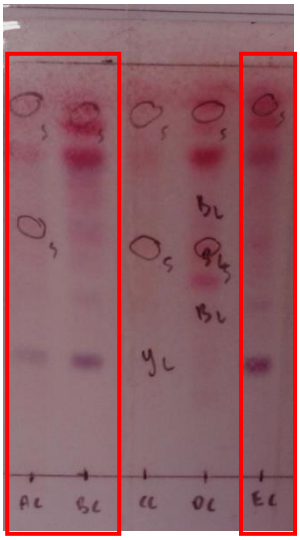

AC BC CC DC EC

Fig. 3.6: TLC of crude propolis samples showing good separation of diverse components. Extracts highlighted in red box were subjected to further fractionation and isolation work.

Table 3.3: Bioactive extracts from Malaysian propolis on A2780 and A549. Highlighted rows indicate bioactivity, causing cell viability ≤ 40% in comparison to the control.

Sample ID	Antiproliferative against ovarian cancer A2780 100µg/ml	Antiproliferative against lung cancer A549 100µg/ml
AC	5.1	88.2
BC	46.1	65.4
CC	89.7	94.2
DC	89.7	89.7
EC	26.3	0.1

Based on the bioassay screening results (**Table 3.3)**, AC and EC extracts exhibited the strongest activity on A2780 cell line. In fact EC extract also gave potent cytotoxicity effects against A549, subjected to ≤ 40% threshold. The HR-LCMS data was processed in a modified version of Mzmine 2.10 then dereplicated using an EXCEL Macro coupled to the DNP database. SIMCA 14.0 was used to generate PCA scores and loadings scatter plots as shown in **Fig 3.7**. There were five variables used in PCA which are AC, BC, CC, DC and EC indicating the type of Malaysian propolis crude extracts used in this study. As observed from the PCA scores scatter plot, BC and EC samples clustered together that indicated a strong similarity of their chemical profiles (**Fig 3.7a)**. AC was nearer to the clustered group while CC and DC were more dispersed. Based on the loadings plot, the metabolite in BC and EC extracts might share the same pattern of compounds because majority of their variables overlapped with each other. Both R^2 and Q^2 values were at 1.0, which indicated a well-fitted model (R^2) and good prediction of variables (Q^2).The end metabolites listed in **Table 3.4** were found to be unknown compounds at the highest intensity in EC and BC extracts, which indicated molecular weight between 690 – 825 g/mol. While AC metabolites were observed at molecular weight between 1365 – 1500 g/mol, coloured in red (**Fig 3.7b**).

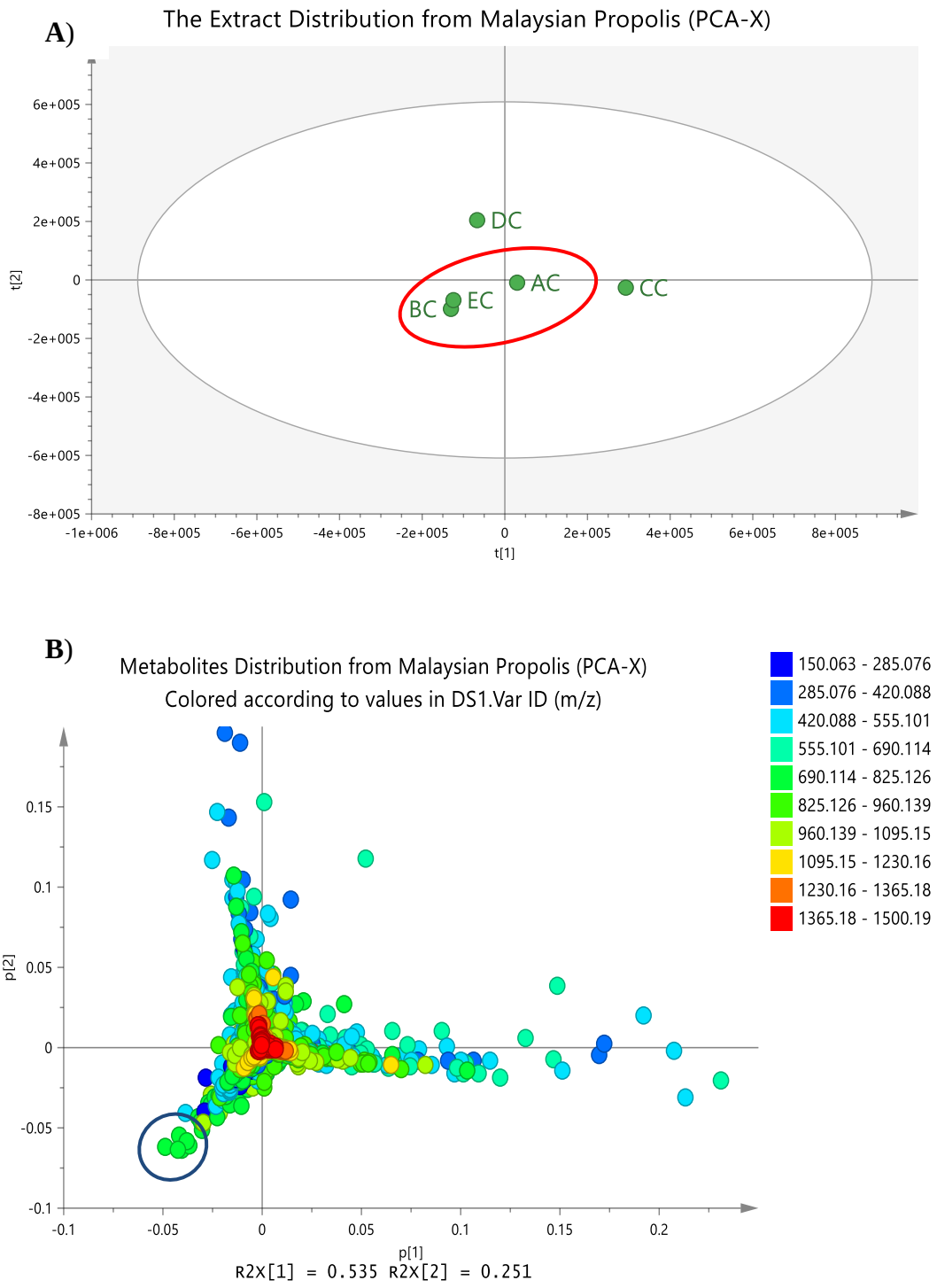

Fig. 3.7: A) The PCA scores scatter plot summarized the similarity and variation between the extracts. **B)** The loadings scatter plot showed the distribution of the metabolites in all extracts, encircled in blue indicate the unique metabolites found in EC and BC extract listed on **Table 3.4**.

Table 3.4: Dereplication table for unique metabolites for BC and EC encircled in blue in **Figure 3.7b**. Peak areas were shown particularly for the active extract EC.

Primary ID	*m/z*	RT	Peak Area	Molecular Weight	Predicted Molecular Formula
N_6881	720.6094	32.65	3.21E+07	721.6167	$C_{40}H_{79}N_7O_4$
N_6834	718.6130	36.66	1.16E+08	719.6203	$C_{34}H_{73}N_{17}$
N_6925	720.6094	35.82	1.28E+08	721.6167	$C_{40}H_{79}N_7O_4$
N_6838	718.6132	37.33	2.19E+08	719.6204	$C_{34}H_{73}N_{17}$
N_6993	745.6316	33.95	2.36E+08	746.6390	$C_{44}H_{78}N_{10}$ $C_{24}H_{74}N_{24}O_3$ $C_{43}H_{82}N_6O_4$ $C_{47}H_{86}O_6$ $C_{38}H_{82}N_8O_6$ $C_{42}H_{86}N_2O_8$
N_11171	719.6163	36.67	1.20E+08	720.6236	$C_{42}H_{76}N_{10}$ $C_{37}H_{76}N_{12}O_2$ $C_{41}H_{80}N_6O_4$ $C_{45}H_{84}O_6$ $C_{36}H_{80}N_8O_6$ $C_{40}H_{84}N_2O_8$

Above all, the BC, EC and AC extracts were chosen for further fractionation and isolation due to their bioactivities, chemical profile similarities, which also matched the information, deduced from the ^{1}H NMR spectra. BC was not active against lung cancer cell line while it showed weak activity against ovarian cancer cell line, but due to its similarity in chemical profile to EC, further isolation was continued on both BC and EC to correct any profiling or bioassay discrepancy performed on the two samples. On the other hand, AC was found the most active against the ovarian cancer cell line as shown in **Table 3.3**.

3.3.2 Secondary metabolites isolated from BC propolis

Chromatographic fractionation of BC extract with DCM and MeOH yielded 11 fractions, which were subjected to TLC profiling. The ^{1}H NMR spectrum for P9BC and P10BC (**Fig. 3.8**) established that these fractions afforded the same pure compound. ^{1}H NMR for P11BC was not performed because of its very low yield. Therefore, 2D NMR experiments including COSY, ^{13}C, DEPT, HMQC and HMBC were performed on P9BC to elucidate the compound and confirm the identity of metabolite as predicted from the dereplication database.

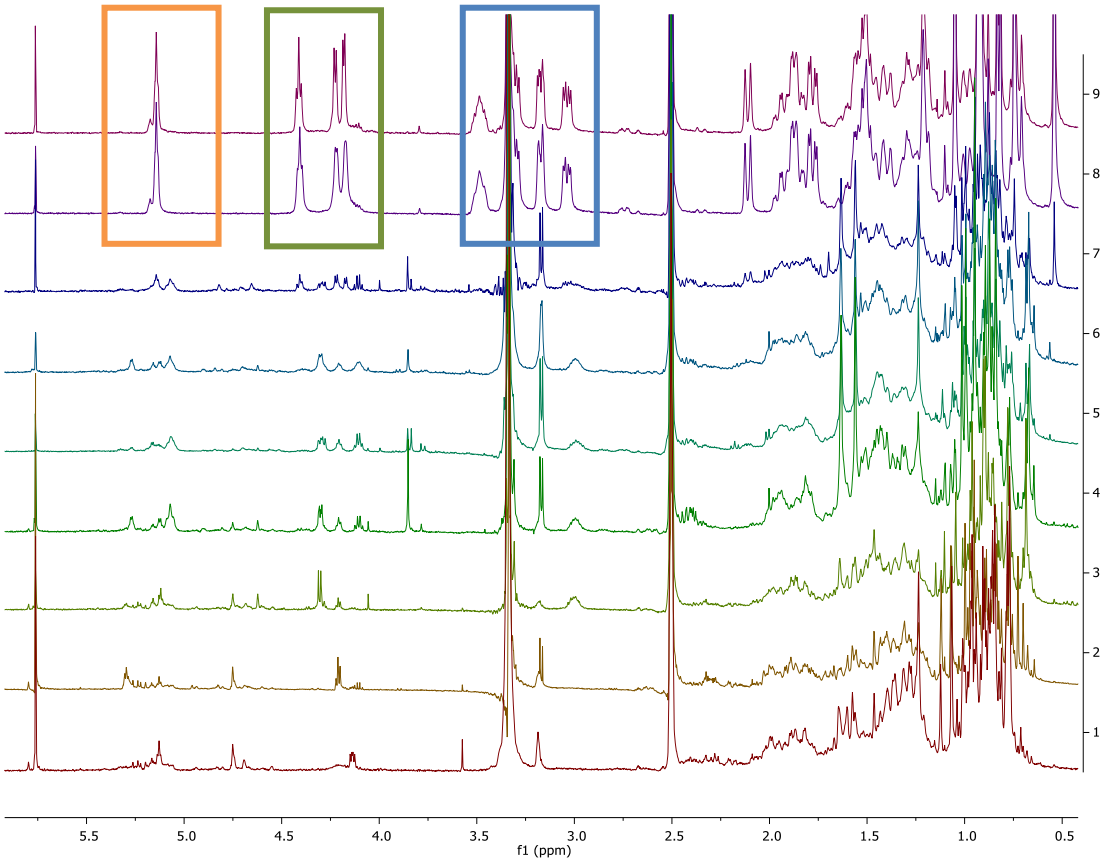

Fig. 3.8: ^{1}H NMR spectra of Malacca green propolis fractions at 400 MHz in DMSO-d_6. Coloured boxes indicate unique resonances for P9BC and P10BC. The spectra were labelled from below; P2BC, P3BC, P4BC, P5BC, P6BC, P7BC, P8BC, P9BC and P10BC.

Based on their TLC (**Fig. 3.9**), P9BC, P10BC and P11BC were observed as clear single band, indicating the same pure compound due to their similar Rf values at 0.56. The bioassay screening of all fractions against A2780 was shown in **Fig 3.10.** Based on the bioactivity at a threshold of 40%, only P8BC, P9BC, P10BC and P11BC gave cytotoxicity effects on A2780. Furthermore, TLC of P8BC also showed good separation of its compounds (**Fig. 3.9**).

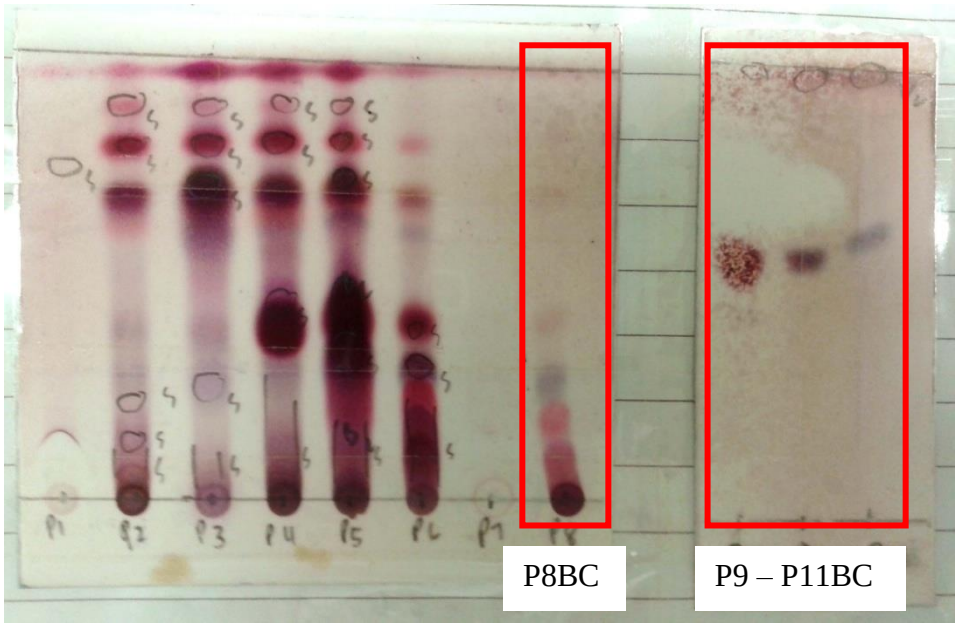

Fig. 3.9: TLC for BC propolis fractions with DCM and MeOH at a ratio of 99:1 for fractions P1 toP8BC. P9BC, P10BC and P11BC fractions were highlighted as they yielded a similar compound and were pure enough for further elucidation work; DCM and MeOH were used at (9:1) ratio.

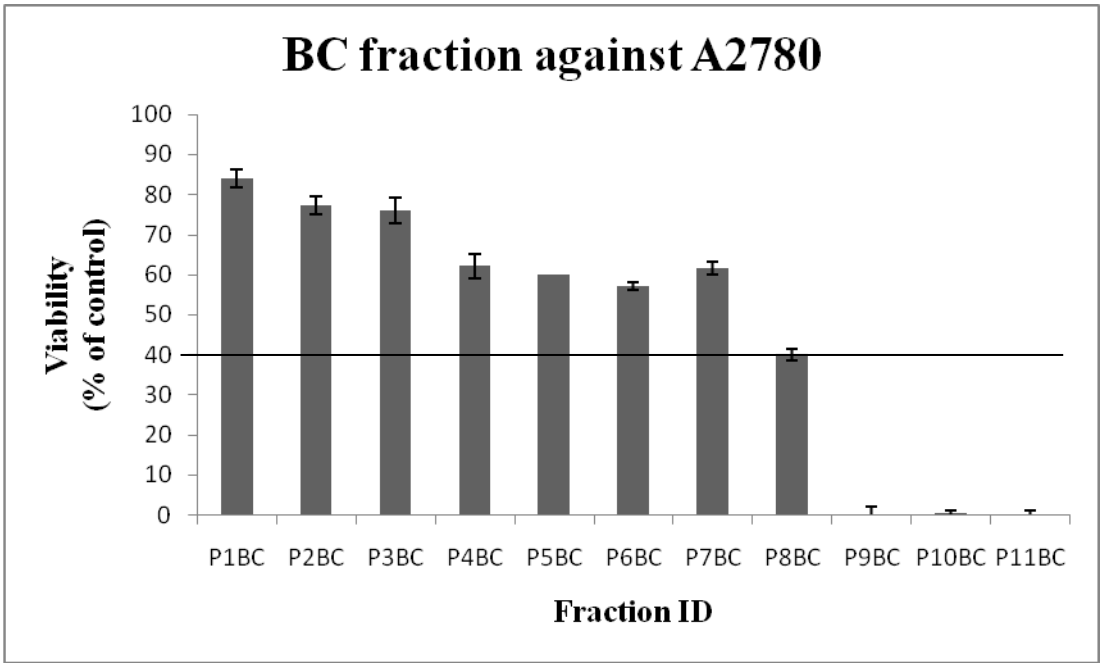

Fig 3.10: Cytotocixity assay of BC fractions on ovarian cancer cell line A2780. P8BC, P9BC, P10BC and P11BC were active against A2780 causing ≤40% cell viability of control.

Furthermore the metabolomic profiling on BC fraction was conducted to identify the unique features of all fractions that responsible for its bioactivity on A2780. The mass spectral data set from the LCMS of the BC fractions was processed using PCA-X multivariate analysis R^2 and Q^2 values of 0.53 and 0.21, respectively. There were 11 variables being analysed in this model including P1BC, P2BC, P3BC, P4BC, P5BC, P6BC, P7BC, P8BC, P9BC, P10BC and P11BC. Based on the result (**Fig. 3.11**), P9BC, P10BC and P11BC were clustered in the same group, which indicated that these fractions were sharing the same set of metabolites. This finding supports the result from the ^{1}H NMR spectra and TLC, which showed similar signals for fractions P9BC to P11BC.

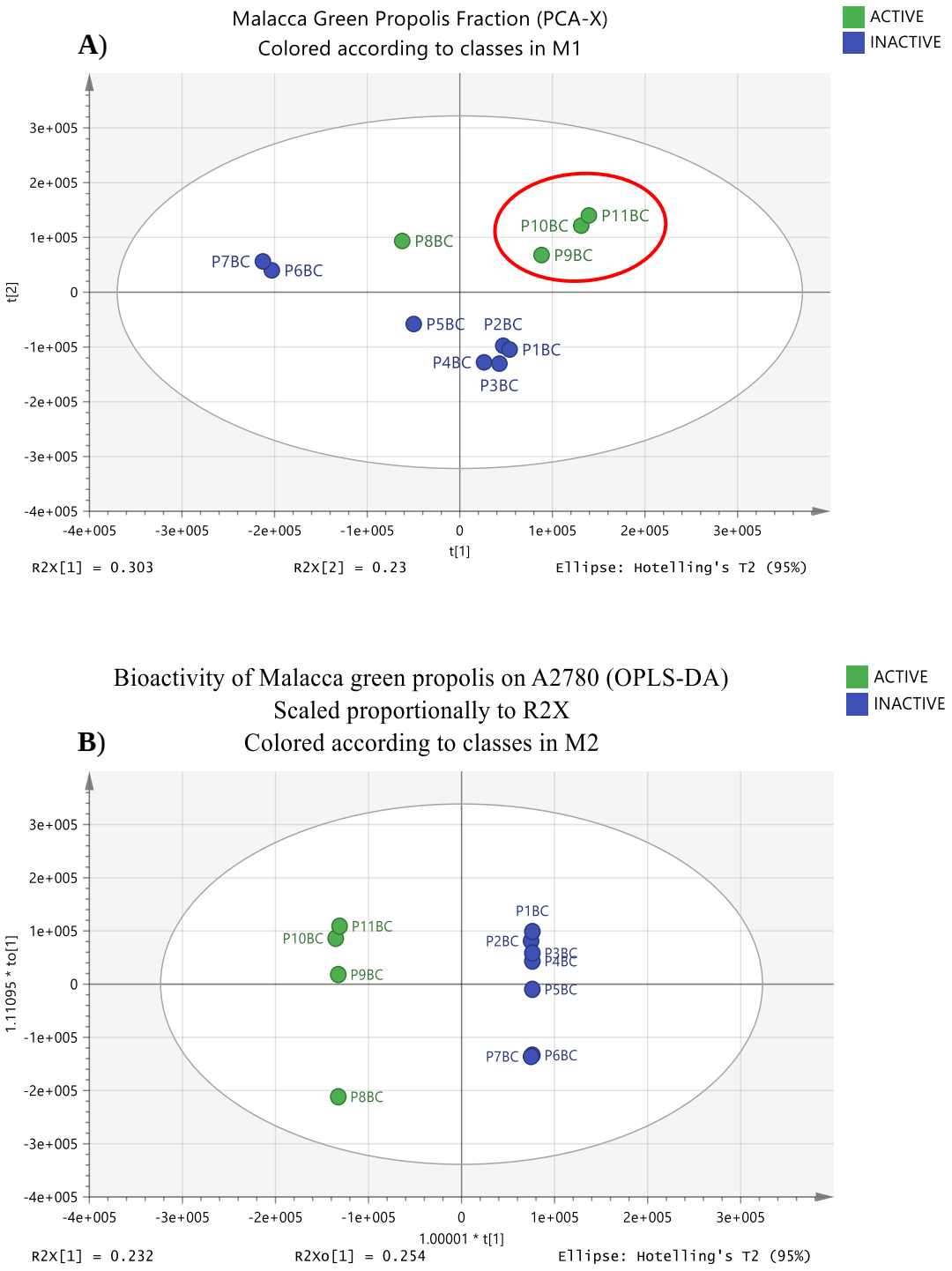

Fig. 3.11: **A**) PCA-X score scatter plot of BC propolis fractions were classified according bioactivity against A2780. The fractions in the red circle were clustered together because of similarity in chemical profile. **B**) Using an OPLS-DA model, fractions were grouped in accordance to their bioactivity against ovarian cancer cell line A2780.

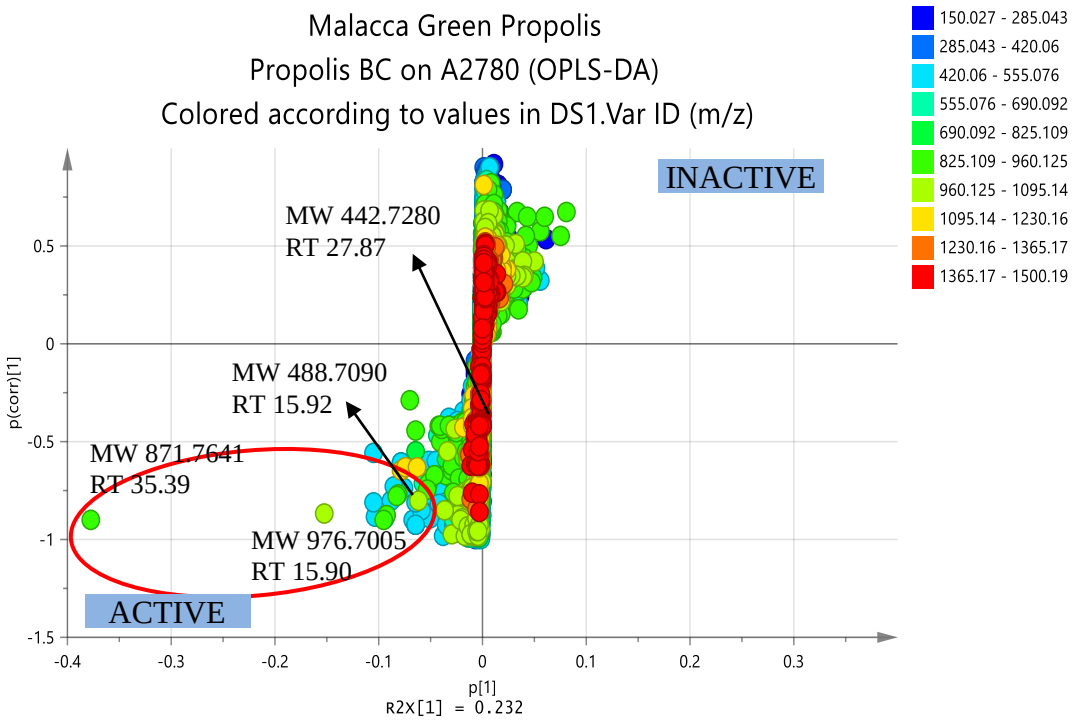

Fig. 3.12: OPLS-DA S-plot generated from LCMS database indicating targeted metabolites responsible for bioactivity against A2780. Dereplication of unique metabolites for the active fractions are listed in **Table 3.5**.

In addition, the aim of performing metabolomic analysis and dereplication by using an in-house Excel Macro coupled to a database (Macintyre et al., 2014) is to generate putative metabolites and to identify the remaining unknown features of all extracts as well as to be able to target the bioactive metabolite. The metabolites potentially contributing to bioactivity were determined using the OPLS-DA S-plot of the BC fractions against A2780 cell line, which gave a R^2 and Q^2 values of 0.99 and 0.93, respectively where the differences between R^2 and Q^2 is <0.3 showing good fitness prediction (**Fig. 3.12**). The permutation test also gave Q2Y value of −0.1 which is <0, showing the validity of the OPLS-DA analysis. All the data were cross-matched with the Dictionary of Natural Products (DNP) database to provide identification of targeted metabolites (**Table 3.5**). Taken together based on bioactivity and metabolites profiling, P8BC fraction was chosen for further fractionation and purification to isolation the targeted bioactive metabolites. The isolation work from BC extract afforded asiatic acid (Furuya et al., 1987) and hydroxydammarenone-II (Asakawa et al., 1977).

Table 3.5: Dereplication of targeted metabolites from fractions P8BC, P9BC, P10BC and P11BC that potentially active against the A2780.

Mzmine ID	*m/z*	RT (min)	Peak Area	MOLECULAR FORMULA	EXACT MASS	NAME	SOURCE
N_739	503.3383	12.56	3734008	$C_{30}H_{48}O_6$	504.3456	16,23:16,24-diepoxy-3,6,7,25-cycloartanetetrol	Constit. of *Astragalus orbiculatus*
N_692	549.3440	12.65	4800309	$C_{31}H_{50}O_8$	550.3513	antibiotic AB 023	Prod. by *Streptomyces* sp. SD581 and *Streptomyces* sp. NCIMB40212
P_1096	453.3360	15.87	8.41E+07	$C_{30}H_{44}O_3$	452.3288	25(9->8)-abeo-3-oxo-4(23)-friedelen-24,1-olide	Constit. of *Schaefferia cuneifolia*
N_640	487.3431	15.89	8.57E+07	$C_{30}H_{48}O_5$	488.3503	asiatic acid	*Prod. By Eucalyptus perriniana*
N_635	533.3486	15.89	9.18E+07	$C_{31}H_{50}O_7$	534.3559	passifloric acid	Isolated from leaves and stems of *Passiflora edulis*
N_643	975.6933	15.90	1.65E+08	$C_{60}H_{96}O_{10}$ $C_{55}H_{96}N_2O_{12}$	976.7005	No hits	
P_1877	443.3885	27.80	4.33E+07	$C_{30}H_{50}O_2$	442.7280	hydroxydammarenone-II	Isolated from Ginseng
P_6619	877.7282	34.41	1.44E+08	$C_{58}H_{92}N_4O_2$ $C_{43}H_{88}N_{16}O_3$ $C_{53}H_{92}N_6O_4$	876.7209	No hits	
P_9703	872.7714	35.39	1.94E+09	$C_{57}H_{96}O_6$ $C_{58}H_{99}N_2O_3$	871.7641	No hits	

Highlighted in grey is the isolated and elucidated metabolite.

*3.3.2.1 Asiatic acid /**P9BC***

Table 3.6: The relative stereochemistry of the isolated asiatic acid is shown as based on the literature (Furuya et al., 1987).

Asiatic acid (N_640)
Source: Malacca green propolis
Sample amount: 23 mg (colourless sticky material)
Molecular formula: $C_{30}H_{48}O_5$
Molecular weight: 488.7090 g/mol
Exact mass: 488.3503
$[\alpha]_D^{20}$: +50.0 (*c* = 0.03, $CHCl_3$)

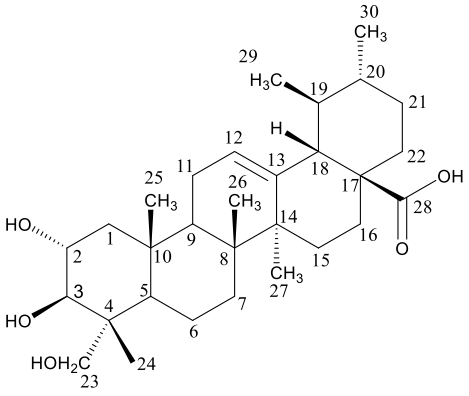

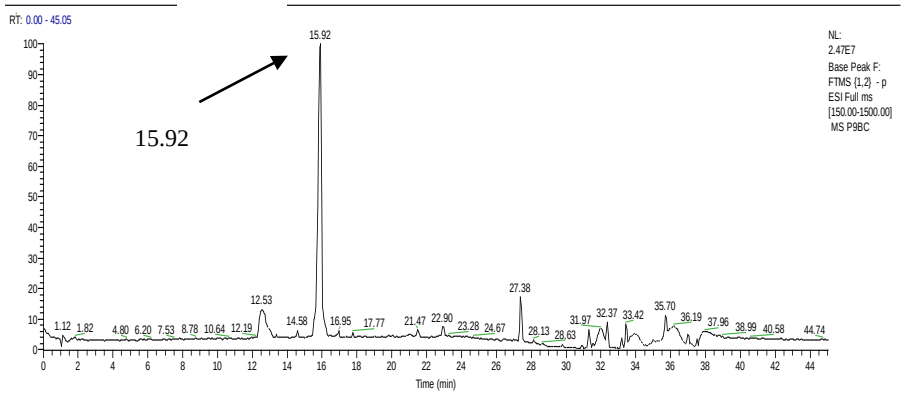

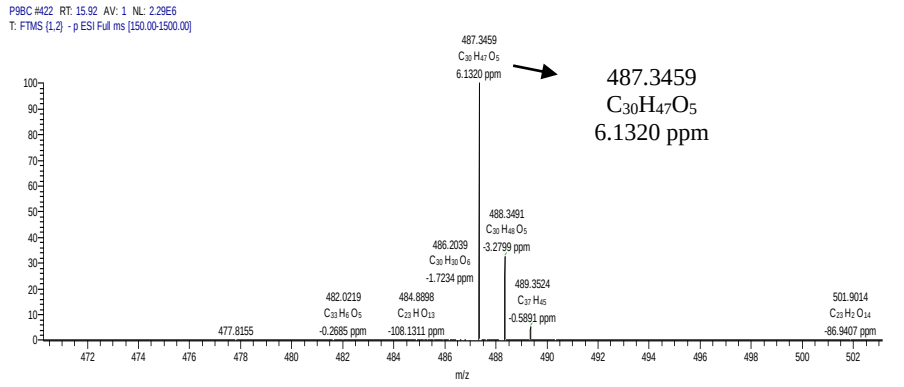

Based on the high resolution mass spectral data, the ESI peak at 15.92 min in the negative mode was found at *m/z* 487.3459 $[M-H]^-$. This revealed the exact mass at 488.3503 g/mol, which established the molecular formula of $C_{30}H_{48}O_5$ (**Table 3.6**). The ^1H NMR spectrum of **P9BC** (**Fig. 3.13**) contained six methyl signals at 0.5 – 1.5 ppm. Two of the signals were observed as doublets at δ0.82 (*d, J* = 6.4 Hz) and 0.92 (*d, J* = 6.4 Hz) and four singlets at δ0.54, 0.74, 1.05 and 0.93. Furthermore, three hydroxyl signals were also observed at 11.94 (*s*), 5.76 (*s*) and 4.41 (*s*). The signals of the hydroxyl-bearing carbons were observed in the ^{13}C and DEPT spectra at δ76.1, 68.0 and 64.5 for C-3, C-2 and C-23, respectively (**Fig. 3.14**). The carbon peak at 125.1 and 138.8 ppm corresponded to the double bond for C-12 and C-13, respectively. The carboxyl carbon was interpreted at position C-28 with carbon peak at 178.9 ppm. Based on this spectrum, it was anticipated that **P9BC** possessed a methyl urs-12-en-28-oate backbone structure. ^1H-^1H COSY (**Fig. 3.15**), HMQC (**Fig. 3.16**) and HMBC (**Fig. 3.17**) were performed to confirm the structure of 2,3,23-trihydroxy-12-ursen-28-oic acid. Comparison of the spectral data with the literature (Furuya et al., 1987) supported that this compound is asiatic acid ($C_{30}H_{48}O_5$) with the structure of 2α,3β,23-trihydroxy-12-ursen-28-oic acid based on its ^1H and ^{13}C NMR spectral data (**Tables 3.7** and **3.8**). The optical rotation was observed at $[\alpha]_D^{20}$ +50.0 (*c*= 0.03, $CHCl_3$) that also comparable with literature $[\alpha]_D^{22}$+53.3 (*c*= 1.03, $CHCl_3$) (Furuya et al., 1987). This compound was first reported by Furuya *et al.,* 1987 which was isolated from *Eucalyptus perriniana* cell culture.

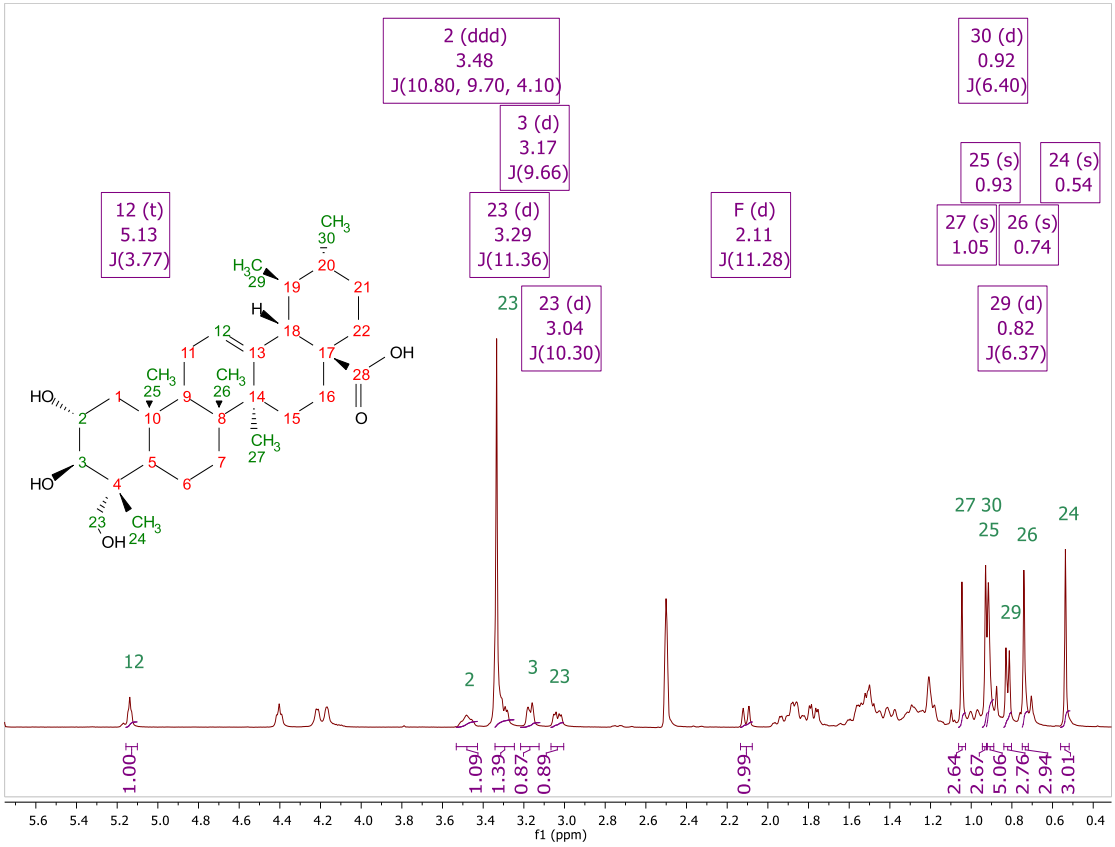

Fig. 3.13: ^{1}H NMR spectrum at 400 MHz of **P9BC** in DMSO-d_6.

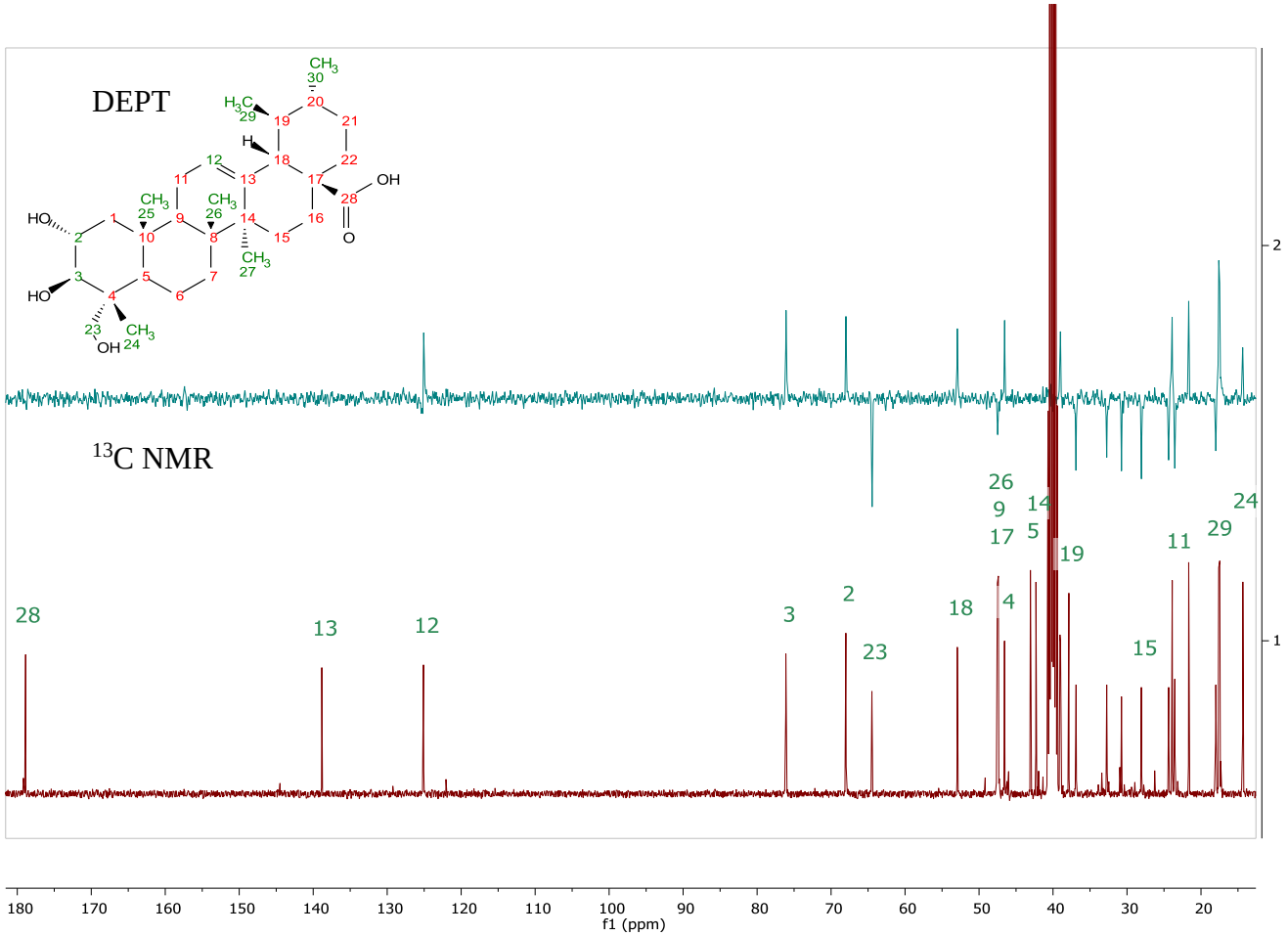

Fig. 3.14: ^{13}C and DEPT (100 MHz) spectra of **P9BC** in DMSO-d_6.

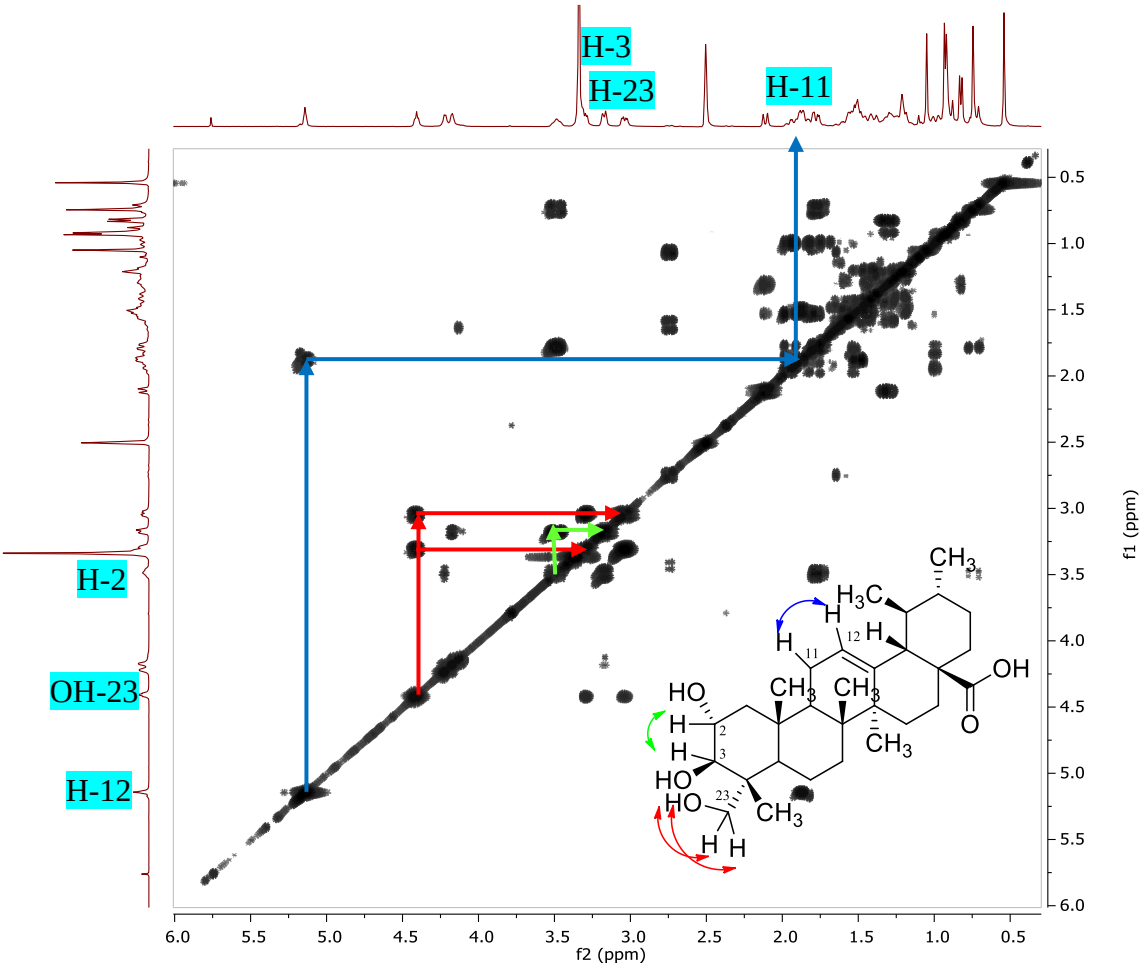

Fig. 3.15: The ^{1}H-^{1}H COSY (400 MHz) spectrum of **P9BC** in DMSO-d_6.

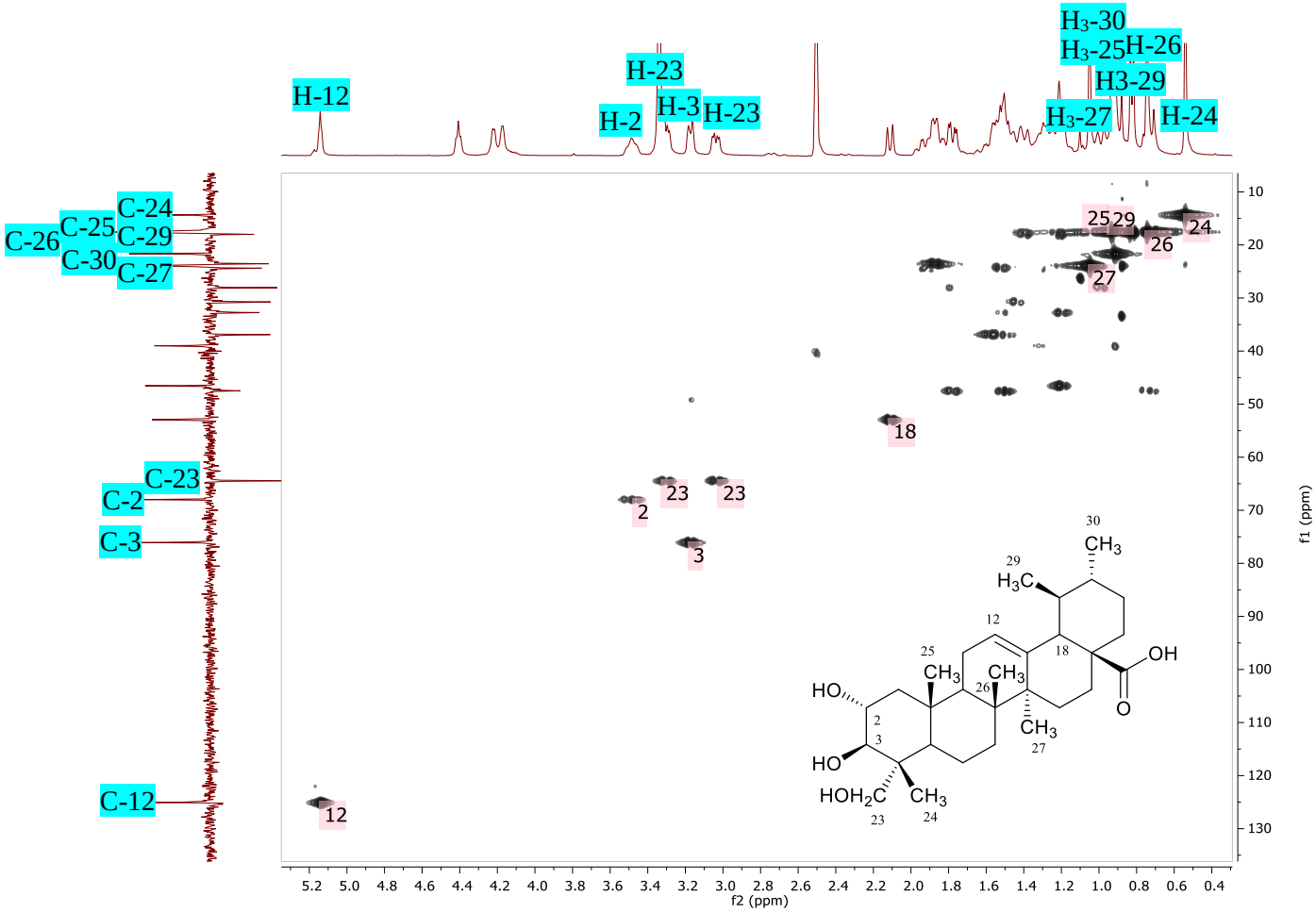

Fig. 3.16: The HMQC showed the correlation of the proton and DEPT spectra at 400 MHz, respectively in DMSO-d_6.

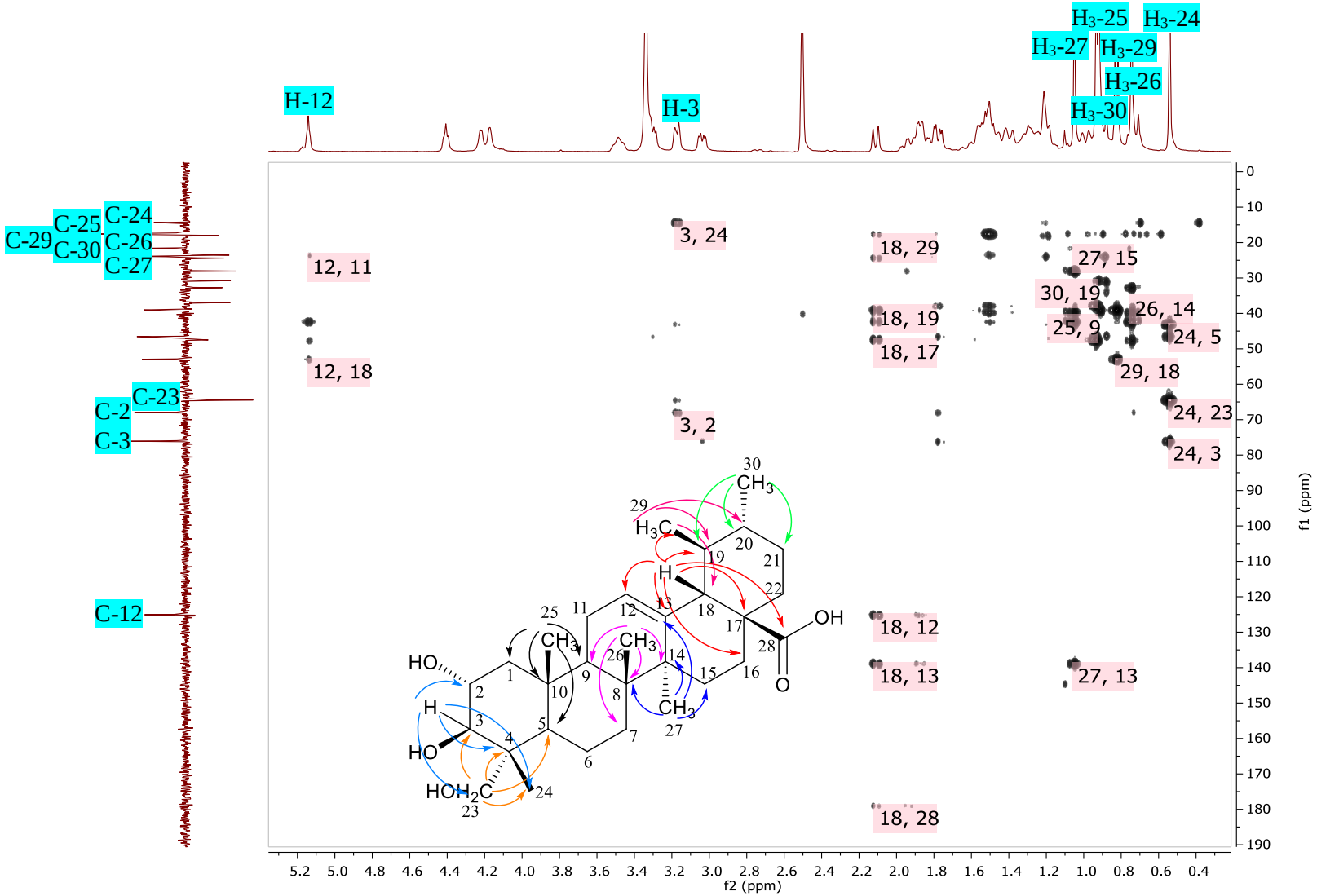

Fig. 3.17: The HMBC of **P9BC**. The X- and Y-axes correspond to the proton and DEPT spectra 400 MHz, respectively in DMSO-d_6.

Table 3.7: ^{1}H NMR (DMSO-d_6, 400MHz) of compound **P9BC** and comparison with asiatic acid from literature. Full assignment was deduced from HMQC in DMSO-d_6 at 400 MHz.

Carbon no.	^{1}H NMR, δ_H (multiplicity *J* in Hz)	
	P9BC in DMSO	**Literature of asiatic acid (Furuya et al., 1987) in $CDCl_3$**
1	1.50, 1.81	-
H-2	3.48 (*ddd*, *J* = 4.1, 9.7, 10.8 Hz)	3.79 (*ddd*, *J* = 4.5, 9.5, 11.5 Hz)
H-3	3.17 (*d*, *J* = 9.7 Hz)	3.48 (*d*, *J* = 9.5 Hz)
5	3.17	-
6	1.22, 1.42	-
7	1.18, 1.50	-
9	1.21	-
11	1.86, 1.92	-
H-12	5.13 (*d*, *J* = 3.8 Hz)	5.24 (*t*, *J* = 4 Hz)
15	0.97, 1.80	-
16	1.50, 1.54	-
H-18	2.11 (*d*, *J* = 11.3 Hz)	2.20 (*d*, *J* = 12 Hz)
19	0.91	-
20	1.32	-
21	1.46, 1.52	-
22	1.48, 1.60	-
H-23	3.04 (*d*, *J* = 10.3 Hz)	3.43 (*d*, *J* = 10.5 Hz)
	3.29 (*d*, *J* = 11.4 Hz)	3.70 (*d*, *J* = 10.5 Hz)
CH_3-24	0.54	0.71
CH_3-25	0.93	1.00
CH_3-26	0.74	0.89
CH_3-27	1.05	1.04
CH_3-29	0.82 (*d*, *J* = 6.4 Hz)	0.82 (*d*, *J* = 6 Hz)
CH_3-30	0.92 (*d*, *J* = 6.4 Hz)	0.91 (*d*, *J* = 6 Hz)

Table 3.8: ^{13}C NMR (100 MHz) of compound **P9BC** in DMSO-d_6 in comparison with the literature (Furuya et al., 1987).

Carbon no.	^{13}C NMR δ_C (ppm)	
	P9BC in DMSO-d_6	**Literature of asiatic acid (Furuya et al., 1987) in $CDCl_3$**
1	47.6 CH_2	46.5 CH_2
2	68.0 CH	68.9 CH
3	76.1 CH	80.7 CH
4	43.1 C	42.7 C
5	49.2 CH	49.2 CH
6	18.0 CH_2	18.5 CH_2
7	32.7 CH_2	32.8 CH_2
8	39.4 C	39.7 C
9	47.4 CH	47.6 CH
10	37.9 C	38.3 C
11	23.5 CH_2	23.5 CH_2
12	125.1 CH	125.4 CH
13	138.8 C	138.4 C
14	42.3 C	42.3 C
15	28.1 CH_2	28.2 CH_2
16	24.4 CH_2	24.4 CH_2
17	47.5 C	48.2 C
18	53.0 CH	53.0 CH
19	39.0 CH	39.2 CH
20	38.9 CH	39.0 CH
21	30.8 CH_2	30.8 CH_2
22	36.9 CH_2	36.8 CH_2
23	64.5 CH_2	70.4 CH_2
24	14.4 CH_3	13.0 CH_3
25	17.5 CH_3	17.1 CH_3
26	17.6 CH_3	17.2 CH_3
27	23.9 CH_3	23.9 CH_3
28	178.9 C	178.2 C
29	17.6 CH_3	17.3 CH_3
30	21.7 CH_3	21.3 CH_3

*3.3.2.2 Hydroxydammarenone-II/**P8BC2-3&4***

Table 3.9: The relative stereochemistry of the isolated hydroxydammarenone-II was illustrated based on the literature (Asakawa et al., 1977).

Hydroxydammarenone-II (N_1877)
Source: Malacca green propolis
Sample amount: 11 mg (colourless sticky material)
Molecular formula: $C_{30}H_{50}O_2$
Molecular weight: 442.7280 g/mol
Exact mass: 442.3812
$[\alpha]_D^{20}$: +64.9 (*c* = 0.07, $CHCl_3$)
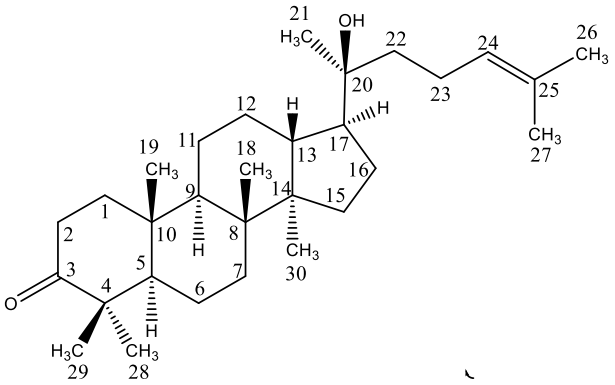
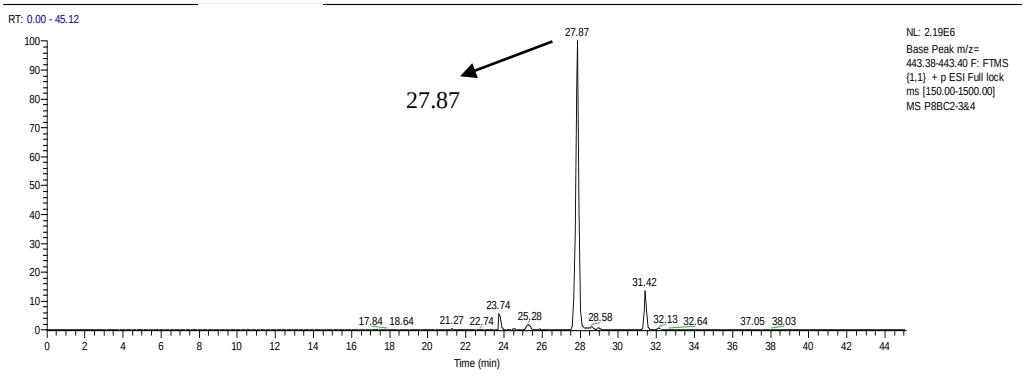
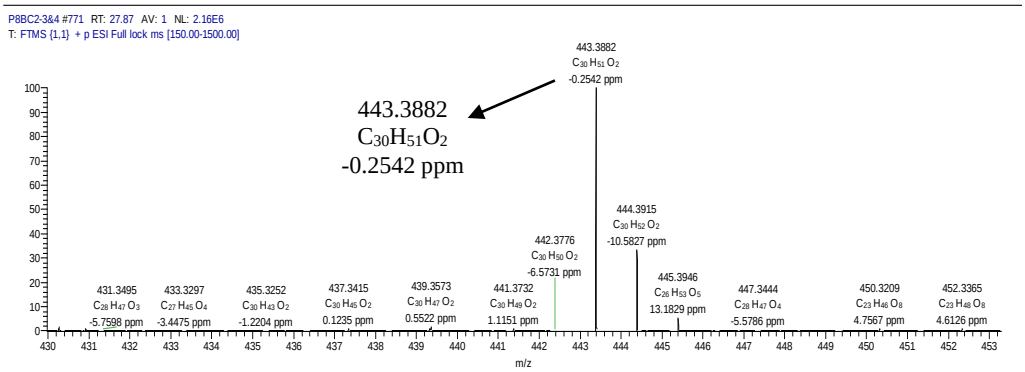

Based on the high-resolution mass spectral data, the ESI ion peak at positive mode was found at *m/z* 443.3882 $[M+H]^+$ and at a retention time of 27.87 min. This revealed the exact mass at 442.3812 g/mol, which established the molecular formula of $C_{30}H_{50}O_2$ (**Table 3.9**). The ^1H NMR spectrum of **P8BC2-3&4** (**Fig. 3.18**) contained eight methyl signals at 0.8 – 1.7 ppm. All methyl signals were observed as singlets (δ0.82, 0.88, 0.94, 0.97, 1.01, 1.09, 1.56, and 1.62). The methyl group signals were also seen in the DEPT spectrum at δ15.2, 16.0, 16.3, 17.7, 21.0, 25.4, 25.7, and 26.7 (**Fig. 3.19**). An olefinic carbon was observed at δ124. Based on this spectrum, it was indicated that **P8BC2-3&4** possessed a triterpene backbone structure. HSQC (**Fig. 3.20**) and HMBC (**Fig. 3.21**) were performed to confirm the structure of hydroxydammarenone-II. The correlation of (5.06, 124.7) ppm marked the position of C24 which was located within olefinic region. All eight methyl group signals were also observed at the aliphatic region in the ^1H spectrum between 1.70 – 0.80 ppm.

An HMBC experiment was used to determine the correlation between neighbouring protons and carbon atoms (**Fig. 3.21**). The position of C24 was observed at 124.7 ppm and showed a strong correlation with neighbouring methyl protons at C26 and C27 at 1.56 and 1.62 ppm, respectively. Meanwhile, C25 was assigned at 131.5 ppm and gave a cross peak with C26 and C27. C25 was also observed as a quaternary carbon with no corresponding proton signal observed on its HSQC spectrum. C3 was a ketone carbon because it was observed at the most downfield chemical shift of 218.1 ppm. C3 correlated with neighbouring methyl protons of C28 and C29 at 1.01 and 0.97 ppm, respectively. C19 was confirmed by its strong correlation with methyl protons of C28 and C29 as well. The methyl protons of C28 and C29 further correlated with C5 at 55.3 ppm. C18 was verified with the cross peaks of the methyl protons of C18 and C19 with C9 at 50.1 ppm. Furthermore, C30 was confirmed by the strong correlation of its proton and the C18 methyl proton with C8 and C14 at 40.2 and 50.2 ppm, respectively. C14 was assigned more downfield compared to C8 because C14 was directly attached to the side chain. In the case of the C21 methyl proton, it correlated with the quaternary hydroxyl-bearing carbon group at 75.0 ppm (C20), the methine doublet, and methylene triplet carbons. As shown by the DEPT

and HSQC spectra, C17 was a methine carbon at 49.7 ppm and C22 at 40.5 ppm was a methylene carbon unit. The carbon spectrum matched with the literature, which confirmed the structure of hydroxydammarenone-II (**Table 3.11**). Comparison of the spectral data with the literature (Asakawa et al., 1977) supported that this compound is indeed hydroxydammarenone-II ($C_{30}H_{50}O_2$) with the structure of 20-hydroxydammar-24-en-3-one based on its high-resolution mass spectral data and ^{13}C NMR spectral data (**Table 3.11**). The optical rotation was observed at $[\alpha]_D^{20}$+64.9 (*c*= 0.07, $CHCl_3$) that also comparable with literature $[\alpha]_D$+66.0 (*c* 1.18, $CHCl_3$) (Asakawa et al., 1977). Hydroxydammarenone-II was first isolated from ginseng, the root of plants in the genus *Panax* (Asakawa et al., 1977).

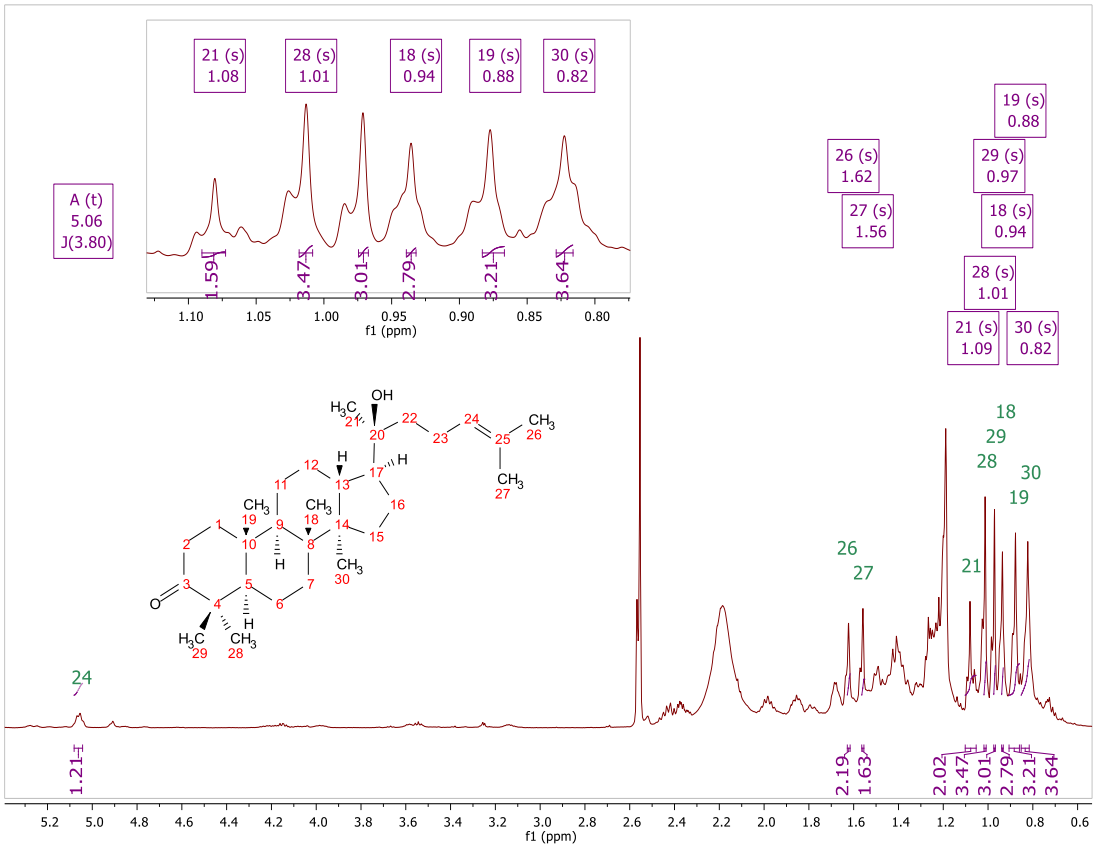

Fig. 3.18: ^1H NMR spectrum of **P8BC2-3&4** at 500 MHz instrument in $CDCl_3$.

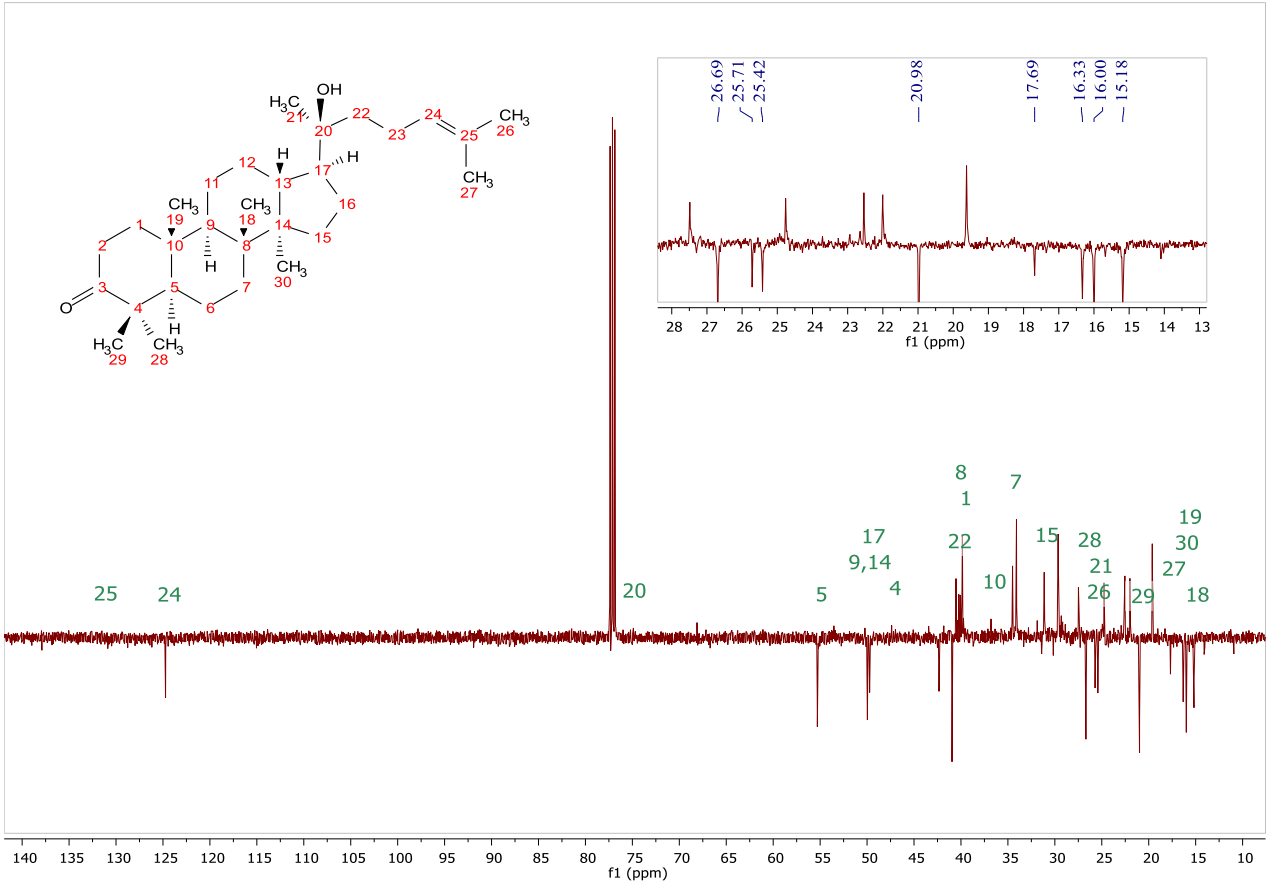

Fig. 3.19: The DEPT (125 MHz) spectrum for **P8BC2-3&4** in $CDCl_3$. Inset shows the most upfield signals in the aliphatic region between 15 to 27 ppm.

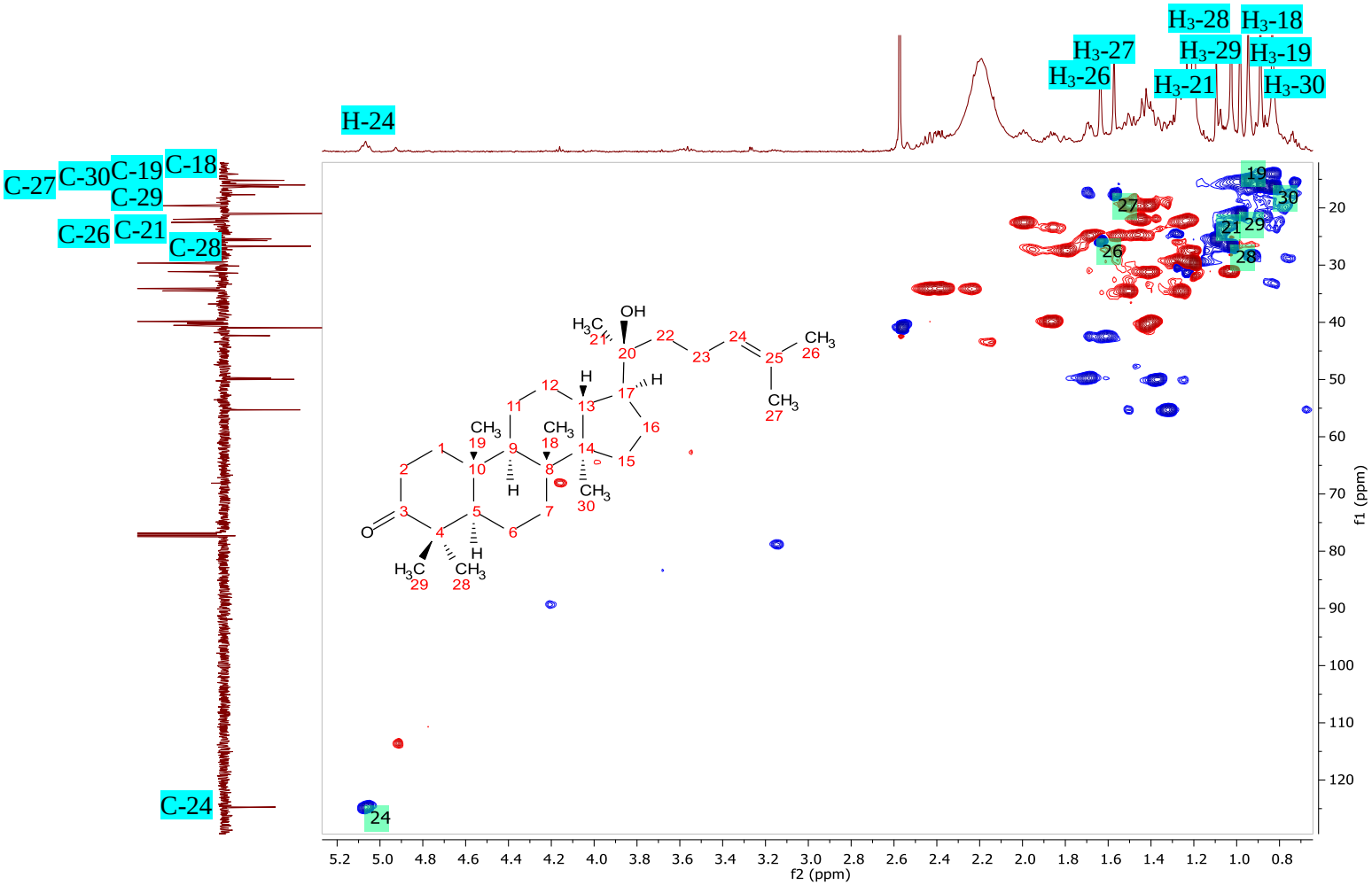

Fig. 3.20: The HSQC of **P8BC2-3&4** in $CDCl_3$. The X and Y-axes indicate the proton and DEPT spectra (500 MHz), respectively.

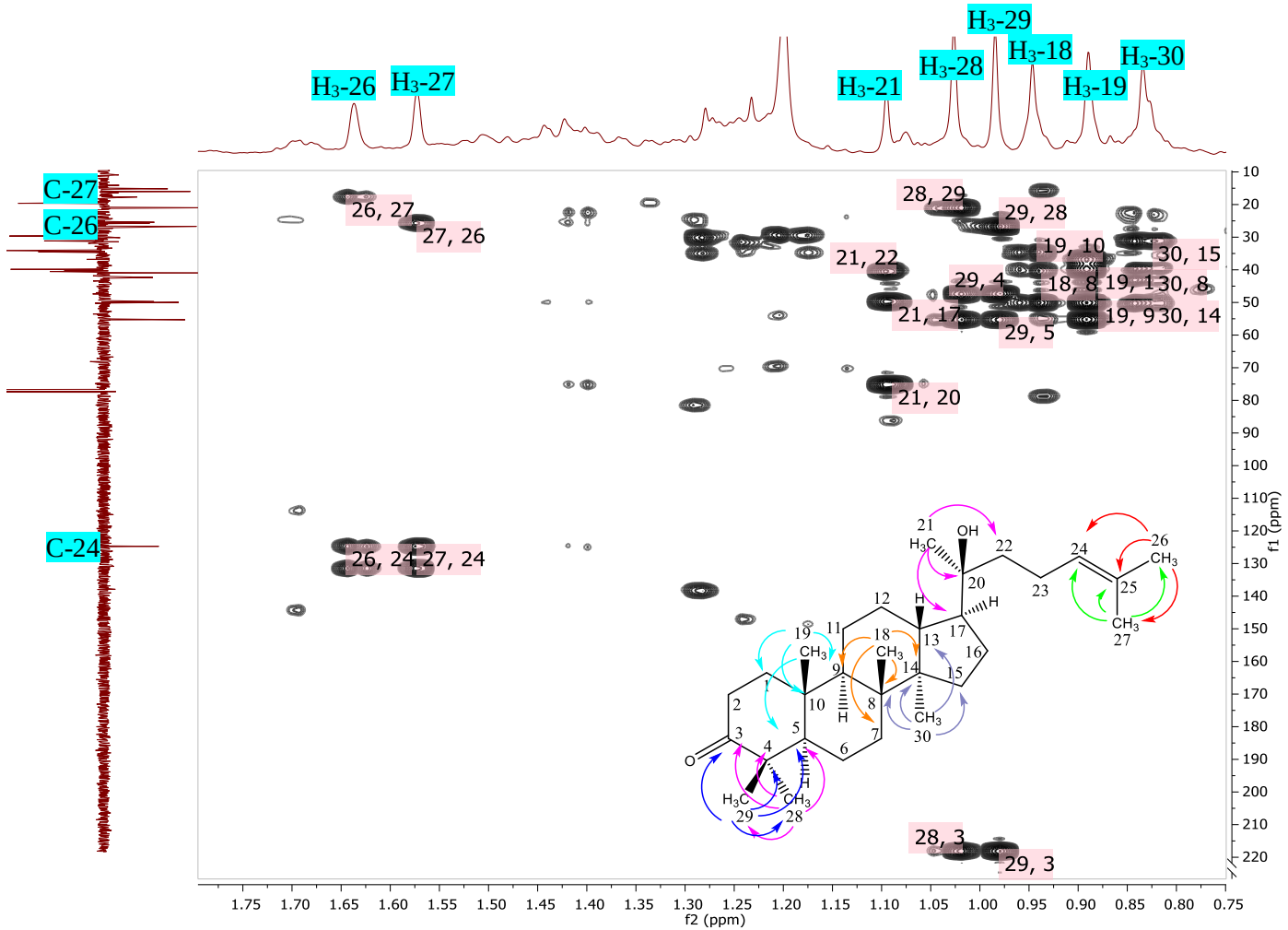

Fig. 3.21: The HMBC of **P8BC2-3&4** in $CDCl_3$. The X and Y axes correspond to the proton and DEPT spectra (500 MHz), respectively.

Table 3.10: ^{1}H NMR (500 MHz) of compound **P8BC2-3&4** in $CDCl_3$. Full assignment was deduced from HSQC in $CDCl_3$ at 500 MHz.

Carbon no.	**^{1}H NMR, δ_H (multiplicity*J* in Hz)**
1	1.41, 1.86
2	2.23, 2.43
5	1.32
6	1.41, 1.50
7	1.26, 1.50
9	1.38
11	1.38, 1.45
12	1.55, 1.68
13	1.47
15	1.03, 1.41
16	1.22, 1.79
17	1.69
CH_3-18	0.94 (*s*)
CH_3-19	0.88 (*s*)
CH_3-21	1.09 (*s*)
22	1.42, 1.43
23	1.24, 1.99
H-24	5.06 (*t*, *J* = 3.8 Hz)
CH_3-26	1.62 (*s*)
CH_3-27	1.56 (*s*)
CH_3-28	1.01 (*s*)
CH_3-29	0.97 (*s*)
CH_3-30	0.82 (*s*)

Table 3.11: ^{13}C NMR (100 MHz) of compound **P8BC2-3&4** in $CDCl_3$ in comparison with literature data.

Carbon no.	^{13}C NMR δ_C (ppm)	
	P8BC2-3&4 in $CDCl_3$	**Literature (Asakawa et al., 1977) in $CDCl_3$**
1	39.9 CH_2	39.8 CH_2
2	34.1 CH_2	34.0 CH_2
3	218.1 C	217.6 C
4	47.4 C	47.3 C
5	55.3 CH	55.3 CH
6	19.6 CH_2	19.6 CH_2
7	34.5 CH_2	34.6 CH_2
8	40.2 C	40.2 C
9	50.1 CH	49.9 CH
10	36.8 C	36.7 C
11	22.0 CH_2	22.0 CH_2
12	24.7 CH_2	25.4 CH_2
13	47.7 CH	47.3 CH
14	50.2 C	50.2 C
15	31.1 CH_2	31.1 CH_2
16	27.4 CH_2	27.5 CH_2
17	49.7 CH	49.7 CH
18	15.3 CH_3	15.9 CH_3
19	16.0 CH_3	15.2 CH_3
20	75.0 C	75.1 C
21	25.5 CH_3	24.7 CH_3
22	40.5 CH_2	40.5 CH_2
23	22.6 CH_2	22.5 CH_2
24	124.7 CH	124.7 CH
25	137.9 C	131.1 C
26	25.7 CH_3	25.7 CH_3
27	17.7 CH_3	17.6 CH_3
28	26.7 CH_3	26.6 CH_3
29	21.1 CH_3	21.0 CH_3
30	16.3 CH_3	16.2 CH_3

3.3.3 Secondary metabolites isolated from EC propolis

MPLC fractionation of the EC extract with n-hexane and EtOAc yielded 11 fractions, which were subjected to TLC profiling. The ^{1}H NMR spectrum for P10EC and P11EC (**Fig. 3.22**) established that these fractions afforded the same pure compound. The spectrum of P10EC and P11EC showed unique chemical fingerprints. Based on their TLC; P9BC and P11EC were observed as a clear single band, indicating the same pure compounds due to its similar Rf value at (0.37) and ^{1}H NMR spectrum (**Fig. 3.23**). Therefore, P10EC and P11EC were identified as asiatic acid, which were identical to the NMR and mass spectral data of P9BC.

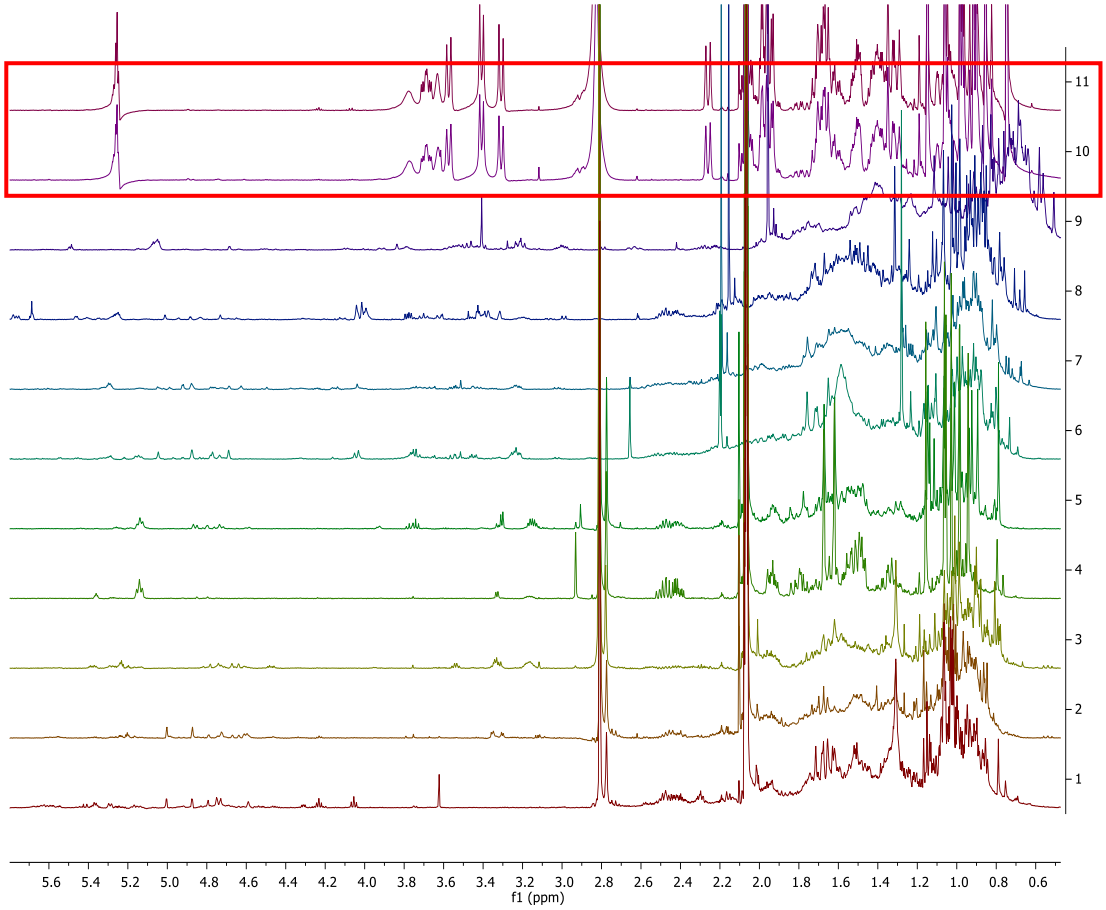

Fig. 3.22: ^{1}H NMR spectra of Johor green propolis fractions at 400 MHz instrument inacetone-d_6. Highlighted by a red box indicated similar spectra for P10EC and P11EC. The spectra were labelled from below; P1EC, P2EC, P3EC, P4EC, P5EC, P6EC, P7EC, P8EC, P9EC, P10EC and P11EC.

A)

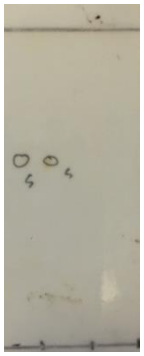

P9BC P11EC

B)

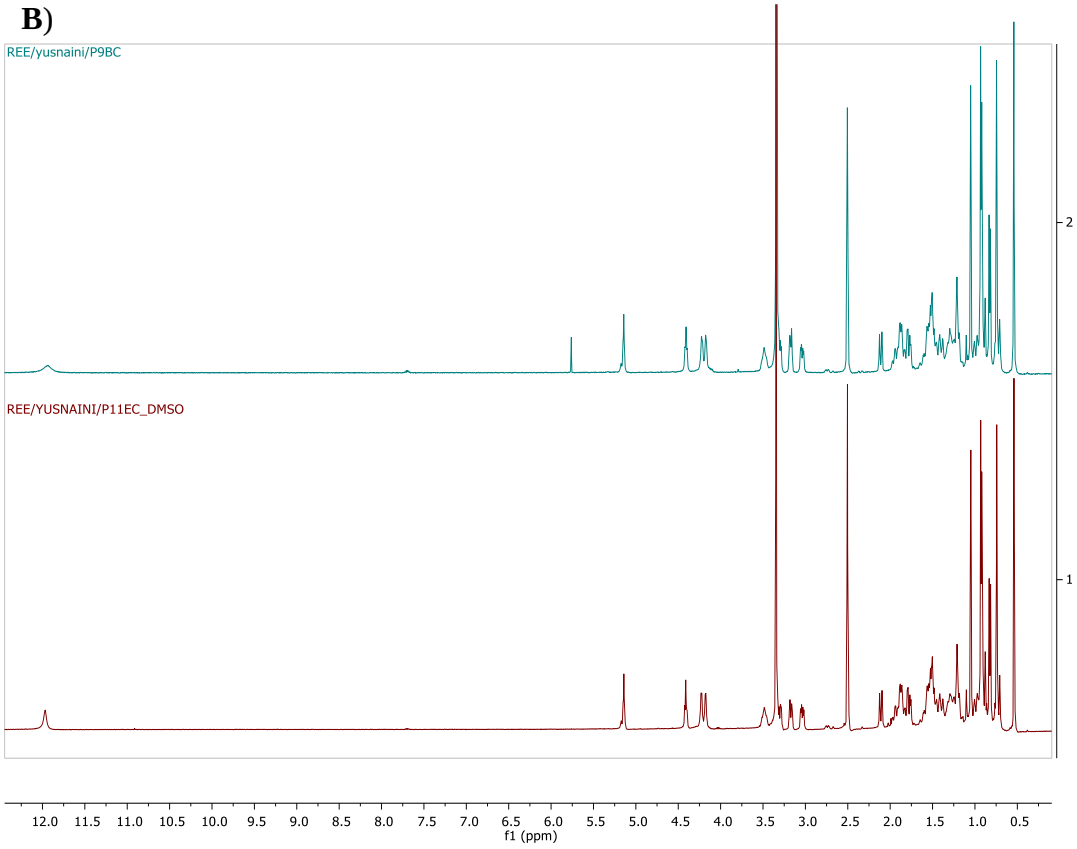

Fig. 3.23: **A**) TLC spots of P9BC and P11EC in DCM and MeOH at a ratio of 9:1. **B**) ^{1}H NMR spectrum of P9BC (above) and P11EC (below) at 400 MHz in DMSO-d_6.

The bioassay screening of all EC fractions showed that several fractions were active against A2780; where potent activity was observed for P10EC and P11EC, whilst P4EC to P9EC exhibited mild to moderate cytotoxicity effect (**Fig 3.24**).

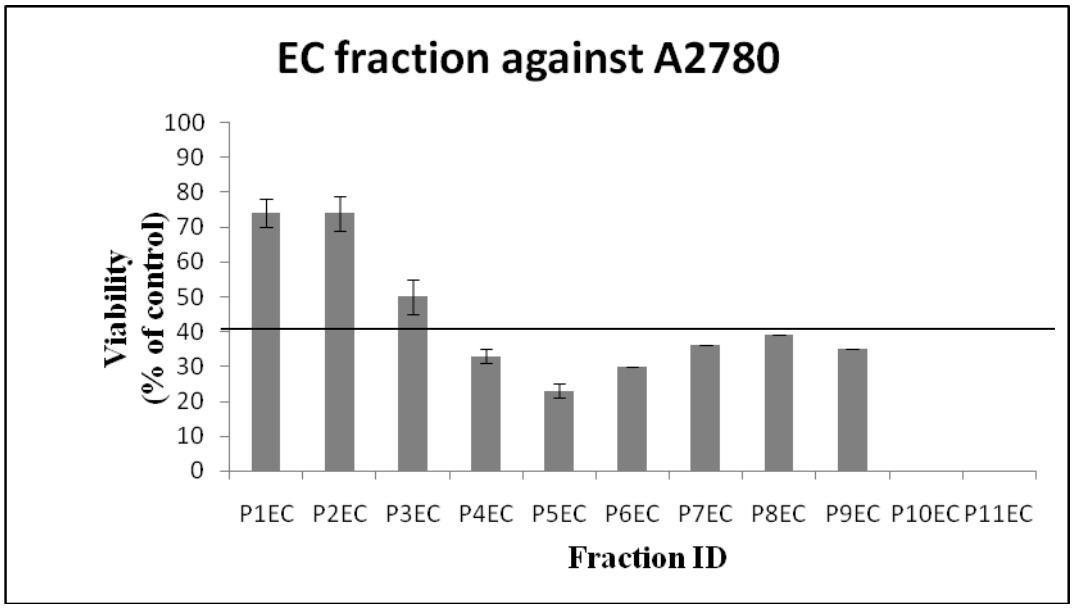

Fig 3.24: Cytotocixity assay of EC fractions on ovarian cancer cell line (A2780), P4EC – P11EC were active against A2780, causing ≤40% cell viability in comparison to control.

A TLC of P4EC and P5EC was performed to determine their similarity in chemical profile. Both fractions afforded high yield and good bioactivity on A2780 (**Fig. 3.25**). The chromatograms and proton NMR spectra of both fractions indicated a unique chemical finger print that might be responsible for the bioactivity against A2780.

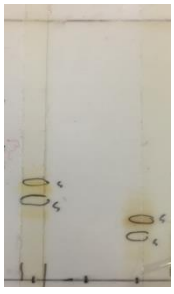

P4EC P5EC

Fig. 3.25: TLC for P4EC and P5EC in n-hexane and EtOAc at a ratio of 8:2.

The HR-LCMS data of the EC fractions was processed and subjected to multivariate analysis using PCA-X multivariate analysis with R^2 and Q^2 values at 0.50 and 0.11, respectively. There were 11 variables being analysed in this model. Based on the result (**Fig. 3.26A**), P1EC -P5EC (in red circle) were clustered in the same group, which indicated that these fractions shared the same chemical profile. The metabolites potentially contributing to bioactivity were determined using the OPLS-DA and S-plot of the EC fractions against A2780 cell line with R^2 and Q^2 of 0.92 and 0.58, respectively, which gave a good fitted model (**Fig. 3.26B** and **3.27**). The permutation test gave Q2Y value of −0.18, showing good validity model. All the data were cross-matched with the DNP database to provide details of on putative bioactive metabolites to be targeted (**Table 3.12**). Taken together based on bioactivity and metabolites profiling, P4EC and P5EC fractions were chosen for further fractionation and purification to isolation the targeted bioactive metabolites. Moreover, both fractions gave high yield (1.8 and 1.2, g, respectively) and also gave good separation which indicated a diverse metabolomic profile. Chromatographic fractionation afforded as dammara-20,24-dien-26-oic acid, 3-oxo-, (24E) (Phan et al., 2011) and dammarenolic acid (Esimone et al., 2010).

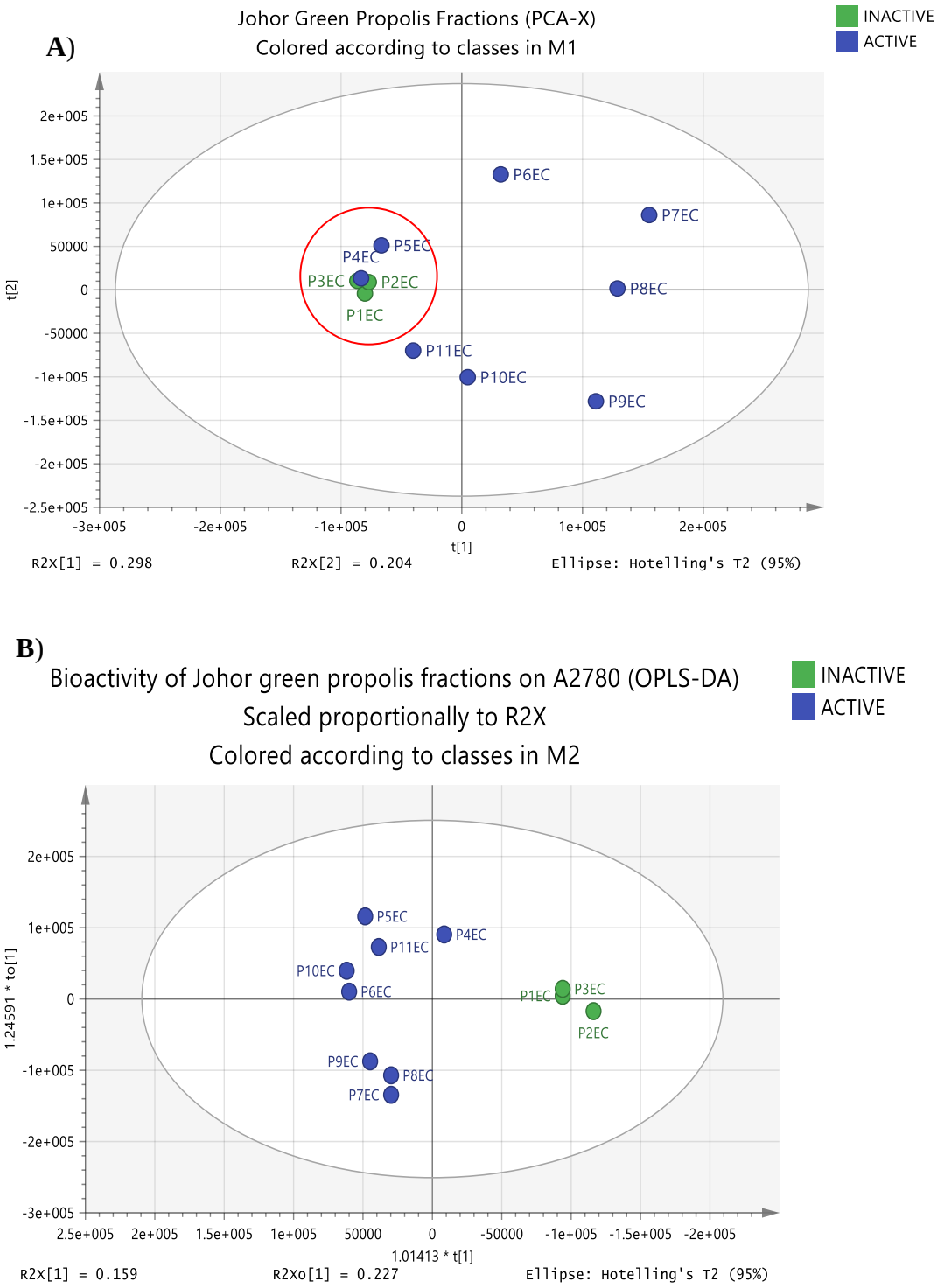

Fig. 3.26: **A**) PCA-X score scatter plot of EC propolis fractions were classified according bioactivity against A2780. The fractions in the red circle were clustered

together because of similarity in chemical profile. **B**) OPLS-DA scores scatter plot of EC propolis fractions group according to bioactivity against ovarian cancer cell line.

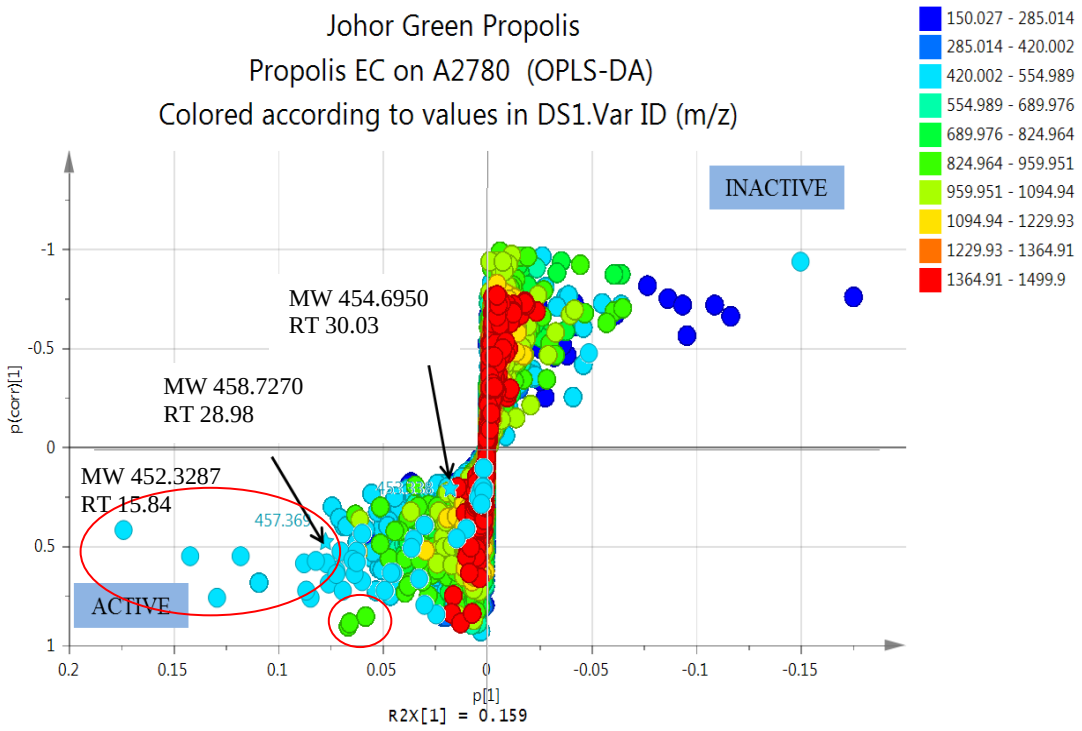

Fig. 3.27: OPLS-DA S-plot generated from LCMS database indicating the target metabolites that were predicted to be responsible for the extract's bioactivity against A2780.

Table 3.12: The accompanying dereplication of selected metabolites measured in P4EC and P5EC that are potentially active against the A2780.

FRACTION ID	M/Z	RT	Peak Area P4EC	Peak Area P5EC	MOLECULAR FORMULA	EXACT MASS	NAME	SOURCE
P_21	453.3360	15.84	1103978	1598028	$C_{30}H_{44}O_3$	452.3287	25(9->8)-abeo-3-oxo-4(23)-friedelen-24,1-olide	*Schaefferia cuneifolia*
P_5598	219.1743	17.34	1258671	5.56E+07	$C_{15}H_{22}O$	218.1670	5-africanen-4-one	*Porella swartziana*
N_5787	457.3684	28.98	31897.74	1.23E+08	$C_{30}H_{50}O_3$	458.3760	dammarenolic acid	dammar resin
N_1900	453.3379	30.03	1.80E+07	3.52E+07	$C_{30}H_{46}O_3$	454.3448	3-oxodammara-20,24-dien-26-al; (24*E*)-form, 26-Carboxylic acid	*Maytenusmacrocarpa*
P_418	1148.3269	34.58	1949327	3.86E+07	$C_{45}H_{53}N_{11}O_{25}$ $C_{49}H_{57}N_5O_{27}$ $C_{39}H_{57}N_9O_{31}$ $C_{43}H_{61}N_3O_{33}$ $C_{49}H_{95}N_{15}O_3$ $C_{53}H_{99}N_9O_5$	1147.3196	No hits	
P_9182	942.7796	35.03	4486470	5.14E+07	$C_{48}H_{99}N_{11}O_7$ $C_{52}H_{103}N_5O_9$ $C_{47}H_{103}N_7O_{11}$ $C_{51}H_{107}NO_{13}$ $C_{62}H_{97}N_3O_2$ $C_{51}H_{97}N_9O_5$	941.7723	No hits	
P_9178	916.7680	35.50	3.37E+07	4.75E+07	$C_{55}H_{101}N_3O_7$ $C_{46}H_{97}N_{11}O_7$ $C_{50}H_{101}N_5O_9$	915.7607	No hits	

Highlighted in grey were the isolated and elucidated metabolites against A2780.

*3.3.3.1 24-(E)-3-oxodammara-20(21),24-dien-27-oic acid/**P4EC7***

Table 3.13: The compound from P4EC fraction (**P4EC7**) was elucidated using NMR spectroscopy. The relative stereochemistry of the isolated 24-(E)-3-oxodammara-20(21),24-dien-27-oic acid was illustrated as indicated from the literature (Phan et al., 2011).

24-(E)-3-oxodammara-20(21),24-dien-27-oic acid (N_1900)
Source: Johor green propolis
Sample amount: 22.1 mg (white crystal)
Molecular formula: $C_{30}H_{46}O_3$
Molecular weight: 454.6950 g/mol
Exact mass: 454.3448
$[\alpha]_D^{20}$: +27.5 (*c* = 0.07, $CHCl_3$)

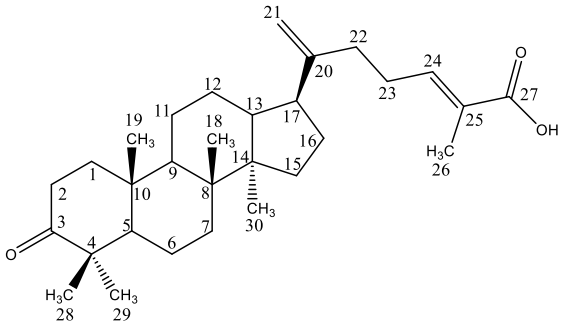

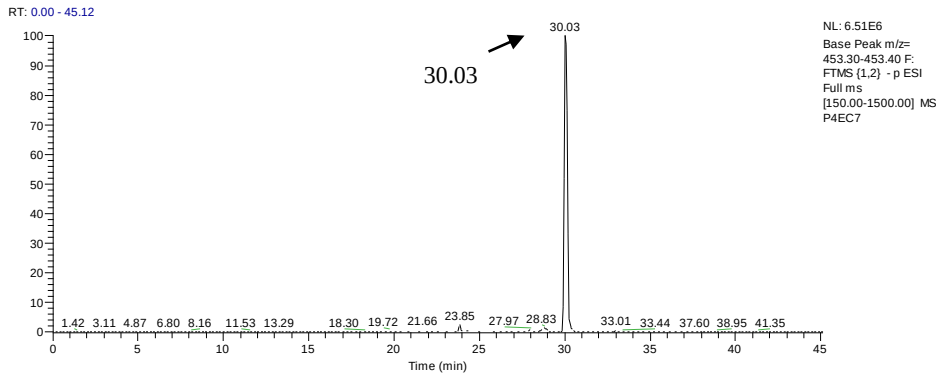

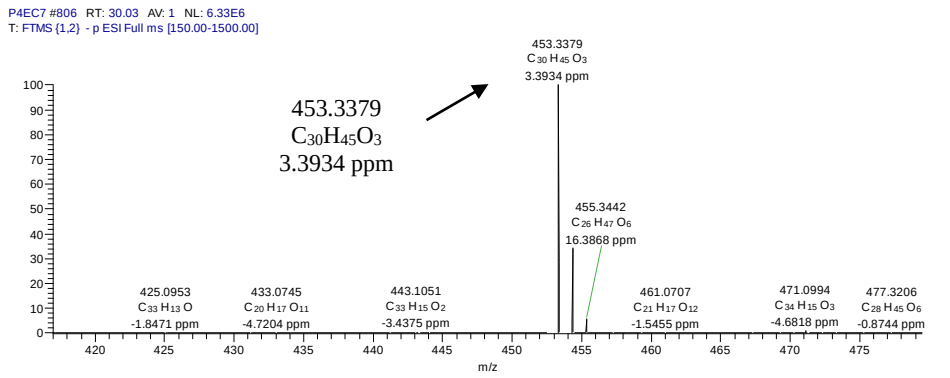

Based on the high resolution mass spectral data, the ESI peak at 30.03 min in the negative mode was found at *m/z* 453.3379 $[M-H]^-$. This revealed the exact mass at 454.3448 g/mol, which established the molecular formula of $C_{30}H_{46}O_3$ (**Table 3.13**). The ^1H NMR spectrum of **P4EC7** (**Fig. 3.28**) contained six methyl signals at 0.8 – 1.9 ppm. All methyl proton signals were observed as singlets (δ0.87, 0.93, 1.00, 1.03, 1.07, 1.84). One olefinic methine proton was observed at δ6.88. Furthermore, two methylene protons were observed at δ4.71 and 4.79. The ^{13}C NMR contained thirty carbon signals (**Fig. 3.29**). Among these, one ketone (C3) and carboxyl (C27) carbon was observed respectively at δ217.7 and δ171.4. Two olefinic quaternary carbons were observed at δ150.9 (C20) and δ126.4 (C25), in addition of one olefinic methine and methylene at δ144.2 and δ107.8, respectively. Based on the ^1H-^1H COSY (**Fig. 3.30**), direct correlation of protons on C24/C23, C23/C22, C21/C21 and C1/C2 were observed which implicated that **P4EC7** had the dammarane backbone structure. The multiplicity of the carbons was determined by an HSQC experiment (**Fig. 3.31**). These were five primary, eleven secondary, six tertiary and eight quaternary carbons. From the HSQC spectrum, the resonances for C21 was illustrated at 4.71 and 4.79 ppm for its protons, which correlated with the olefinic carbon at 107.8 ppm that indicated the methylene unit. C24 was observed as an olefinic methine at 6.89 and 144.2 ppm for its proton and carbon signals, respectively.

The key HMBC correlations for the structure of 24-(E)-3-oxodammara-20(21),24-dien-27-oic acid was first determined through C3, C17, C22, C24, C25, C26 and C27. C3 and C5 at δ217.7 and 54.9, respectively, gave strong correlations with neighbouring methyl protons on C29 and C28 at 1.03 and 1.07 ppm, respectively (**Fig. 3.32**). Furthermore, based on the HSQC spectrum, C5 was observed as a methine carbon. Meanwhile, the quaternary C22 was assigned at 32.1 ppm that gave a strong correlation with neighbouring olefinic protons of C21 at 4.71 and 4.79 ppm as well as the methylene protons of C23 at 2.35 ppm. Nonetheless, the position of C21 was further confirmed by the correlation of its protons with C22 and C17 at 32.1 and 47.2 ppm, respectively. C17 is a methine carbon, which was determined from the HSQC spectrum. The position of C23 was confirmed by the strong correlation of its proton with C22, C24, and C25 at 32.1, 144.2 and 126.4 ppm, respectively). C26 was

determined as a tertiary carbon based on its ^{1}H integral and HSQC correlation. C26 proton was observed at 1.84 ppm, which correlated with olefinic carbons C24 and C25 as well as the carboxylic carbon (C27) at 144.2, 126.4 and 171.4 ppm, respectively. In addition, the olefinic proton of C24 was deshielded at 6.88 ppm and showed a cross peak with C26 and C27 thus confirmed the position of C24.Whereas, the position of C5 was confirmed by the strong correlation of its carbon at 54.9 ppm with methyl protons of C19, C28 and C29 at 0.93, 1.07 and 1.03 ppm, respectively. C9 was elucidated by the cross peaks of the methyl protons of C19 and C18 at 0.93 and 1.00 ppm, respectively with C9 at 49.8 ppm. Furthermore, C8 was confirmed by the strong correlation of the methyl protons of C18 and C30 (0.87 ppm) with C8 at 39.9 ppm. In the case of C14, its assignment was indicated by cross peaks of the methyl protons of C18 and C19 with C14 at 48.9 ppm. By comparison of the spectral data (**Tables 3.14** and **3.15**) of **P4EC7** with the literature (Phan et al., 2011), the compound was elucidated as 24-(E)-3-oxodammara-20(21),24-dien-27-oic acid. The optical rotation was observed at $[\alpha]_D^{20}$ +27.5 (*c*= 0.07, $CHCl_3$) that also comparable with literature $[\alpha]_D^{26}$ +37.9 (*c*= 0.09, $CHCl_3$) (Phan et al., 2011). This compound with (E)-configuration was first isolated from the leaves of *Alnus nepalensis,* a native species in Vietnam (Phan et al., 2011).

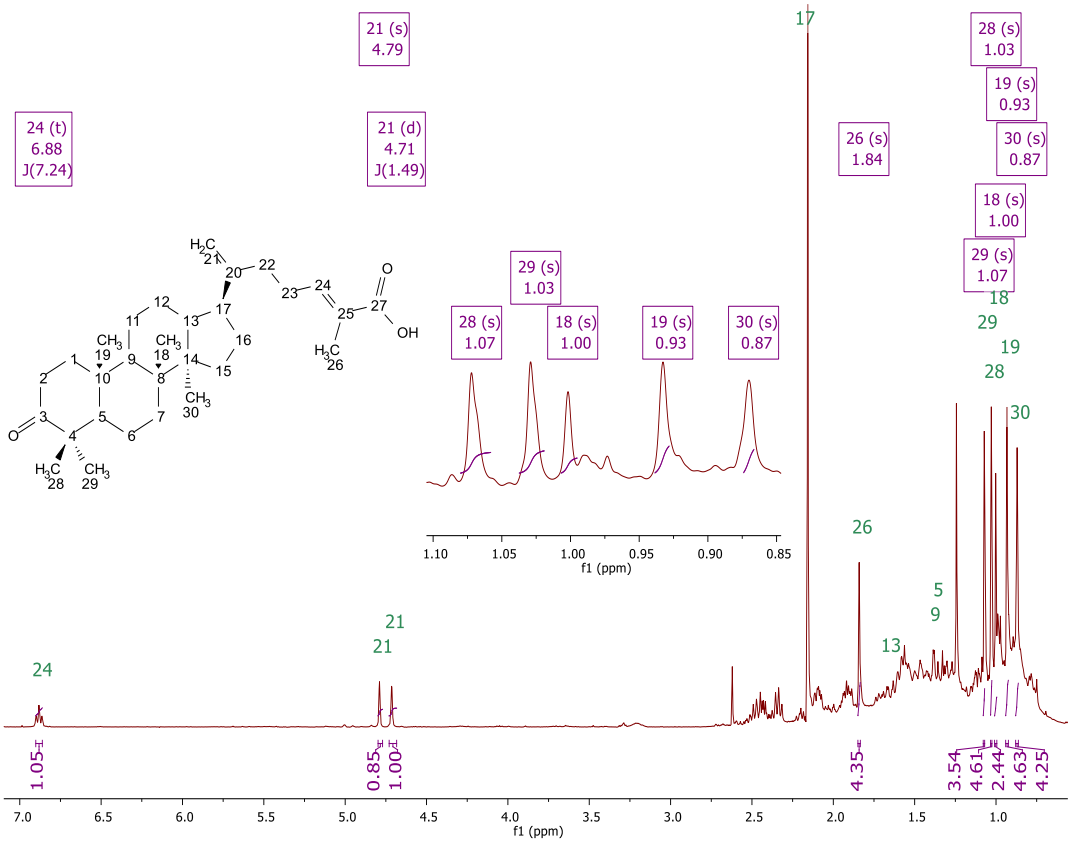

Fig. 3.28: ^{1}H NMR spectrum at 400 MHz of **P4EC7** in $CDCl_3$.

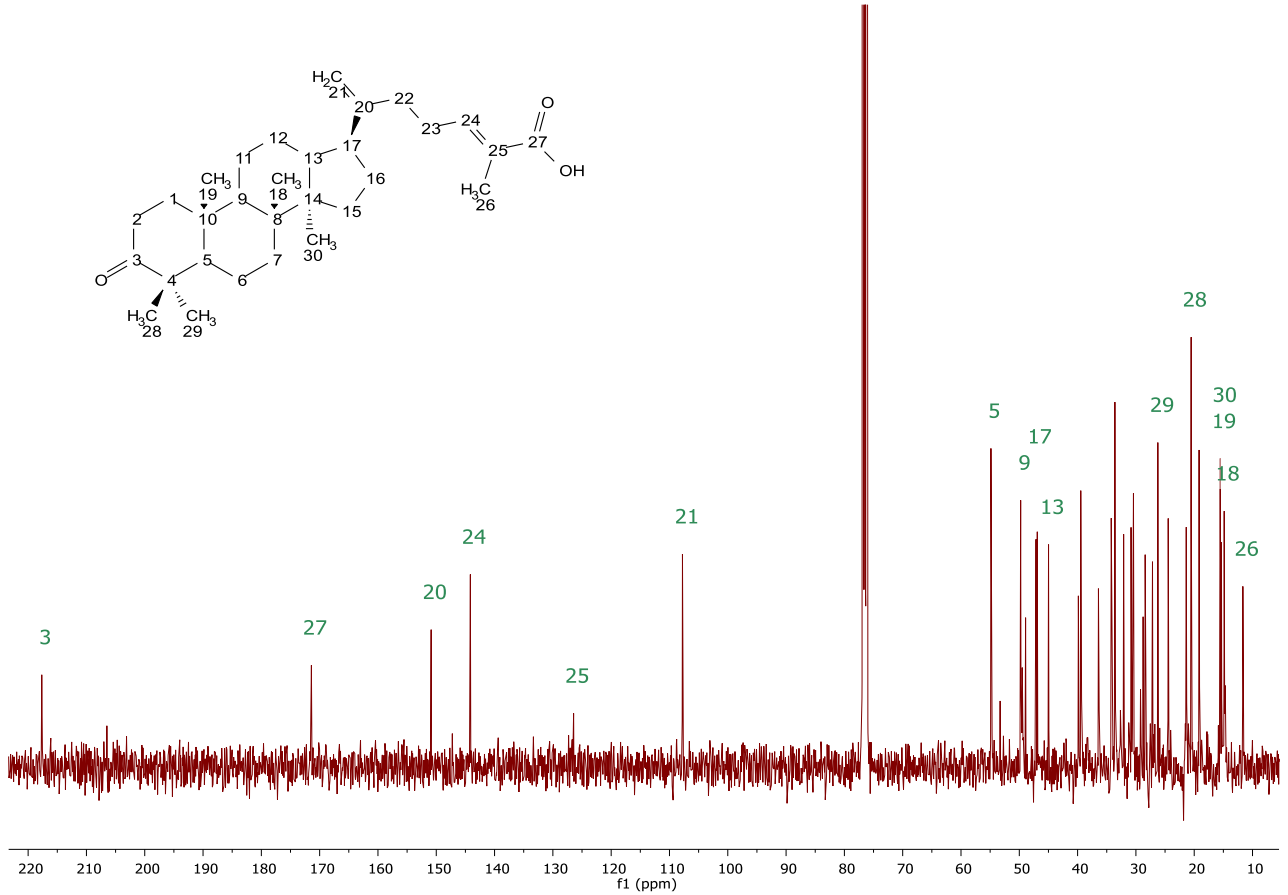

Fig. 3.29: ^{13}C (100 MHz) spectrum of **P4EC7** in $CDCl_3$.

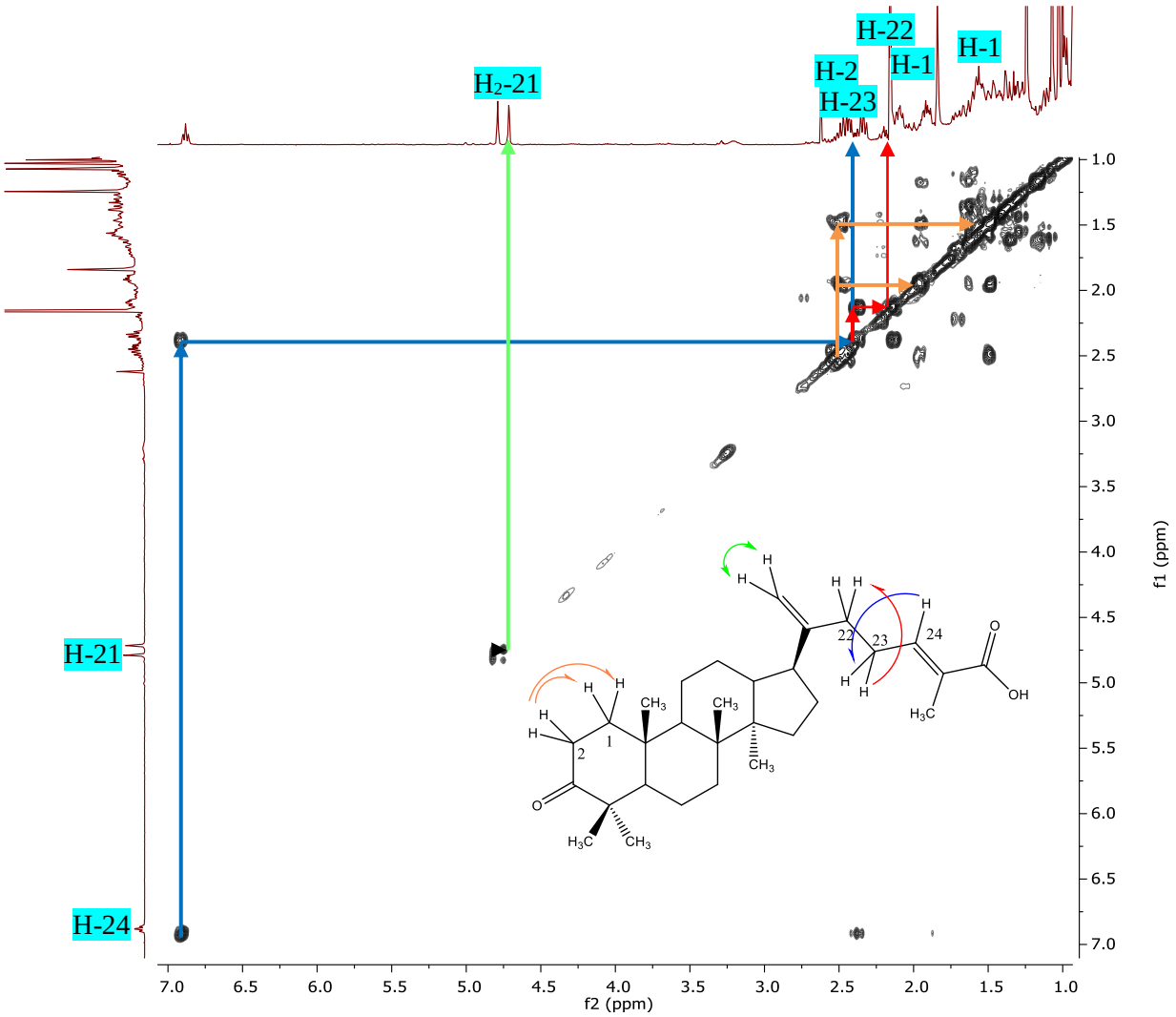

Fig. 3.30: ^{1}H-^{1}H COSY (400 MHz) spectrum in $CDCl_3$ showed partial correlations in the substructure of 24-(E)-3-oxodammara-20(21),24-dien-27-oic acid for **P4EC7**.

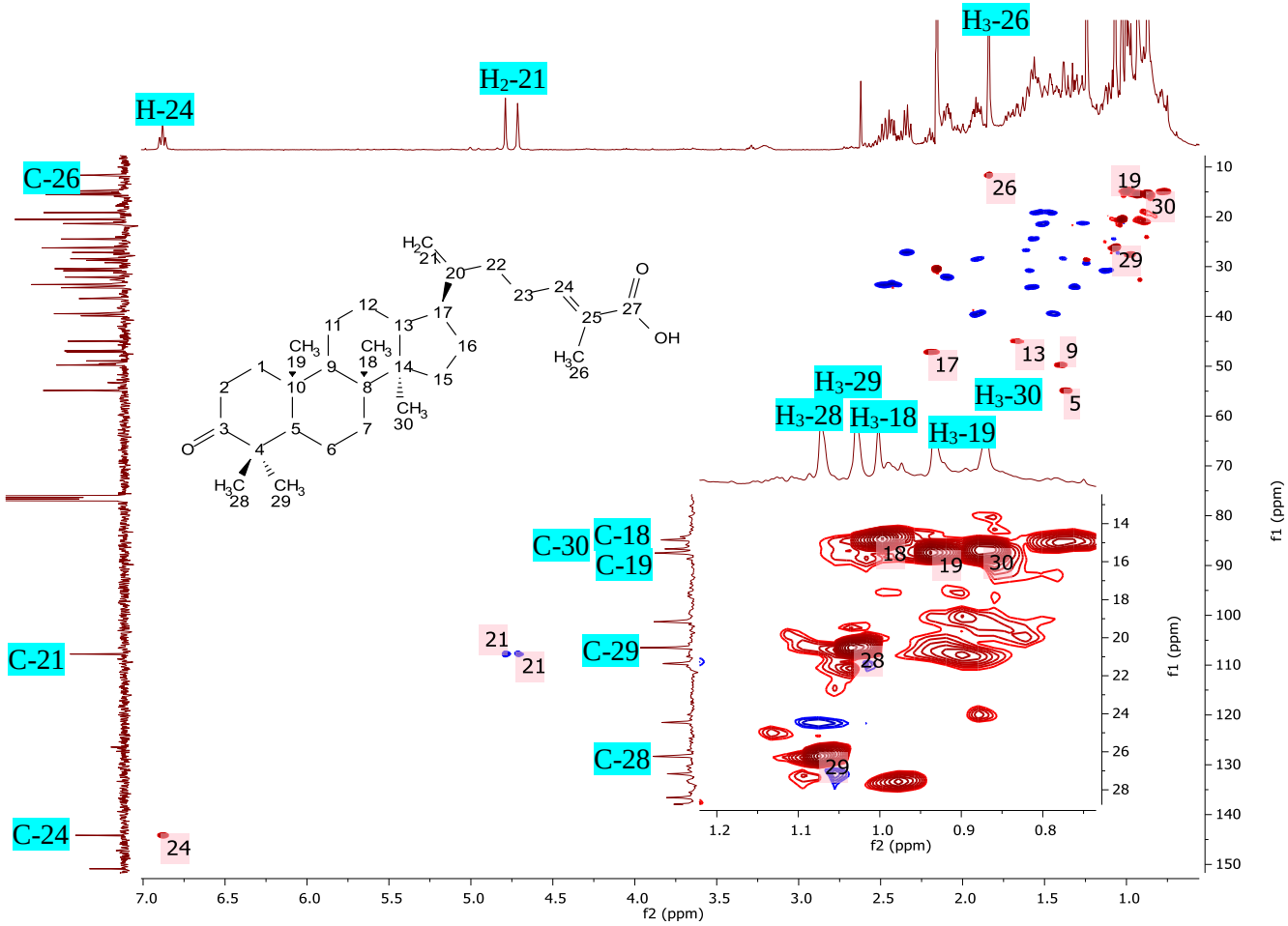

Fig. 3.31: HSQC of **P4EC7** in $CDCl_3$. The X- and Y-axes indicate the proton and carbon spectra (400 MHz), respectively. Inset showed all six methyl group signals observed at the aliphatic region.

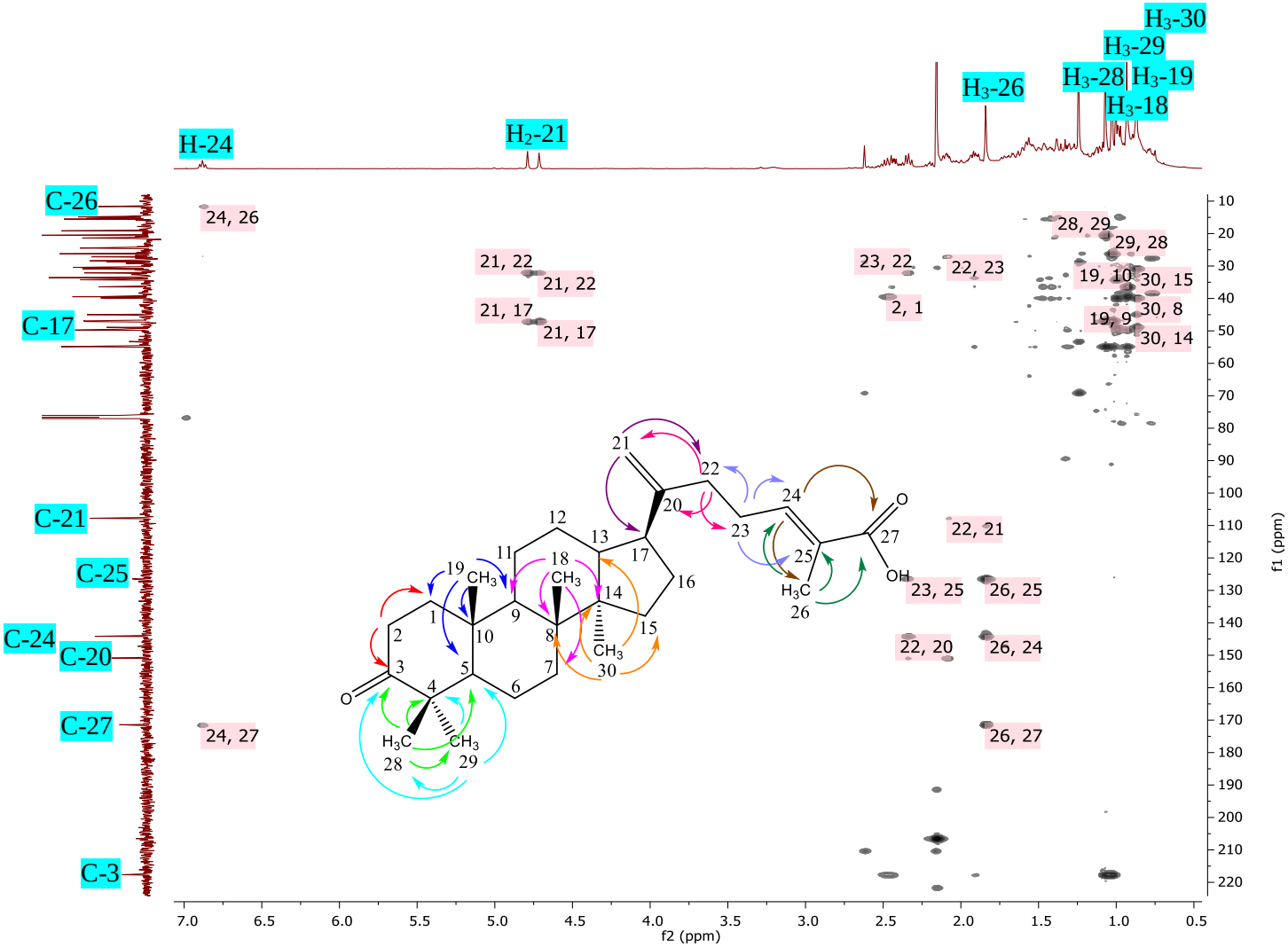

Fig. 3.32: The HMBC of **P4EC7** in $CDCl_3$. The X- and Y-axes correspond to the proton and carbon spectra (400 MHz), respectively.

Table 3.14: ^{1}H NMR (400MHz) of compound **P4EC7** in $CDCl_3$ in comparison with literature data (Phan et al., 2011). Full assignment was deduced from HSQC in $CDCl_3$ at 400 MHz.

Carbon no.	^{1}H NMR, δ_H (multiplicity *J* in Hz)	
	P4EC7 in $CDCl_3$	**Literature (Phan et al., 2011) in $CDCl_3$**
1	1.45, 1.89	-
2	2.43, 2.47	-
5	1.37	-
6	1.46, 1.56	-
7	1.32, 1.57	-
9	1.39	-
11	1.27, 1.51	-
12	1.08, 1.58	-
13	1.66	-
15	1.13, 1.59	-
16	1.39, 1.90	-
17	2.19	-
CH_3-18	1.00 (*s*)	1.04 (*s*)
CH_3-19	0.93 (*s*)	0.97 (*s*)
H-21	4.71 (*d*, *J* = 1.5 Hz)	4.75 (*d*, *J* = 1.0 Hz)
	4.79 (*s*)	4.82 (*br.s*)
22	2.09, 2.17	-
23	1.05, 2.34	-
H-24	6.88 (*t*, *J* = 7.2 Hz)	6.92 (*br.t*, *J* = 7.0 Hz)
CH_3-26	1.84 (*s*)	1.87 (*s*)
CH_3-28	1.07 (*s*)	1.11 (*s*)
CH_3-29	1.03 (*s*)	1.06 (*s*)
CH_3-30	0.87 (*s*)	0.90 (*s*)

Table 3.15: ^{13}C NMR (100 MHz) of compound **P4EC7** in $CDCl_3$ in comparison with literature data (Phan et al., 2011).

Carbon no.	13C NMR δC (ppm)	
	P4EC7 in $CDCl_3$	**Literature (Phan et al., 2011) in $CDCl_3$**
1	39.4 CH_2	39.9 CH_2
2	33.6 CH_2	34.1 CH_2
3	217.7 C	218.1 C
4	46.9 C	47.4 C
5	54.9 CH	55.4 CH
6	19.2 CH_2	19.7 CH_2
7	34.3 CH_2	34.8 CH_2
8	39.9 C	40.4 C
9	49.8 CH	50.3 CH
10	36.5 C	36.9 C
11	21.5 CH_2	21.9 CH_2
12	24.2 CH_2	24.9 CH_2
13	45.0 CH	45.6 CH
14	48.9 C	49.5 C
15	30.9 CH_2	31.4 CH_2
16	28.4 CH_2	28.9 CH_2
17	47.2 CH	47.7 CH
18	14.8 CH_3	15.4 CH_3
19	15.5 CH_3	16.1 CH_3
20	150.9 C	151.4 C
21	107.8 CH_2	108.3 CH_2
22	32.1 CH_2	33.7 CH_2
23	27.1 CH_2	27.7 CH_2
24	144.2 CH	144.7 CH
25	126.4 C	127.1 C
26	11.6 CH_3	12.1 CH_3
27	171.4 C	172.5 C
28	26.2 CH_3	26.8 CH_3
29	20.5 CH_3	21.0 CH_3
30	15.4 CH_3	15.9 CH_3

*3.3.3.2 Dammarenolic acid/**P5EC12***

Table 3.16: The compound from P5EC fraction (**P5EC12**) was elucidated using NMR spectroscopy. The relative stereochemistry of the isolated dammarenolic acid was illustrated based on the literature.

Dammarenolic acid (N_5787)
Source: Johor green propolis
Sample amount: 16.1 mg (colourless oily material)
Molecular formula: $C_{30}H_{50}O_3$
Molecular weight: 458.7270g/mol
Exact mass: 458.3760
$[\alpha]_D^{20}$: +23.9 (*c* = 0.07, $CHCl_3$)

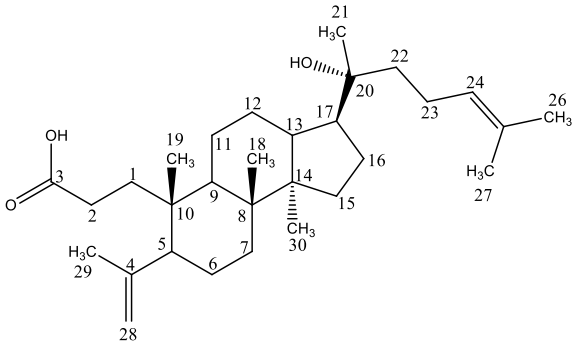

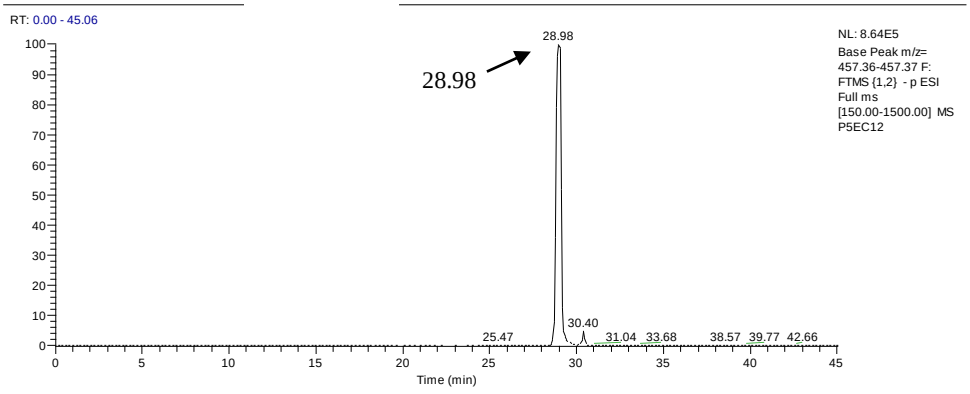

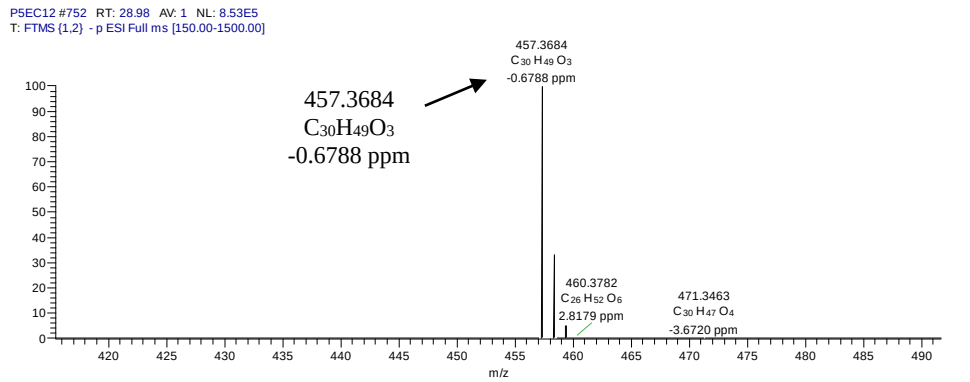

Based on the high resolution mass spectral data, the ESI peak at 28.98 min in the negative mode was found at *m/z* 457.3684 $[M-H]^-$. This revealed the exact mass at 458.3760 g/mol, which established the molecular formula of $C_{30}H_{50}O_3$ (**Table 3.16**). The ^1H NMR spectrum (**Fig. 3.33**) of P5EC12 contained seven methyl signals within 0.8 – 1.9 ppm. All methyl proton signals were observed as singlets (δ0.85, 0.89, 1.01, 1.15, 1.62, 1.69 and 1.73). As found in the COSY spectrum, two olefinic signals at 4.66 and 4.85 ppm bearing carbon at C28 was correlated with each other indicating the presence of an unsaturated exomethylene moiety. Another olefinic methine proton was shown at 5.12 ppm. The ^{13}C NMR contained one carboxyl carbon (C3) at δ178.1 (**Fig. 3.34**). Four olefinic carbons for C28, C4, C24 and C25 were observed at 113.0, 147.0, 124.2 and 131.2, respectively. In addition, C20 was also observed as a hydroxyl-bearing carbon at δ75.0. Based on this spectrum, it was implied that **P5EC12** also has the dammarane backbone structure. Other 2D NMR experiments including ^1H-^1H COSY (**Fig. 3.35**), HSQC (**Fig. 3.36**) and HMBC (**Fig. 3.37**) were performed to confirm the structure.

The position of the carboxyl carbon C3 was observed at δ178.1 and displayed strong correlations with the methylene protons of C2 at 2.40 and 2.24 ppm. Both proton signals from C2 then showed further correlation with C1 at δ33.8. The position of C4 at δ147.0 was confirmed by the cross peaks with the methyl protons of C29 at δ1.73, methylene protons of C28 at δ4.66 and 4.85 as well as the methine proton of C5 at δ1.98 ppm. The position of C5 was further confirmed by its correlation with the methyl protons of C29 and C19 at 1.73 and 0.85 ppm, respectively and with the methylene protons of C28. Furthermore, the assignment of C28 was confirmed at δ113.0 due the correlation of its unsaturated olefinic protons with C4, C29, and C5. Meanwhile, C9 was assigned at δ41.9, which exhibited cross peaks with methyl protons of C19 and C18 at 0.85 and 1.01ppm, respectively. The assignment of the quaternary carbons C8 and C14 at 39.9 and 50.1 ppm, respectively were established from the HMBC correlation with the methyl protons of C18 and C30 at 1.01 and 0.89 ppm, respectively. Meanwhile, the hydroxyl-bearing quaternary carbon C20 was assigned at δ75.0 with its strong correlation with the methyl protons of C21 at 1.15

ppm. Furthermore, correlations between methyl protons of C21 with C20, C17, and C22 at δ75.0, δ49.3 and δ40.1, respectively were also observed, which confirmed the position of C21. Nonetheless, the positions of the olefinic carbons C24 and C25 were confirmed by their strong correlations with the methyl protons of C26 and C27 at 1.69 and 1.62 ppm, respectively. Comparison of the spectral data of **P5EC12** as presented in **Tables 3.17** and **3.18** with the literature (Esimone et al., 2010) supported that this compound is dammarenolic acid. The optical rotation was observed at $[\alpha]_D^{20}$ +23.9 (*c*= 0.07, $CHCl_3$) that also comparable with literature $[\alpha]_D^{20}$ +19.0 (*c*= 0.03, $CHCl_3$) (Esimone et al., 2010). This compound was previously isolated from the bark of *Aglaia ignea* found in Southeast Asian region (Esimone et al., 2008).

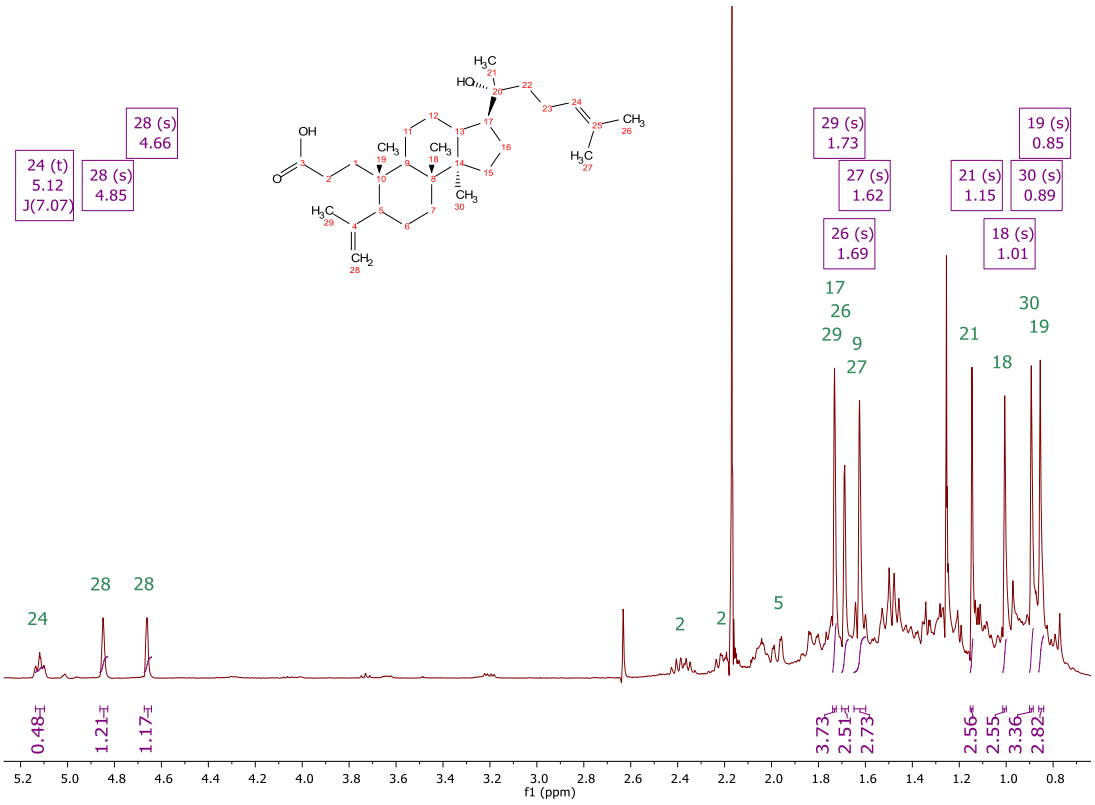

Fig. 3.33: ^{1}H NMR spectrum at 400 MHz of **P5EC12** in $CDCl_3$.

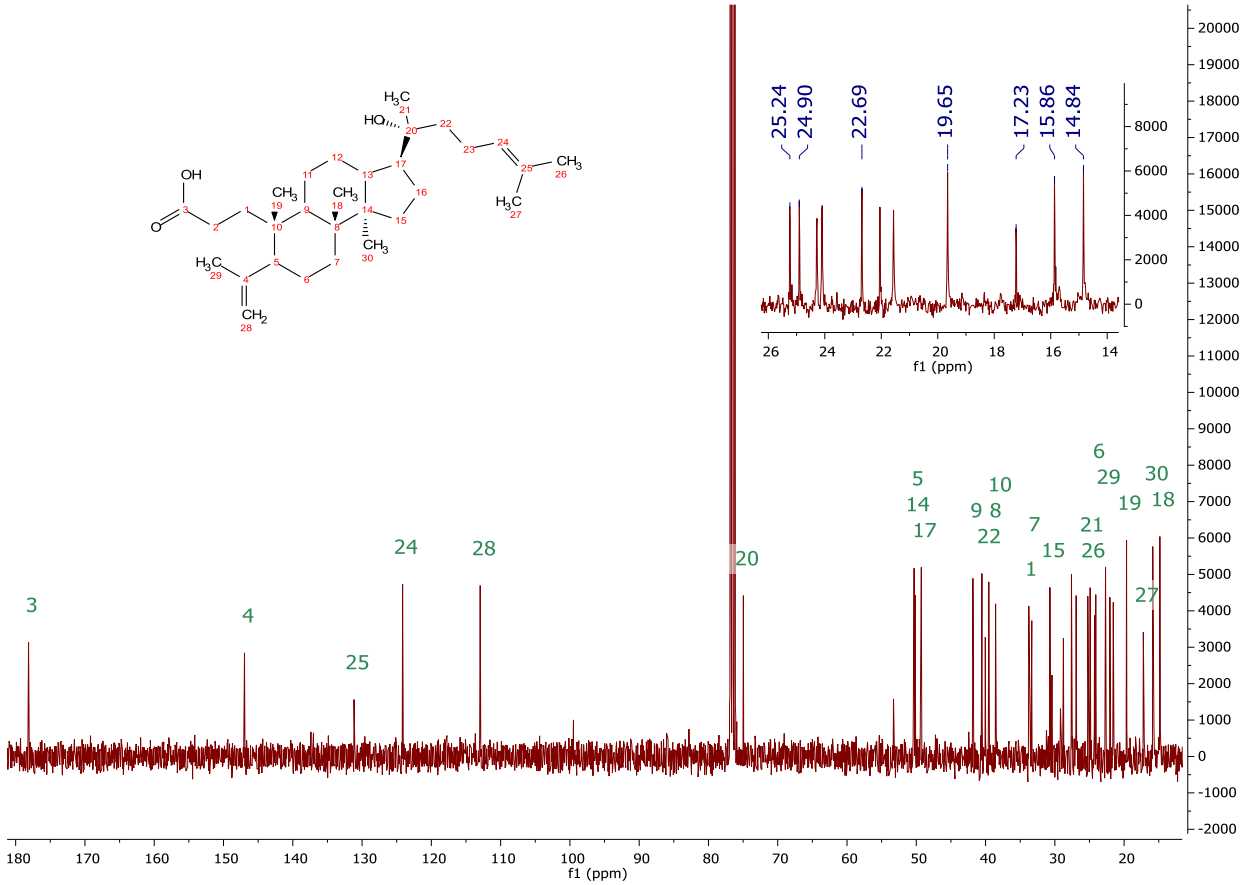

Fig. 3.34: ^{13}C spectrum at 100 MHz of **P5EC12** in $CDCl_3$. Inset showed the methyl signals between 14.0 to 26.0 ppm.

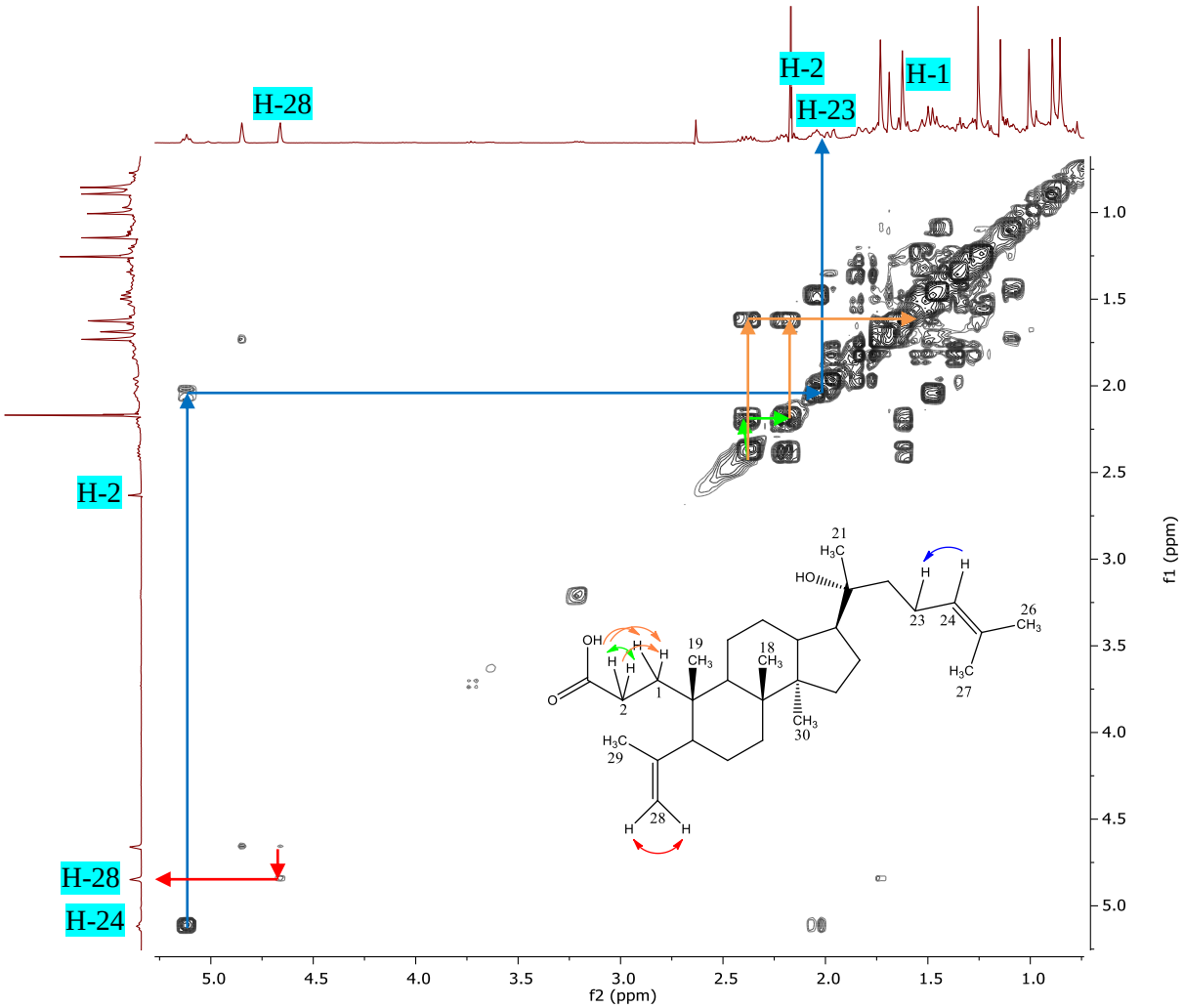

Fig. 3.35: ^{1}H-^{1}H COSY (400 MHz) spectrum in $CDCl_3$ showing substructure of dammarenolic acid in **P5EC12**.

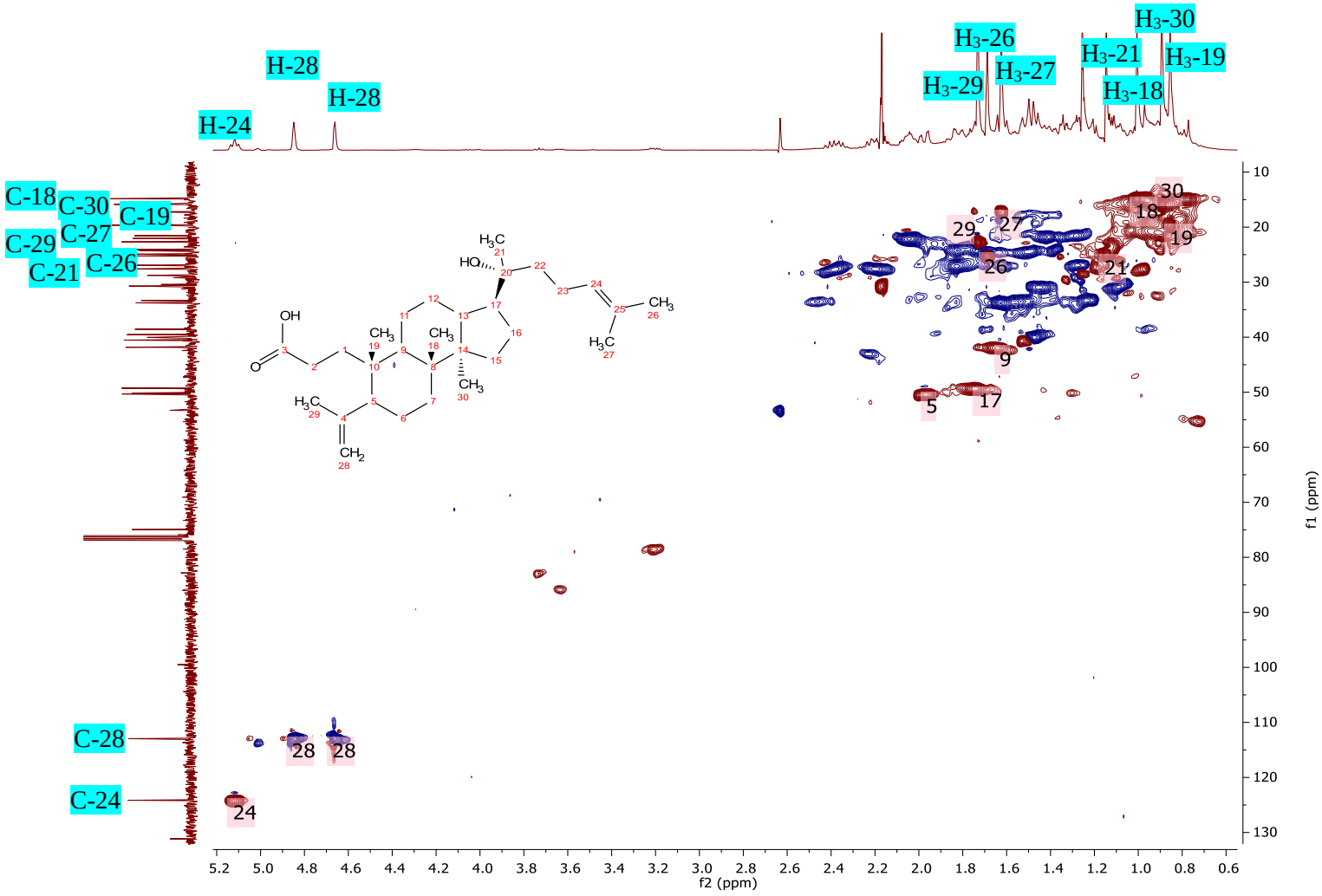

Fig. 3.36: HSQC (400 MHz) of **P5EC12** in $CDCl_3$.

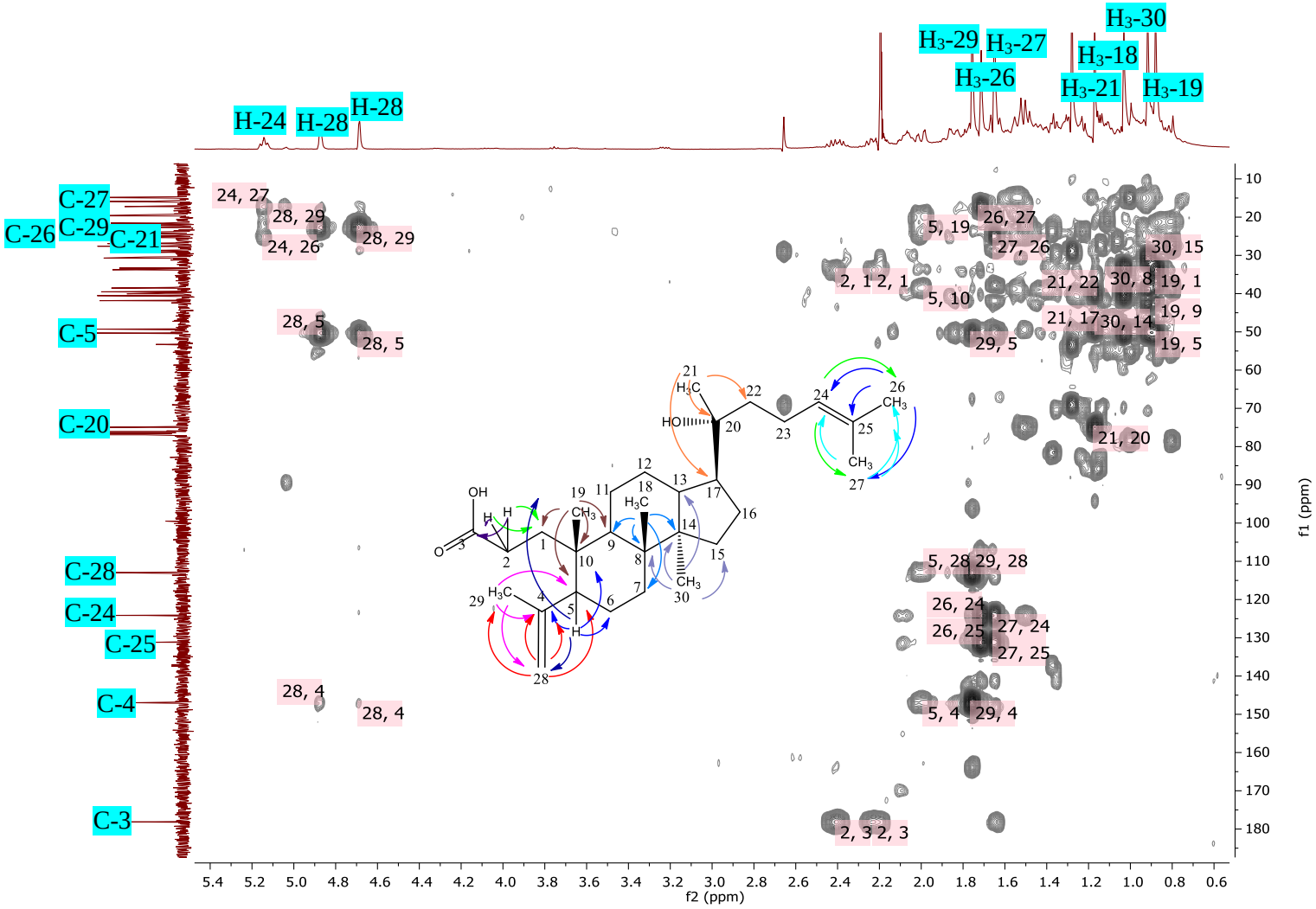

Fig. 3.37: The HMBC at 400 MHz of **P5EC12** in $CDCl_3$. The X and Y-axes correspond to the proton and ^{13}C spectra, respectively.

Table 3.17: ^{1}H NMR (400 MHz) of compound **P5EC12** in $CDCl_3$ in comparison with literature data (Esimone et al., 2010). Full assignment was deduced from HSQC in $CDCl_3$ at 400 MHz.

Carbon no.	^{1}H NMR, δ_H (multiplicity J in Hz)	
	P5EC12 in $CDCl_3$	**Literature (Esimone et al., 2010) in $CDCl_3$**
1	1.62, 2.46	-
2	2.20, 2.38	-
5	1.97	-
6	1.38, 1.51	-
7	1.24, 1.54	-
9	1.65	-
11	1.28, 1.42	-
12	1.28, 1.62	-
13	1.53	-
15	1.09, 1.45	-
16	1.75, 1.82	-
17	1.74	-
CH_3-18	1.01 (s)	0.99 (s)
CH_3-19	0.85 (s)	0.86 (s)
CH_3-21	1.15 (s)	1.14 (s)
22	1.40, 1.47	-
23	1.42, 2.04	-
H-24	5.12 (*t*, *J* = 7.1 Hz)	5.10 (t)
CH_3-26	1.69 (s)	1.68 (s)
CH_3-27	1.62 (s)	1.63 (s)
H-28	4.66 (s)	4.66 (br s)
	4.85 (s)	4.85 (br s)
CH_3-29	1.73 (s)	1.72 (s)
CH_3-30	0.89 (s)	0.89 (s)

Table 3.18: ^{13}C NMR (100 MHz) of compound **P5EC12** in $CDCl_3$ in comparison with literature data (Esimone et al., 2010).

Carbon no.	13C NMR δC (m)	
	P5EC12 in $CDCl_3$	**Literature (Esimone et al., 2010) in $CDCl_3$**
1	33.8 CH_2	34.3 CH_2
2	27.6 CH_2	28.3 CH_2
3	178.1 C	179.8 C
4	147.0 C	147.5 C
5	50.4 CH	50.8 CH
6	24.3 CH_2	24.6 CH_2
7	33.3 CH_2	33.9 CH_2
8	39.9 C	40.1 C
9	41.9 CH	41.1 CH
10	38.0 C	39.1 C
11	21.4 CH_2	22.1 CH_2
12	27.0 CH_2	27.5 CH_2
13	40.7 CH	42.4 CH
14	50.1 C	50.7 C
15	30.9 CH_2	31.2 CH_2
16	24.3 CH_2	24.8 CH_2
17	49.3 CH	49.7 CH
18	14.9 CH_3	15.4 CH_3
19	19.8 CH_3	20.2 CH_3
20	75.0 C	75.6 C
21	25.2 CH_3	25.4 CH_3
22	40.1 CH_2	40.6 CH_2
23	22.1 CH_2	22.6 CH_2
24	124.2 CH	124.7 CH
25	131.2 C	131.7 C
26	25.0 CH_3	23.8 CH_3
27	17.3 CH_3	17.8 CH_3
28	113.0 CH_2	113.5 CH_2
29	22.7 CH_3	23.2 CH_3
30	15.8 CH_3	16.4 CH_3

3.3.4 Secondary metabolites isolated from AC propolis

Chromatographic fractionation of AC extract with n-hexane and ethyl acetate yielded 23 fractions that were further subjected to TLC profiling. The ^{1}H NMR spectrum and TLC for AC17 and AC18 (**Fig. 3.38 and 3.39**) indicated that these fractions were having similar or almost identical chemical profiles.

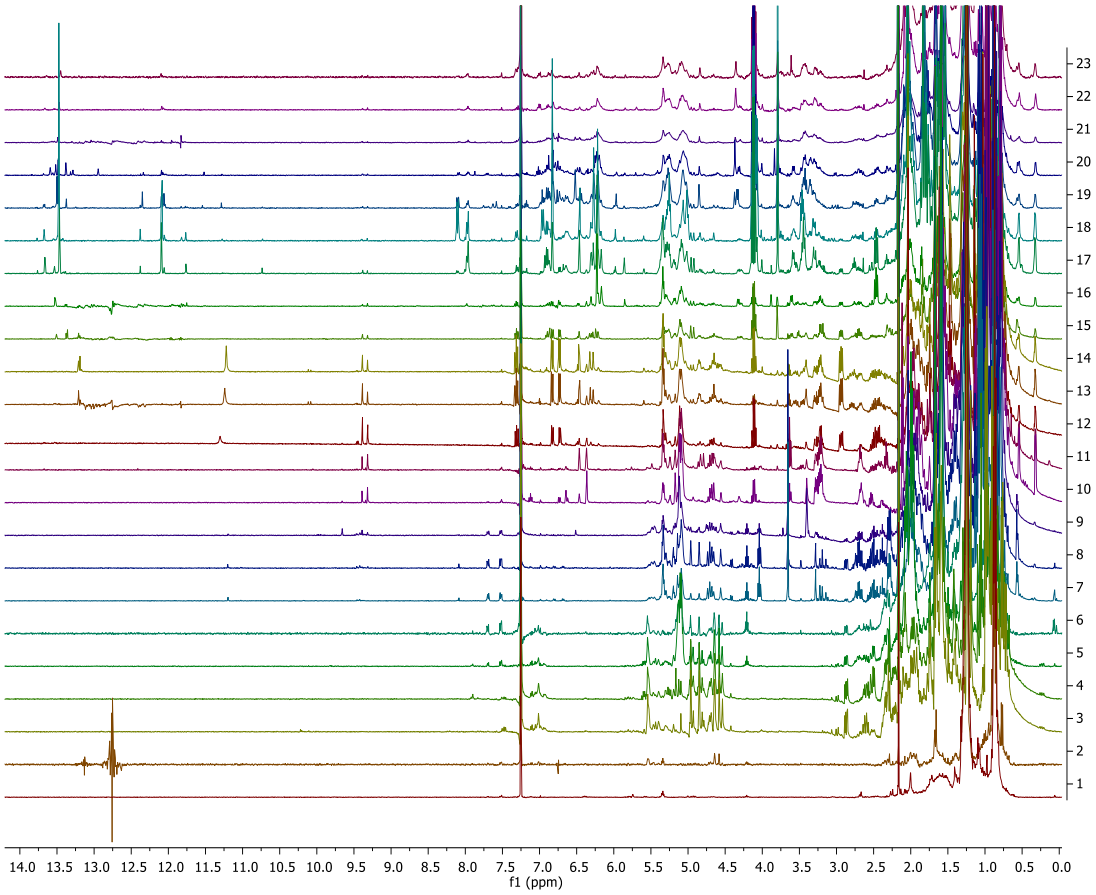

Fig. 3.38: ^{1}H NMR spectra at 400 MHz of Malacca yellow propolis fractions in $CDCl_3$. The spectra were labelled from below; AC1, AC2, AC3, AC4, AC5, AC6, AC7, AC8, AC9, AC10, AC11, AC12, AC13, AC14, AC15, AC16, A17, A18, AC19, AC20, AC21, AC22 and AC23.

A)

AC17 AC18

B)

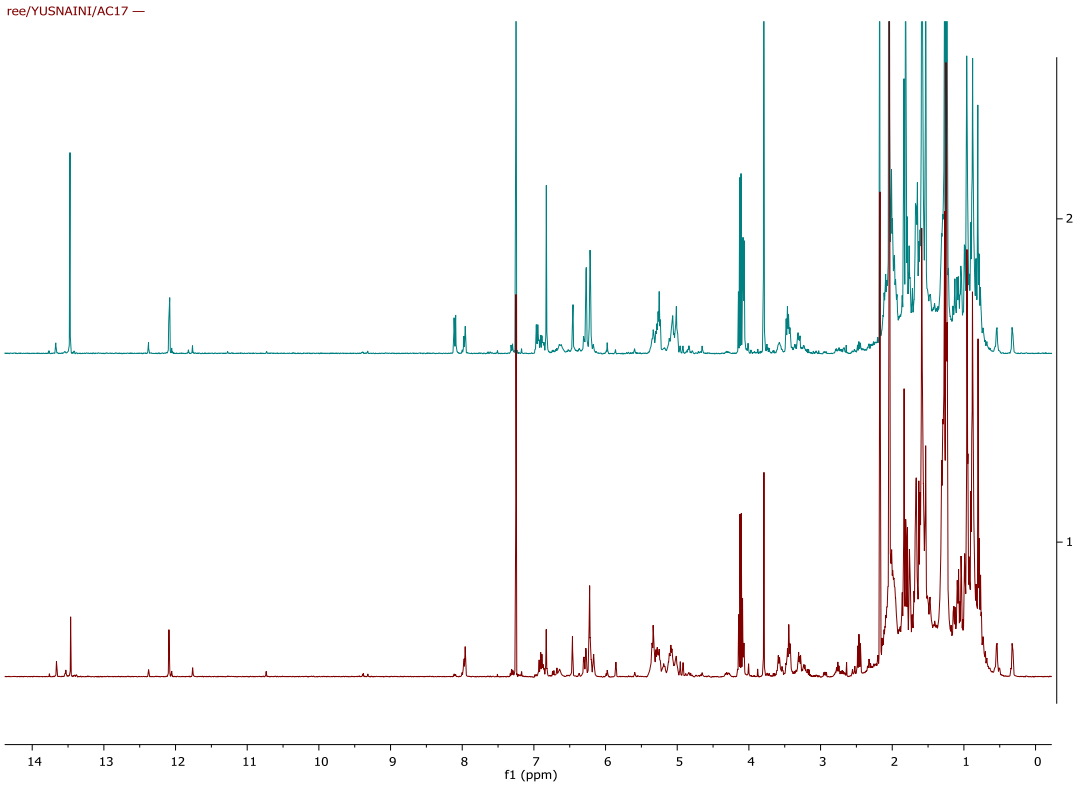

Fig. 3.39: **A**) TLC for AC17 and AC18 in n-hexane and EtOAc at a ratio of 7:3.**B**) ^{1}H NMR of AC17 (above) and AC18 (below), showing identical chemical finger print in both fractions.

Metabolomics-guided isolation work was also performed on the AC fractions for the characterization of unique metabolites, thus giving an insight on how further fractionation and isolation of the pure compounds could be accomplished. The cytotoxicity effects on A2780 were exhibited by fractions AC13 to AC23 (**Fig 3.40**).

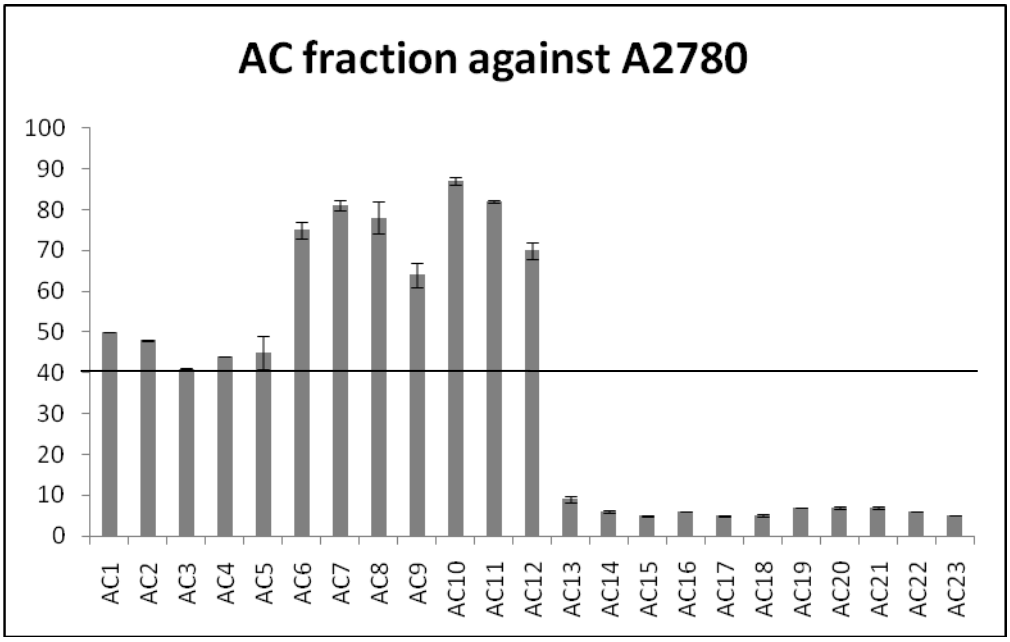

Fig 3.40: Cytotocixity assay of AC fractions on ovarian cancer cell line (A2780), the active fraction was determined at threshold ≤40%.

HR-LCMS data set for AC fractions was processed and statistically analysed for their similarities and differences using PCA-X multivariate analysis (**Fig. 3.41**). There were 23 variables being analysed in this model. R^2 and Q^2 values at 0.99 and 0.31, respectively was quite low for Q^2 value due to the high diversity in chemical profiles between fractions, as well as the existence of outlier (AC19). The metabolites potentially contributing to the bioactivity of the AC fractions against A2780 cell line were determined using the OPLS-DA S-plot. R^2 and Q^2 values were calculated at 0.99 and 0.85, respectively, showing good fitness and predictability of the model (**Fig. 3.42**). The permutation test showed a Q2Y value of -0.26, showing good validity of the prediction model. The data was cross-matched with the DNP database to provide structural details on targeted metabolites (**Table 3.19**). AC17 and AC18 were combined and renamed to AC17 based on the similarity of their ^{1}H NMR spectrum and TLC chromatogram. Based on their bioactivity against A2780, metabolomic profile and their high yield, AC17 was chosen for further fractionation and isolation, which afforded nepetadiol (Khan et al., 2011).

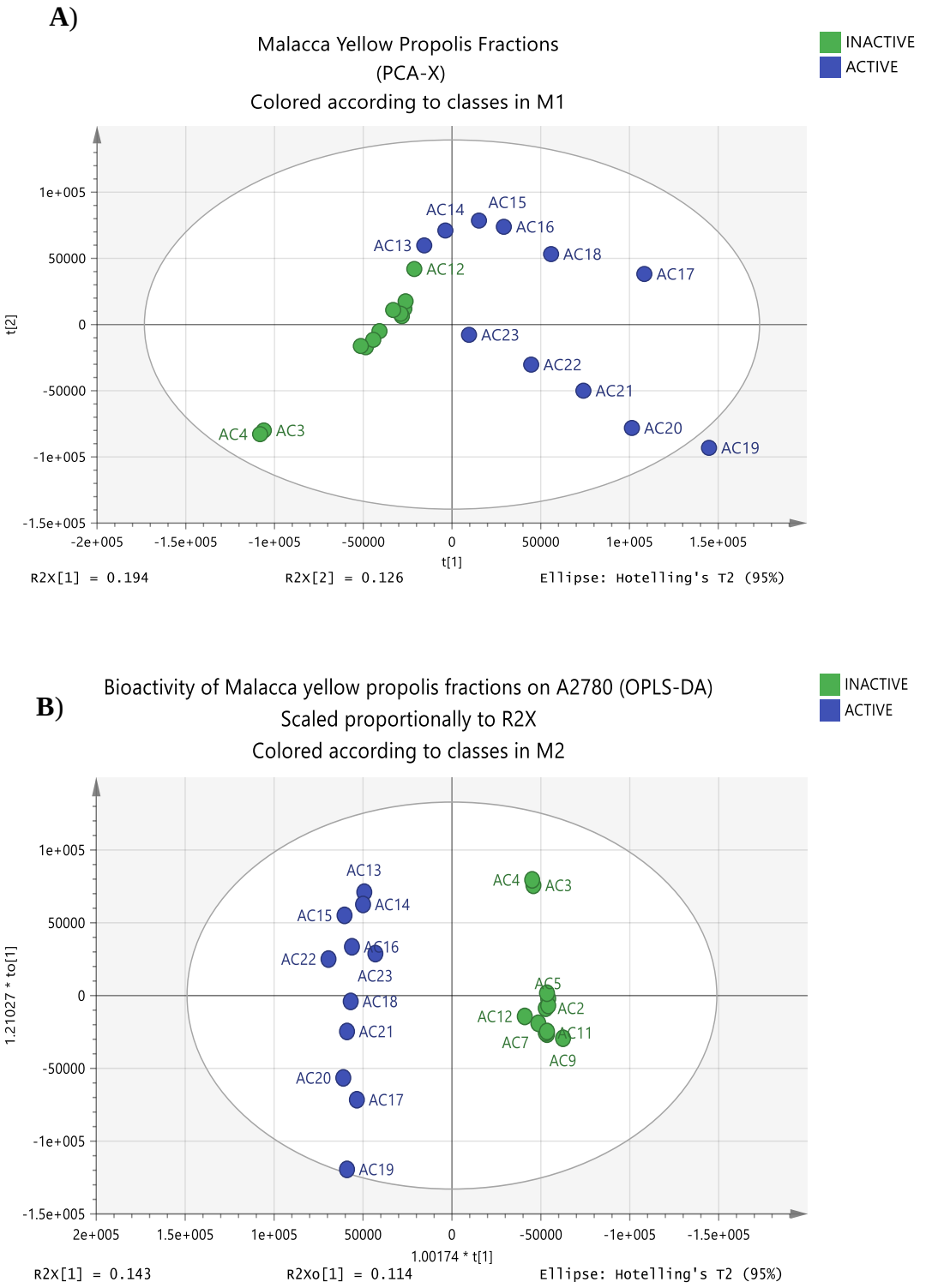

Fig. 3.41: **A**) PCA-X score scatter plot of AC propolis fractions were classified according bioactivity against A2780. **B**) The fractions were grouped based on their bioactivity, where the variations between the groups are larger than within the group by 14 and 11, %, respectively.

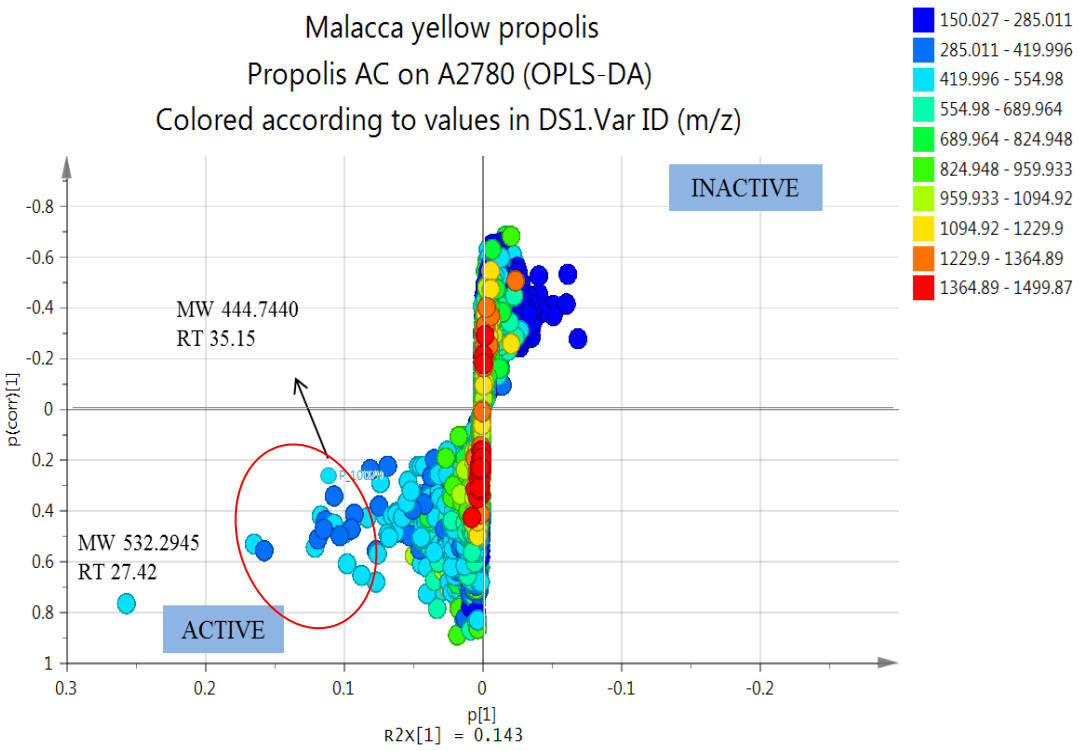

Fig. 3.42: OPLS-DA S-plot generated from the LCMS data indicating the encircled putative target metabolites responsible for the bioactivity of AC fractions against A2780. The targeted metabolites are presented on **Table 3.19**.

Table 3.19: Dereplication of target metabolites in P17AC and P18AC that are potentially active against the A2780.

Mzmine ID	M/Z	RT	Peak Area	MOLECULAR FORMULA	EXACT MASS	NAME	SOURCE
P_6764	423.1800	21.42	5.35E+08	$C_{25}H_{26}O_6$	422.1727	albanin E	Isol. from *Morus alba* (white mulberry)
N_653	409.1749	21.94	6.61E+08	$C_{21}H_{24}N_5O_4$ $C_{20}H_{28}NO_8$	410.1821	No hits	
P_1481	411.1803	22.45	4.88E+08	$C_{24}H_{26}O_6$ $C_{26}H_{26}N_9$	410.1730	caloxanthone B	*Calophyllum soulattri*
N_1474	463.2231	22.61	1.14E+09	$C_{25}H_{30}N_5O_4$ $C_{27}H_{32}N_2O_5$ $C_{24}H_{34}NO_8$	464.2304	No hits	
P_3041	465.2274	23.45	3.01E+08	$C_{28}H_{32}O_6$	464.2201	1-(3,7-dimethyl-2,6-octadienyl)-2,3,6,8-tetrahydroxy-7-(3-methyl-2-butenyl)xanthone	Isol. from *Garcinia cowa*
P_1317	533.2902	23.60	1.58E+08	$C_{33}H_{40}O_6$	532.2830	hanburin	Constit. of *Garcinia hanburyi*
N_1440	531.2872	26.90	7.36E+08	$C_{33}H_{36}N_6O$ $C_{35}H_{38}N_3O_2$ $C_{30}H_{38}N_5O_4$ $C_{32}H_{40}N_2O_5$	532.2945	No hits	
N_341	371.2677	27.42	4.14E+07	$C_{21}H_{34}N_5O$ $C_{20}H_{38}NO_5$	372.2749	No hits	
P_10029	445.4032	30.43	6.76E+04	$C_{30}H_{52}O_2$	444.3967	nepetadiol	Constit. of *Nepeta suavis*

Highlighted in grey is the isolated and elucidated metabolite.

*3.3.4.1 Nepetadiol/**P17AC2-2***

Table 3.20: The compound from P17AC2 fraction (**P17AC2-2**) was elucidated using NMR spectroscopy. The relative stereochemistry of the isolated nepetadiol was shown based on the literature (Khan et al., 2011).

Nepetadiol (P_10029)
Source: Malacca yellow propolis
Sample amount: 22.4 mg (white powder)
Molecular formula: $C_{30}H_{52}O_2$
Molecular weight: 444.7440g/mol
Exact mass: 444.3967
$[\alpha]_D^{20}$: +25.4 (*c* = 0.07, MeOH)

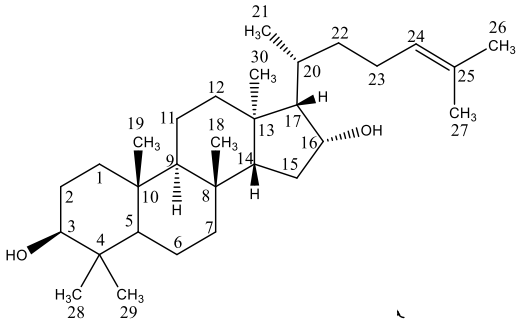

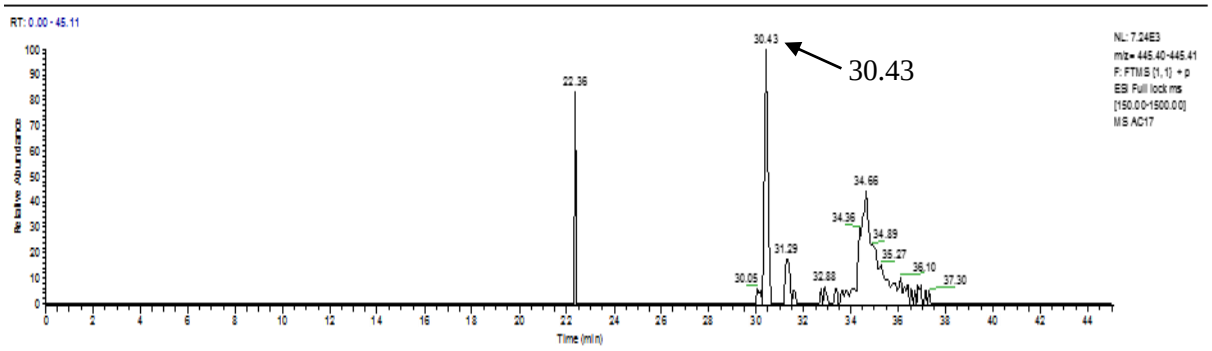

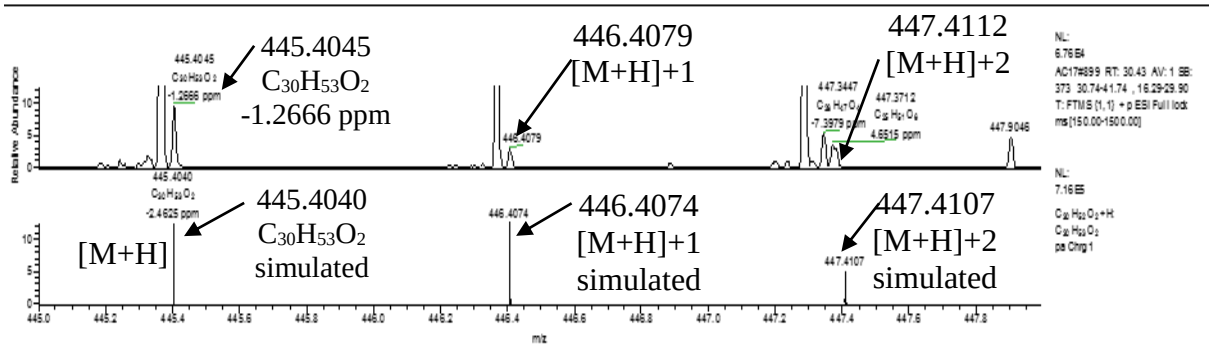

Based on the high resolution mass spectral data, the ESI peak at 30.43 min in the positive mode was found at *m/z* 445.4032 $[M+H]^+$. This revealed the exact mass at 444.3967 g/mol, which established the molecular formula of $C_{30}H_{52}O_2$ (**Table 3.20**). Although nepetadiol was detected in the dereplication study, the compound itself was poorly ionised in both the positive and negative mode by ESI resulting to poor ion peak intensities. The ^{1}H NMR spectrum of **P17AC2-2** (**Fig. 3.43**) had eight methyl signals within 0.8 – 1.7 ppm. All methyl proton signals were observed as singlets at δ0.78, 0.79, 0.87, 0.94, 0.98, 1.59 and 1.67, except for the resonance at δ0.95, which was observed as a doublet. Two hydroxyl-bearing methine protons were observed at 3.21 and 3.27 ppm. One olefinic methine proton was shown at 5.11 ppm. The ^{13}C and DEPT NMR spectra exhibited two olefinic carbons at δ125.4 and 131.0 for C24 and C25, respectively (**Fig. 3.44**). In addition, C3 and C16 also were observed as hydroxyl-bearing carbons at δ78.9 and 79.0. Based on this spectral data, **P17AC2-2** was described to have the dammarane-type triterpenoid backbone (Hill and Connolly, 2013). 2D NMR experiments that included ^{1}H-^{1}H NOESY (**Fig. 3.45**), HSQC (**Fig. 3.46**) and HMBC (**Fig. 3.47**) were performed to confirm the structure of P17AC2-2. Based on ^{1}H-^{1}H NOESY experiment (**Fig. 3.45**), the position and orientation of C3 was confirmed by its oxygenated proton correlating with the methyl protons of C28. The strong ^{1}H-^{1}H NOESY correlation was also observed between H-16/H-20, H_3-21/H-17, H-20/H-24.

The HMBC spectrum (**Fig. 3.47**) was quite informative in determining the structure of nepetadiol. The olefinic carbons C24 and C25 were observed at δ125.4 and 131.0, respectively, and illustrated strong correlations with the methyl protons of C26 and C27 at 1.67 and 1.59 ppm, respectively. Both methyl proton signals correlated with each other's carbons at δ25.8 and 17.7, which confirmed the terminal and germinal positions of C26 and C27. The position of C3 was further validated by its cross peaks with the methyl protons of C28 and C29 at 0.98 and 0.78 ppm, respectively. The position of the methine carbon C5 found at δ55.4 was further confirmed by its correlation with the methyl protons at 0.98, 0.78, and 0.94 ppm assigned for C28, C29, and C19, respectively. Furthermore, the position of methine carbon C14 at δ47.3 was confirmed through its correlation with the methyl protons of C18 and C30

at 0.88 and 0.79 ppm, respectively. Meanwhile, methine carbons C16 and C20 were observed at δ79.0 and δ40.7, respectively. The hydroxyl substituent on C16 caused its downfield shift to 79 ppm. C16 and C20 correlated with the methyl protons of C30 and C21 at 0.79 and 0.95 ppm, respectively. The proton and carbon spectral data of **P17AC2-2** (**Table 3.21 and 3.22**) were compared with the literature (Khan et al., 2011), which confirmed the structure of nepetadiol. The optical rotation was observed at $[\alpha]_D^{20}$ +25.4 (*c*= 0.07, MeOH) that also comparable with literature $[\alpha]_D^{25}$ +19.4 (*c*= 0.16, MeOH) (Khan et al., 2011). This compound was first described from *Nepeta suavis* (Khan et al., 2011).

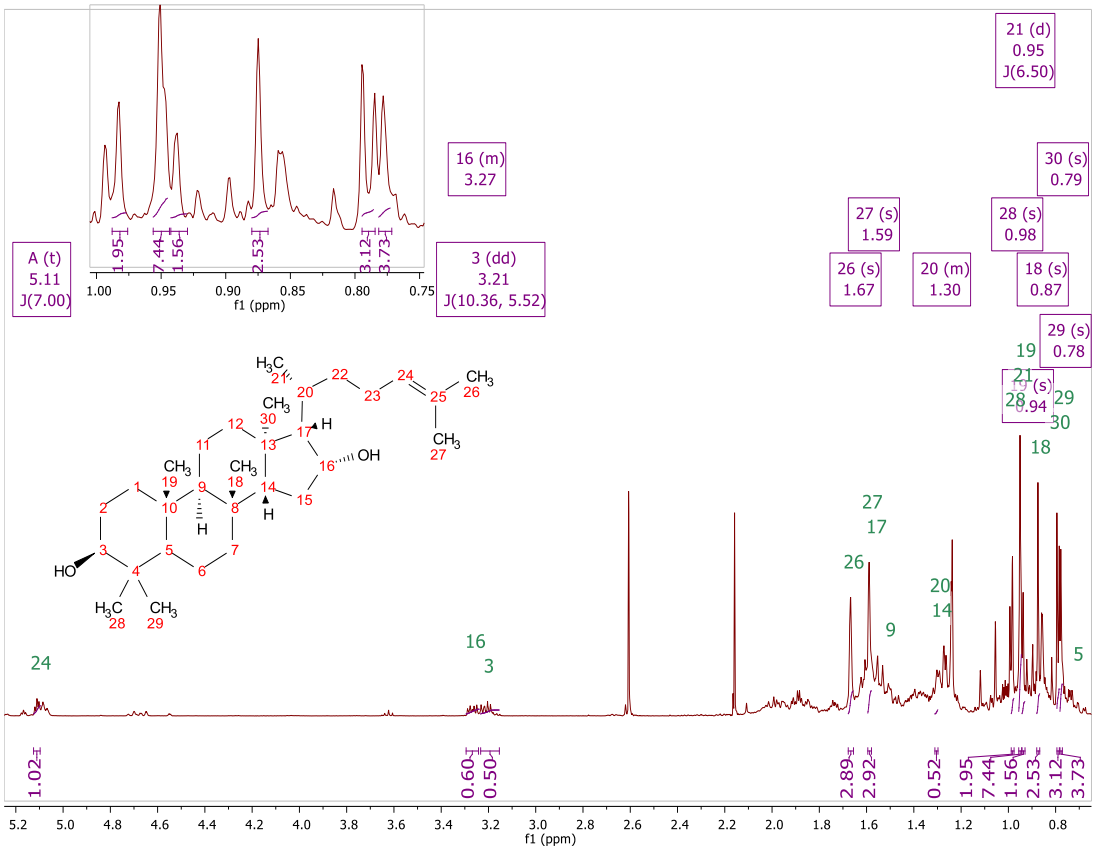

Fig. 3.43: ^{1}H NMR (400 MHz) spectrum of **P17AC2-2** in $CDCl_3$ was obtained on a JEOL-LA400 FT-NMR instrument.

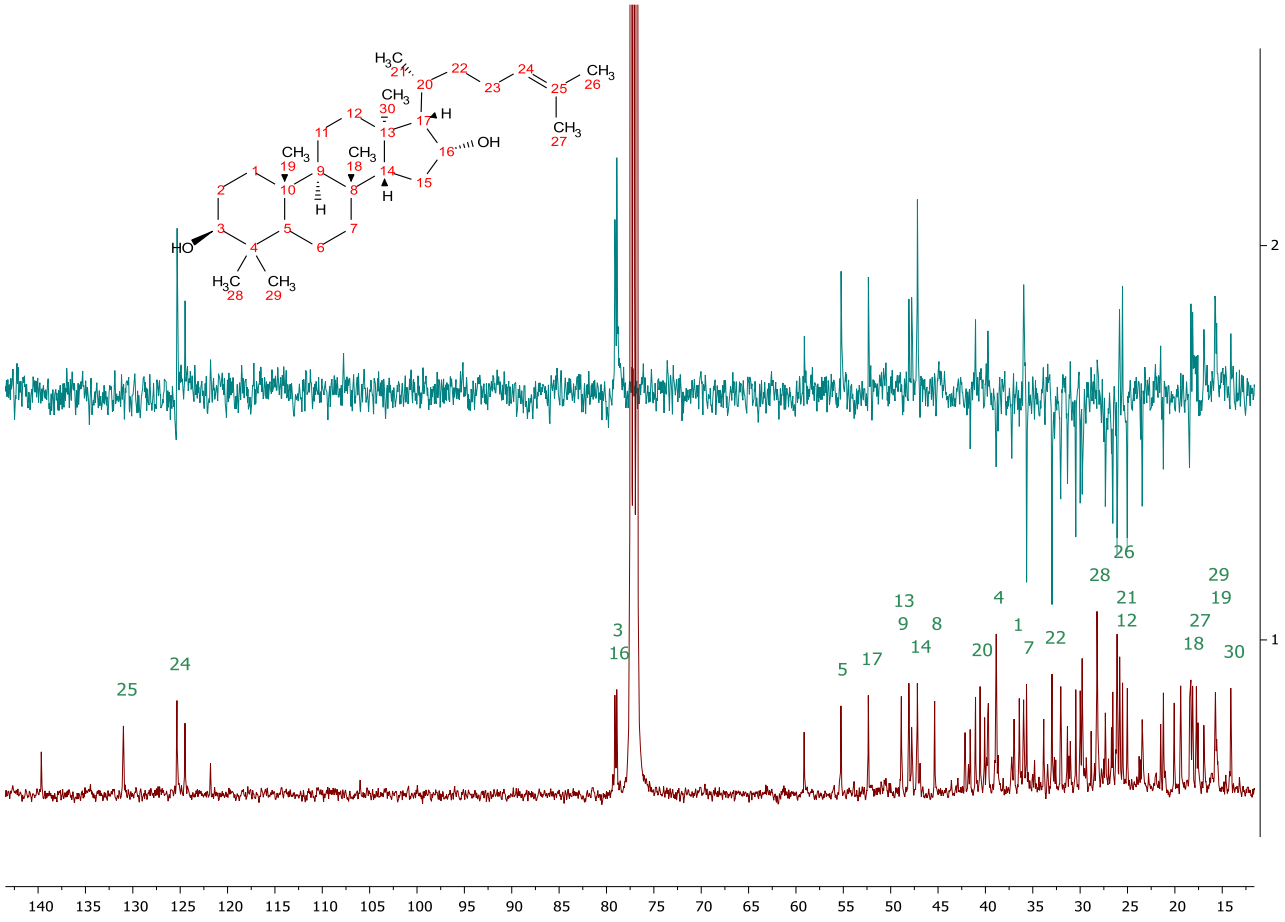

Fig. 3.44: DEPT (above) and ^{13}C (below) spectra of **P17AC2-2** in $CDCl_3$ at 100 MHz.

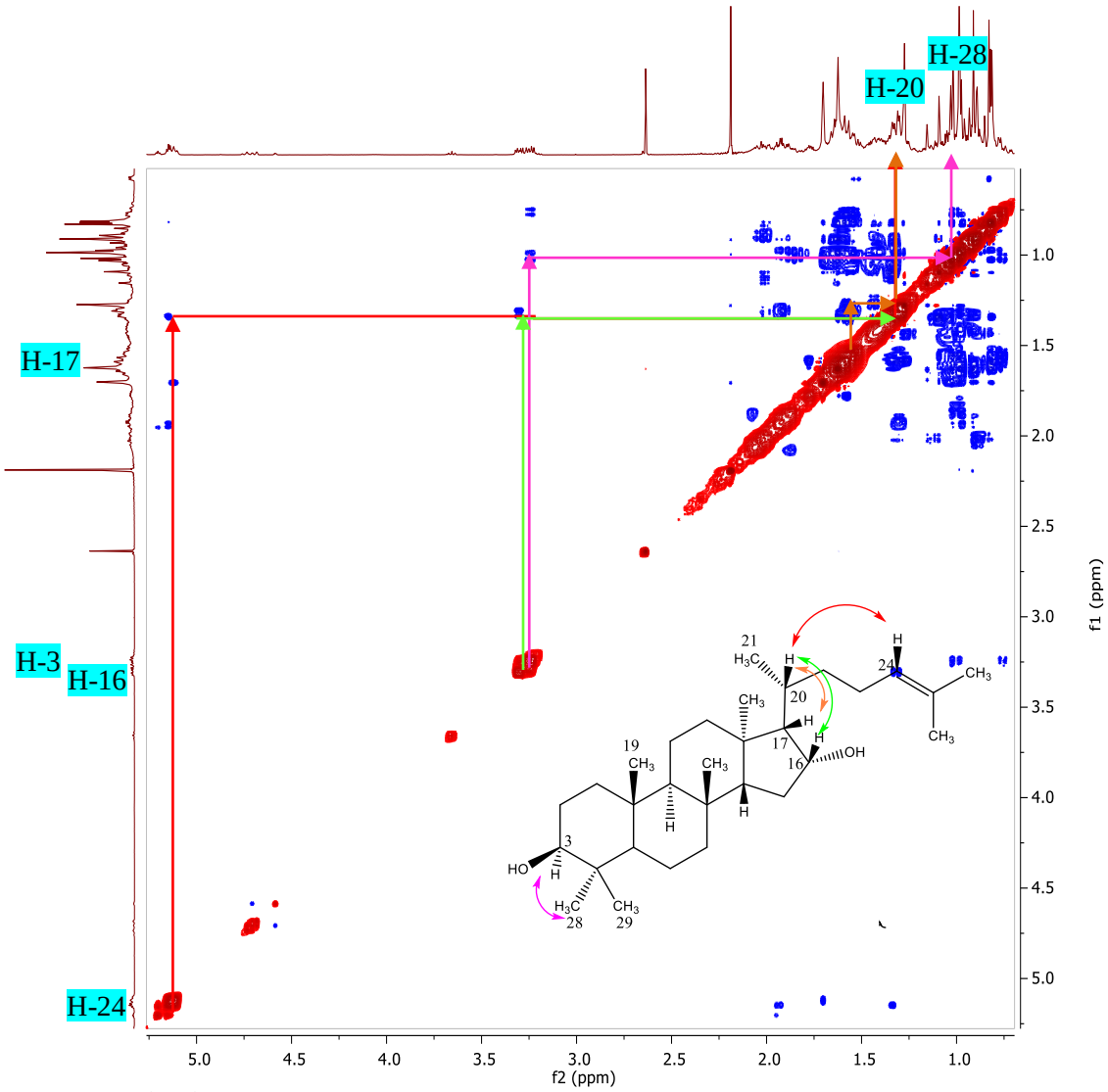

Fig. 3.45: ^{1}H-^{1}H NOESY (400 MHz) spectrum in $CDCl_3$ indicated through space correlation of protons in **P17AC2-2** fraction to establish relative stereochemistry in the isolated nepetadiol.

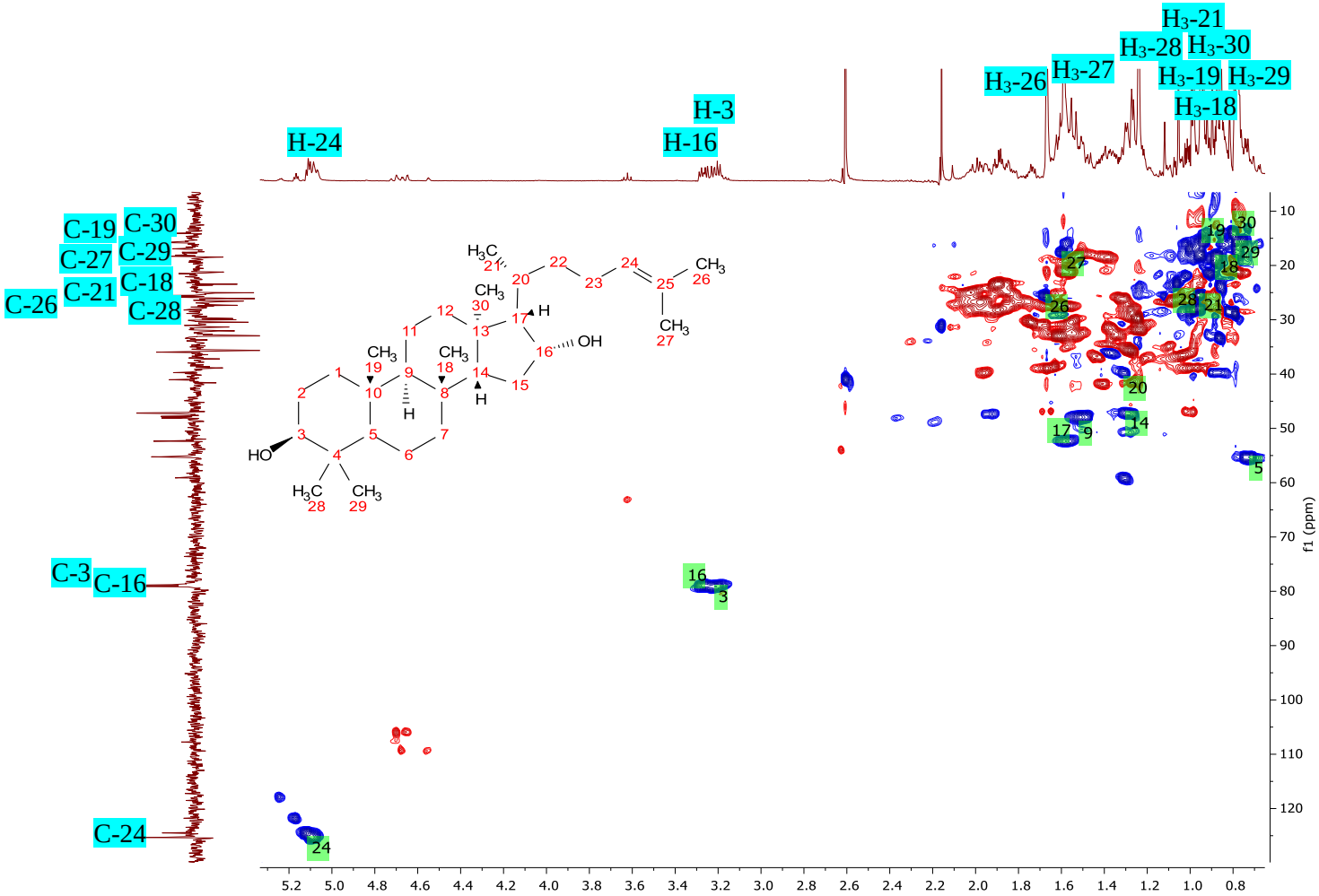

Fig. 3.46: HSQC of **P17AC2-2** in $CDCl_3$ at 400 MHz.

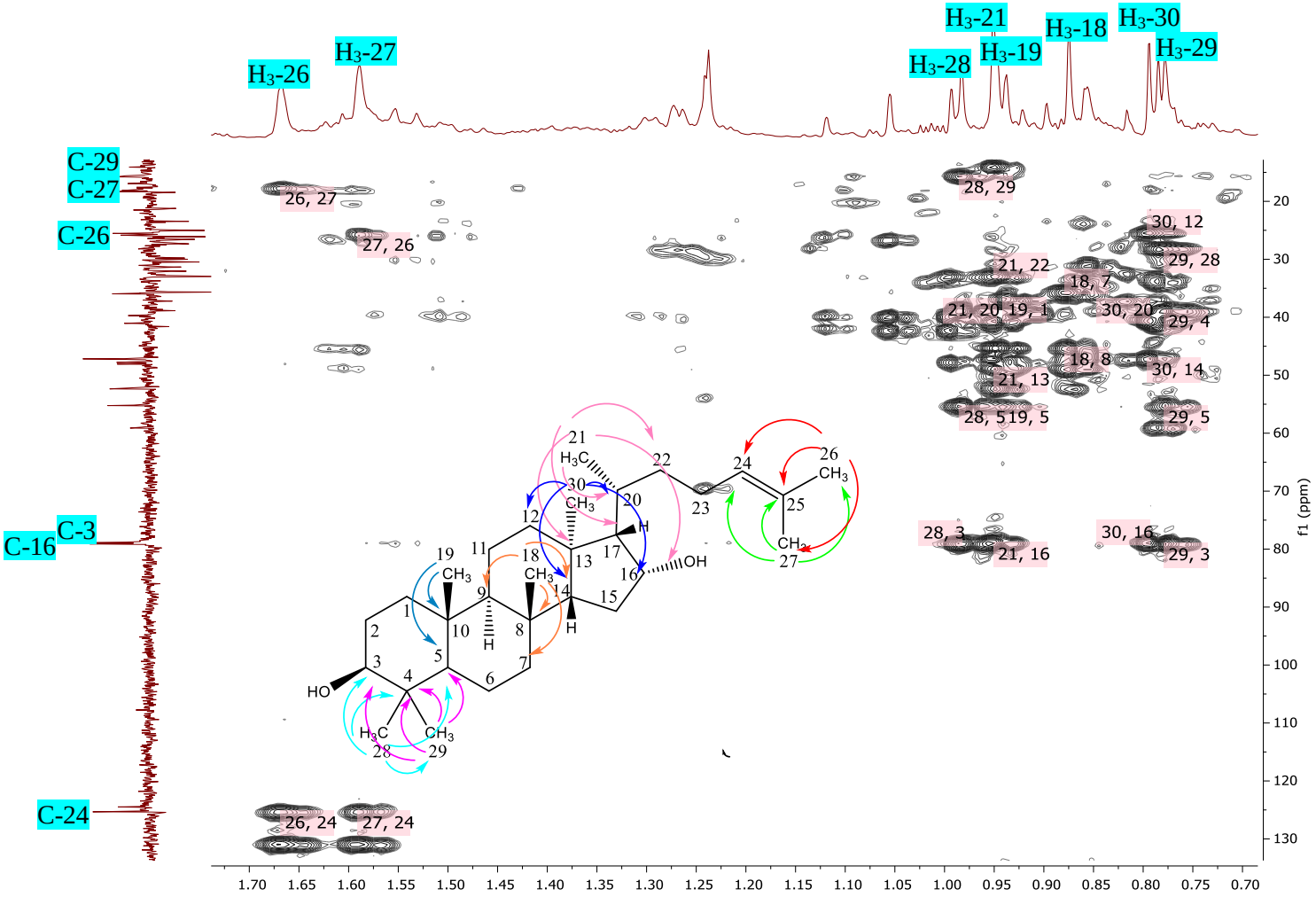

Fig. 3.47: HMBC of **P17AC2-2** in $CDCl_3$ at 400 MHz. The X and Y-axes correspond to the proton and DEPT spectra, respectively.

Table 3.21: ^{1}H NMR ($CDCl_3$, 400 MHz) of compound **P17AC2-2** and comparison with previous data (Khan et al., 2011). Full assignment was deduced from HSQC in $CDCl_3$ at 400 MHz.

Carbon no.	^{1}H NMR, δ_H (multiplicity *J* in Hz)	
	P17AC2-2 in $CDCl_3$	**Literature (Khan et al., 2011) in CD_3OD**
1	1.03, 1.43	-
2	1.60, 1.65	-
OH-3	3.21 (*dd, J* = 5.5, 10.4 Hz)	3.19 (*dd, J* = 4.0, 10.8 Hz)
5	0.72	-
6	1.08, 1.98	-
7	1.00, 1.27	-
9	1.51	-
11	1.31, 1.98	-
12	1.62, 2.03	-
15	1.24, 1.41	-
OH-16	3.27 (*m*)	4.10 (*m*)
17	1.57	-
CH_3-18	0.88 (*s*)	1.04 (*s*)
CH_3-19	0.94 (*s*)	0.94 (*s*)
H-20	1.30 (*m*)	0.98 (*m*)
CH_3-21	0.95 (*d, J* = 6.5 Hz)	1.10 (*d, J* = 6.5 Hz)
22	1.35, 1.61	-
23	1.15, 1.98	-
H-24	5.11 (*t, J* = 7 Hz)	5.23 (*t, J* = 7 Hz)
CH_3-26	1.67 (*s*)	1.68 (*s*)
CH_3-27	1.59 (*s*)	1.69 (*s*)
CH_3-28	0.98 (*s*)	1.18 (*s*)
CH_3-29	0.78 (*s*)	0.93 (*s*)
CH_3-30	0.79 (*s*)	1.11 (*s*)

Table 3.22: DEPT NMR ($CDCl_3$, 100MHz) of compound **P17AC2-2** and comparison with previous data (Khan et al., 2011).

Carbon no.	^{13}C NMR δ_C (ppm)	
	P17AC2-2 in $CDCl_3$	**Literature (Khan et al., 2011) in CD_3OD**
1	36.9 CH_2	40.1 CH_2
2	27.3 CH_2	27.8 CH_2
3	78.9 CH	79.0 CH
4	38.8 C	40.5 C
5	55.4 CH	62.8 CH
6	26.5 CH_2	26.6 CH_2
7	35.8 CH_2	47.8 CH_2
8	45.4 C	42.4 C
9	49.0 CH	50.8 CH
10	40.1 C	40.3 C
11	26.2 CH_2	22.4 CH_2
12	25.5 CH_2	27.7 CH_2
13	49.0 C	50.0 C
14	47.3 CH	42.9 CH
15	41.1 CH_2	42.3 CH_2
16	79.0 CH	77.3 CH
17	52.4 CH	55.2 CH
18	18.4 CH_3	17.8 CH_3
19	15.7 CH_3	17.6 CH_3
20	40.7 CH	39.8 CH
21	25.5 CH_3	25.3 CH_3
22	33.0 CH_2	27.7 CH_2
23	26.8 CH_2	22.9 CH_2
24	125.4 CH	125.9 CH
25	131.0 C	135.5 C
26	25.8 CH_3	23.6 CH_3
27	17.7 CH_3	21.2 CH_3
28	28.3 CH_3	31.4 CH_3
29	15.6 CH_3	16.1 CH_3
30	14.2 CH_3	18.1 CH_3

3.3.5 Biological activities of isolated compounds

As described earlier, five compounds were isolated from Malaysian propolis, namely asiatic acid, hydroxydammarenone-II, 24-(E)-3-oxodammara-20(21),24-dien-27-oic acid, dammarenolic acid and nepetadiol (**Fig. 3.48**). Each of these compounds has selective bioactivities against some cancer cell lines that included lung cancer (A549), ovarian cancer (A2780) and breast cancer (ZR75), as well as its toxicity on normal prostate epithelial (PNT2A) cell lines (**Table 3.23**). Based on *in vitro* experiments, asiatic acid acid was highly effective in preventing the growth of A549, A2780 and ZR75 at IC_{50} values of 52.15, 48.07 and 43.13 µM, respectively. Although asiatic acid was also found toxic on PNT2A at an IC_{50} value of 20.12 µM. Meanwhile, in the case of dammarenolic acid, even though it was toxic on PNT2A, it showed higher IC_{50} value at 49.39 µM, which indicated lesser toxicity than asiatic acid. Moreover, it was also showed mild activity against A549, A2780 and ZR75 with IC_{50} values of 53.58, 41.97 and 45.53 µM. Interestingly, hydroxydammarenone-II, 24-(E)-3-oxodammara-20(21),24-dien-27-oic acid and nepetadiol were nontoxic on PNT2A with their IC_{50} values >100 µM. These latter compounds also exhibited mild cytotoxicity on A2780 with IC_{50} values of 53.58, 44.31, and 50.75 µM, respectively. Based on an *in vivo* experiment, for those compounds that have been tested on zebrafish, only dammarenolic acid gave potent activity on the phenotypic assay at 10 and 20 µM causing curved and curled tails or trunks on zebrafish. Such effects on zebrafish can be related with the interfering of Notch-signalling in cancer cells (**Table 3.24, Fig. 3.49**). None of isolated compounds gave an effect in angiogenicity.

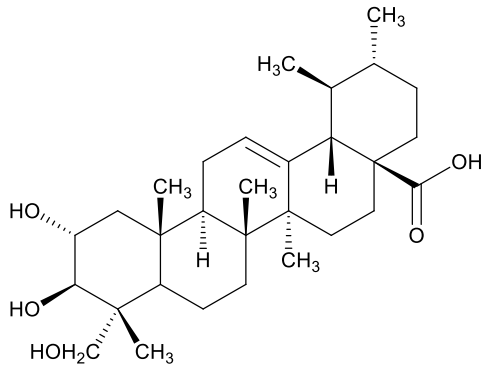

asiatic acid

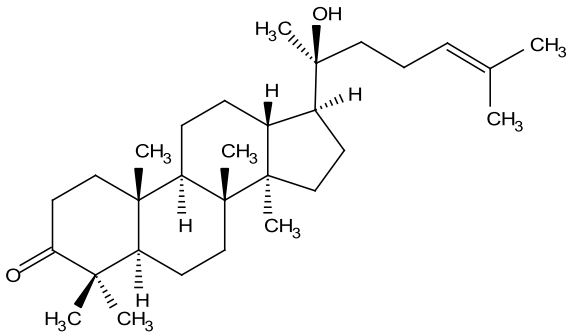

hydroxydammarenone-II

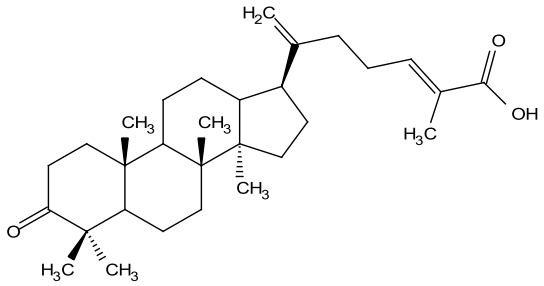

24-(E)-3-oxodammara-20(21),24-dien-27-oic acid

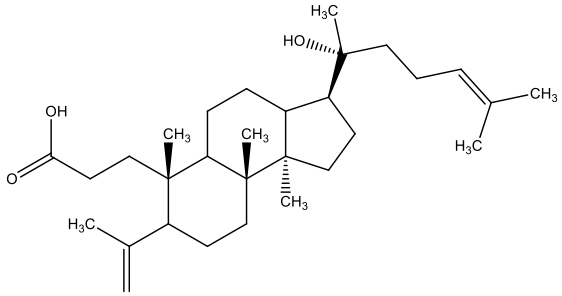

dammarenolic acid

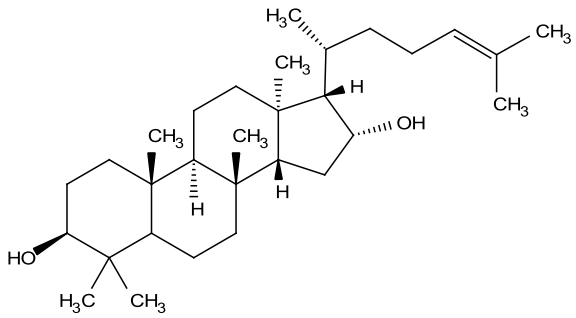

nepetadiol

Fig. 3.48: Structure of isolated compounds from Malaysian propolis indicated that the stereochemistry asiatic acid, hydroxydammarenone-II, 24-(E)-3-oxodammara-20(21),24-dien-27-oic acid, dammarenolic acid and nepetadiolare relative and based on literature data (Cheung and Feng, 1968, Mills, 1956, Torpocco et al., 2007, Brewis and Halsall, 1961, Khan et al., 2011).

Table 3.23: Summary of In-vitro assays of isolated compound. Highlighted cells showed cytoxicity effects on cancer cell lines as compared to PNT2A.

Chemical Name	Cell line [a)]			
	Lung cancer (A549)	**Ovary cancer (A2780)**	**Breast cancer (ZR75)**	**Normal prostate epithelial(PNT2A)**
asiatic acid	52.15±0.658	48.07±0.106	43.13±0.010	20.18±0.191
hydroxydammarenone-II	>100±0.916	53.58±0.535	>100±0.126	>100±0.829
24-(E)-3-oxodammara-20(21),24-dien-27-oic acid	>100±0.457	44.31±0.111	>100±0.027	>100±0.974
dammarenolic acid	53.58±0.777	41.97±0.174	45.53±0.106	49.39±0.081
nepetadiol	>100±0.521	50.75±0.051	>100±0.640	>100±1.000

[a)] IC_{50}(µM), N=3

Table 3.24: Summary of In-vivo phenotypic zebrafish assay treated with isolated compounds.

No.	Chemical Name	Appearance of curved/curled tail/trunk[a]	
		20µM	10µM
1	asiatic acid	N	N
2	hydroxydammarenone-II	N	N
3	24-(E)-3-oxodammara-20(21),24-dien-27-oic acid	N	N
4	dammarenolic acid	Y	Y
5	nepetadiol	N	N

Vehicle control DMSO 0.5%, positive control DAPT 50 µM,
[a)] N=No, Y=Yes
N=3

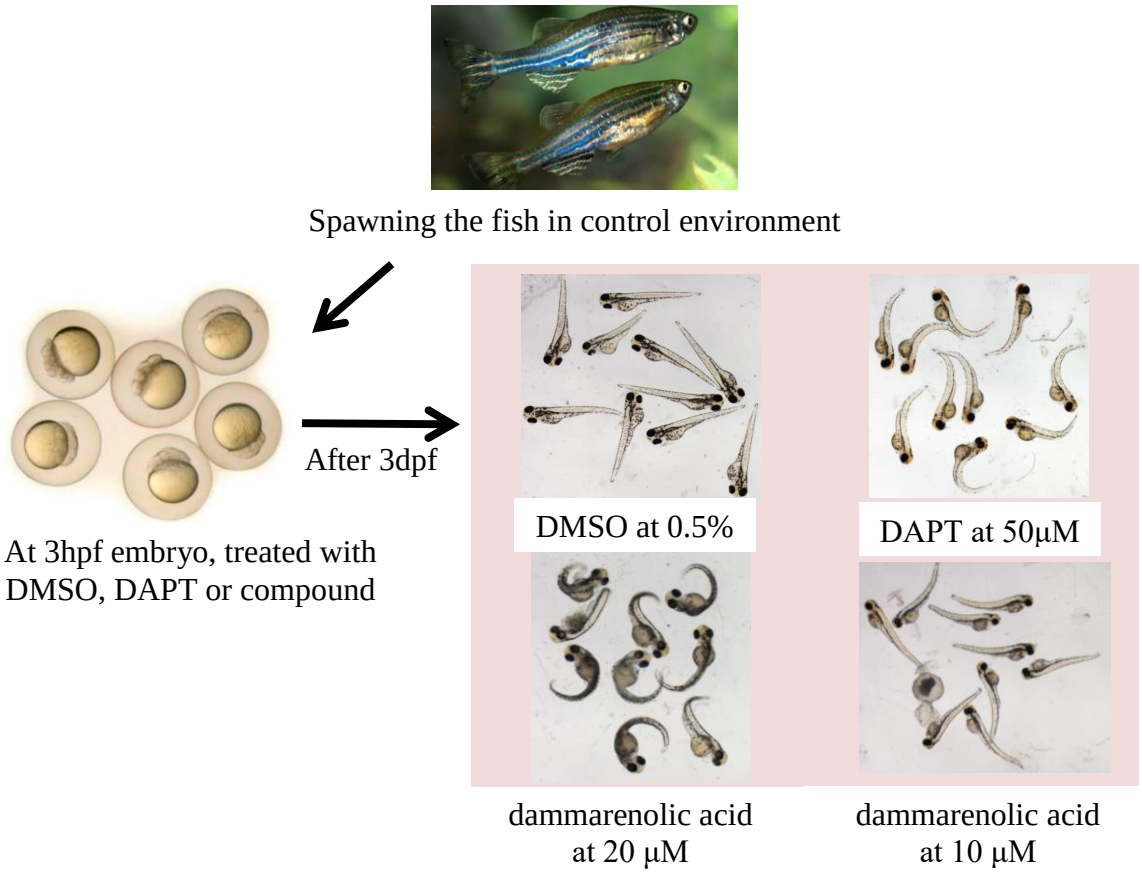

Fig. 3.49: Stages of phenotypic assay. Zebrafish treated with dammarenolic acid at 10 µM and 20 µM were comparable with the negative control showing curled/curved for its tails/trunks as shown in the red box.

3.4 Discussion

3.4.1 Secondary metabolites isolated from Malaysian propolis

3.4.1.1 Triterpenoids from Malaysian propolis

Organic compounds from plant based natural product have played a significant role in preventing and treating human diseases (Newman,Cragg and Snader, 2000). In general, natural products contribute at least 60% and 75% of therapeutic drugs for cancer and infectious diseases, respectively (Newman,Cragg and Snader, 2003). Among this group, terpenes are the largest group of natural products, which is significantly applied in different branch of the industry sectors involving not only in the production of food ingredients, cosmetics, fragrances but as well as pharmaceuticals. The basic unit of a terpene is derived from an isoprene, 2-methylbuta-1,3-diene (C_5H_8) moiety, which undergoes different degree of unsaturation, oxidation, cyclization and rearrangement of the functional groups and ring closures which give rise to other terpene groups (**Table 3.25**) (Ludwiczuk et al., 2017).

Table 3.25: The classification of terpenes.

Name	No. of isoprene units	No. of carbon atom	General formula
Hemiterpenes	1	5	C_5H_8
Monoterpenes	2	10	$C_{10}H_{16}$
Sesquiterpenes	3	15	$C_{15}H_{24}$
Diterpenes	4	20	$C_{20}H_{32}$
Sesterterpenes	5	25	$C_{25}H_{40}$
Triterpenes	6	30	$C_{30}H_{48}$
Tetraterpenes	8	40	$C_{40}H_{64}$
Polyterpenes	More than 8	More than 40	$(C_5H_8)_n$

Based on the number of isoprene units, all five compounds isolated from Malaysian propolis in the present study are classified as triterpenes, particularly triterpenes which carry ursane and dammarane carbon skeleton. The asiatic acid was classified as ursane (Furuya et al., 1987), while hydroxydammarenone-II (Asakawa et al., 1977), 24-(E)-3-oxodammara-20(21),24-dien-27-oic acid (Phan et al., 2011), dammarenolic acid (Esimone et al., 2010) and nepetadiol (Hill and Connolly, 2013) were characterized as dammaranes. According to their biosynthetic pathway, these carbon skeletons were derived from the isopentenyl diphosphate (IPP) and dimethylallyl diphosphate (DMAPP) which are produced from acetyl-CoA via the mevalonic acid pathway (MVA) (Ghosh, 2016). In plants, the MVA pathway operates independently in the cytoplasm to supply IPP and DMAPP for the biosynthesis of triterpenes. Two units of C_5-IPP and a unit of C_5-DMAPP are joined to generate C_{15} farnesyl pyrophosphate (FPP) that is the precursor for the biosynthesis of sesquiterpenes (C_{15}). When two units of FPP are fused together, it generates the linear C_{30} triterpene squalene that serves as a precursor for the biosynthesis of other diverse triterpenes. The epoxidation and cyclization of 2,3-oxidosqualene, which is catalyzed by a family of enzymes known as oxido squalene cyclases (OSC) results in the formation of diverse triterpene carbon skeletons including tetra- and pentacyclic triterpenes, thus forming ursane, dammarane and lanostane triterpene backbone structures. Triterpene biosynthesis pathway has been summarized in **Fig. 3.50**.

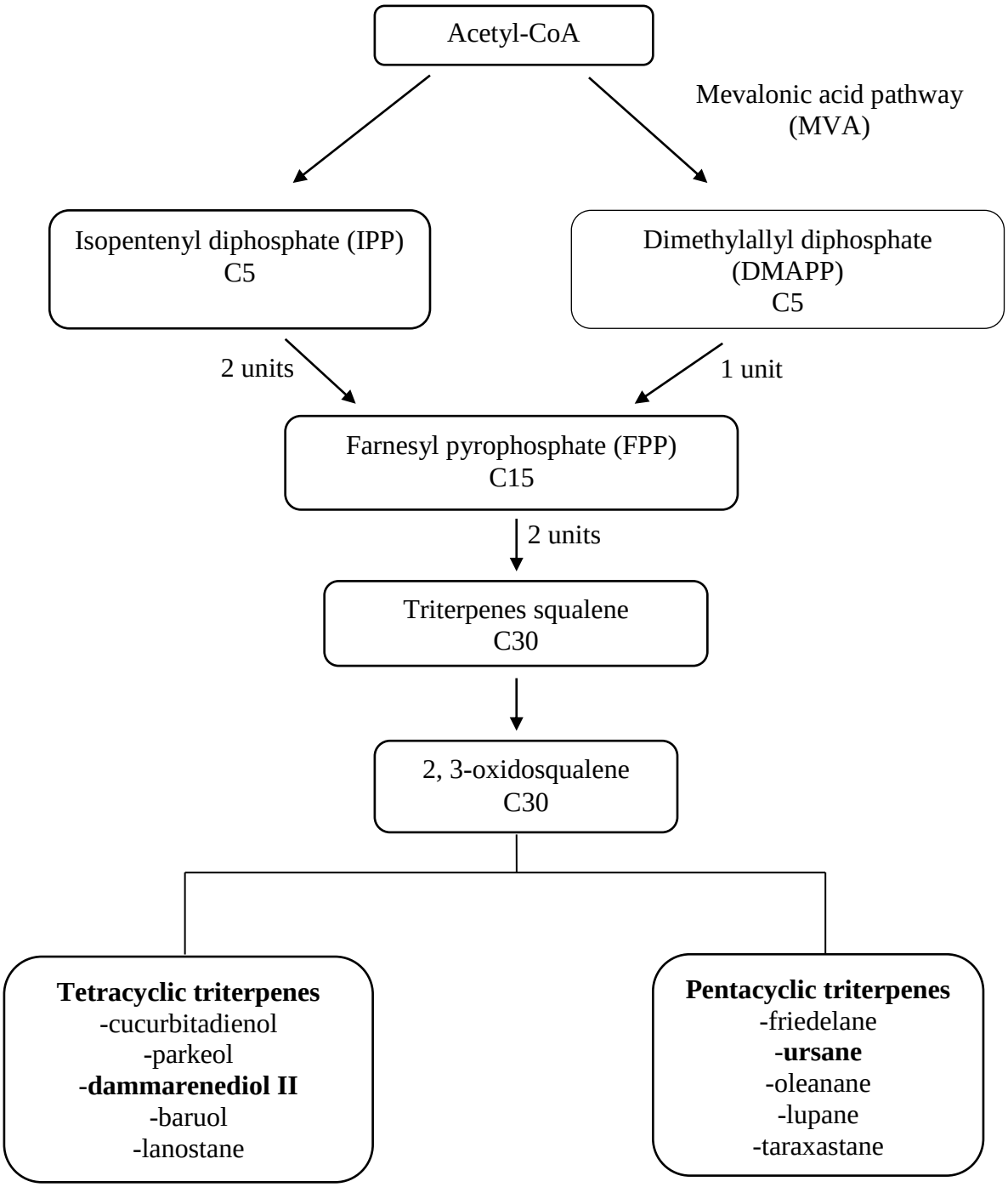

Fig. 3.50: Simplified diagram of biosynthesis pathway for the production of dammarenediol II and ursane (Ghosh, 2016).

Back in nature, terpenes have a specific role in plants to defend itself from pathogens and herbivores (Singh and Sharma, 2015). The direct defence system in plants include physical structures such as trichomes and thorns, as well as phytochemicals derived from diterpenes, for example phytoalexin which is accumulated in the leaves in response to microbial pathogens such as, *Magnaporthe grisea* (Prisic et al., 2004). Besides that, indirect defence system refers to the response towards herbivore threats. The synergistic effects of patchoulol synthase and farnesyl diphosphate synthase, which synthesised the sesquiterpene patchoulol that is accumulated at high levels in *Pogostemoncabli* L., were incorporated into plastids in transgenic tobacco, *Nicotianatabacum* L., thus significantly prevented tobacco hornworms and pine beetles from feeding on leaves (Wu et al., 2006, Bohlmann, 2012).

Interestingly, approximately 30, 000 terpene compounds have been discovered from natural products and to date more of these compounds have been discovered to give promising therapeutic effects on human diseases. Artemisinin and paclitaxel (Taxol®) are respectively among the established drugs for antimalaria and anticancer that were derived from terpenes (Wang et al., 2005). The derived sesquiterpene lactone endoperoxide, artemisinin is highly active against the multidrug-resistant form of *Plasmodium falciparum*. Meanwhile, paclitaxel is an anticancer diterpene-derived agent, while others including ginkgolides, gibberellins and phorbol esters are bioactive diterpenes for PAF inhibitors, plant growth hormones and tumor promoters, respectively. Moreover, among other bioactive triterpenes that includes ginsenosides, betulinic acid, brusatol and boswellic acids have been as adaptogens, anti-melanoma, chemo preventive, anti-inflammatory and anti-arthritic, respectively. In fact, several terpenes were investigated for their medicinal properties via several stages of various clinical trials (**Table 3.26**). Despite many discoveries about the effectiveness of terpenes in different types of human diseases, the ongoing and future phytochemical investigations of terpenes will continue to be a field of exciting new discoveries.

Table 3.26: Several terpenes that under clinical trial.

Classification of terpenes	Terpenes-based drug	Source	Medicinal applications	Literature
sesquiterpene	artemisinin	*Artemisia annua* L	antimalaria	(Brown, 2010)
diterpene	tanshinones	*Salvia miltiorrhiza*	anticancer (breast, liver, colon, stomach, prostate, lung, leukaemia)	(Zhang et al., 2012)
diterpene	ingenol 3-angelate	*Euphorbia peplus* L.	Basal cell carcinoma, squamous cell carcinoma, intraepidermal carcinoma, antileukemic	(Vasas et al., 2012)
diterpene	ginkgolides	*Ginkgo biloba*	Neuro degenerative disorder (Alzheimer, dementia)	(Solfrizzi and Panza, 2015)
triterpene	betulinic acid	*Betula pubescens*	dysplastic nevi (melanoma)	(Csuk, 2014)
triterpene	boswellic acid	*Boswellia serrata*	anti inflammatory	(Abdel-Tawab et al., 2011)
tetraterpene	lycopene	Tomato	prostate cancer	(Huang et al., 2012)
sesterterpene	β-sitosterol	Avocados	anti oxidant, anti inflammatory	(Singh and Sharma, 2015)
monoterpene	D-limonene	*Mentha* spp.	prostate cancer	(Liu et al., 2003)
Diterpene	paclitaxel (taxol®)	*Taxus brevifolia*	anticancer	(Wang et al., 1999)
triterpene	ursolic acid	*Rosemarinus officinalis* *Eriobotrya japonica* *Calluna vulgaris* *Ocimum sanctum* *Eugenia jumbolana*	prostate cancer	(Shanmugam et al., 2012)
monoterpene	1,8 cineole	*Eucalyptus globulus* oil.	skin irritation	(Takaishi et al., 2012)
sesquiterpene	germacranolide, guaianolide, eudesmanolide	*Inula helenium,* *Rudbeckia Subtomentosa*	tuberculosis	(Cantrell et al., 2001)

3.4.1.2 Isolated triterpenes and its configuration-related biological activities.

In the present study, **P9BC (N-640)** appeared as a white powder and was elucidated as asiatic acid. This compound was first described from *Eucalyptus perriniana* cell cuture. The backbone structure of the ursane derivative was validated by the occurrence of six methyl groups where two appeared as doublets and four as singlets, (Furuya et al., 1987). It possessed the structure of 2α, 3β, 23-trihydroxyurs-12-en-28-oic acid based on the coupling constants of H-2 (J = 4.1, 9.7, 10.8 Hz) and H-3 (J = 8.1 Hz), respectively at 3.47 and 3.03 ppm. In 1990, a fraction containing three terpenes including asiatic acid was extracted from *Centella asiatica* (Maquart et al., 1990). For the first time asiatic acid was isolated from a plant, the bark of *Schefflera octophylla* was in 1992 (Sung et al., 1992). Yang and colleagues (2011) have demonstrated potent inhibitory activity of ursane-type triterpenoids isolated from leaves and twigs of *Juglans sinensis* on cell proliferation of immortalized rat hepatic stellate cell line (HSC-T6) by 3-(4,5-dimethylthiazol-2-yl)-2,5-diphenyltetrazolium bromide (MTT) assay. The inhibition of HSC-T6 was considered to delay the fibrosis in the liver, the thickening and scarring of connective tissue in liver due to injury. According to Yang et al., (2011), the ursane type skeleton with the presence of free carboxyl group at C-28 was very important in inhibiting the cell proliferation at 80% of HSC-T6 at 100 μM in comparison with a β-glucopyranoside at C-28 with only 16% inhibition (Yang et al., 2011b). In contrast, other study has reported more potent activities of ursane-type triterpenoids isolated from *Forsythia suspense* leaves with the presence of β-glucopyranoside at C-28 against BGC-823 and/or MCF-7, respectively gastric and breast cancer cell lines, with IC_{50} values of $\leq$19 μM by MTT assay in comparison with a carboxyl group at the same position with IC_{50} value at 40 μM (Ge et al., 2016). The present study has determined the anti-cancer activities of **P9BC** by the Alamar blue assay and was shown to effectively prevent the growth of A549, A2780 and ZR75 at IC_{50} values of 52.15, 48.07 and 43.13 μM, respectively. However, **P9BC** was also toxic on PNT2A at IC_{50} value 20.12 μM.

P8BC2-3&4 (P_10706) was elucidated as hydroxydammarenone-II, which was isolated as a white sticky material. Hydroxydammarenone-II was isolated from ginseng (Asakawa et al., 1977). Later in 1987, hydroxydammarenone-II was isolated from *Dipterocarpus crinitus* locally known as Keruing mempelas, collected from reserve forest of Malacca, Malaysia (Shimadad et al., 1987). In 1991, hydroxydammarenone-II was also isolated from another species of the genus *Dipterocarpus* known as *D.tubinatus* (Wang et al., 1991). The structure of hydroxydammarenone-II that is an 18S-isomer was distinguished from hydroxydammarenone-I, an 18R-isomer by the ^{13}C NMR chemical shift of C-28 reported at δ25.4 from the literature (Yamashita et al., 1998), which was observed at δ26.7 in the present study that is compatible for the 18S-isomer. The cytotoxicity activity of hydroxydammarenone-II on leukemia (HL60) and melanoma (CRL1579) human cell lines were demonstrated by MTT assay to give EC_{50} values of 19.2 and >100 µM, respectively (Ukiya et al., 2010). In addition, hydroxydammarenone-II also exhibited an IC_{50} value of 341 molar ratio/32 pmol TPA against Epstein – Barr Virus Early Antigen (EBV-EA) derived from Burkitt's lymphoma. On the other hand, the present study showed the cytotoxicity effects of the isolated hydroxydammarenone-II on A2780 with an IC_{50} value of 53.58 µM.

P4EC7 (N_1900) was isolated as a white crystal and elucidated as 24-(E)-3-oxodammara-20(21), 24-dien-27-oic acid that was first isolated from the leaves of *Alnus nepalensis*, a native species in Vietnam (Phan et al., 2011). The position of the C-24/C-25 double bond was confirmed to follow the (E) configuration by comparing the ^{13}C NMR chemical shifts of C-24, C-25 and C-26 at δ144.2, 126.4 and 11.6, respectively with those reported in the literature for C-24 (δ144.7), C-25 (δ127.1) and C-26 (δ12.1). Furthermore, the (E) geometry in the isolated compound was also comparable with previous reports. Ganoderic acid AP2 was described to have the 24-(E) geometry reported similar chemical shifts for C-24 at δ144.7, C-25 at 127, and C-26 at 12.1(Wang and Liu, 2008). Alternatively, for 24-dien-27-oic acid, 24-(Z)-3-oxodammara-20(21),24-dien-27-oic acid, C-24, C-25and C-26 were observed at δ146.2, 137.8, and 20.5 (Torpocco et al., 2007) ,which were incompatible with the chemical shifts of the isolated compound **P4EC7**. Thus confirming the structure of

P4EC7 as 24-(E)-3-oxodammara-20(21), 24-dien-27-oic acid. 24-(E)-3-oxodammara-20(21), 24-dien-27-oic acid was found to be nontoxic on a set of isogenic yeast strains defective for the G1/S and G2/M DNA damage checkpoint, which suggested not to exhibit antifungal activity. The present study demonstrated the cytotoxicity of the isolated 24-(E)-3-oxodammara-20(21), 24-dien-27-oic acid on A2780 with an IC_{50} value of 44.31 µM.

P5EC12 (P_98) was isolated as a colourless oily material, which have been previously isolated from the bark of *Aglaia ignea* found in Southeast Asian region (Esimone et al., 2008). It has shown strong inhibitory activity against respiratory syncytial virus (RSV) with an IC_{50} value of 0.1 µg/ml. A complete structure elucidation of dammarenolic acid (ignT1) was reported by Esimone and colleagues in 2010. Dammarenolic acid also showed potent response against several viruses including human immunodeficiency virus (HIV-1), simian immunodeficiency virus (SIV) and murine leukaemia virus (MLV) atleast with IC_{50} values of 3 µg/ml (Esimone et al., 2010). The ^{13}C NMR chemical shift from the literature for C-4 and C-20 at δ179.8 and δ75.6, respectively were consistent with those of P5EC12 for C-4 (δ178.1) and C-20 (δ75.0), thus indicating the presence of carboxyl and hydroxyl group in the structure. Furthermore, the relative stereochemistry of the isolated compound was comparable with the 1D and 2D NMR data from the literature. Therefore, confirming the structure of **P5EC12** to be dammarenolic acid. Furthermore, dammarenolic acid have been isolated from *Shorea javanica* exhibiting an IC_{50} value of 226 molar ratio/32 pmol TPA and EC_{50} at 13.5 µM against Epstein – Barr Virus Early Antigen (EBV-EA) derived from Burkitt's lymphoma and human leukaemia cell line (HL-60), respectively (Ukiya et al., 2010). The weak cytotoxicity effect on CRL-1579 was reported with EC_{50} values >100 µM. In the present study, the isolated dammarenolic acid demonstrated cytotoxicity effects on A549, A2780 and ZR75 with IC_{50} values of 53.58, 41.97 and 45.53 µM, respectively. On the other hand, the notch-signalling pathway is crucial in cell proliferation, differentiation and for stem cell maintenance. Notch signalling is active during trunk/tail development in embryogenesis of zebrafish (Velaithan et al., 2017). Over expression of Notch signalling could be associated with acute human T

cell lymphoblastic leukemia, head and neck squamous cell carcinomas, brain tumor, renal carcinoma and oral cancer (Weng et al., 2004, Sun et al., 2014, Purow et al., 2005, Sjölund et al., 2008, Velaithan et al., 2017). Therefore, through a zebrafish phenotypic assay, identifying the phenotypic alteration in zebrafish could provide a promising biomarker in human disease study. Interestingly, dammarenolic acid demonstrated to give positive effects on the alteration of zebrafish phenotype at concentrations of 10 and 20 µM.

P17AC2-2 (P_10029) was isolated as a white powder and elucidated as nepetadiol, which was first described from *Nepeta suavis* (Khan et al., 2011). *Nepeta* is a genus of flowering plant consists of atleast 250 species are native to Europe, Asia and Africa (Cotrim et al., 1994). Nowadays a few *Nepeta* species is cultivated for ornamental plant, including *N. suavis, N. cataria, N. grandiflora and N. racemosa.* The β configuration of the hydroxyl-bearing C-3 with a proton coupling constants of 5.5 and 10.4 Hz at 3.21 ppm for P17AC2-2 was compatible with that reported in the literature. Furthermore, the ^{13}C NMR chemical shift of C-28 was observed more downfield at δ28.3 caused by the coupling effects of the β-oriented hydroxyl unit on C-3. Moreover, based on the NOESY spectra, a cross peak was observed between H_3-28 and H-3 which further confirmed the 3β-orientation of the hydroxyl moiety. Meanwhile the position of C-16 was determined based on its ^{13}C NMR and HSQC spectra at δ79.0, thus indicating the presence of hydroxyl group on its carbon, which caused the chemical shift of C-17 to be more downfield at δ52.4. In addition, the β-orientation of hydroxyl-bearingC-16 was determined by comparing the ^{13}C NMR of C-15 (δ41.1), C-16 (δ79.0) and C-17 (δ52.4) of **P17AC2-2** with the literature for C-15 (δ42.3), C-16 (δ77.3) and C-17 (δ55.2). Therefore, this compound was confirmed to be 3β, 16β- dihydroxy-dammar-24-ane. The present study demonstrated the cytotoxicity of nepetadiol on A2780 with an IC_{50} value of 50.75 µM.

Table 3.27 summarised the biological activities of the isolated reported in the literature since 2010. Taken together, it can be summarised that the biological activities of the triterpenes were quite selective and could be related with the different targeted bioassay as well as affected by the conjugation of carboxylic or hydroxyl groups in their structures. All the biological activities of the isolated triterpenes in this study against A2780, A549 and ZR75 were reported for the first time. The fractionation of BC, EC, and AC propolis extracts were performed using high-throughput flash and MPLC chromatography. The BC extract yielded two triterpeniod derivatives, namely asiatic acid (Furuya et al., 1987) and hydroxydammarenone-II (Asakawa et al., 1977). Meanwhile the EC extract afforded two triterpenoids elucidated as dammara-20, 24-dien-26-oic acid, 3-oxo-, 24*E* (Phan et al., 2011) and dammarenolic acid (Esimone et al., 2010). The AC extract yielded only one triterpenoid, elucidated as nepetadiol (Khan et al., 2011). Highest cytotoxicity against A2780 was observed with a carboxylic moiety as in the structures of dammarenolic acid, 24-(E)-3-oxodammara-20(21),24-dien-27-oic acid and asiatic acid, followed by nepetadiol and hydroxydammarenone-II. In addition, only asiatic acid and dammarenolic acid showed cytotoxicity against A549 and ZR75 which can also be related with the occurrence of carboxyl and hydroxyl units in their structures. Notably, dammarenolic acid was the only triterpenoid that can interfere the Notch signalling in zebrafish which could be due to the presence of carboxyl, hydroxyl and olefinic groups in its structure. It was also concluded that the major bioactive compounds isolated from both Johor and Malacca propolis were all triterpenes, which suggested the high incidence of homogenous plants at the southeast part of Peninsular Malaysia which was dominated by *Dipterocarpaceae* species. Hence, the present study also suggested that *Trigona* sp. bees were more favourable to collect propolis from the same species of plants even though they were breeding at different areas in Johor and Malacca.

Table 3.27: Biological activities of isolated compounds as reported in the literature since 2010.

Chemical Name	Reported Activity/Literature	Source
asiatic acid	1) Stimulated the effect on collagen synthesis in human skin fibroblasts (Bylka et al., 2014)	*Centella asiatica*
	2) Antimalaria agent (Zhang et al., 2013)	Synthetic
	3) Inhibit liver fibrosis (Tang et al., 2012)	Purified natural product
	4) Inhibit pro-angiogenic effects of VEGF and human glioma (Kavitha et al., 2011)	Synthetic
hydroxydammarenone-II	1) Treatment of hypercholesterolemia or atherosclerosis via inhibitory effect on hACAT (Kim et al., 2010)	*Rhus chinensis*
	2) Inhibit HL-60 and EBV-EA (Ukiya et al., 2010)	*Shorea javanica*
	3) Antiparasitic on *T. bruceigambiense* (Mai et al., 2016)	*Gardenia urvillei*
24-(*E*)-3-oxodammara-20(21),24-dien-27-oic acid	1) Nontoxic to isogenic yeast defective DNA damage (Z type) (Torpocco et al., 2007)	*Maytenus macrocarpa*
dammarenolic acid	1) Antiretroviral in HIV-1, SIV and MLV (Esimone et al., 2010)	*Aglaia* sp.
	2) Inhibit HL-60 and EBV-EA (Ukiya et al., 2010)	*Shorea javanica*
Nepetadiol	NA	NA

NA= Not applicable

CHAPTER 4

4 Manuka New Zealand propolis secondary metabolites and its bioactivities

4.1 Introduction

Much research has been done to investigate the major compounds in honey from Manuka. Some have been identified as caffeic acid, isoferulic acid, p-coumaric acid, gallic acid, 4-hydrobenzoic acid, syringin acid, quercetin, luteolin, 8-methoxykaempferol, pinocembrin, isorhamnetin, kaempferol, chrysin, galangin, pinobanksin, phenyllactic acid, 4-methoxyphenolactic acid, kojic acid, 5-hydroxymethylfurfural, 2-methoxybenzoic acid, phenylacetic acid, methyl syringate, dehydrovomifoliol, leptosin, glyoxal, methylglyoxal, and 3-deoxyglucosulose (Oelschlaegel et al., 2012, Adams et al., 2009, Mavric et al., 2008, Chan et al., 2013). Meanwhile, the major organic constituents in New Zealand propolis have been identified in tincture solution. These include cinnamic acid, pinobanksin, pinocembrin, pinobanksin 3-acetate, 1,1-dimethyl-allylcaffeic acid, chrysin, galangin, pinocembrin 7-methyl ether, chrysin 7-methyl ether and galangin 7-methyl ether (Markham et al., 1996). Other studies reported isoprenylcaffeate as a major compound in Manuka propolis, in addition to pinocembrin, galangin, chrysin, apigenin, caffeic acid phenethyl ester and caffeic acid and other non-flavonoid constituents (Gemiarto et al., 2015, Demestre et al., 2009). Processed Manuka propolis was safe to consume as food supplement at a dose of 25 mg/kg via oral intake for melanoma and pancreas cancer patients. It can mutate the secretion of RAS thus deactivating the production of PAK1 that is responsible for triggering the disease (Demestre et al., 2009). A recent study also investigated the anti-pathogenic ability of New Zealand propolis through inhibiting the growth of *Chromobacterium violaceum,* as an initiative to develop an antibiotic for antibiotic-resistant bacterial infections (Gemiarto et al., 2015). Even though the therapeutic properties of propolis from New Zealand have been explored for quite some time, the study is not as thorough as those that have been done on honey. Therefore, the present study was focused on the isolation of bioactive compounds from New Zealand Manuka propolis

on A549, ZR75, A2780 on lung, breast and ovary cancer cell lines respectively, as well as on the cytotoxicity on normal prostate epithelial cell line (PNT2A).

4.2 Materials and methods

4.2.1 Propolis

Fresh New Zealand propolis was obtained from Dr. Young from the Honey New Zealand (International) Ltd. The sample was kept at room temperature until further use (**Table 4.1**). The extractions of crude propolis were conducted as mentioned in section *2.4.1* and **Table 4.2** showed the weights of propolis extracts after solvent partitioning.

Table 4.1: Summary details about the New Zealand propolis used.

ID	TYPE OF BEE	COLOUR	GEOGRAPHICAL AREA	DISTRIBUTOR
F	*Apis mellifera*	Yellow	North and South Island of New Zealand	Honey New Zealand (International) Ltd (Dr. Young)

Table 4.2: The weights of propolis extracts after solvent partitioning.

Sample ID	Initial raw sample weight (g)	Sample ID	MeOH:H_2O (1:1) extract weight (g)	Sample ID	MeOH:Acetone (1:1) extract weight (g)
F	25.0	FO	10.0	FC	10.0

4.2.2 Isolation of New Zealand crude yellow propolis extract (FC) using GRACE® MPLC

Medium pressure liquid chromatography (MPLC) was used to isolate the pure compounds from FC extract (10.0g). Two solvents, Solvent A (MeOH) and Solvent B (DCM), were used for elution at a flow rate of 40 ml/min, which was suitable for a sample load of 40 mg to 8.0g. A silica column from Reveleris® (GRACE, USA) was used in MPLC with a particle size of 40 µm and a column volume of 48 ml. The chromatographic run started with elution of 100% B for 5 min for equilibration, followed by a linear gradient elution from 0% to 1% A for 15 min, continued with 5% A for 25 min and then 50% A for another 20 min. The column was washed with 50% A for the last 15 min. The fractions were collected by peak detection through a fraction collector in 20 ml test tubes, resulting in 57 fractions. All fractions were subjected to TLC profiling and those with the same chromatogram were pooled together, yielding 11 fractions (**Fig. 4.1**).

4.2.2.1: Isolation and purification of secondary metabolites from FC extract.

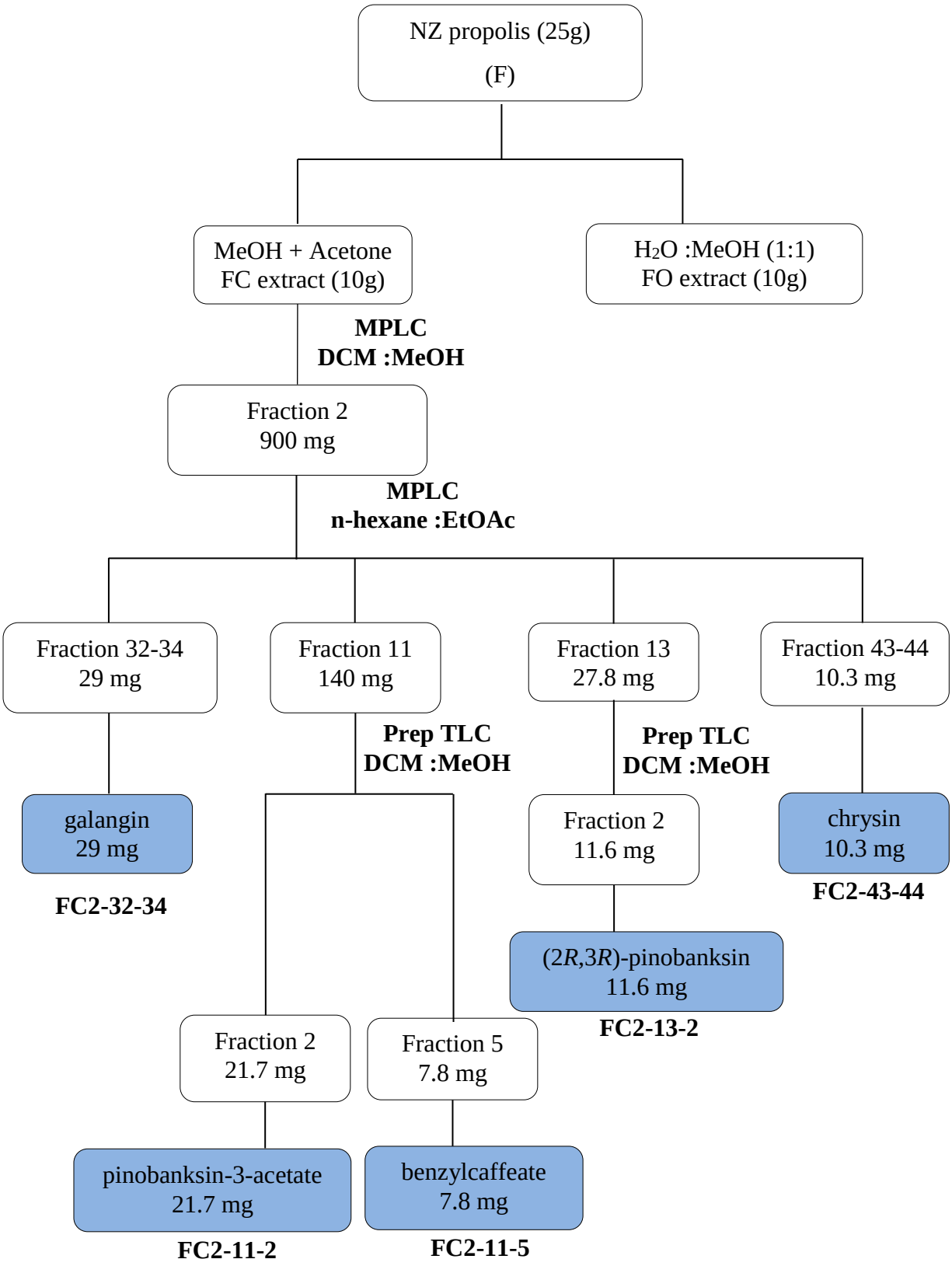

Fig. 4.1: Summary diagram of the New Zealand (NZ) propolis extraction and fractionation.

4.3 Results

4.3.1 Metabolomic- and bioassay-guided decision making for further isolation of secondary metabolites from New Zealand propolis

The propolis sample from New Zealand was extracted using a 1:1 ratio of water to MeOH, followed by using acetone and MeOH to obtain the organic and crude extracts, respectively. All extracts were subjected to ^{1}H NMR analysis (**Fig. 4.2**). The FC extract (10g) was chosen for further isolation work because this extract was less complex but contained interesting^{1}H NMR resonances. Dense signals were observed at 5.0 – 8.5 ppm within the aromatic region, which indicated the presence of phenolic compound derivatives (highlighted blue). The signals at the most downfield region were observed within 9.5 – 13.0 ppm, which were possibly related to oxygenated proton such as hydroxyl group (highlighted green). Meanwhile, FO extract was not chosen because the compounds it contained were relatively similar to FC but with a denser set of resonances at the sugar region (3-5 ppm), therefore the more interesting compounds will be more complicated to isolate.

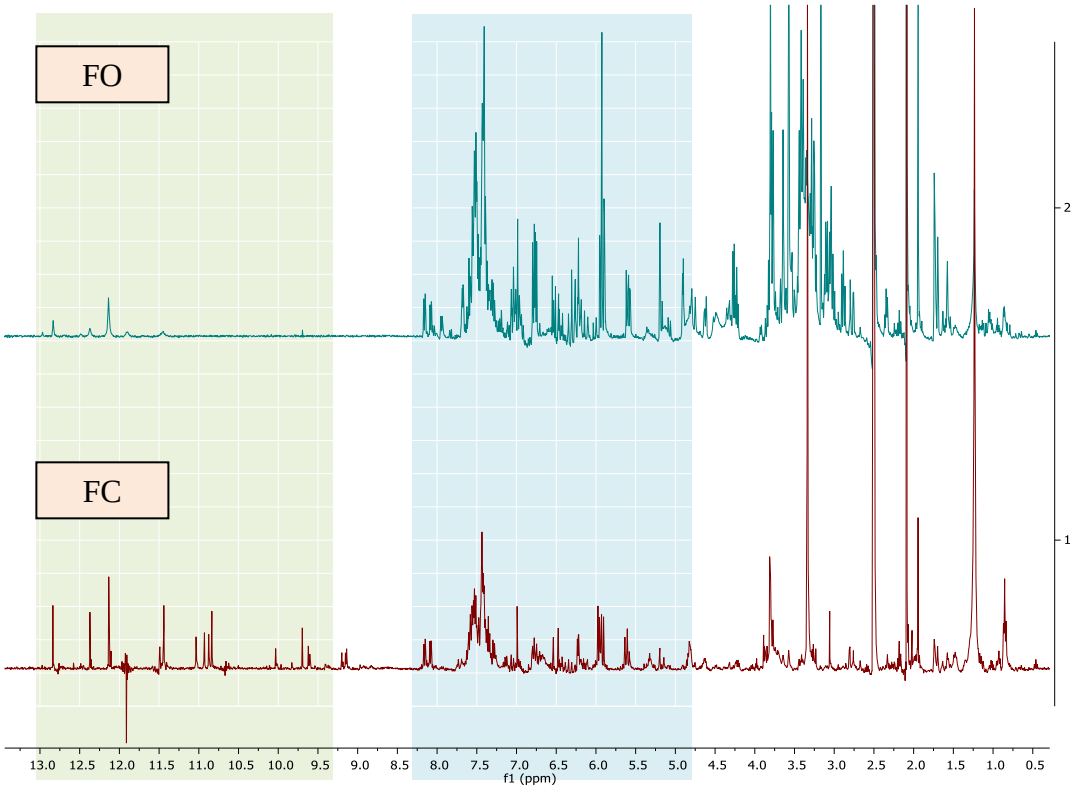

Fig. 4.2: ^{1}H NMR spectra of crude extracts. DMSO-d_6 was used as solvent.

Fig. 4.3 shows the TLC of crude extracts that were eluted using 9:1 DCM:MeOH, which further demonstrated the similarity of FO and FC extracts. Both extracts exhibited good separation of the diverse components contained in those extracts. The isolation of FC extract was considered less complicated as compared to FO extract, in support of the appearance of UV-active bands on the TLC, which indicated the occurrence of aromatic compounds as supported by the ^{1}H NMR spectrums.

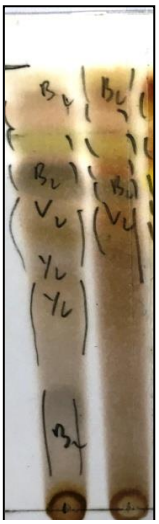

FO FC

Fig. 4.3: TLC of crude New Zealand propolis samples showing good separation of diverse components.

Table 4.3: Biology assay screening of New Zealand propolis extracts on A549 and A2780 cell line. Bioactivity threshold was set at ≤40%.

Sample ID	**Antiproliferative effects at 100µg/ml (Viability % of control)**	
	Lung cancer cell line (A549)	**Ovarian cancer cell line (A2780)**
FC	39	15
FO	43	30

Based on the bioassay screening results (**Table 4.3)**, the FC extract exhibited stronger bioactivity on A549 and A2780 cell line. Therefore, the FC extract was chosen for further fractionation and isolation based on ^{1}H NMR resonances, TLC, and its potent bioactivity against A549 and A2780.

4.3.2 Secondary metabolites isolated from FC propolis

The fractionation of FC extract was done by MPLC technique using DCM and MeOH as eluting solvents affording 45 fractions. TLC was done to monitor the fractions that will be pooled together, yielding eleven fractions from FC extract (FC1, FC2, FC3, FC4, FC5, FC6, FC7, FC8, FC9, FC10 and FC11). The ^{1}H NMR spectrum for FC1 (264 mg), FC2 (900 mg) and FC4 (750 mg) (**Fig. 4.4**) showed unique chemical fingerprints only observed in these respective fractions with high intensity resonances. Based on the cytotoxicity assay of the fractions on A549, bioactivity was observed at a concentration of 100 µg/ml for FC2 exhibiting 24% cell viability in comparison to the control, followed by FC4 at 32% on the same concentration (**Table 4.4**). TLC of FC2, FC3, and FC4 showed good separation with diverse components (**Fig. 4.5**).

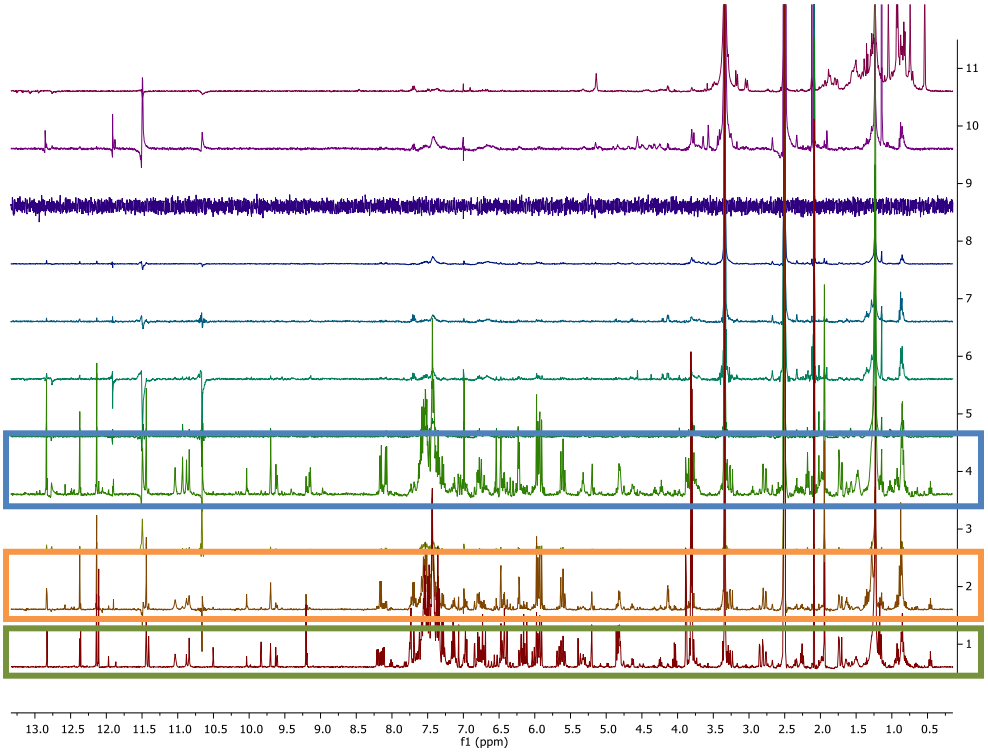

Fig. 4.4: ^{1}H NMR spectra from New Zealand propolis fractions using JEOL-LA400 FT-NMR instrument in DMSO-d_6. The spectrum of FC1, FC2 and FC4 showed several unique chemical fingerprints highlighted with coloured boxes. The spectra shown were labelled from bottom; FC1, FC2, FC3, FC4, FC5, FC6, FC7, FC8, FC9, FC10 and FC11.

Table 4.4: Biology assay screening of FC fractions on A549, cytotoxicity effects on cell line viability in comparison to control. Bioactivity threshold was set at ≤40%.

Sample ID	Antiproliferative against lung cancer A549 100µg/ml (Viability % of control)
FC1	62
FC2	24
FC3	34
FC4	32
FC5	100
FC6	100
FC7	100
FC8	100
FC9	91
FC10	93
FC11	100

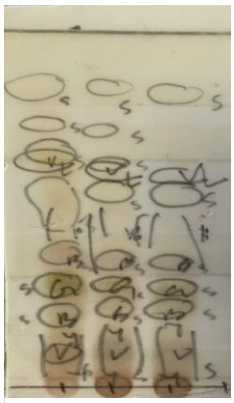

FC2 FC3 FC4

Fig. 4.5: TLC for FC propolis fractions that showed the highest activity against A549.

As observed from the PCA scores scatter plot in **Fig. 4.6A**; FC1, FC2, FC3, and FC4 were all found on the right side of the ellipse but were dispersed into two quadrants, indicating unique chemical profiles for each of this fraction. There were 11 variables being analysed in this model. Both R^2 and Q^2 values were measured at 0.99 and 0.69, respectively. On the OPLS-DA scores scatter plot (**Fig. 4.6B**), the biological fractions FC2, FC3, and FC4 were clustered on one part of the ellipse but were still considered discrete from each other. For the OPLS-DA model, both R^2 and Q^2 values were measured at 0.93 and 0.83, respectively, which indicated a good-fitted model (R^2), and good prediction of variables (Q^2). The permutation test was observed at -0.4 of Q^2 value, indicating a good-valid model. The discriminating metabolites obtained from the S-plot (**Fig. 4.7**) and listed in **Table 4.5** could be predicted as the compounds that could be responsible for the bioactivity in both fractions. Unknown compounds with molecular weights between 150 – 417 g/mol were at their highest intensity in FC2 and FC3 fractions.

A)

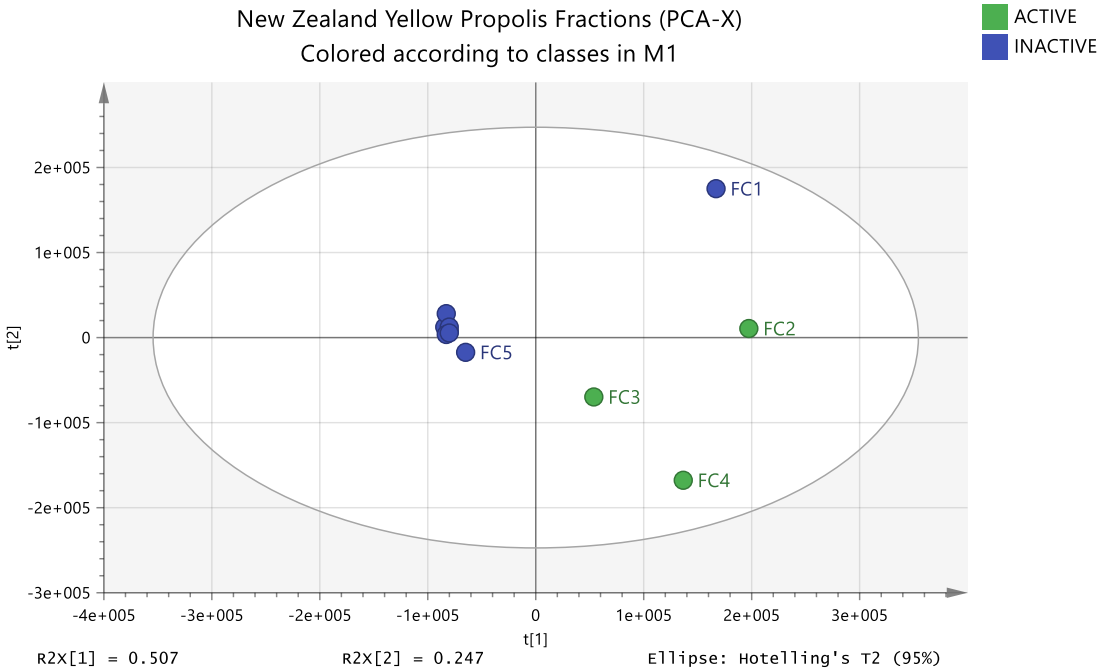

B)

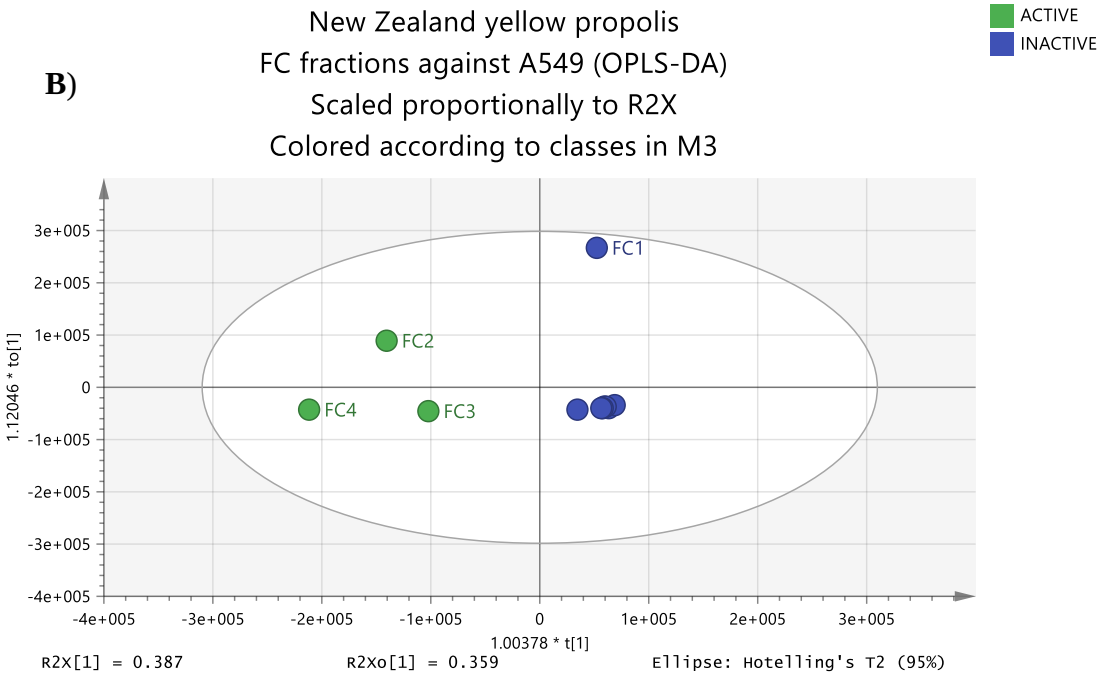

Fig. 4.6: **A**) PCA-X score scatter plot of FC propolis fractions were classified according bioactivity against A549. **B**) OPLS-DA between groups on the cytotoxicity effects on A549.

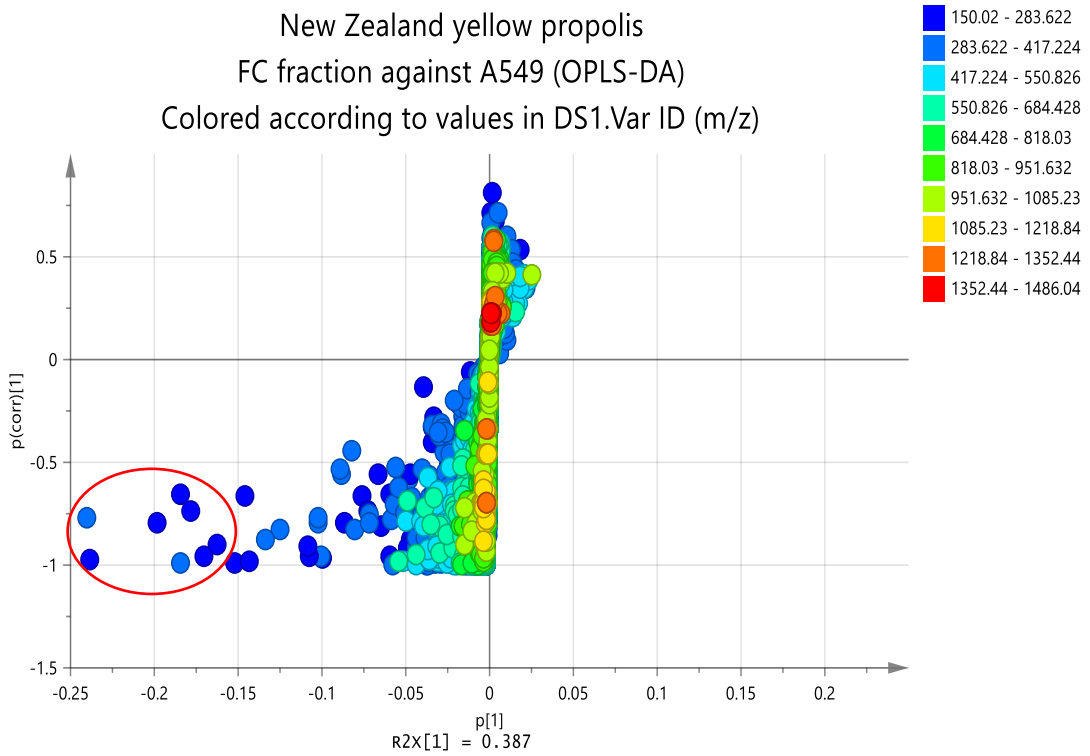

Fig. 4.7: S-plot of FC fraction, 'end' point or discriminating metabolites (in red circle) were predicted to be responsible for bioactivity on A549.

Table 4.5: Dereplication data on the 'end' or unique discriminating metabolites from the S-plot (**Fig. 4.7**).

Fraction ID	*m/z*	RT (Fraction found)	PREDICTED MOLECULAR FORMULA	EXACT MASS	NAME	SOURCE
N_151	271.0623	11.56 (FC2)	$C_{16}H_8N_4O$	272.0696	No hits	
N_144	247.0991	14.74 (FC3)	$C_{15}H_{12}N_4$	248.1064	No hits	
P_6511	255.0652	14.90 (FC3)	$C_{15}H_{10}O_4$	254.0579	5H-Phenanthro[4,5-bcd]pyran-2,6,7-triol	*Phalaenopsis equestris*
N_938	255.0678	15.29 (FC3)	$C_{16}H_8N_4$	256.0750	No hits	
P_832	271.0601	15.42 (FC4)	$C_{15}H_{10}O_5$	270.0528	galangin	*Helichrysum aureonitens*
N_141	269.0472	15.43 (FC3)	$C_{16}H_6N_4O$	270.0545	No hits	
N_142	313.0736	15.62 (FC2)	$C_{18}H_{10}N_4O_2$	314.0809	No hits	
N_147	295.0993	16.55 (FC2)	$C_{19}H_{12}N_4$	296.1066	No hits	

Therefore, based on ^{1}H NMR, TLC profiling, bioactivity against A549, high yield and metabolomic profiling, FC2 was chosen for further fractionation and isolation work. Using n-hexane and EtOAc as eluting solvents, MPLC was applied on FC2 fraction (900 mg) for further purification of the bioactive compounds yielding 88 fractions. Fractions were pooled together depending on the similarity of TLC trace, which afforded 16 unique fractions. In addition, two fractions that precipitated colourless needles were separated and labelled FC2-32-34 and FC2-43-44. These two fractions were run through 1D and 2D NMR for structure elucidation. FC1 was later abandoned for further analytical work due to its very low yield (1.3 mg). ^{1}H NMR and HR-LCMS were performed on the remaining 15 fractions. The datasets obtained were processed and statistically evaluated by PCA multivariate analysis to assess their similarities in chemical profiles in relation to their bioactivity. The spectral dataset generated from the ^{1}H NMR, HR-LCMS and concatenated datasets from both MS and NMR were used for PCA-X and hierarchy-clustering analysis (HCA) (**Fig. 4.9 – 4.11**). For HCA, the ward method is used to calculate the distance, where the cut off chosen in those dendrograms were set randomly in accordance to have the best fraction's clustering order. The three approaches demonstrated that fractions clustered together share the same chemical profile or similar major metabolites. However, best clustering was observed from the fused MS-NMR datasets, which could have correlated a similar set of metabolites with cytotoxicity effects of FC2 fractions on A549 (**Fig. 4.8**) with R^2 (1.00) and Q^2 (0.99) which indicated good fitted model and good prediction model (**Fig. 4.11**). It is interesting to note that FC2-32-34 will have its similarity with FC2-11 and FC2-12 while FC2-43-44 clustered with FC2-9 and FC2-10, which were sources of the supernatant solution for the respective precipitants.

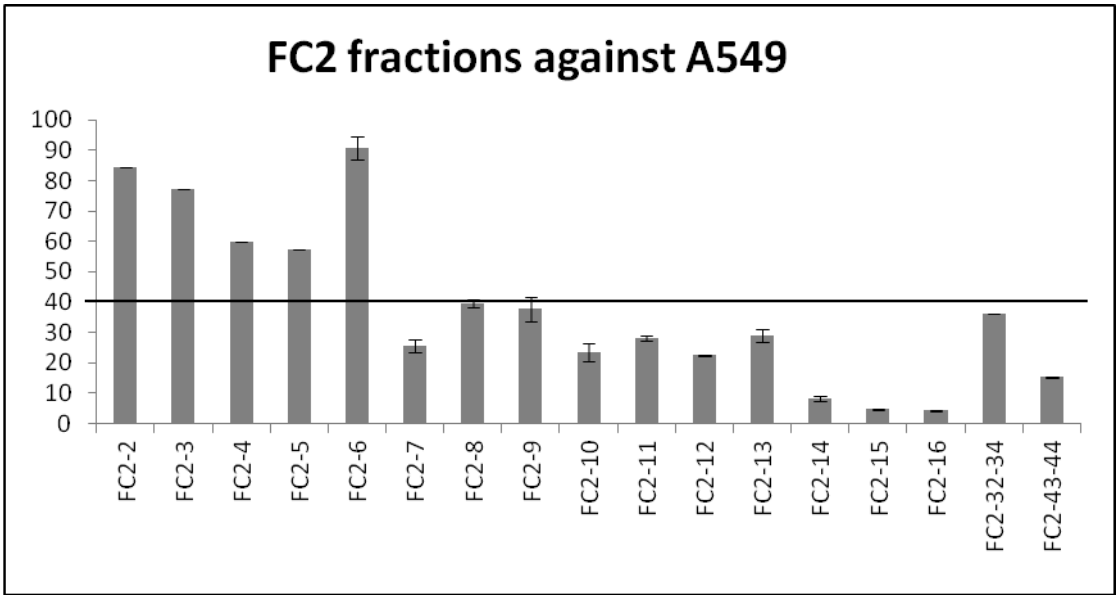

Fig. 4.8: The bioactivity of FC2 fractions on A549, subjected to cell viability of control at a threshold of ≤40%.

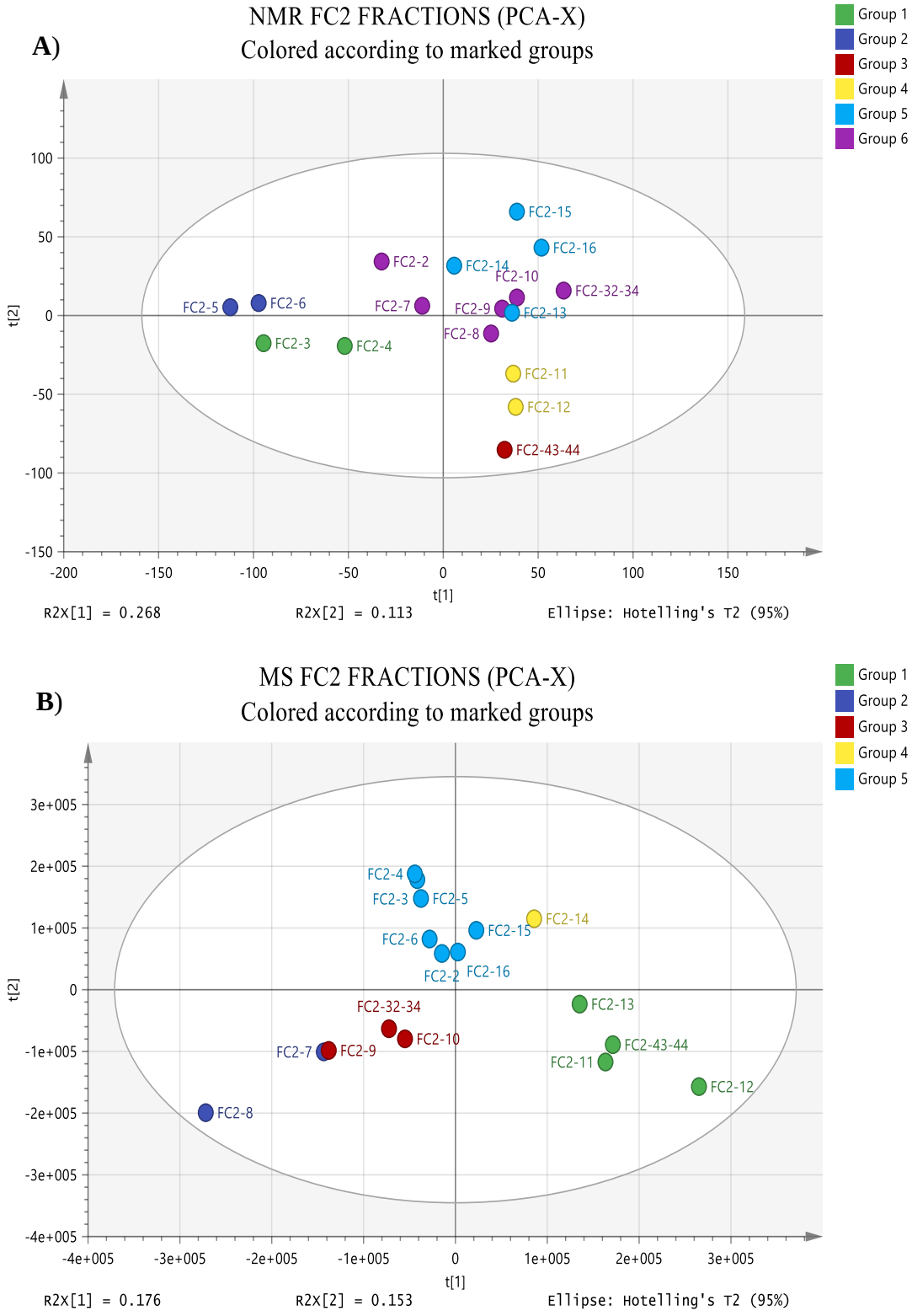

Fig. 4.9: **A**) PCA-X score scatter plot of FC2 fractions based on NMR (R^2=0.99, Q^2=0.74) and **B**) HR-LCMS (R^2=1, Q^2=0.99) data. The fractions that clustered together as marked with their respective colours possibly consist of similar major metabolites.

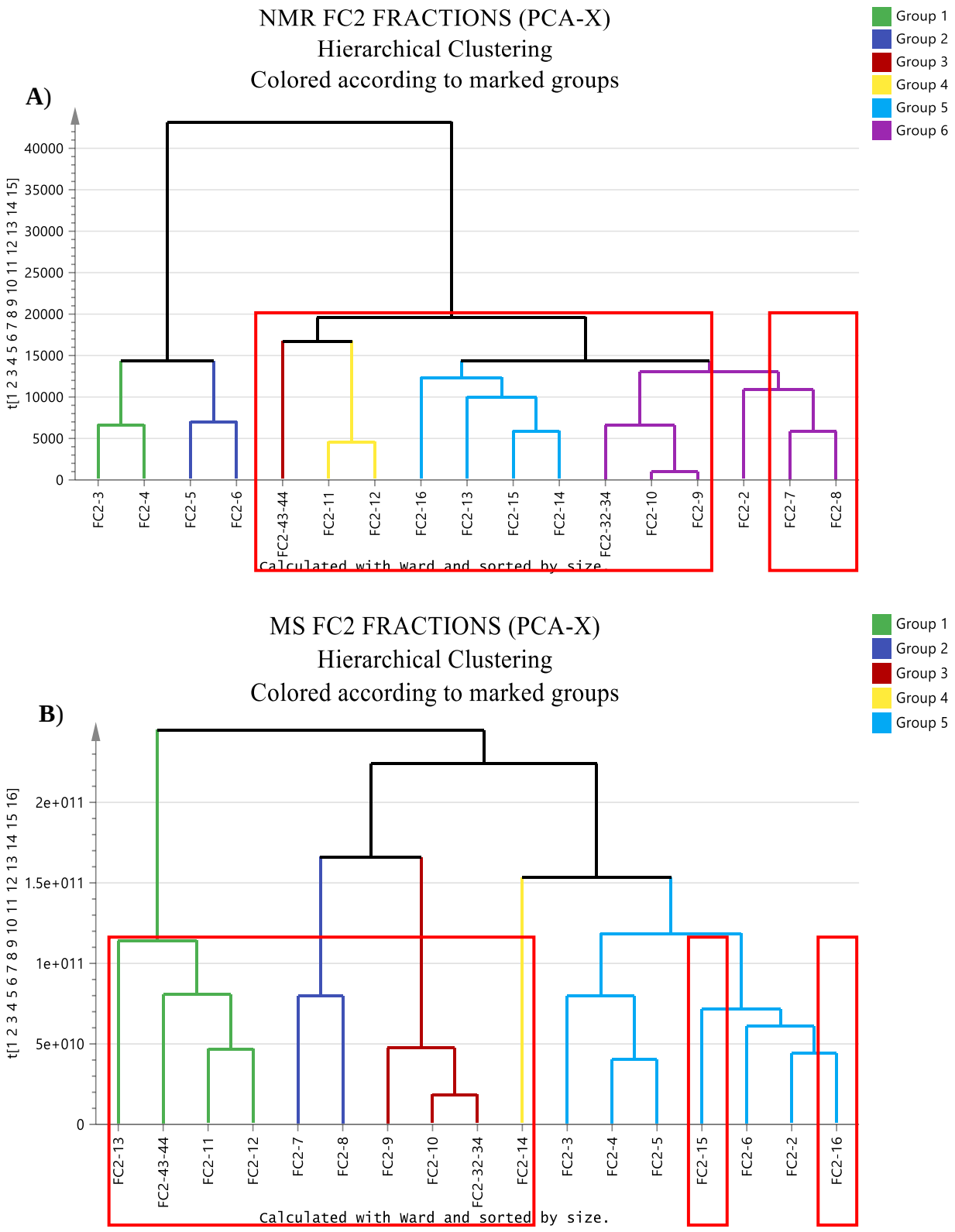

Fig. 4.10: Hierarchical PCA-X plot of FC2 fractions based on **A**) NMR and **B**) HR-LCMS data. The fractions that clustered together as marked by their respective colours possibly consist of similar major metabolites. Active fractions against A549 (red box).

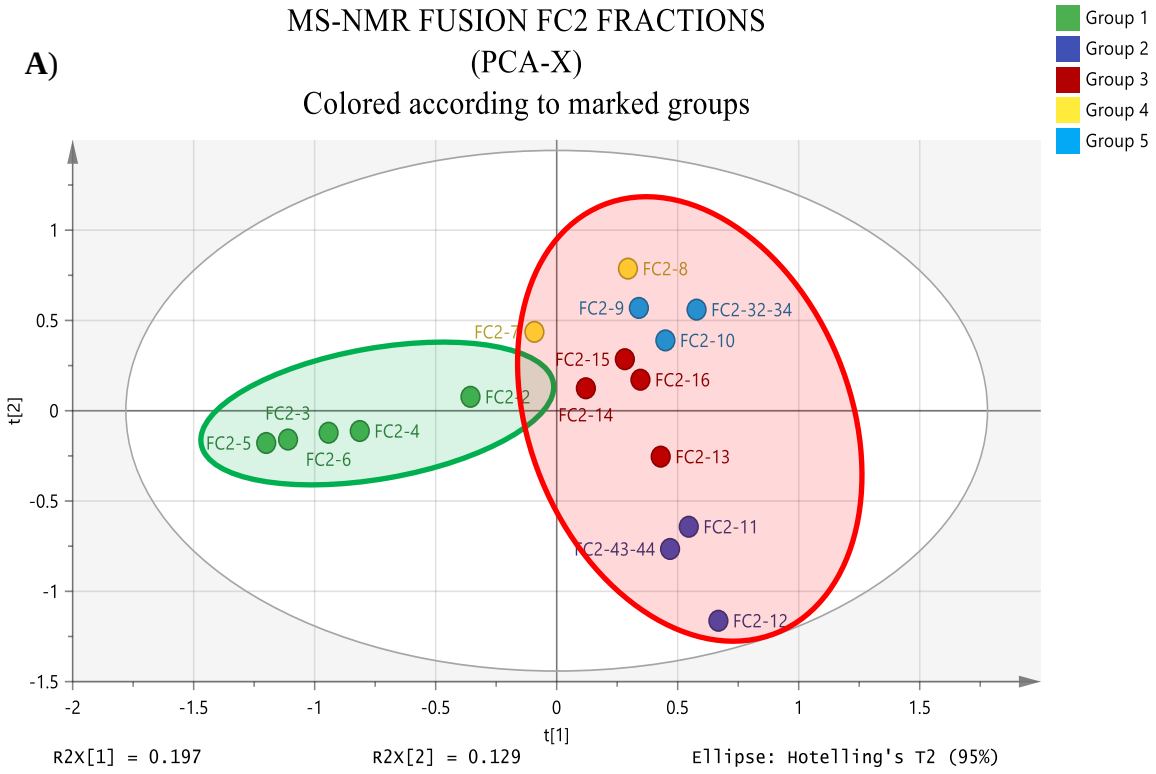

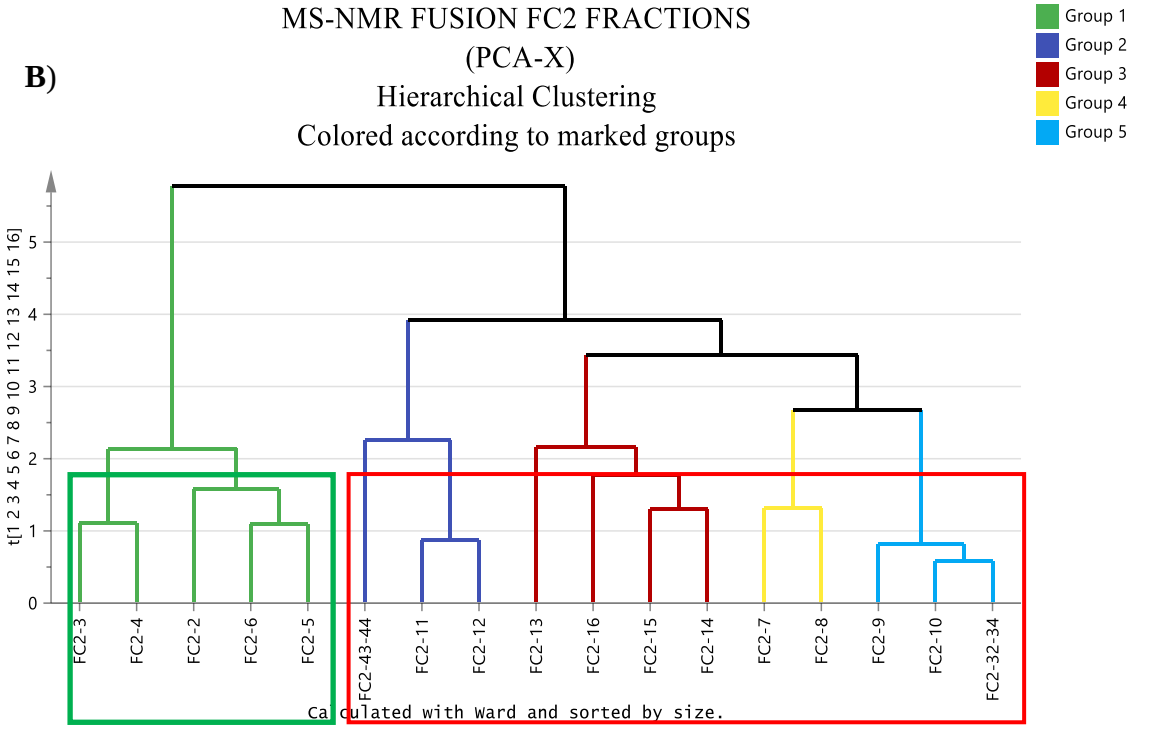

Fig. 4.11: **A**) PCA score scatter plot and **B**) hierarchical clustering of FC2 fractions based on MS-NMR fusion data. Active fractions against A549 were highlighted in red in PCA, while in HCA in red box. Meanwhile the green box marked for inactive fractions.

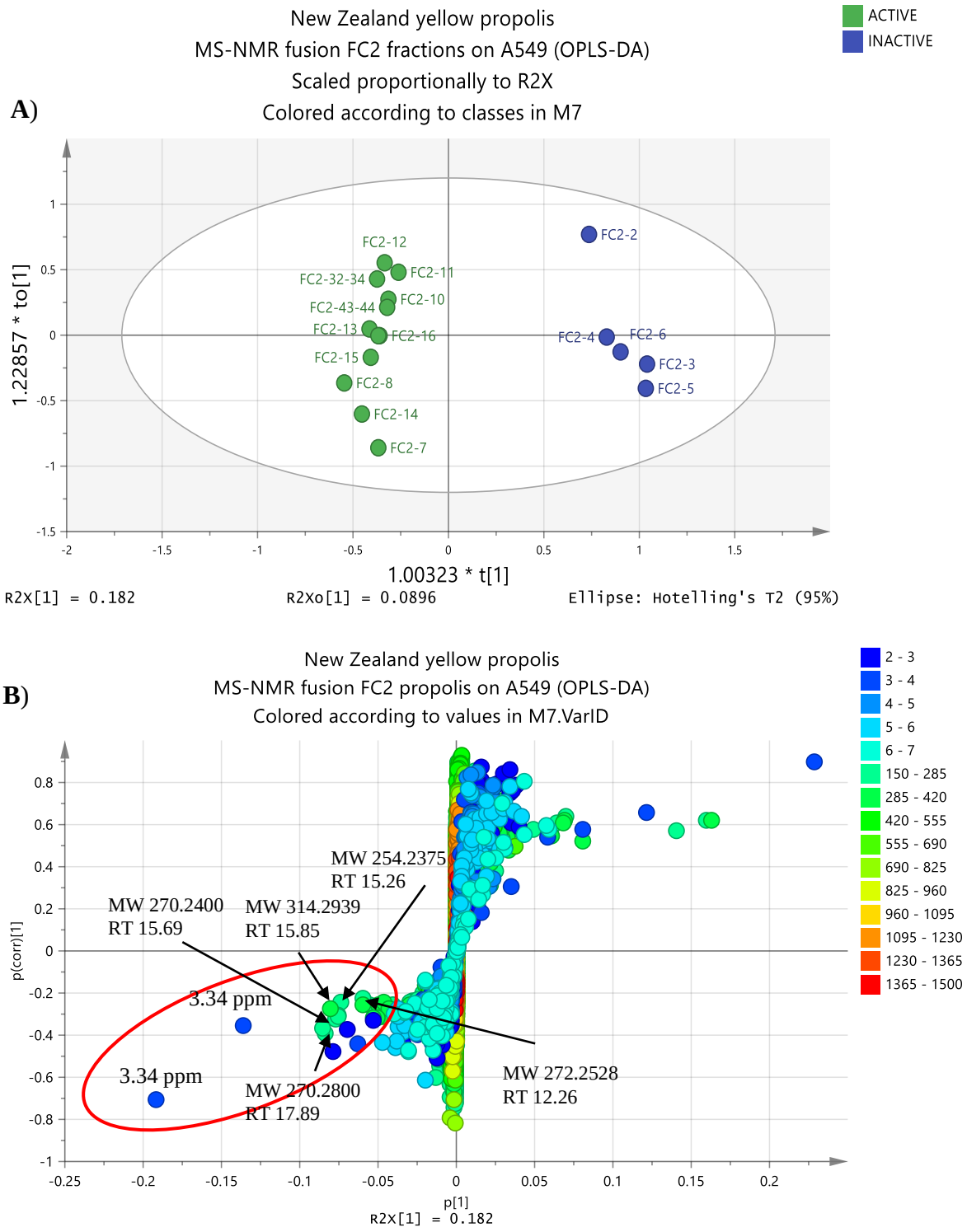

Fig. 4.12: **A)** OPLS-DA and **B)** S-plot generated from MS-NMR fusion database indicating targeted metabolites that were predicted to be responsible for the bioactivity of the fractions against A549.

The putative metabolites predicted to be responsible for the bioactivity were identified from the OPLS-DA S-plot based on generated MS-NMR fused dataset (**Fig. 4.12**). Both R^2 and Q^2 value were observed at 0.98 and 0.82, respectively, showing a model with both good fitness and predictability. The permutation test also gave a good validation score with Q^2 value of −0.5. The metabolites potentially contributing to the bioactivity against A549 cell line were cross-referenced with the Dictionary of Natural Products (DNP) database to dereplicate the target metabolites (**Table 4.6**). There were five flavonoid derivatives isolated and elucidated, namely galangin (Lee *et al.*, 2008), pinobanksin-3-acetate (Neacsu2007), benzyl caffeate (Yamauchi *et al.*, 1992), (2*R*,3*R*)-pinobanksin (Kuroyanagi *et al.*, 1982) and chrysin (Park *et al.*, 2007).

Table 4.6: Dereplication of target metabolites found in bioactive FC2 fractions against the A549.

NO.	FRACTION ID	M/Z	RT (Fraction)	Peak area in FC2	MOLECULAR FORMULA	EXACT MASS	NAME	SOURCE
1	**P_5286**	273.0757	12.26 (FC2-13-2)	1.80E+09	$C_{15}H_{12}O_5$	272.0685	pinobanksin	Constit. of the stem bark of *Annona squamosa* and Nepalese propolis
2	**P_1853**	255.0652	15.26 (FC2-43-44)	3.10E+07	$C_{15}H_{10}O_4$	254.0579	chrysin	Isol. from *Ulmus sieboldiana*, *Flourensia resinosa, Oroxylum indicum*, *Populus* sp., *Muntingia calabura*, *Prunus cerasus,Pinus monticola*, *Scutellaria baicalensis*, *Oroxylum indicum*
3	**P_53**	271.0602	15.69 (FC2-32-34)	6.27E+09	$C_{15}H_{10}O_5$	270.0530	galangin	Constit. of Galanga root (*Alpinia officinarum*) and many other plants
4	**P_623**	315.0868	15.84 (FC2-11-2)	3.71E+09	$C_{17}H_{14}O_6$	314.0789	pinobanksin-3-acetate	Constit. of *Achillea* spp.
5	**P_1910**	273.0757	15.85 (FC2-11-2)	2.25E+08	$C_{15}H_{12}O_5$	272.0685	pinobanksin	Constit. of the stem bark of *Annona squamosa* and Nepalese propolis
6	**P_1863**	271.0965	17.89 (FC2-11-5)	2.85E+08	$C_{16}H_{14}O_4$	270.0892	3-(3,4-dihydroxyphenyl)-2-propenoic acid; (E)-form, Benzyl ester	Constit. of propolis and *Populus* sp.

Highlighted in grey were the isolated and elucidated metabolites against A549.

*4.3.2.1 Galangin/**FC2-32-34***

Table 4.7: Spectral data of **FC2-32-34** was compared to galangin (Lee et al., 2008).

Galangin (P_53)
Source: New Zealand yellow propolis
Sample amount: 29 mg (colourless needle)
Molecular formula: $C_{15}H_{10}O_5$
Molecular weight: 270.2400 g/mol
Exact mass: 270.0528

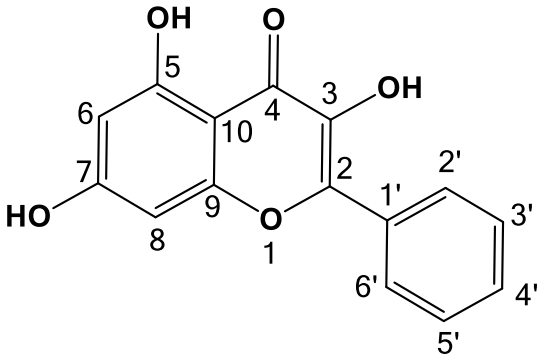

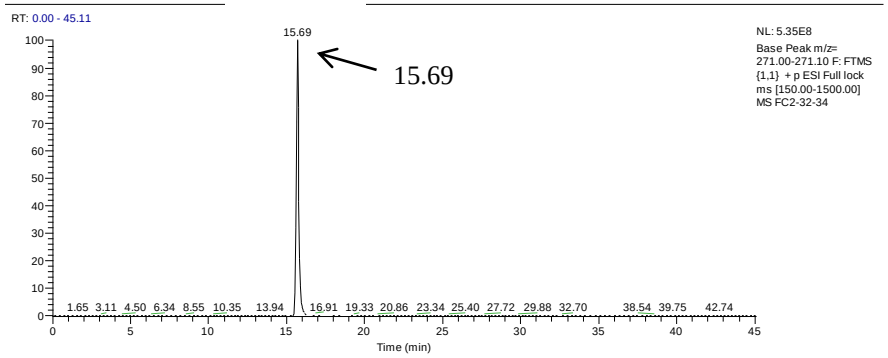

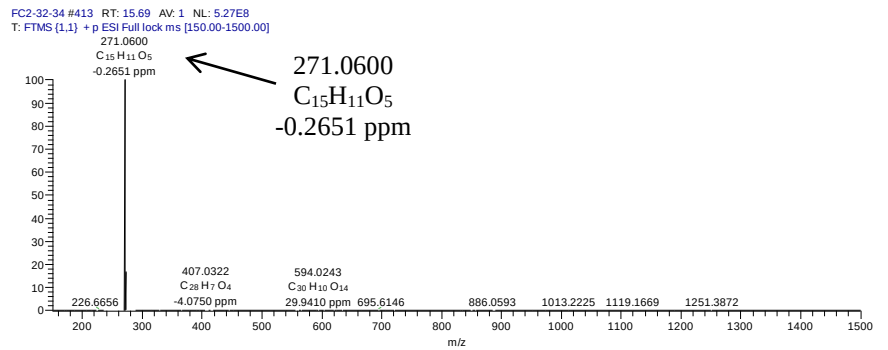

Based on the high-resolution mass spectral data, the ESI peak at 15.69 min in the positive mode was found at *m/z* 271.0600 $[M+H]^+$. This established the exact mass of 270.0528 g/mol, which established the molecular formula of $C_{15}H_{10}O_5$ (**Table 4.7**). The degrees of unsaturation in a molecule can be calculated from its molecular formula using the following formula:

$$\text{Degree of unsaturation} = \frac{2C + 2 + N - H - X}{2}$$

(C = no. carbon, N = no. nitrogen, H = no. hydrogen, X = no. halogen)

The degree of unsaturation for $C_{15}H_{10}O_5$ was calculated to be eleven, which indicated the total number of double bonds and rings in the structure. The ^{1}H NMR spectrum of **FC2-32-34** (**Fig. 4.13**) contained proton signals between 6.0–12.5 ppm. Three of the signals were observed as doublets at δ6.23 (1H, *J*=2.0 Hz), 6.48 (1H, *J*=2.0 Hz) and 8.16 (2H, *J*=7.3 Hz) and one signal as a multiplet at δ7.55 (3H). Based on the chemical shifts, which were greater than or downfield to 5 ppm, those signals were interpreted as protons that were attached to benzene rings. Furthermore, three hydroxyl signals were also observed as singlets at δ9.65, 10.87, and 12.37. The signals for oxygen-bearing carbons can be seen in the JMOD spectrum at δ 146.2, 176.8, 161.3, 164.7, and 156.9 (**Fig. 4.14**). The most upfield signals, shielded by two hydroxyl moieties in the aromatic region were δ94.1 and 98.8, showing the existence of two methine carbons for C-8 and C-6, respectively. The carbonyl carbon was interpreted at position C-4 with carbon peak at δ176.8. Based on this spectrum, it was projected that **FC2-32-34** possessed a flavonoid backbone structure.^{1}H-^{1}H COSY (**Fig. 4.15**), HSQC (**Fig. 4.16**) and HMBC (**Fig. 4.17**) confirmed the structure of galangin. The correlations of δ_H6.23, δ_C98.8 and δ_H6.48, δ_C94.1 marked the positions for C-6 and C-8, respectively. The proton and carbon assignments for C-2'/C-6', C-3'/C-5' and C-4' were deduced at δ8.17, 128.0; 7.55, 129.0; and 7.55, 130.4; respectively (**Fig. 4.16**). Comparison of the ^{1}H and ^{13}C NMR spectral data (**Table 4.8** and **4.9**) to the literature (Lee et al., 2008) confirmed that **FC2-32-34** is galangin with the structure of 3,5,7-trihydroxyflavone.

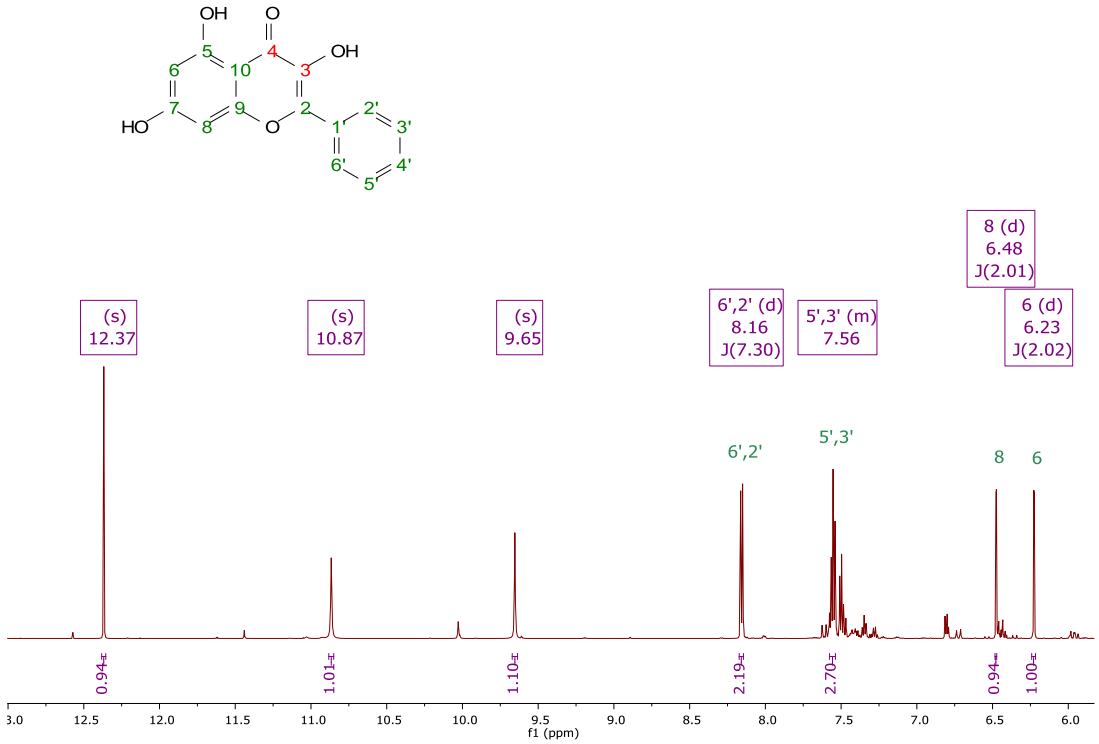

Fig. 4.13: ^{1}H NMR (600 MHz) spectrum of **FC2-32-34** in DMSO-d_6.

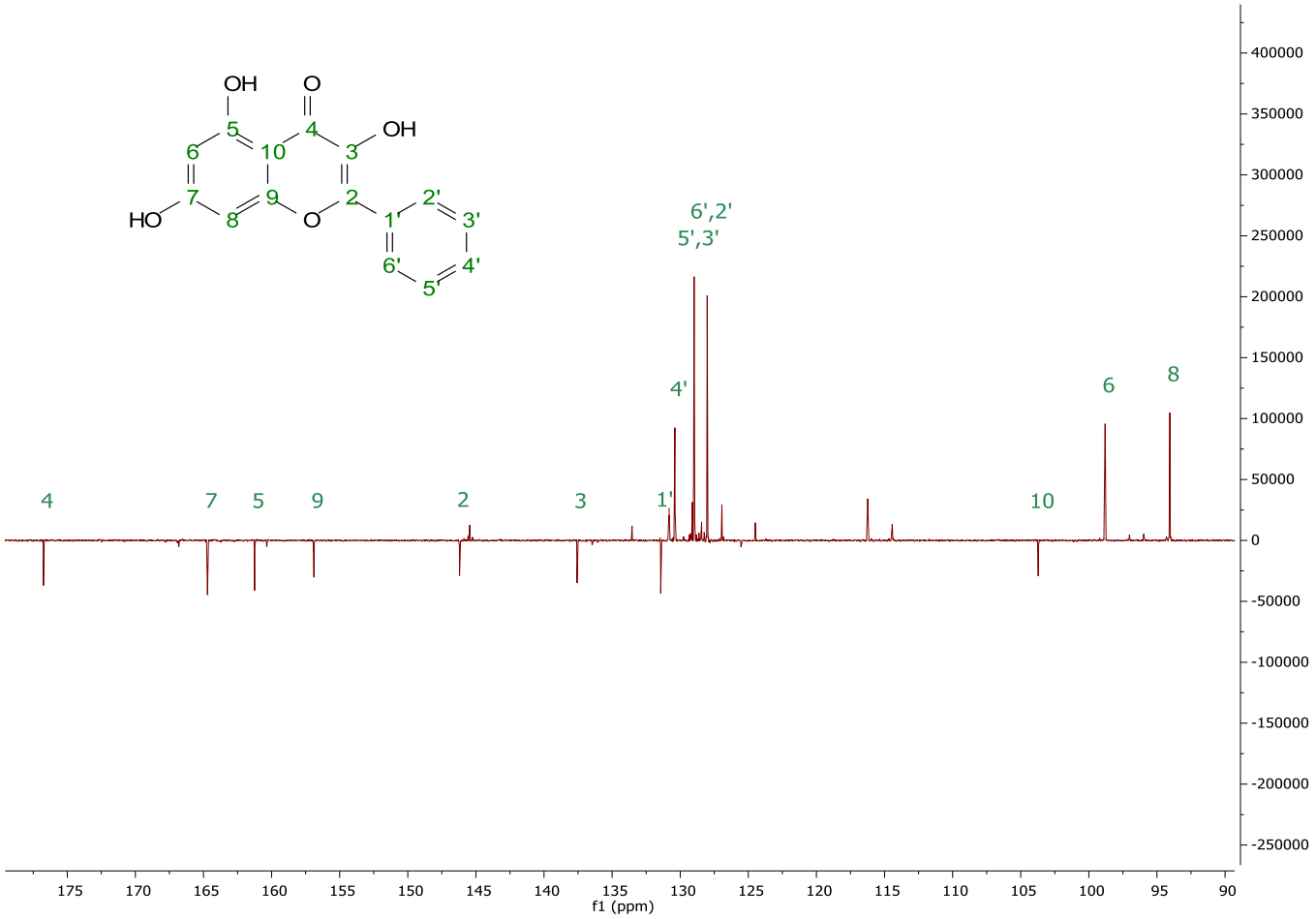

Fig. 4.14: JMOD spectrum of **FC2-32-34** in DMSO-d_6 at 150 MHz.

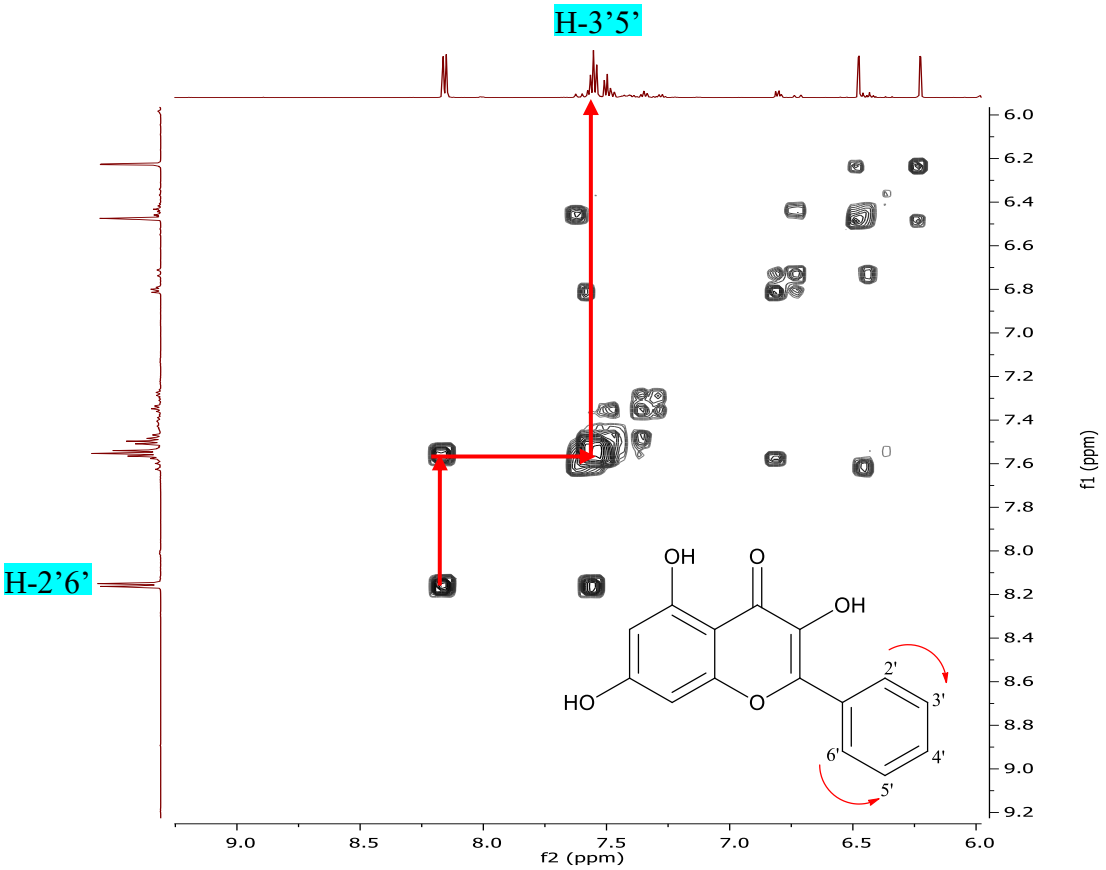

Fig. 4.15: ^{1}H-^{1}H COSY spectrum of **FC2-32-34** in DMSO-*d*$_6$ at 600 MHz.

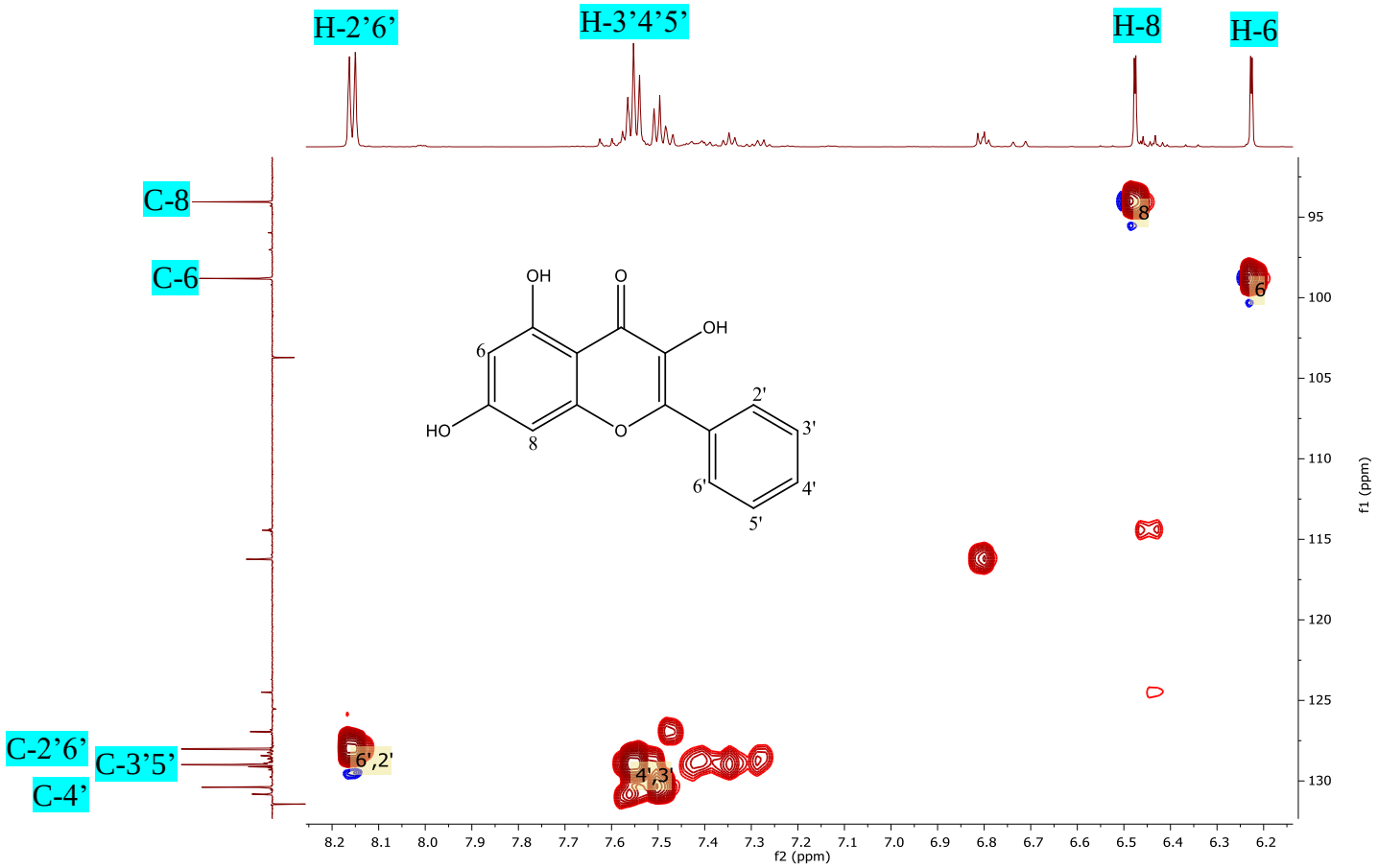

Fig. 4.16: HSQC spectrum of **FC2-32-34** in DMSO-d_6 at 600 MHz showed the correlation of the proton and JMOD spectra at X- and Y-axis, respectively.

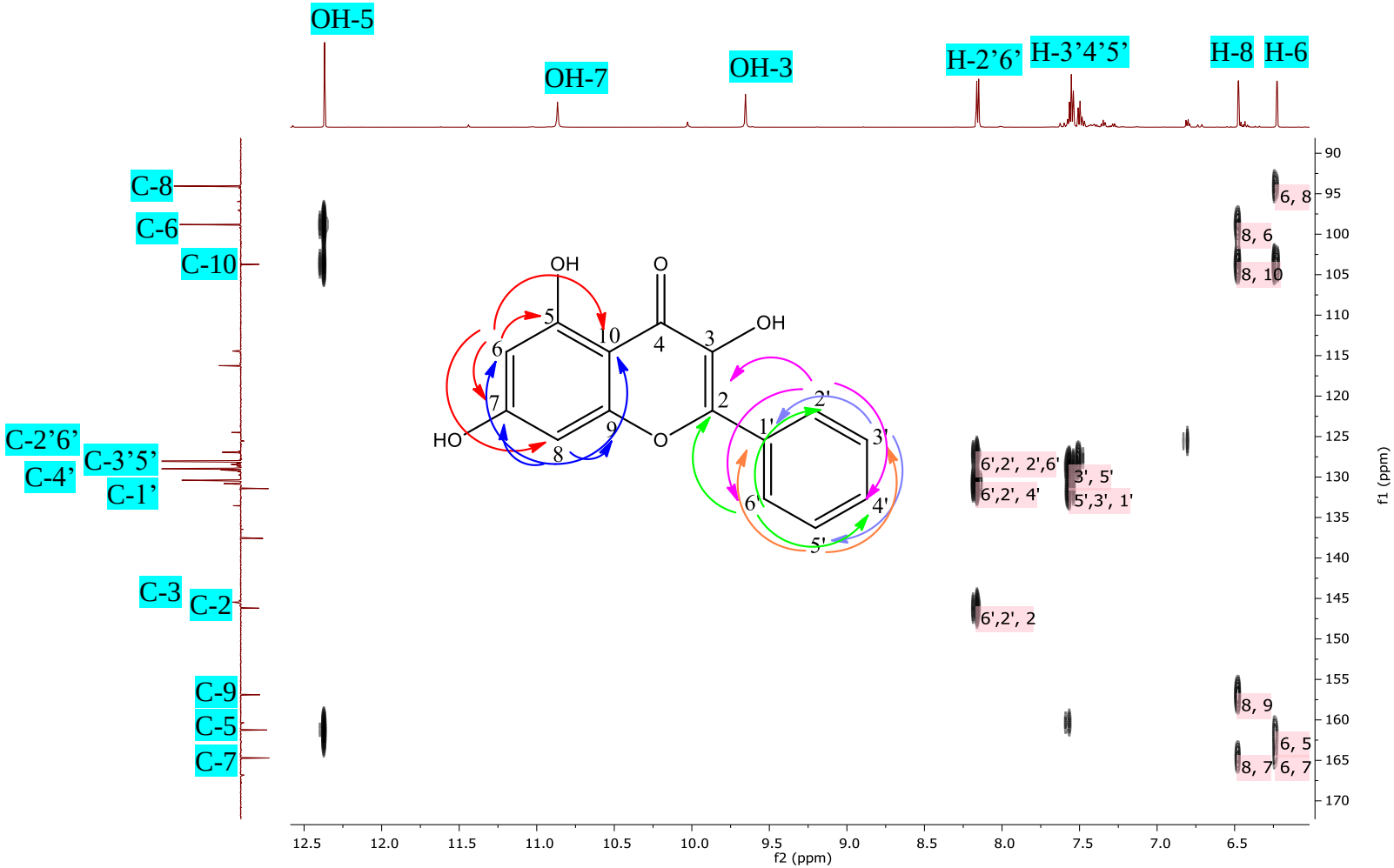

Fig. 4.17: HMBC of **FC2-32-34** in DMSO-d_6 at 600 MHz. The X- and Y-axes correspond to the proton and JMOD spectra, respectively.

Table 4.8: ^{1}H NMR (DMSO-d_6, 400 MHz) of **FC2-32-34** and galangin (Lee et al., 2008).

No.	^{1}H NMR, δ_H (ppm, multiplicity *J* in Hz)	
	FC2-32-34 in DMSO	**Literature (Lee et al., 2008) in DMSO**
H-6	6.23 (*d*, *J*=2.0 Hz)	6.12 (*d*, *J*=2.0 Hz)
H-8	6.48 (*d*, *J*=2.0 Hz)	6.46 (*d*, *J*=2.0 Hz)
H-2'	8.16 (*d*, *J*=7.3 Hz)	8.13 (*d*, *J*=7.3 Hz)
H-3'	7.56 (*m*)	7.50 (*m*)
H-4'	7.56 (*m*)	7.50 (*m*)
H-5'	7.56 (*m*)	7.50 (*m*)
H-6'	8.17 (*d*, *J*=7.3 Hz)	8.13 (*d*, *J*=7.3 Hz)
OH-3	9.65 (*br*, *s*)	9.62
OH-5	12.37	12.44
OH-7	10.87 (*br*, *s*)	10.87

Table 4.9: ^{13}C NMR (DMSO-d_6, 100MHz) of **FC2-32-34** and galangin (Lee et al., 2008)

Carbon no.	**^{13}C NMR δ_C (ppm)**	
	FC2-32-34 in DMSO	**Literature(Lee et al., 2008) in DMSO**
2	146.2 C	145.8 C
3	137.6 C	137.2 C
4	176.8 C	176.3 C
5	161.3 C	160.9 C
6	98.8 CH	98.4 CH
7	164.7 C	164.3 C
8	94.1 CH	93.7 CH
9	156.9 C	156.5 C
10	103.7 C	103.3 C
1'	131.4 C	131.3 C
2'	128.0 CH	127.6 CH
3'	129.0 CH	128.6 CH
4'	130.4 CH	130.0 CH
5'	129.0 CH	128.6 CH
6'	128.0 CH	127.6 CH

*4.3.2.2 (2R, 3R)-Pinobanksin/**FC2-13-2***

Table 4.10: The absolute stereochemistry of **FC2-13-2** was illustrated as found for (2*R*,3*R*)-pinobanksin from the literature (Kuroyanagi et al., 1982).

(2*R*, 3*R*)-Pinobanksin (P_5286)
Source: New Zealand yellow propolis
Sample amount: 11.6 mg (white powder)
Molecular formula: $C_{15}H_{12}O_5$
Molecular weight: 272.2528 g/mol
Exact mass: 272.0685
$[\alpha]_D^{20}$: +44.0 (*c* = 0.05, MeOH)

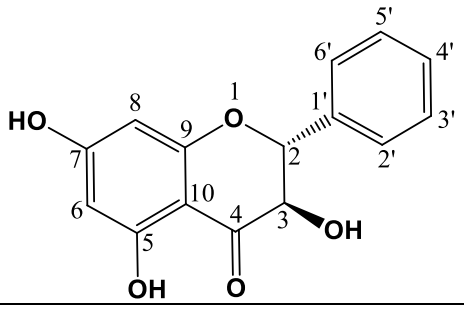

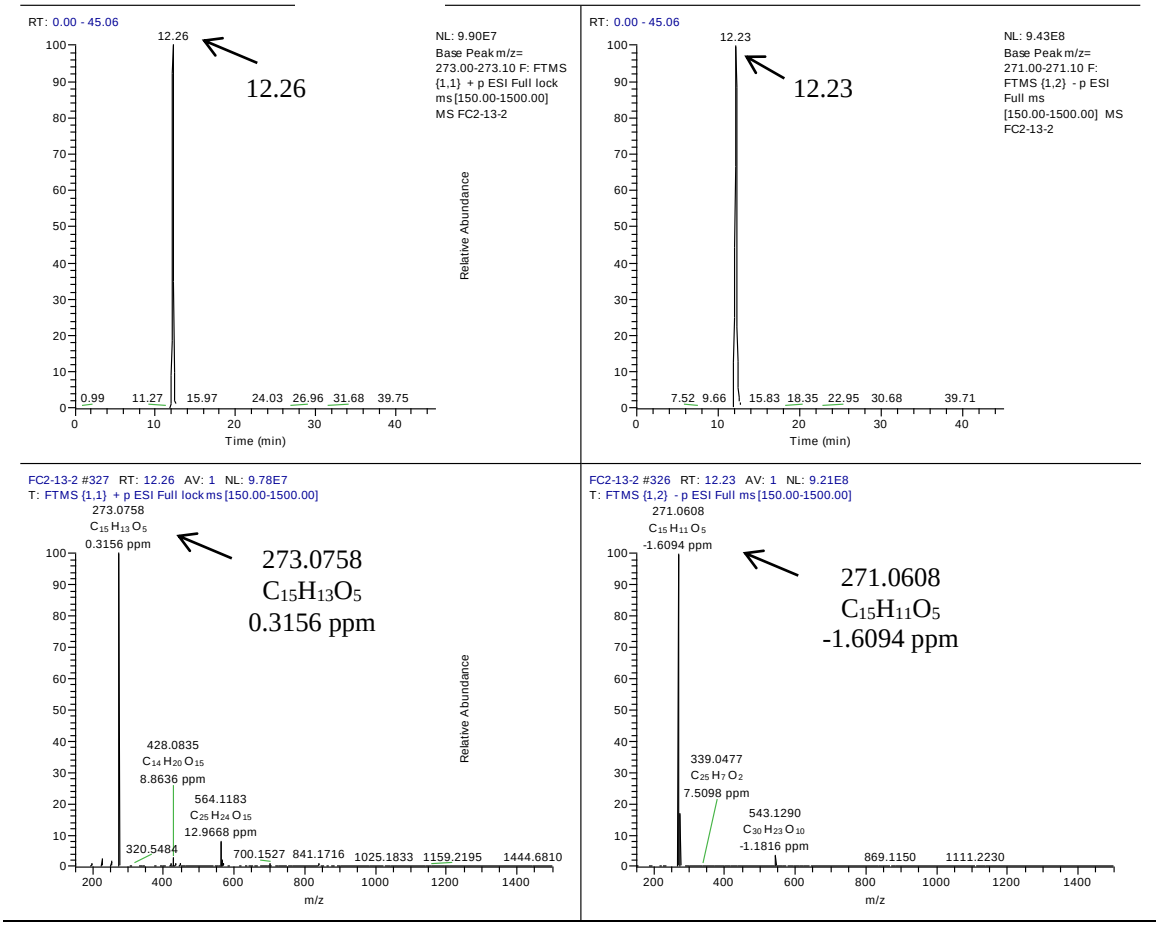

Based on the high-resolution mass spectral data, the ESI peak at 12.26 and 12.23 min in both positive and negative were found at *m/z* 273.0758 $[M+H]^+$and *m/z* 271.0608 $[M-H]^-$, respectively. This revealed the exact mass of 272.0685 g/mol, which is represented by the molecular formula of $C_{15}H_{12}O_5$ (**Table 4.10**). The degree of unsaturation of $C_{15}H_{12}O_5$ was calculated to be ten, which indicated the total of double bonds and rings in the structure that is one double bond less than **FC2-32-34**. The ^1H NMR spectrum of **FC2-13-2** (**Fig. 4.19**) is comparable to **FC2-32-34** with additional proton resonances at the 5-ppm region. As in **FC2-32-34**, a pair of *meta* doublets for H-6 and H-8 with coupling constant of 2.1 Hz were detected at δ5.93 and 5.89, respectively, which went upfield in FC2-13-2. Three coupling resonances were observed at δ5.18 (*d*, *J* = 11.4 Hz), 4.64 (*dd*, *J* = 11.4, 6.0 Hz), and 5.87 (*d*, *J* = 6.0 Hz), for carbon H-2, H-3 and H-3-OH, respectively.

Based on their coupling constants, the doublet at δ5.18 for H-2 correlating with the resonance at δ4.64 for H-3 with a coupling constant of 11.4 Hz indicated axially oriented oxymethine protons as demonstrated in **Fig. 4.18**. The *meta* doublets, representing the shielded protons H-6 and H-8, were both vicinal to a hydroxyl substituent. The signals for the oxygen-bearing carbon can also be seen in the ^{13}C spectrum (**Fig. 4.20**) at δ198.2, 163.0, 167.4, 163.9, 83.5, and 72.1 for positions C-4, C-9, C-7, C-5, C-2, and C-3, respectively. The most downfield signal at δ198.2 was the carbonyl carbon at C-4. Based on this spectrum, **FC2-13-2** possessed a flavonoid backbone structure like FC2-32-34 similar to galangin and is a dihydro derivative of **FC2-32-34**.

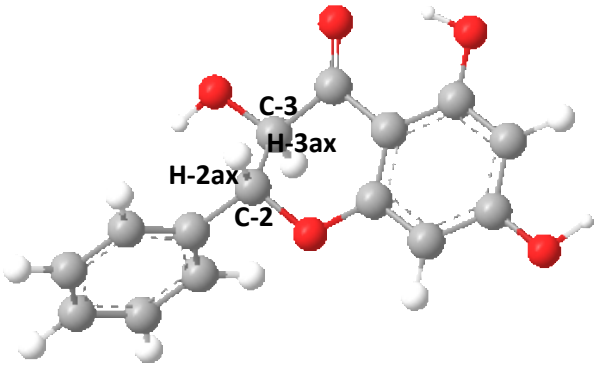

Fig 4.18: Structure of **FC2-13-2** illustrating the stereochemistry at C-2 and C-3.

^{1}H-^{1}H COSY (**Fig. 4.21**), HMQC (**Fig. 4.22**) and HMBC (**Fig. 4.23**) confirmed the structure of **FC2-13-2** as pinobanksin. From the ^{1}H-^{1}H COSY spectrum, H-2'/6' showed direct proton correlation with H-3'/5' and also between H-2 and H-3 proton signals. Based on the HMBC spectrum, H-3 observed at δ4.64 correlated with C-4, C-2, C-1', and C-2'/6' at δ198.2, 83.5, 137.9 and 128.8, respectively. Furthermore, H-2 at 5.18 ppm exhibited cross peaks with C-4, C-3 and C-1' at δ198.2, 72.1 and 137.9, respectively. H-8 correlated with C-7, C-6, C-9, and C-10 at δ167.4, 96.7, 163.0 and 101.0, respectively. Meanwhile, H-6 showed cross peaks with C-7, C-5, C-8 and C-10 at δ167.4, 163.9, 95.6 and 101.0, respectively. On the other hand, the proton signals on phenyl unit also showed strong correlations with each other's carbons. Proton signals at 7.52 and 7.41 ppm correlated with C-2 at δ83.5 and C-1' at δ137.9, respectively. The structure of **FC2-11-2** was elucidated as3,5,7-trihydroxyflavanone. The optical rotation value of **FC2-13-2**, given $[\alpha]_D^{20}$+44.0 (*c* = 0.05, MeOH) was comparable with the literature $[\alpha]_D$ +6.1 (*c* = 0.45, MeOH) (Kuroyanagi et al., 1982). The ^{1}H and ^{13}C NMR spectral data (**Table 4.11** and **4.12**) of **FC2-13-2** was similar to that reported in the literature for (2*R,* 3*R*)-pinobanksin (Kuroyanagi et al., 1982).

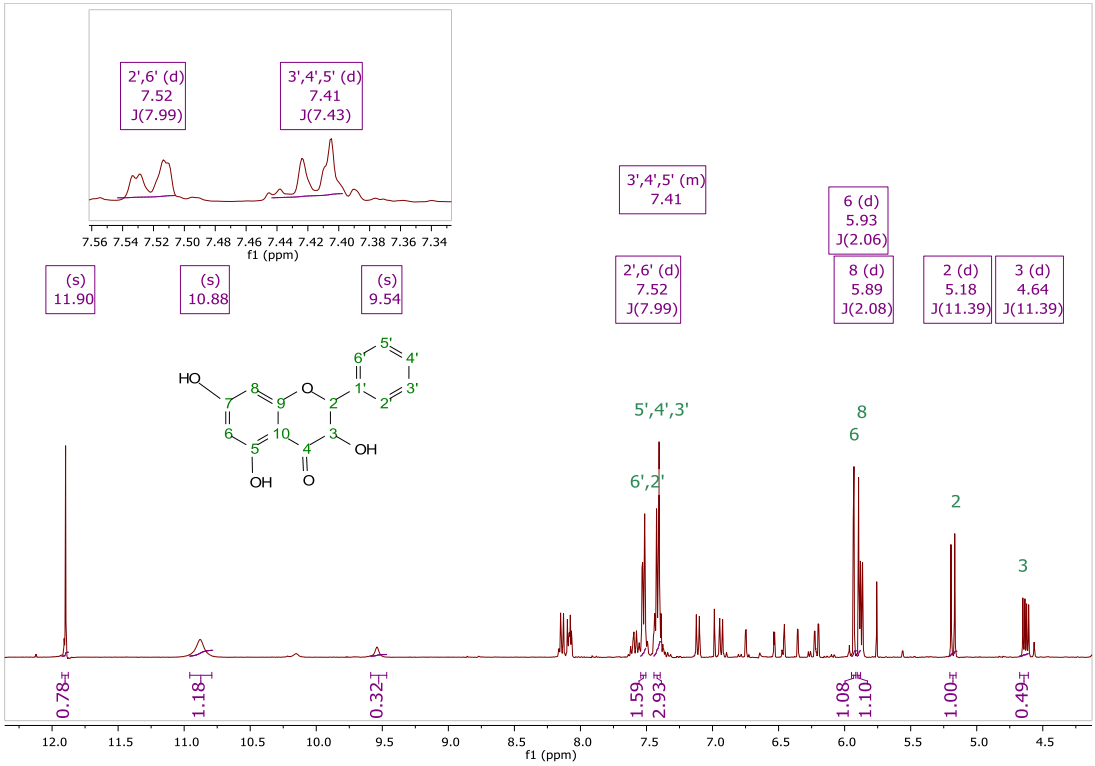

Fig. 4.19: ^{1}H NMR spectrum of **FC2-13-2** in DMSO-d_6 using JEOL-LA400 FT-NMR.

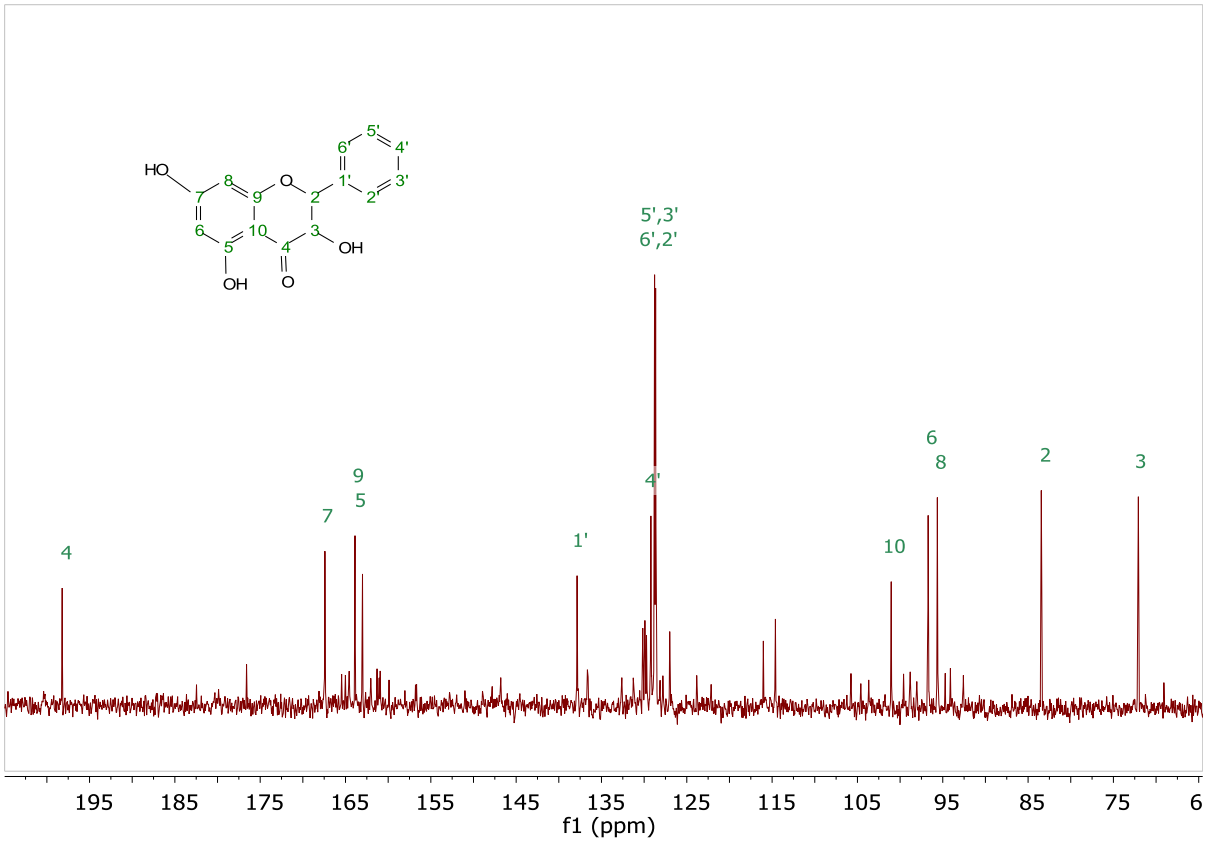

Fig. 4.20: ^{13}C spectrum of **FC2-13-2** in DMSO-d_6 at 100 MHz.

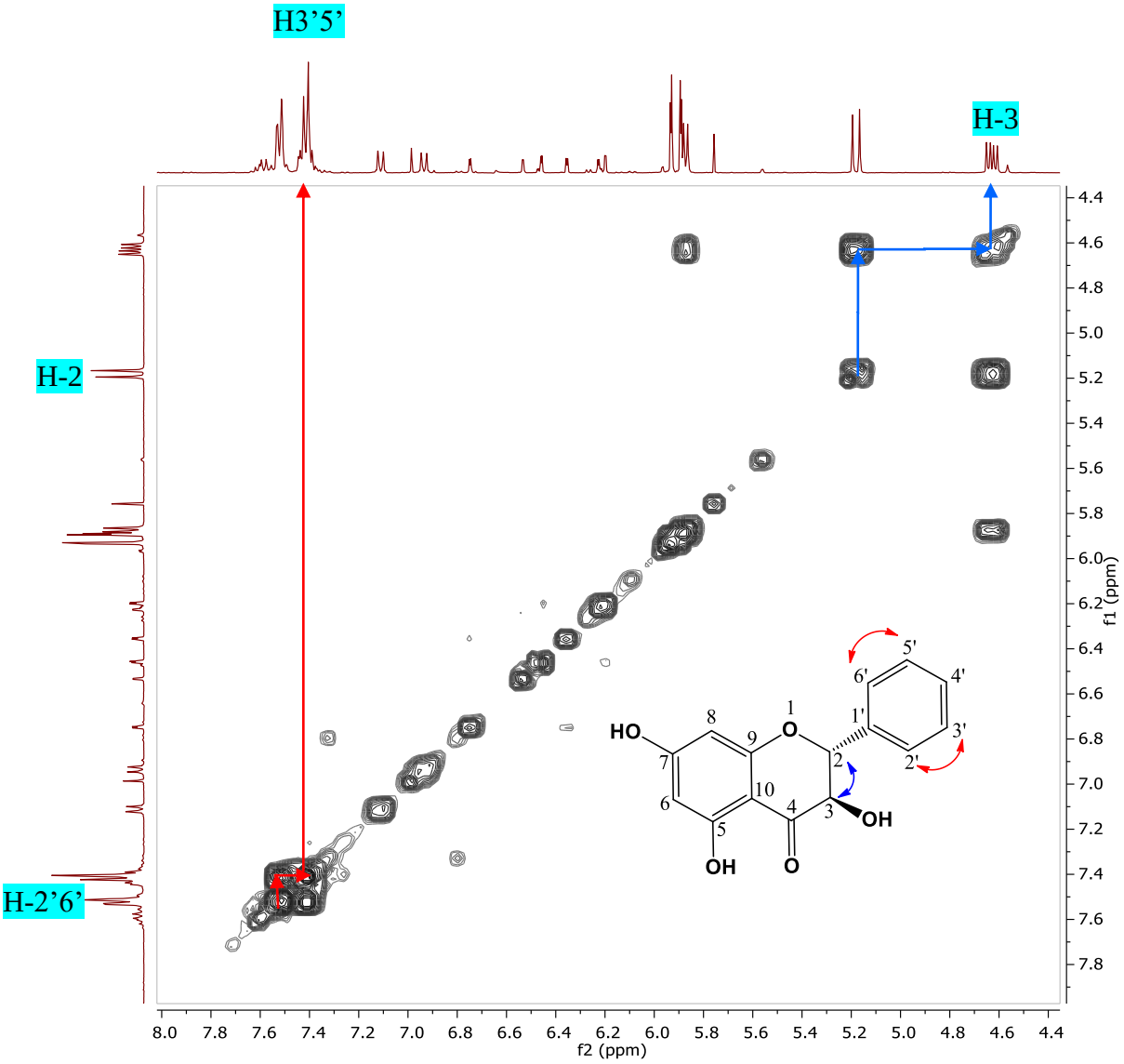

Fig. 4.21: ^{1}H-^{1}H COSY spectrum of **FC2-13-2** in DMSO-d_6 at 400 MHz.

.

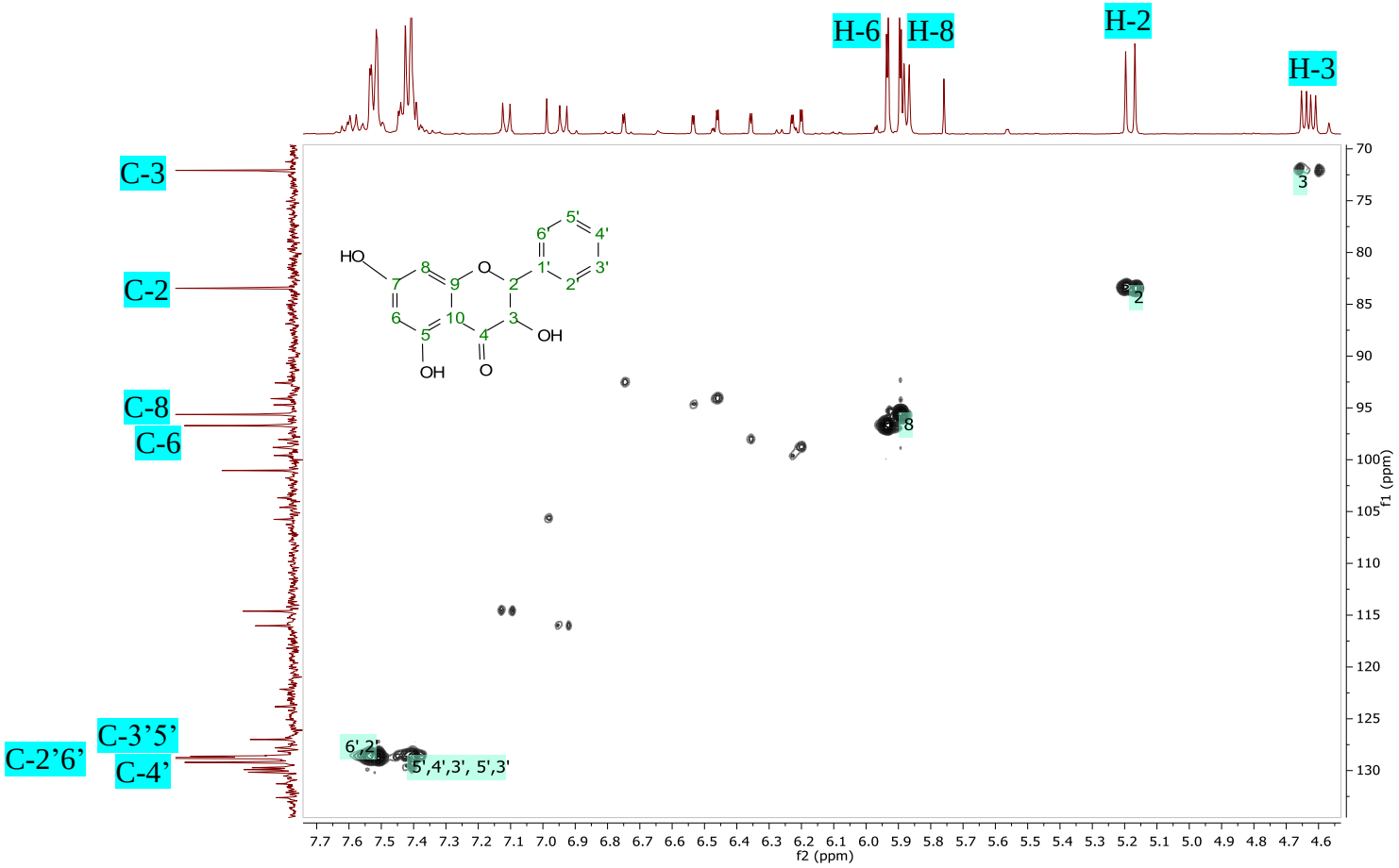

Fig. 4.22: HMQC of **FC2-13-2** in DMSO-$d_6$at 400 MHz. The X-and Y-axes correspond to the proton and ^{13}C spectra, respectively.

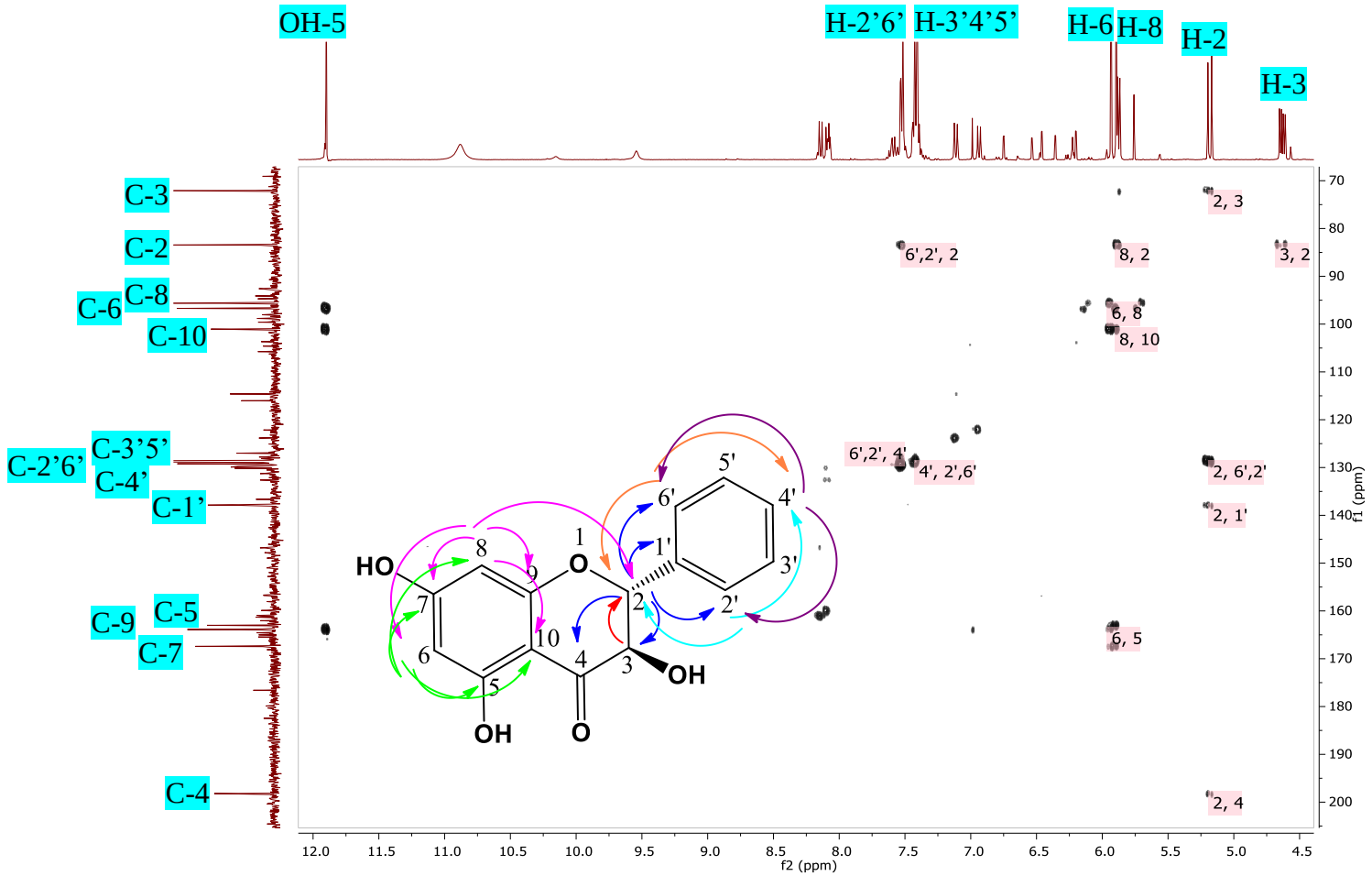

Fig. 4.23: HMBC of **FC2-13-2** in DMSO-d_6 at 400 MHz. The X- and Y-axes correspond to the proton and ^{13}C spectra, respectively.

Table 4.11: ^{1}H NMR (DMSO-d_6, 400MHz) of **FC2-13-2** and (2*R*,3*R*)-pinobanksin (Kuroyanagi et al., 1982).

No.	**^{1}H NMR, δ_H (ppm, multiplicity *J* in Hz)**	
	FC2-13-2 in DMSO-d_6	**(Kuroyanagi et al., 1982) in CD_3OD**
H-2	5.18 (*d, J* = 11.4 Hz)	5.03 (*d, J* = 12.0 Hz)
H-3	4.64 (*d, J* = 11.4 Hz)	4.48 (d, J = 12.0 Hz)
H-6	5.93 (*d, J* = 2.1 Hz)	5.90 (*s*)
H-8	5.89 (*d, J* = 2.1 Hz)	5.90 (*s*)
H-2'/6'	7.52 (*d, J* = 7.9 Hz)	7.25 - 7.52 (*m*)
H-3'/4'/5'	7.41 (*m*)	
OH-3	9.54 (*s*)	-
OH-5	11.90 (*s*)	-
OH-7	10.88 (*s*)	

Table 4.12: ^{13}C NMR (DMSO, 100MHz) of **FC2-13-2** and pinobanksin (Kuroyanagi et al., 1982).

Carbon no.	^{13}C NMR δ_C (ppm)	
	FC2-13-2 in DMSO	**(Kuroyanagi et al., 1982) in $CDCl_3$**
2	72.1 CH	83.5 CH
3	83.5 CH	72.5 CH
4	198.2 C	196.0 C
5	163.0 C	163.0 C
6	96.7 CH	96.9 CH
7	167.4 C	163.6 C
8	95.6 CH	96.0 CH
9	163.9 C	167.5 C
10	101.0 C	100.5 C
1'	137.9 C	136.5 C
2'	128.8 CH	127.6 CH
3'	128.6 CH	128.6 CH
4'	128.6 CH	129.2 CH
5'	128.6 CH	128.6 CH
6'	128.8 CH	127.6 CH

*4.3.2.3 Pinobanksin-3-acetate/**FC2-11-2***

Table 4.13: Spectral data of **FC2-11-2** was compared to pinobanksin-3-acetate (Neacsu et al., 2007).

Pinobanksin-3-acetate (P_1910)
Source: New Zealand yellow propolis
Sample amount: 21.7 mg (white powder)
Molecular formula: $C_{17}H_{14}O_6$
Molecular weight: 314.2930 g/mol
Exact mass: 314.0789
$[\alpha]_D^{20}$: −2.0 (*c* = 0.05, MeOH)

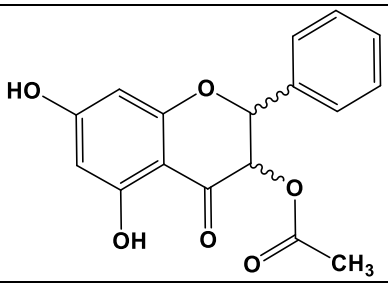

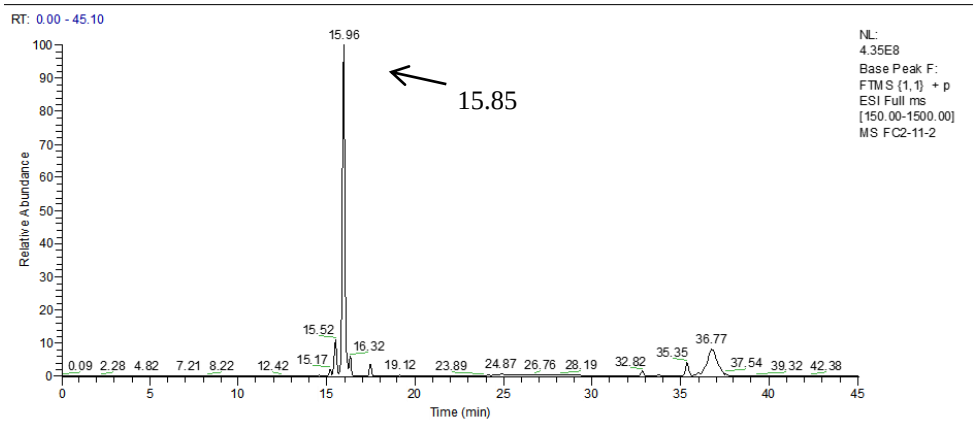

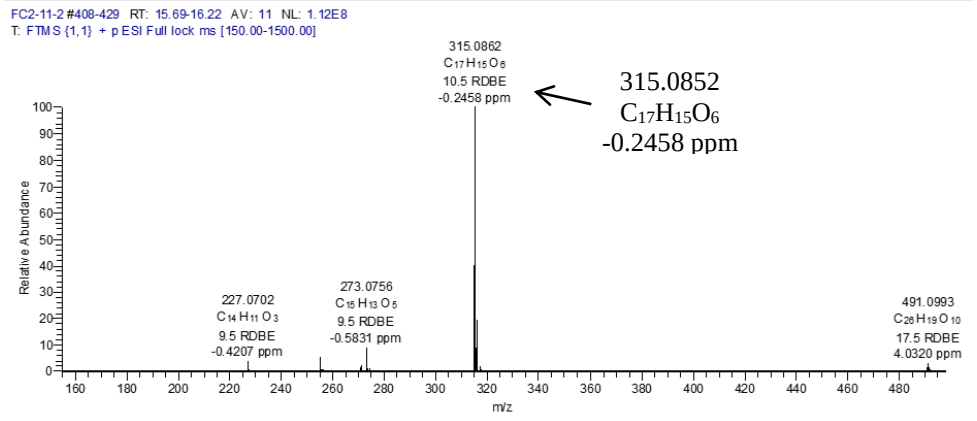

Based on the high-resolution mass spectral data, the ESI peak at 15.85 min in the positive mode was found at *m/z* 315.0852 $[M+H]^+$. This revealed the exact mass of 314.0789 g/mol, which established the molecular formula $C_{17}H_{14}O_6$ (**Table 4.10**). The ^1H NMR spectrum of **FC2-11-2** (**Fig. 4.24**) exhibited proton signals between 5.5–12.0 ppm. A doublet was observed at δ5.62 (1H, *J* = 11.8 Hz) and overlapping resonances at δ5.96 integrating for three protons. Based on their coupling constants, it can be deduced that the overlapping protons consisted of two meta doublets at δ5.98 and 5.95 with coupling constant of 2.0 Hz representing and a pair of axial doublets at δ5.96 (H-2) and 5.62 (H-3) with a coupling constant of 11.8 Hz similar to that found in **FC2-13-2**. However, the axial doublets were shifted downfield in **FC2-11-2**. Like in **FC2-13-2**, the *meta* doublets of H-6 and H-8 were also shifted upfield due to the shielding effects of adjacent hydroxyl substituent. The signals for the oxygen-bearing carbon can also be perceived in the ^{13}C spectrum (**Fig. 4.25**) at δ191.8, 169.3, 167.9, 163.8, 80.6, and 72.6 for positions C-4, C-9, C-7, C-5, C-2, and C-3, respectively. The most downfield signal at δ191.8 was the carbonyl at C-4, which was shifted upfield when compared to **FC2-13-2.** Based on this spectrum, FC2-11-2 possessed a very similar flavonoid backbone structure to **FC2-13-2** with the addition of an acetyl unit, hence the difference of 42 mass units. Additional proton and carbon resonances were also observed at 1.95 and 169.3 ppm, respectively, which further indicated the presence of the acetyl moiety.

^1H-^1H COSY (**Fig. 4.26**) and HMBC (**Fig. 4.27**) established the structure of **FC2-11-2** that gave similar patterns of correlations as in **FC2-13-2**. An additional HMBC correlation was observed between the proton singlet at 1.95 ppm and the quaternary carbon at 169.3. The acylation occurred at C-3, as evidenced from the significant changes in chemical shifts for H-2, H-3, and C-4. The proton NMR chemical shift for doublets H-2 and H-3 were deshielded in comparison to those respective upfield shifts at δ5.18 and 4.64 reported for **FC2-13-2** while C-4 was shifted 4 ppm upfield in **FC2-11-2**. The structure of **FC2-11-2** was elucidated as the acetylated congener of **FC2-13-2**. The ^1H and ^{13}C NMR spectral data (**Table 4.14** and **4.15**) of **FC2-11-2** were similar to those reported in the literature for pinobanksin-3-acetate (Neacsu et al., 2007, Tran et al., 2012). The optical rotation value of **FC2-11-2** was found to be

$[\alpha]_D^{20}$–2.0 (*c* = 0.05, MeOH), which was incompatible with the reported optical rotation value for pinobanksin-3-acetate at $[\alpha]_D$ +48.1 (*c* = 0.85, MeOH) (Neacsu et al., 2007). The small magnitude of the optical rotation of **FC2-11-2** also indicated that the isolated compound was not enantiomeric pure or was a racemic mixture of (*2R*, *3R*) and (*2S*, *3S*).

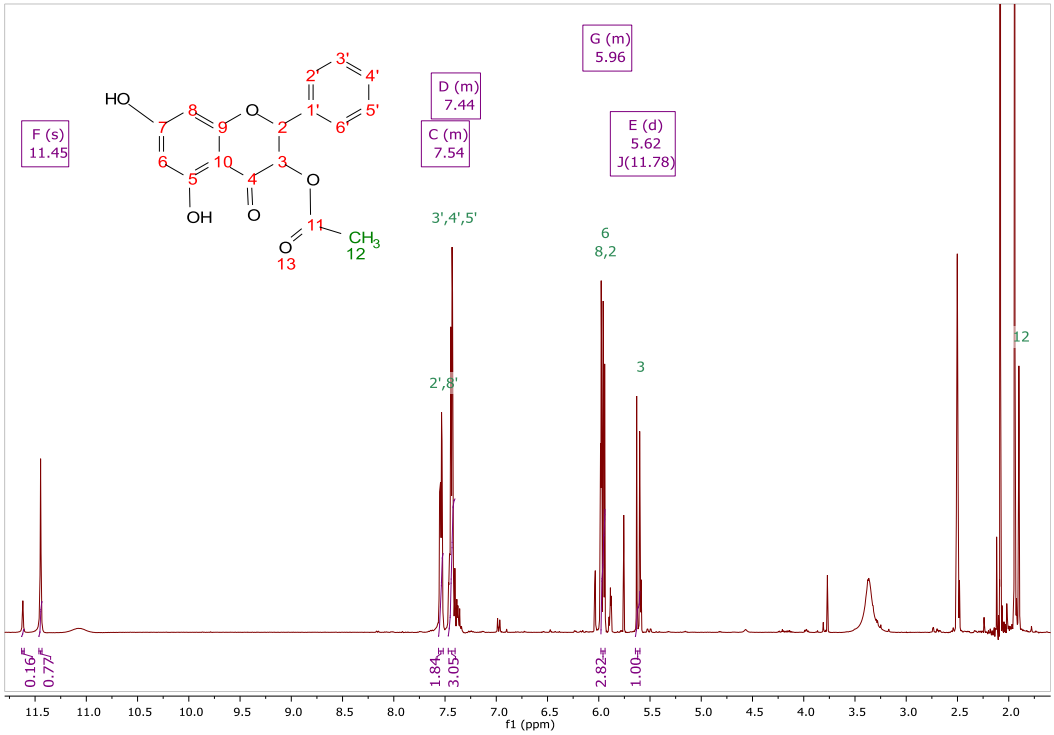

Fig. 4.24: ^{1}H NMR spectrum of **FC2-11-2** in DMSO-d_6 using JEOL-LA400 FT-NMR.

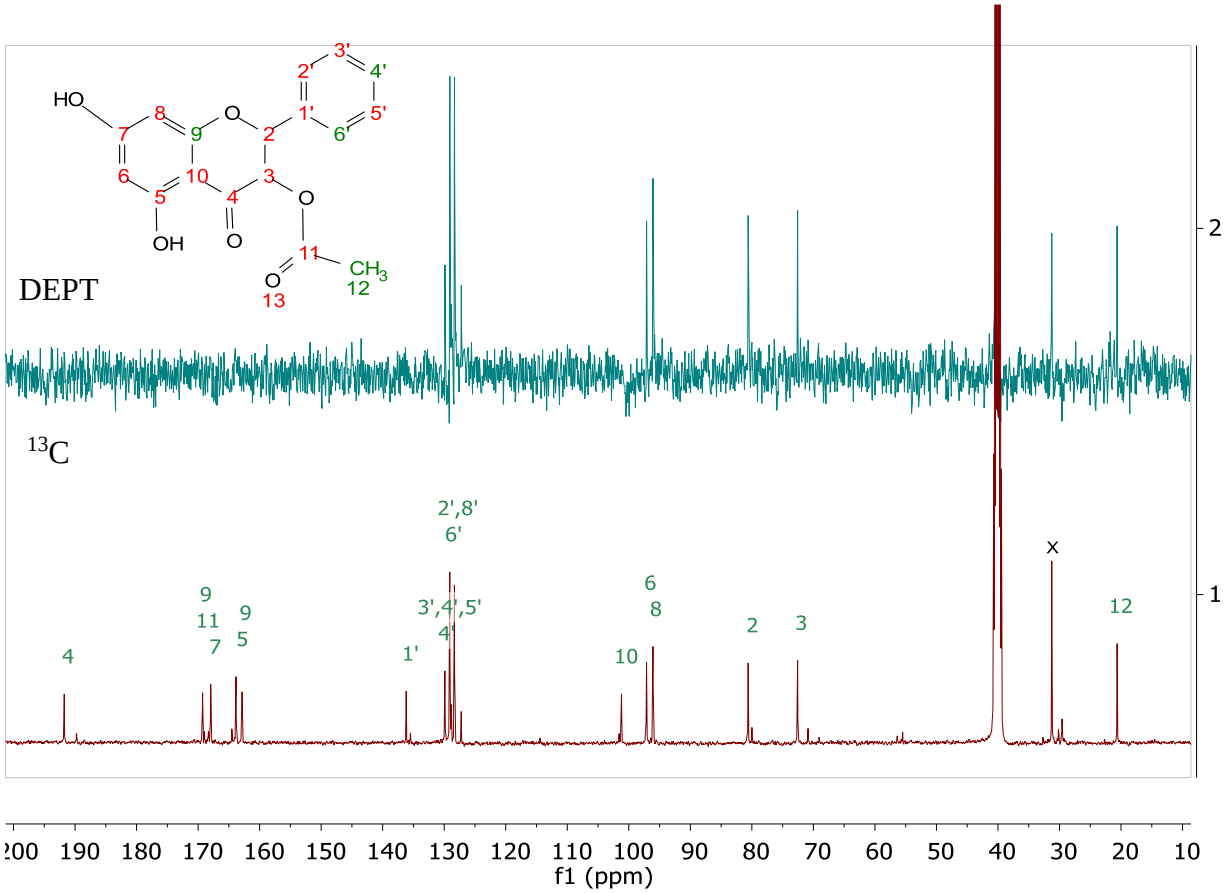

Fig. 4.25: DEPT and ^{13}C spectraof **FC2-11-2** in DMSO-d_6 at 100 MHz.

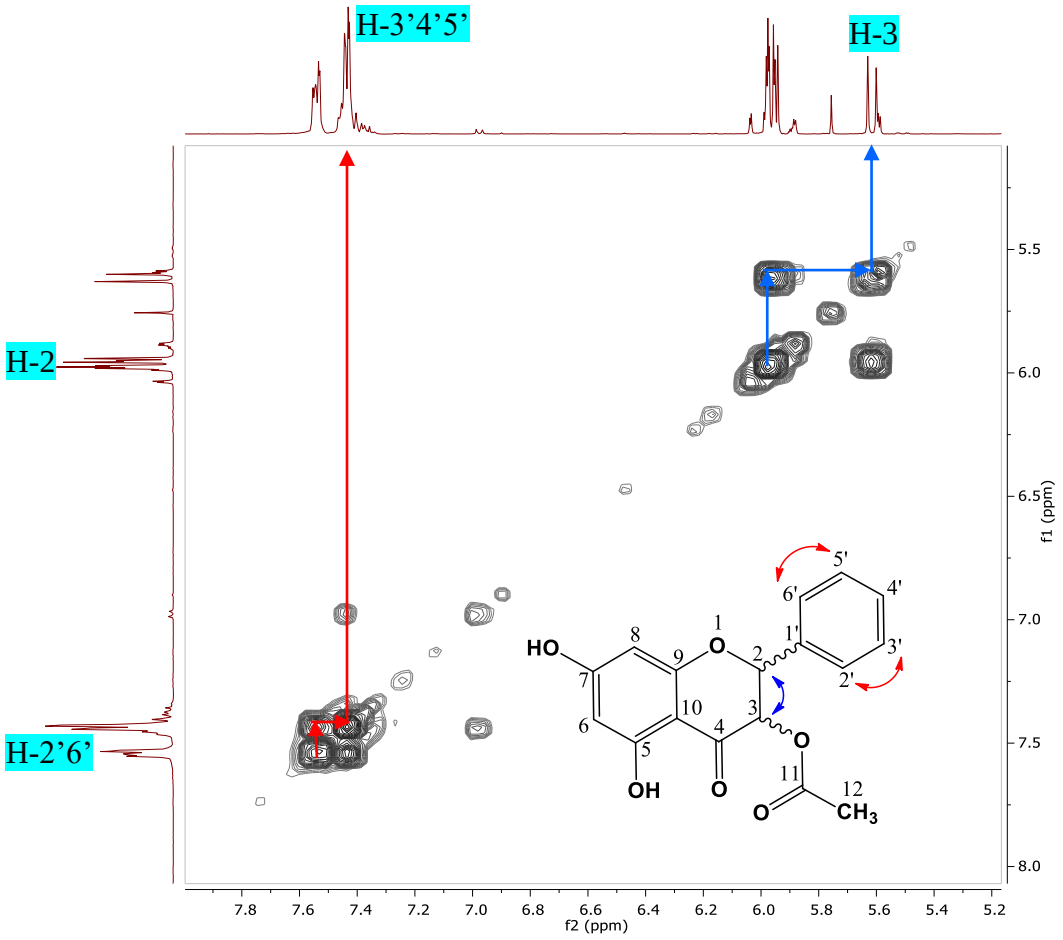

Fig. 4.26: ^{1}H-^{1}H COSY spectrum of **FC2-11-2** in DMSO-d_6 at 400 MHz.

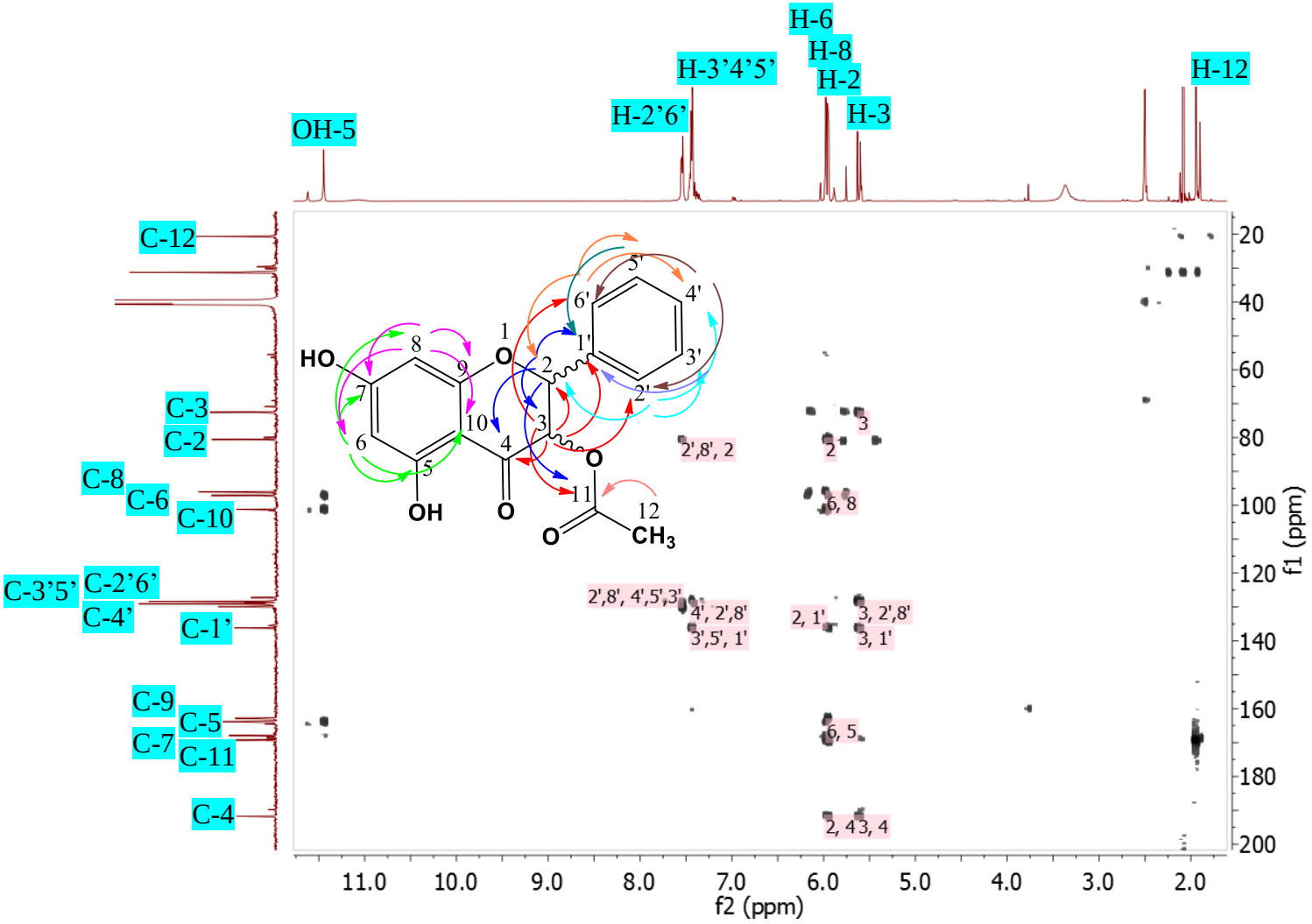

Fig. 4.27: HMBC of **FC2-11-2** in DMSO-d_6 at 400 MHz. The X- and Y-axes correspond to the proton and ^{13}C spectra, respectively.

Table 4.14: ^{1}H NMR (DMSO-d_6, 400 MHz) of **FC2-11-2** and pinobanksin-3-acetate (Neacsu et al., 2007, Tran et al., 2012).

No.	^{1}H NMR, δ_H (multiplicity *J* in Hz)		
	FC2-11-2 in DMSO-d_6	**Neascu et al in MeOD-d_4**	**Tran et al in $CDCl_3$**
H-2	5.96 (*d*, *J* = 11.8 Hz)	5.83 (*d*, *J* = 11.7 Hz)	5.81 (*d*, *J* = 11.7 Hz)
H-3	5.62 (*d*, *J* = 11.8 Hz)	5.41 (*d*, *J* = 11.7 Hz)	5.36 (*d*, *J* = 11.7 Hz)
H-6	5.98 (*d*, *J* = 2.0 Hz)	5.97 (*d*, *J* = 2.0 Hz)	6.04 (*d*, *J* = 2.2 Hz)
H-8	5.95 (*d*, *J* = 2.0 Hz)	5.95 (*d*, *J* = 2.0 Hz)	6.00 (*d*, *J* = 2.2 Hz)
H-phenyl	7.44 - 7.54 (*m*)	7.44 - 7.54 (m)	7.44 m
OH-5	11.45 (*s*)	-	11.47(*s*)
OAc	1.90 (*s*)	1.95 *(s*)	2.02 *(s*)

Table 4.15: ^{13}C NMR (DMSO-d_6, 100 MHz) of **FC2-11-2** and pinobanksin-3-acetate (Neacsu et al., 2007, Tran et al., 2012).

Carbon no.	^{13}C NMR δ_C (ppm)		
	FC2-11-2 in DMSO-d_6	**Neascu et al in MeOD-d_4**	**Tran et al in $CDCl_3$**
2	80.6 CH	85.1 CH	81.3
3	72.6 CH	73.7 CH	72.4
4	191.8 C	193.0 C	191.6
5	163.8 C	165.5 C	164.1
6	97.1 CH	97.8 CH	97.4
7	168.0 C	169.1 C	165.2
8	96.1 CH	96.6 CH	95.9
9	162.8 C	164.1 C	162.5
10	101.2 C	102.1 C	101.9
11	169.3 C	170.7 C	169.5
12	20.1 C	No data	20.3
1'	136.2 C	137.2 C	135.1
2'	128.3 CH	128.7 CH	127.3
3'	129.9 CH	129.6 CH	128.7
4'	130.2 CH	130.4 CH	129.6
5'	129.9 CH	129.6 CH	128.7
6'	128.3 CH	128.7 CH	127.3

*4.3.2.4 Chrysin /**FC2-43-44***

Table 4.16: The spectral data of **FC2-43-44** was compared to chrysin (Park et al., 2007).

Chrysin (P_1853)
Source: New Zealand yellow propolis
Sample amount: 10.3 mg (colourless needle)
Molecular formula: $C_{15}H_{10}O_4$
Molecular weight: 254.2375 g/mol
Exact mass: 254.0579

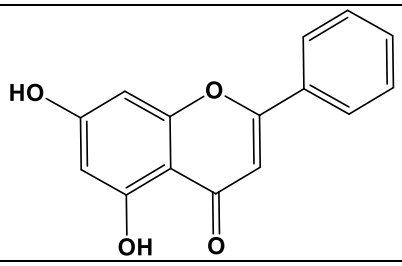

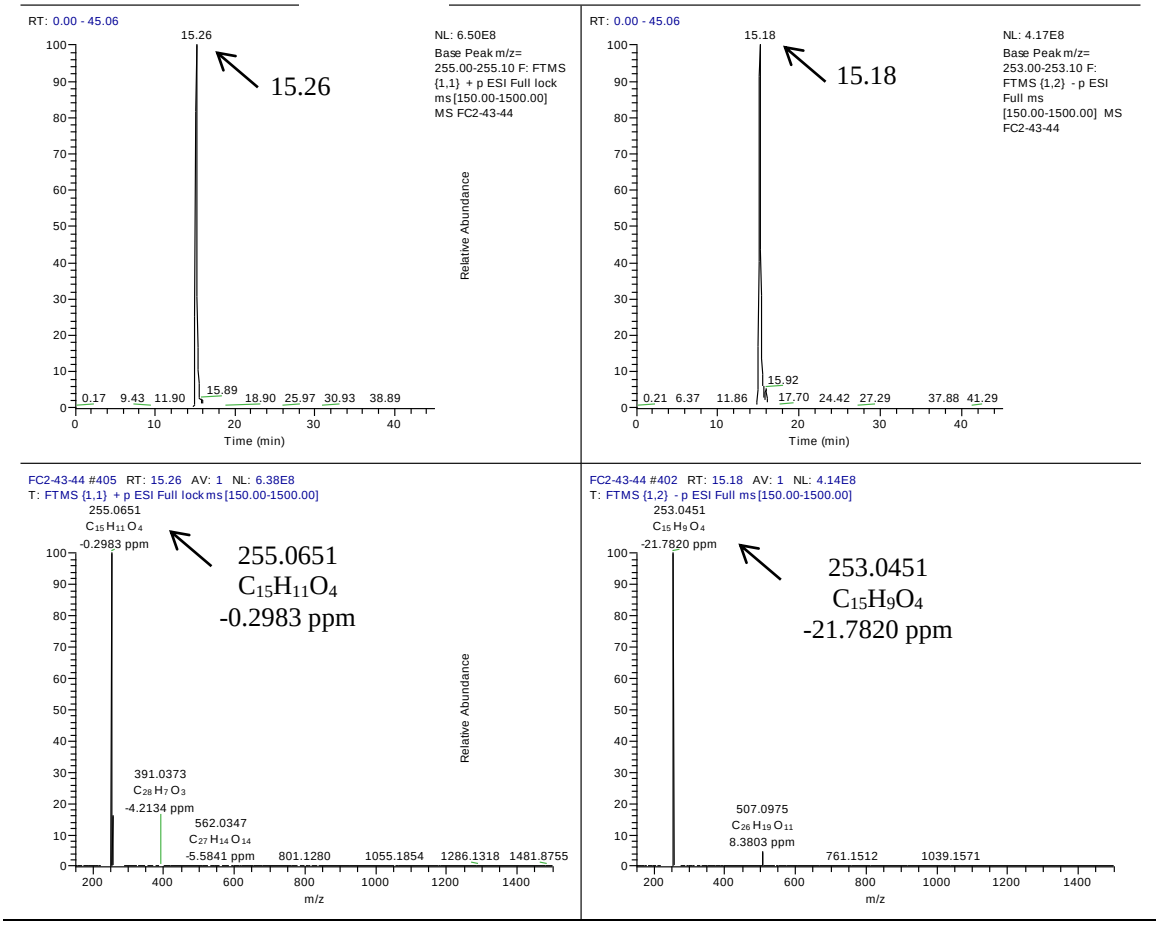

Based on the high-resolution mass spectral data of **FC2-43-44**, the ESI peak at 15.26 and 15.18 min afforded ion peaks at *m/z* 255.0651 $[M+H]^+$ and 253.0451 $[M-H]^-$ in both positive and negative, respectively. This revealed the exact mass of 254.0579 g/mol, established the molecular formula $C_{15}H_{10}O_4$ (**Table 4.16**). The degree of unsaturation for $C_{15}H_{10}O_4$ was calculated to be eleven, which indicated the total number of double bonds and rings in the structure.

The ^{1}H NMR spectrum of **FC2-43-44** (**Fig. 4.28**) contained proton signals between 6.0– 13.0 ppm and was comparable to FC2-32-34, which was elucidated as galangin. As in galangin, a pair of *meta* doublets vicinal to hydroxyl substituents was observed at δ6.22 and 6.52. Proton signals for phenyl unit resonated between 7.59 – 8.07 ppm. When compared to the ^{1}H NMR spectrum of **FC2-32-34**, there is an additional singlet at 6.96 ppm, which signified the loss of a hydroxyl moiety at C-3. This was further confirmed by the 16 mass unit difference of **FC2-43-44** with **FC2-32-34**. The JMOD spectrum (**Fig. 4.29**) of **FC2-43-44** gave the same number of carbons as **FC2-32-34** except for the loss of the quaternary carbon at 137.3 ppm in exchange for the appearance of a shielded methine carbon at 105.7 ppm. It was also observed that the carbon shift for C-2 (163.6) and C-4 (182.3) in **FC2-43-44** went downfield by 20 and 10 ppm, respectively. Based on the 1D spectra, it was assumed that **FC2-43-44** is a dehydroxyl congener of **FC2-32-34**.

^{1}H-^{1}H COSY (**Fig. 4.30**), HMQC (**Fig. 4.31**) and HMBC (**Fig. 4.32**) were performed to confirm the structure of **FC2-43-44**. The ^{1}H-^{1}H COSY and HMBC correlation patterns observed in **FC2-43-44** were comparable to those found in **FC2-32-34**, particularly for rings A and B**.** Additional HMBC cross peaks were observed for H-3. The proton singlet of C-3 at 6.96 ppm correlated with C-4, C-10, C-2 and C-1' at δ182.3, 104.4, 163.6 and 131.2, respectively. The structure of **FC2-43-44** was elucidated as 5,7-dihydroxyflavone. The ^{1}H and ^{13}C NMR spectral data (**Table 4.17** and **4.18**) were comparable to those reported or chrysin (Park et al., 2007).

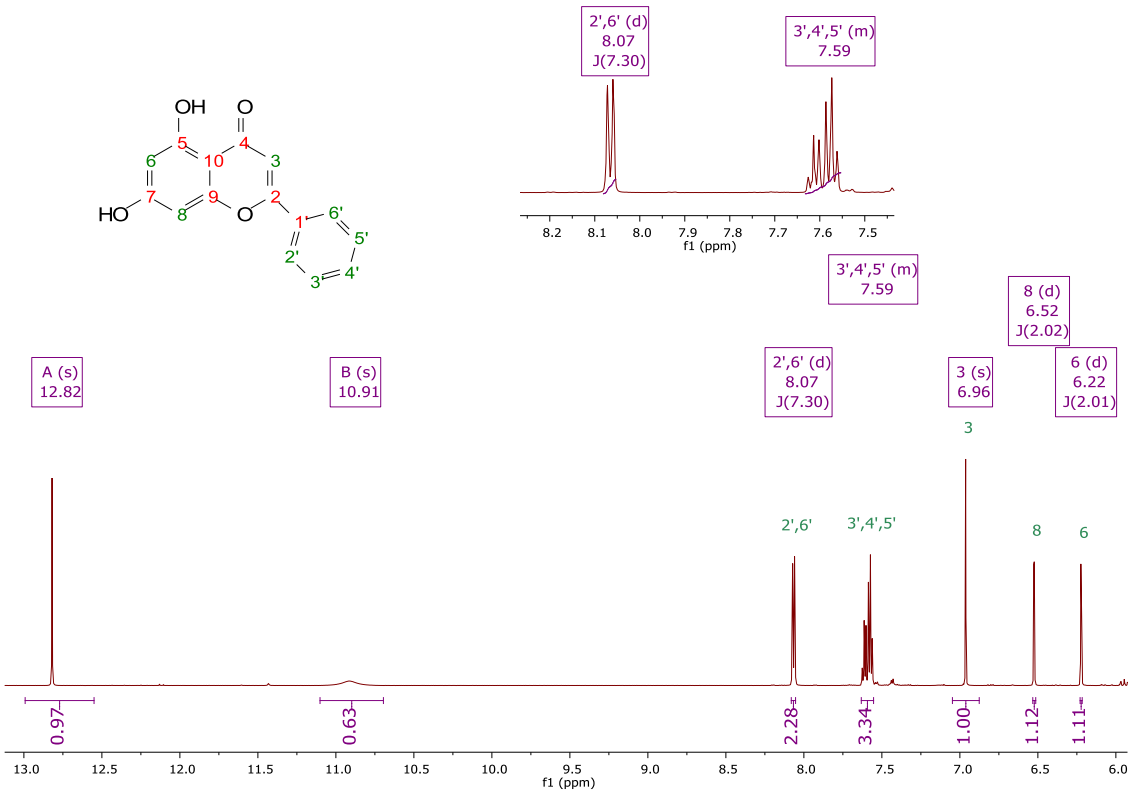

Fig. 4.28: ^{1}H NMR spectrum of **FC2-43-44** in DMSO-d_6 at 600 MHz.

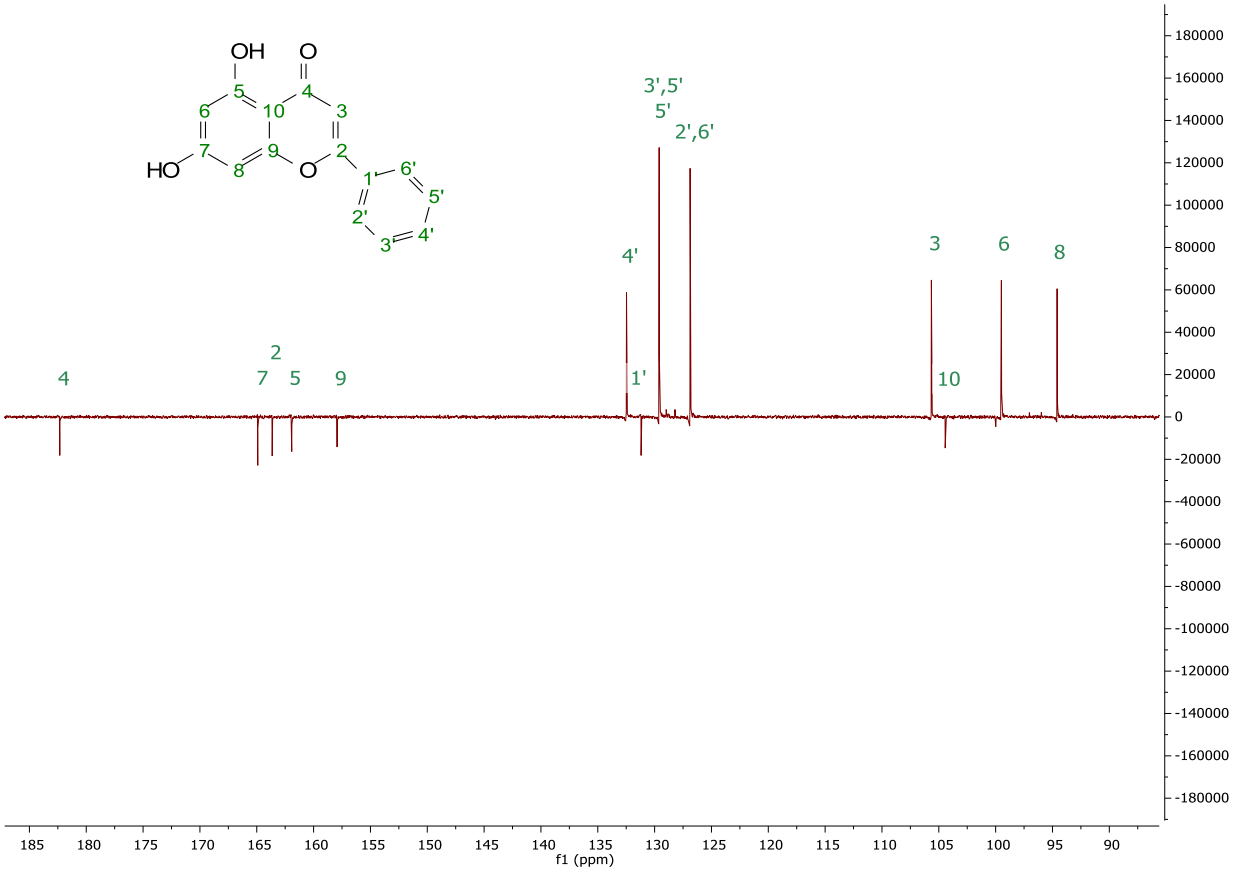

Fig. 4.29: JMOD spectrum of **FC2-43-44** in DMSO-d_6 at 150 MHz.

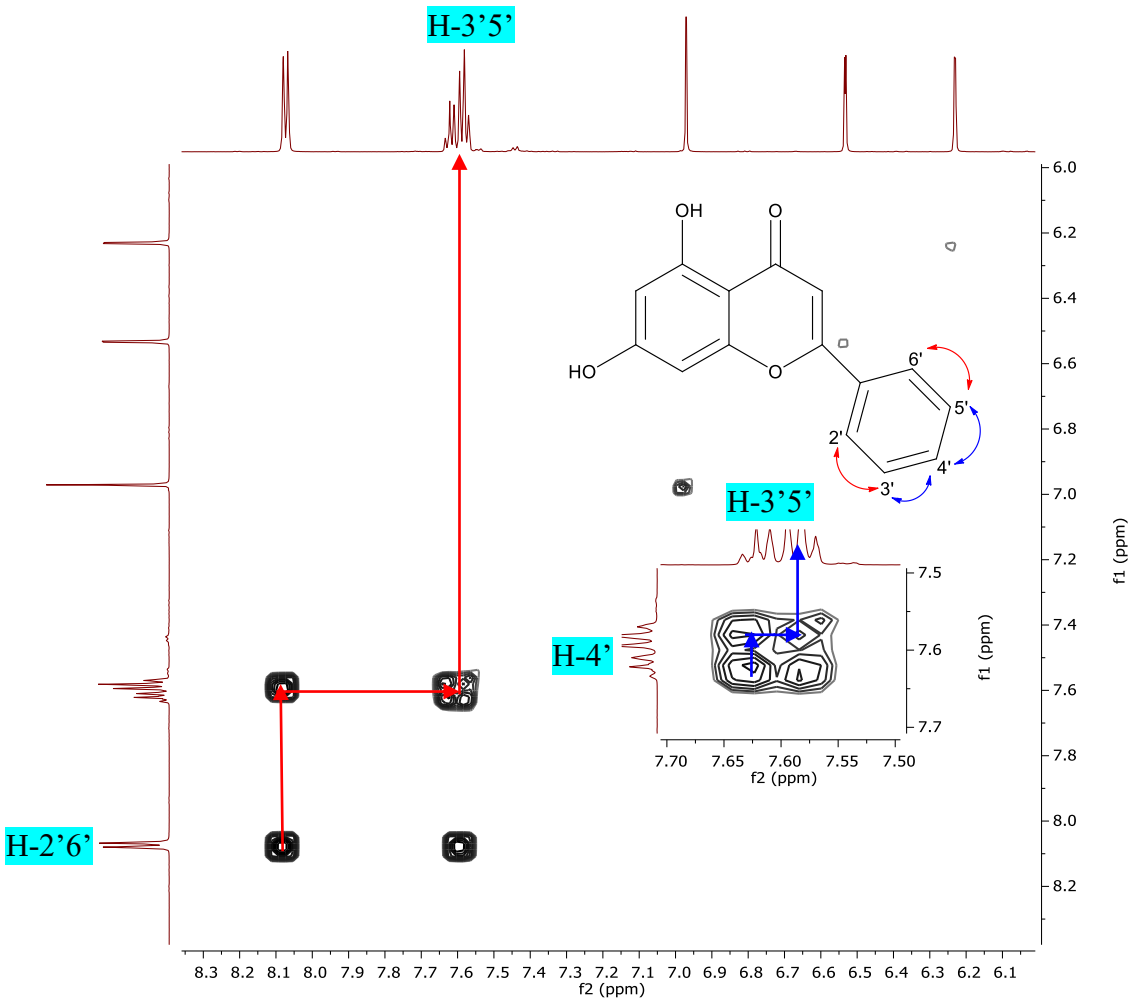

Fig. 4.30: ^{1}H-^{1}H COSY spectrum of **FC2-43-44** in DMSO-d_6 at 600 MHz.

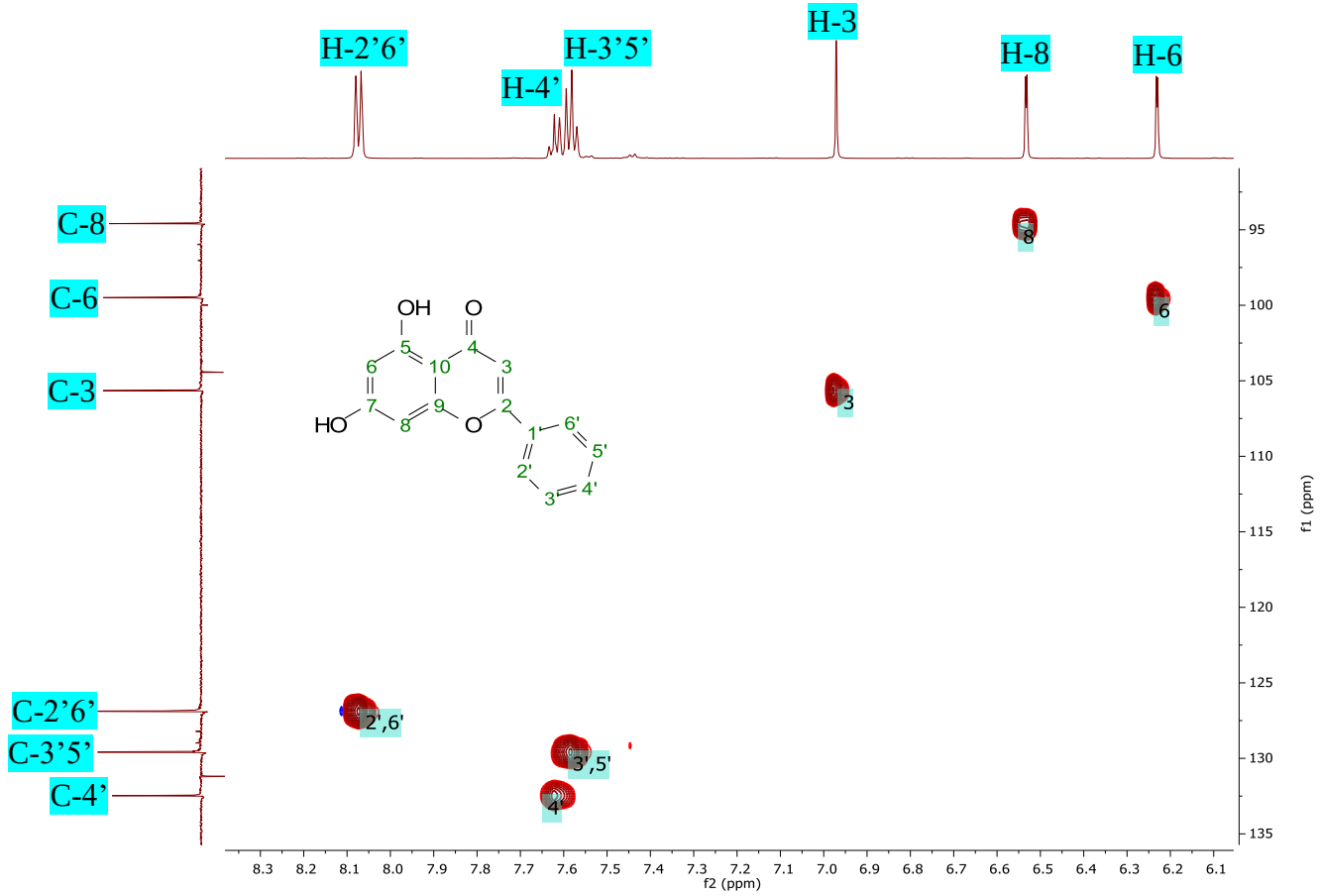

Fig. 4.31: HSQC of **FC2-43-44** in DMSO-d_6 at 600 MHz. The X- and Y-axes correspond to the proton and JMOD spectra, respectively.

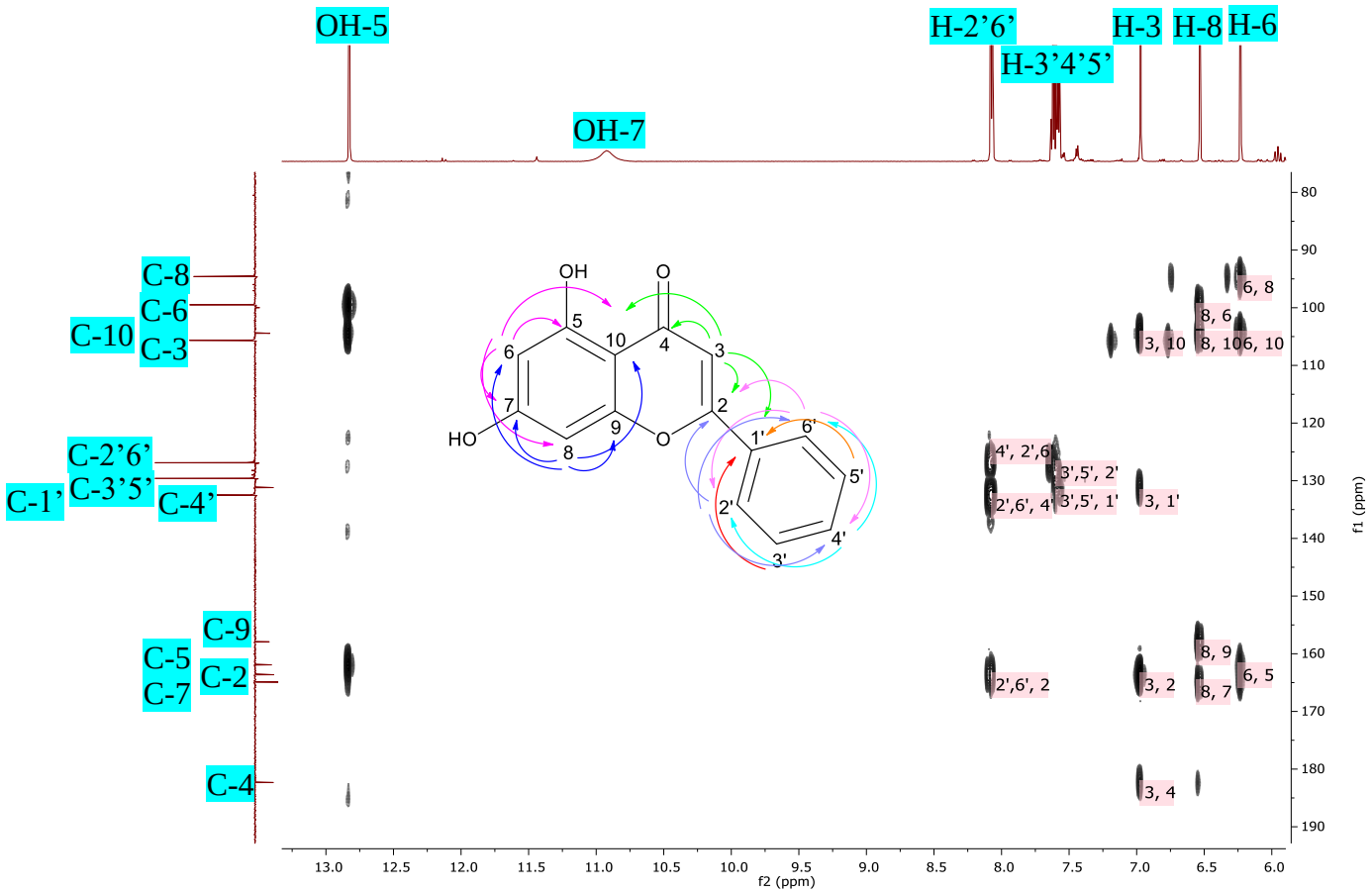

Fig. 4.32: HMBC of **FC2-43-44** in DMSO-$d_6$at 600 MHz. The X- and Y-axes correspond to the proton and JMOD spectra, respectively.

Table 4.17: ^{1}H NMR (DMSO-d_6, 600 MHz) of **FC2-43-44** and chrysin (Park et al., 2007).

No.	^{1}H NMR, δ_H (ppm, multiplicity J in Hz)	
	FC2-43-44in DMSO	**(Park et al., 2007) in DMSO**
H-3	6.96 (*s*)	6.91 (*s*)
H-6	6.22 (*d*, *J* = 2.0 Hz)	6.21 (*d*, *J* = 2.0 Hz)
H-8	6.52 (*d*, *J* = 2.0 Hz)	6.50 (*d*, *J* = 2.0 Hz)
H-2'	8.07 (*d*, *J* = 7.3 Hz)	8.02 (*d*, *J* = 6.8 Hz)
H-3'	7.59 (*m*)	7.55 (*m*)
H-4'	7.59 (*m*)	7.56 (*m*)
H-5'	7.59 (*m*)	7.55 (*m*)
H-6'	8.07 (*d*, *J* = 7.3 Hz)	8.02 (*d*, *J* = 6.8 Hz)
OH-5	12.82 (*s*)	12.80 (*s*)
OH-7	10.91 (*br, s*)	10.90 (*br, s*)

Table 4.18: ^{13}C NMR (DMSO-d_6, 150 MHz) of **FC2-43-44** and chrysin (Park et al., 2007).

Carbon no.	^{13}C NMR δ_C (ppm)	
	FC2-43-44 in DMSO	**(Park et al., 2007) in DMSO**
2	163.6 C	163.2 C
3	105.7 CH	105.2 CH
4	182.3 C	181.8 C
5	161.9 C	161.5 C
6	99.5 CH	99.0 CH
7	164.9 C	164.4 C
8	94.6 CH	94.1 CH
9	157.9 C	157.5 C
10	104.4 C	103.9 C
1'	131.2 C	130.7 C
2'	126.9 CH	126.4 CH
3'	129.6 CH	129.1 CH
4'	132.5 CH	131.9 CH
5'	129.6 CH	129.1 CH
6'	126.9 CH	126.4 CH

*4.3.2.5 Benzyl caffeate/**FC2-11-5***

Table 4.19: Spectral data of **FC2-11-5** compared to benzyl caffeate (Yamauchi et al., 1992).

Benzyl caffeate (P_1863)

Source: New Zealand yellow propolis

Sample amount: 7.8 mg (colourless sticky material)

Molecular formula: $C_{16}H_{14}O_4$

Molecular weight: 270.2800 g/mol

Exact mass: 270.0892

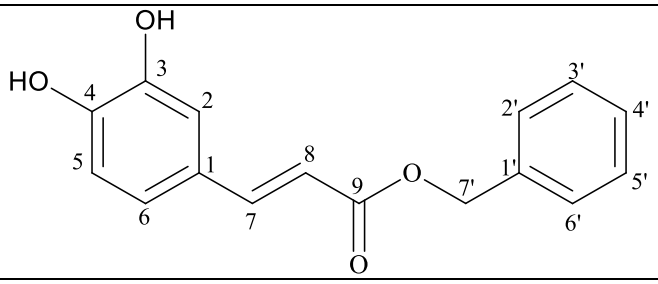

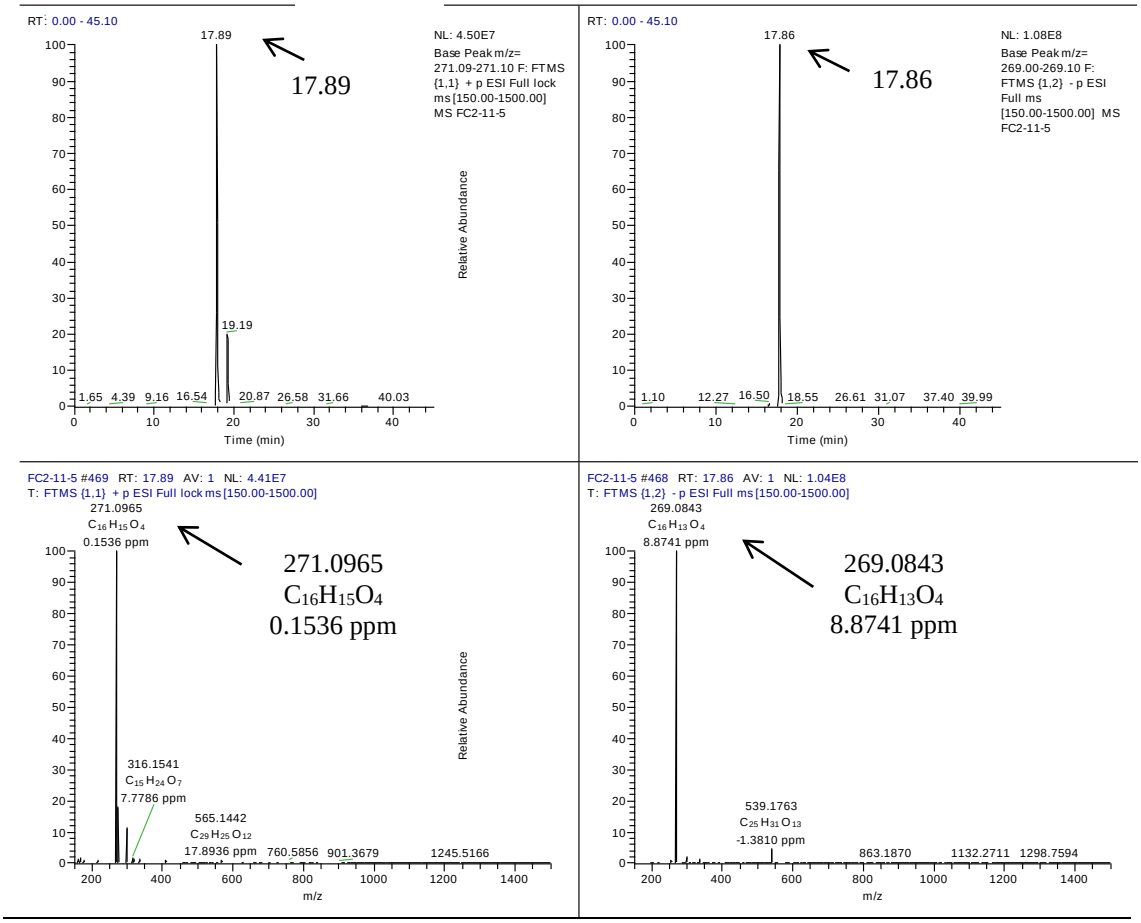

Based on the high-resolution mass spectral data, the ESI peak at 17.89 and 17.86 min in both positive and negative were found at *m/z* 271.0965 $[M+H]^+$ and *m/z* 269.0843 $[M-H]^-$, respectively. This revealed the exact mass of 270.0892 g/mol, which established the molecular formula $C_{16}H_{14}O_4$ (**Table 4.19**). The degree of unsaturation of $C_{16}H_{14}O_4$ was calculated to be ten, which indicates the total of double bonds and rings in the structure.

The ^1H NMR spectrum of **FC2-11-5** (**Fig. 4.33**) contained proton signals between 5.0– 9.5 ppm. A set of shielded ABC proton resonances was observed at δ7.12 (*d*, *J* = 2.1 Hz), 7.15 (*dd*, *J* = 8.4, 2.1 Hz), and 6.96 (*d*, *J* = 8.3 Hz) for a tri-substituted phenyl system. These signals were interpreted as protons for H-2, H-6, and H-5, respectively at *meta*, *ortho*, and *para* positions with each other. The shielding effect was evidenced by the presence of two hydroxyl substituents, one of which is vicinal to the *ortho*-proton. *Trans*-olefinic doublets resonated at δ7.57 and 6.41 with a coupling constant of 15.9 Hz for H-7 and H-8, respectively. A benzylic methylene singlet was detected at 5.20 ppm for H-7'. Protons of the phenyl moiety were observed between 7.28 – 7.48 ppm. The signals at δ166.8 for an ester carbon can be seen in ^{13}C spectrum at position C-9 (**Fig. 4.34**). The corresponding olefinic carbons were observed at δ145.6 and 115.5 for C-7 and C-8, respectively. Meanwhile, the methylene carbon resonated at δ64.9. Based on this spectrum, it was assumed that the structure of **FC2-11-5** possessed a benzyl ester backbone. ^1H-^1H COSY (**Fig. 4.35**), HMQC (**Fig. 4.36**), and HMBC (**Fig. 4.37**) were performed to confirm the structure of **FC2-11-5**. From the ^1H-^1H COSY spectrum, three sets of spin systems were observed. The ABC spin system could be followed through for H-2, H-5 and H-6. Proton correlations were observed between coupling protons H2'/6' and H3'/5'as well as between the olefinic protons, H-7 and H-8.

Based on HMBC spectrum, the *meta*-proton H-2 at δ7.12 showed correlations with C-3, C-4, C-6 and C-7 at δ150.7, 147.2, 150.7, 121.9, and 145.6, respectively. Meanwhile, the *ortho-meta*-proton H-6 at δ6.96 showed cross peaks with C-5, C-4, C-3, C-2 and C-7 at δ112.5, 147.2, 150.7, 114.8, and 145.6, respectively.The olefinic methine doublet at δ7.57 for H-7 showed correlations with C-2, C-6 and C-9 at

δ114.8, 121.9 and 166.8, respectively while the coupling partner H-8 at δ6.41 correlated with C-1 and C-7' at δ127.4 and 64.9, respectively. Furthermore, the benzylic methylene singlet at 5.20 ppm for H-7' afforded cross peaks with C-1', C-2'/6' and C-9 at δ136.6, 129.3 and 166.8, respectively. On the other hand, the proton signals on phenyl moiety yielded cross peaks with its corresponding phenyl carbons. The structure of **FC2-11-5** was elucidated as 3,5,7-trihydroxyflavanone based on its ^{1}H and ^{13}C NMR spectral data (**Table 4.20** and **4.21**) and was compatible to benzyl caffeate (Yamauchi et al., 1992) .

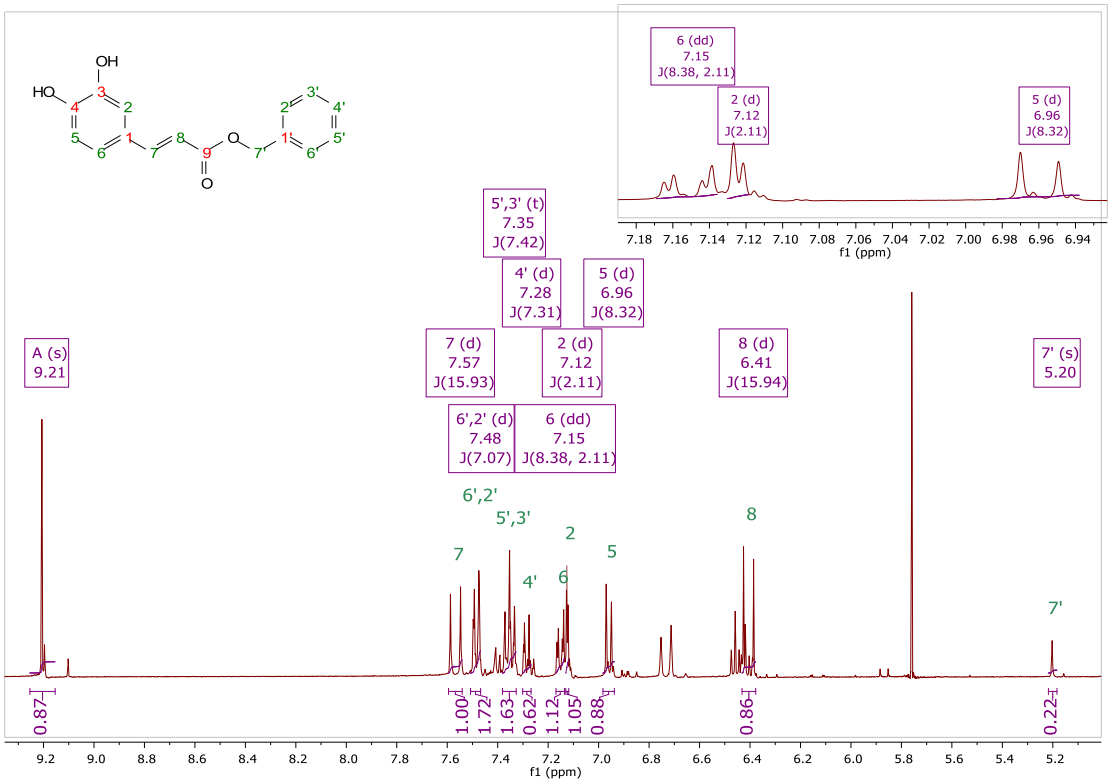

Fig. 4.33: ^{1}H NMR spectrum of **FC2-11-5** in DMSO-d_6 using JEOL-LA400 FT-NMR instrument.

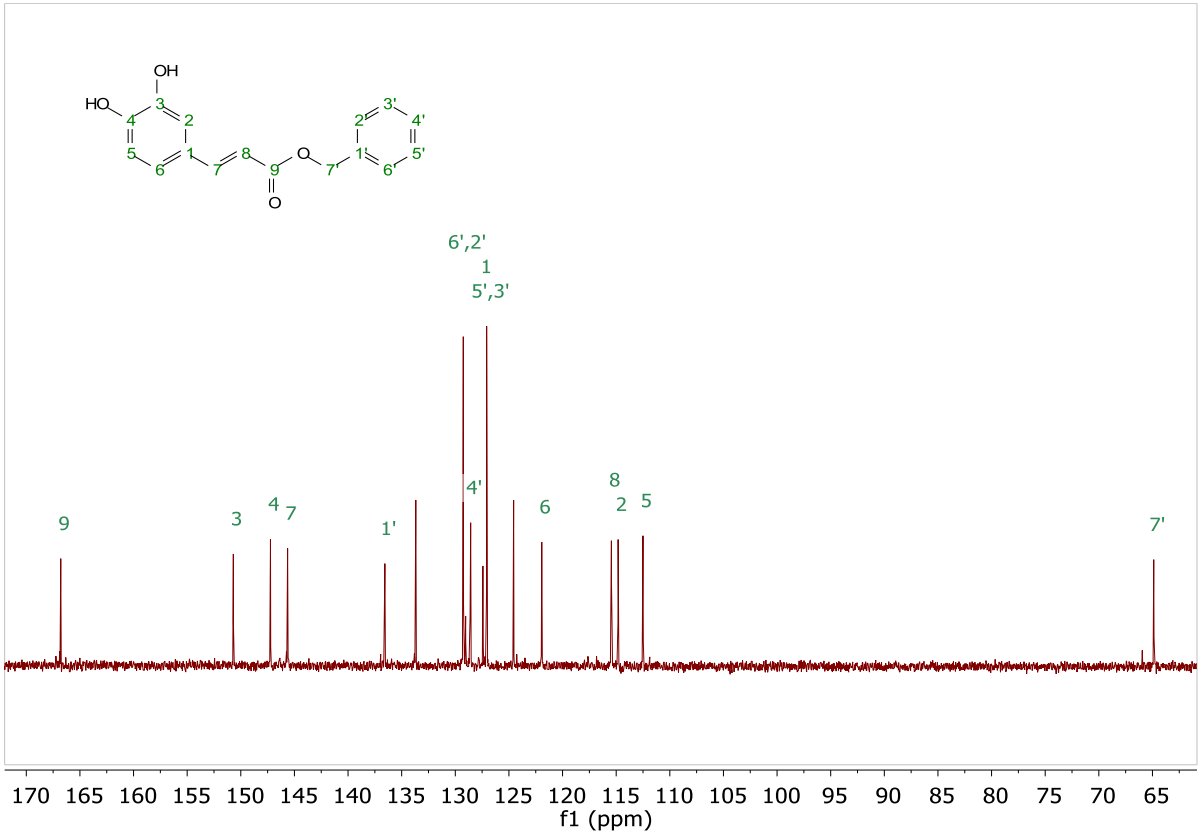

Fig. 4.34: ^{13}C spectrum of **FC2-11-5** in DMSO-d_6 at 100 MHz.

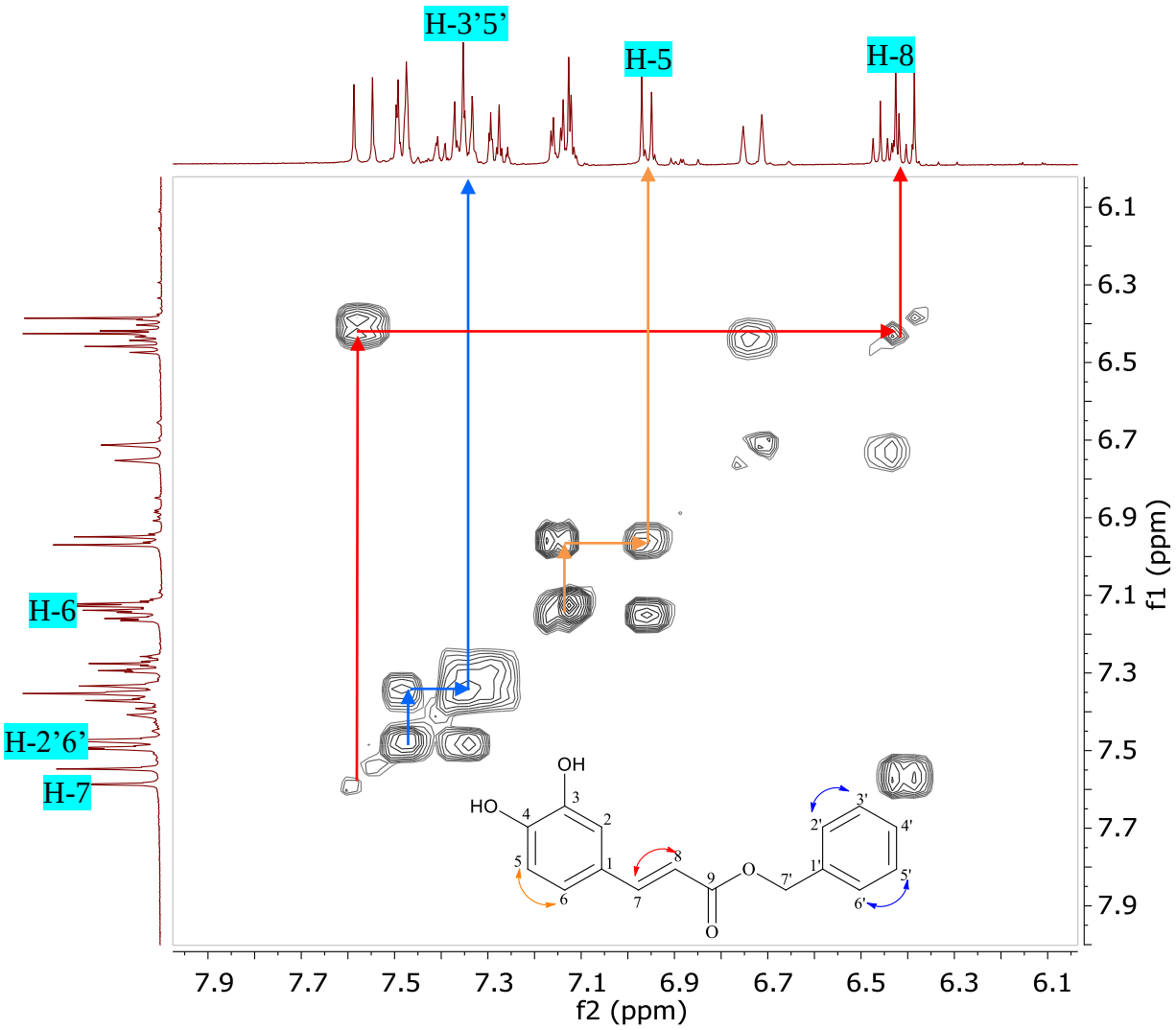

Fig. 4.35: ^{1}H-^{1}H COSY spectrum of **FC2-11-5** in DMSO-d_6 at 400 MHz.

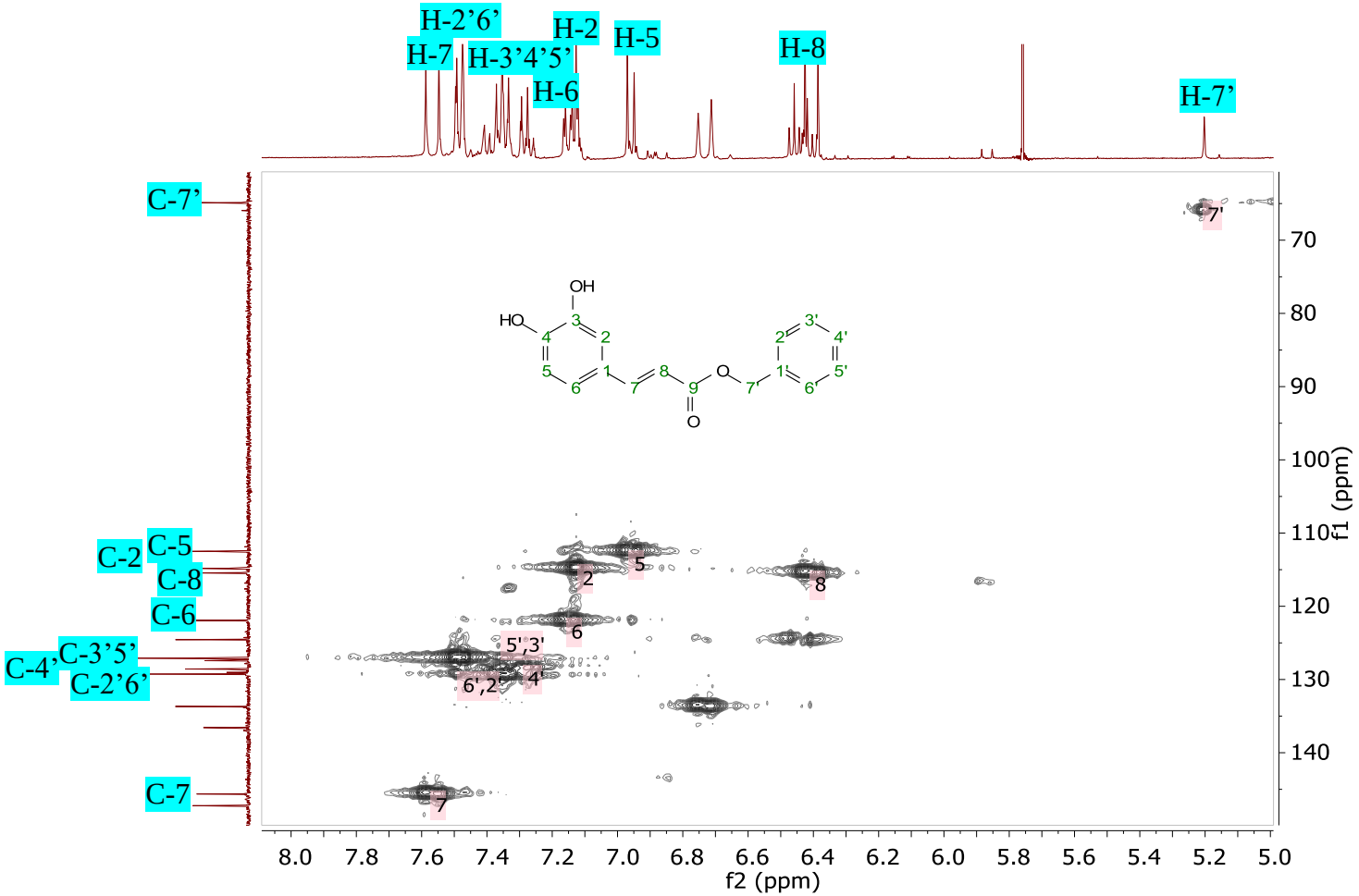

Fig. 4.36: HMQC spectrum of **FC2-11-5** in DMSO-d_6 at 400 MHz.

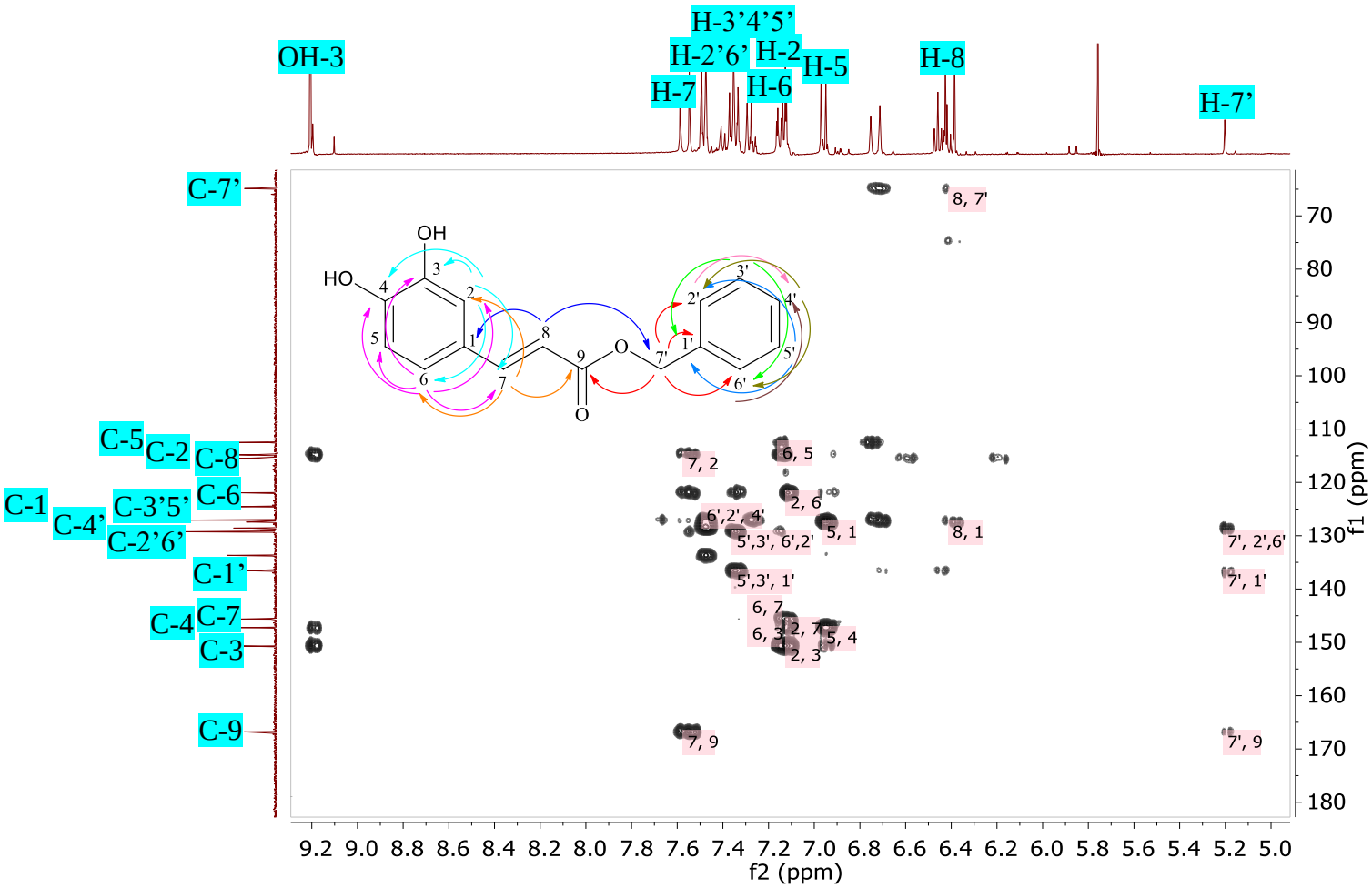

Fig. 4.37: HMBC of **FC2-11-5** in DMSO-d_6 at 400 MHz. The X- and Y-axes correspond to the proton and ^{13}C spectra, respectively.

Table 4.20: ^{1}H NMR (DMSO-d_6, 400 MHz) of **FC2-11-5** and benzyl caffeate (Yamauchi et al., 1992).

No.	^{1}H NMR, δ_H (multiplicity *J* in Hz)	
	FC2-11-5 in DMSO	**(Yamauchi et al., 1992) in CD_3OD**
OH	-	5.04 (*br, s*)
OH-3	9.21 (*s*)	-
H-7'	5.20 (*s*)	5.19 (*s*)
H-8	6.41 (*d, J*=15.9Hz)	6.30 (*d, J*=15.8Hz)
H-5	6.96 (*d, J*=8.3Hz)	6.79 (*d, J*=8.1Hz)
H-6	7.15 (*dd, J*=2.1, 8.4Hz)	6.93 (*dd, J*=2.1, 8.1Hz)
H-2	7.12 (*d, J*=2.1Hz)	7.06 (*d, J*=2.1Hz)
H-2'3'4'5'6'	7.28 - 7.48 (*m*)	7.26 - 7.40 (*m*)
H-7	7.57 (*d, J*=15.9Hz)	7.58 (*d, J*=15.8Hz)

Table 4.21: ^{13}C NMR (DMSO-d_6, 100 MHz) of **FC2-11-5** and benzyl caffeate (Yamauchi et al., 1992).

Carbon no.	^{13}C NMR δ_C (ppm)	
	FC2-11-5 in DMSO	**(Yamauchi et al., 1992) in CD_3OD**
7'	64.9 CH_2	67.1 CH_2
8	115.5 CH	114.9 CH
2	114.8 CH	115.2 CH
5	112.5 CH	116.5 CH
6	121.9 CH	123.0 CH
1	127.4 C	127.7 C
2'6'	129.3 CH	129.1 or 129.5 CH
3'5'	127.1 CH	129.1 or 129.5 CH
4'	128.6 CH	129.1 or 129.5 CH
1'	136.6 C	137.7 C
3	150.7 C	146.7 C
7	145.6 CH	147.1 CH
4	147.2 C	149.5 C
9	166.8 C	169.0 C

4.3.3 Biological activities of isolated compounds

Five compounds were isolated from New Zealand propolis, namely: galangin, (2*R*,3*R*)-pinobanksin, pinobanksin-3-acetate, chrysin, and benzyl caffeate (**Fig. 4.38**). Each of these compounds has selective bioactivities *In-vitro* on lung cancer (A549), ovarian cancer (A2780) and breast cancer (ZR75) cell line, as well as their toxicity on normal cell line (PNT2A) (**Table 4.22**). Based on *In-vitro* experiments, benzyl caffeate gave the most potent cytotoxicity effects on A549 at IC_{50} value of 15.81 µM, followed by chrysin, pinobanksin-3-acetate, (2*R*,3*R*)-pinobanksin, and galangin with IC_{50} values of 23.74, 30.07, 36.65 and 64.79 µM, respectively. Meanwhile, for cytotoxicity activity against A2780, pinobanksin-3-acetate showed the highest IC_{50} value of 1.22 µM, followed by benzyl caffeate at 15.38 µM, galangin at 21.30 µM, (2*R*,3*R*)-pinobanksin at 66.57 µM, and chrysin at 89.72 µM. Moreover, benzyl caffeate demonstrated the most potent cytotoxicity effects on ZR75 at IC_{50} value of 52.15 µM, followed by galangin and chrysin with IC_{50} values of 80.49 and 100 µM, respectively. Interestingly, both pinobanksin congeners were inactive on the normal cell line (PNT2A) while they exhibited cytotoxicity effects on cancer cell lines, A549 and A2780. However, none of the isolated compounds from New Zealand propolis had any effects on zebrafish assay.

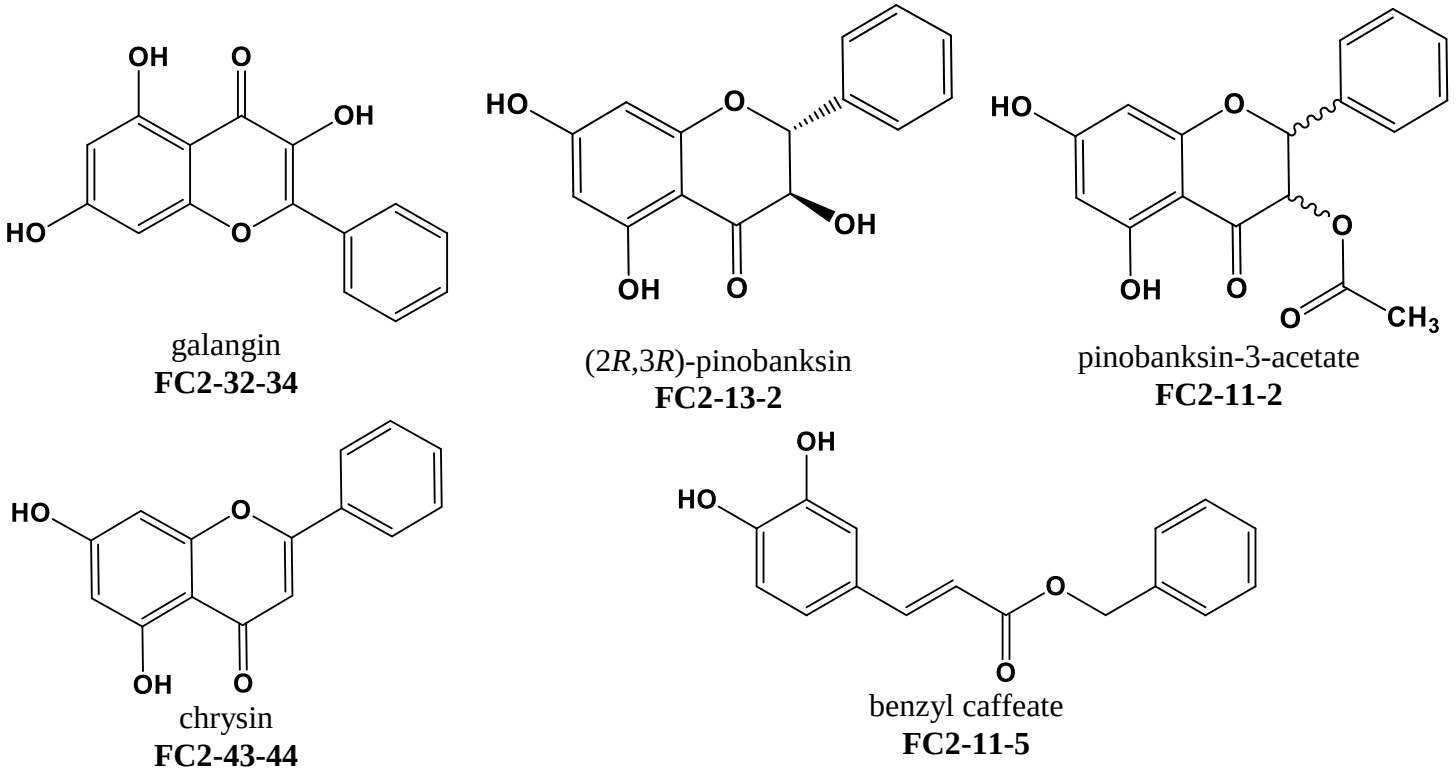

Fig. 4.38: Structures of isolated compounds from New Zealand yellow propolis.

Table 4.22: Summary of *In-vitro* and *In-vivo* assays of isolated compound (n=3). Highlighted cells showed cytoxicity effects on cancer cell lines as compared to PNT2A.

Chemical Name	Cell line[a)]				Zebrafish assay			
	Lung cancer (A549)	Ovary cancer (A2780)	Breast cancer (ZR75)	Normal prostate epithelial (PNT2A)	Phenotypic[b)] (appearance of curved/curled tail/trunk)		Angiogenic[c] (The absent of blood vessel)	
	IC_{50}(μM)				**20μM**	**10μM**	**20μM**	**10μM**
galangin	64.79±0.240	21.30±0.200	80.49±0.017	48.07±0.209	N	N	N	-
(2*R*,3*R*)-pinobanksin	36.65±0.606	66.57±0.617	>100±0.371	>100±0.433	N	N	N	-
pinobanksin-3-acetate	30.07±0.482	1.22±0.247	>100±0.828	>100±0.187	N	N	N	N
chrysin	23.74±0.133	89.72±0.057	100±0.193	29.50±0.088	N	N	N	-
benzyl caffeate	15.81±0.289	15.38±0.203	52.15±0.082	20.18±0.097	N	N	N	N

a) an identical medium volume as vehicle control, whereas Triton-X 4% positive control
b) vehicle control DMSO 0.5%, positive control DAPT 50 μM
c) vehicle control DMSO 0.5%, positive control Sunitinib malate (SM) 20μM, N=No

4.4 Discussion

4.4.1 Secondary metabolites isolated from New Zealand propolis

4.4.1.1 Flavonoid from New Zealand propolis

Flavonoids are found in nature from several plant parts and belong to a large group of phenolic plant constituents. They were derived from 2-phenyl-benzo-γ-pyrone which were assembled in two benzene rings, denoted as A and B rings that connected by an oxygen containing pyrene (C) ring (Brodowska, 2017). Based on a flavan system, flavonoids can be regarded as a C_6-C_3-C_6 carbon skeleton. In some cases, the six-membered ring C could occur in an isomeric open form or replaced by a five-membered ring. Commonly, they are easily recognised by colour pigments in flowers and fruits but also can be found in leaves, rhizomes, seeds and other part of plants. The core structures of flavonoids possesses fifteen carbon atoms with low molecular weight compounds. However, flavonoids could also occur as polyphenolics. The biosynthesis of flavonoids starts with the synthesis of 4-coumaroyl-CoA from phenylalanine by three enzymatic reactions involving phenylalanine ammonia lyase (PAL), cinnamate-4-hydroxylase (C4H), 4-coumarate:CoA ligase (4CL) (**Fig. 4.39**). Collectively, this reaction is called the general phenylpropanoid pathway (GPP). The condensation of 4-coumaroyl-CoA with three molecules malonyl-CoA by chalcone synthase (CHS) producednaringenin chalcone, the precursor of flavonoid synthesis. Subsequently, naringenin chalcone is isomerised by chalcone isomerase (CHI) to produce flavanone, the central intermediate for the further synthesis of the different classes of flavonoid (Koes et al., 1994, Song et al., 2014). In general, flavonoids can be divided into several classes namely: flavanols, flavanones, flavonols, isoflavones, flavones, chalcones and anthocyanidins. In plants, the biosynthesis of flavonoids has its specific role during nodulation (Wasson et al., 2006), plant reproduction and fertility (Van Der Meer et al., 1992), prevents damage caused by high UV-B exposure (Casati and Walbot, 2005), as well as protects against pathogens and herbivores (Kliebenstein, 2004, Bidart-Bouzat and Imeh-Nathaniel, 2008).

Based on the chemical structure, the compounds that have been isolated from New Zealand propolis were classified as flavone, dihydroflavonol, flavonol and caffeate, for chrysin, pinobanksin, galangin and benzyl caffeate, respectively (Van Acker et al., 2017, Clark and Verwoerd, 2011). These major flavonoid skeletons are synthesised from flavanone, which involve several enzymes including flavone synthase I/II (FNSI/II), flavanone-3β-hydroxylase (F3H), flavonol synthase from populus (PFLS), hydroxycinnamoyl-CoA shikimate hydroxyl cinnamoyl tranferase (HCT) and cinnamate-4-hydroxylase (C4H). Flavones have a double bond between C-2 and C-3 in the C ring, also two hydroxyl groups attached to the A or B rings. They are widely found in fruits and vegetables such as orange, apple skin, chamomile, celery, parsley, red pepper, carrot, onion, broccoli and cabbage. Several studies have reported anti-inflammatory, anti-carcinogenic and antioxidant properties of apigenin and luteolin, which were also derived, from flavones but with extra hydroxyl groups attached to the B ring (Patel et al., 2007, Horinaka et al., 2006, Galati and O'Brien, 2004, Lapidot et al., 2002).

Flavanols or dihydroflavonols, also referred to as flavan-3-ols, have a hydroxyl group attached on C-3 of the C ring but unlike flavones, the double bond between C-2 and C-3 is absent in flavanols. They are found mainly in fruits such as kiwis, bananas, apples, blueberries, pears and peaches but are almost absent in vegetables and legumes. They also can be found in tea, cocoa, as well as fruit skin. Catechin, one of the flavanol constitutes, has been reported to have preventative effects on atherosclerosis, carcinogenic and diabetic diseases (Rein et al., 2000, Murphy et al., 2003, Kwon et al., 2008). Meanwhile the basic skeleton structure of flavonol or 3-hydroxyflavone is close to flavones, but with additional hydroxyl group on C-3 of the C ring. Significant amounts of flavonols occur in fruits and vegetables such as grapes, apples, berries, tomatoes, onions, broccoli, red lettuce, tea and kale (Brodowska, 2017, Panche et al., 2016). The two hydroxyl groups that are attached to C-5 and C-7 of A ring, a double bond between C-2 and C-3 and a ketone on C-4 of the C ring are responsible for flavonols antioxidant properties (Makris et al., 2006). On top of that, kaempferol, one of flavonols derivatives, demonstrated anti-cancer activities on cancer cells while being inactive on normal cells (Chen and Chen,

2013). Whereas myricetin is effective in preventing smoking habits, as well as being anti-inflammatory, antihyperlipidemic, antioxidant and antidiabetic. It also can prevent eye and nerve damage related with diabetic disease (Li and Ding, 2012). On the other hand, caffeates derived from chalcones (subclasses of flavonoids) are characterised by the absence of the C ring, appearing as open-chain flavonoids. They are mainly found in fruits and vegetables such as tomatoes, pears, strawberries, bearberries and some from wheat products (Panche et al., 2016). Anti-proliferative properties of some caffeate derivatives have been described (Fiuza et al., 2004), which showed the effect of structure-activity relationships (SARs) on their biological activities. The substitution of hydroxyl group in the ring was found to rule the anti-carcinogenic effects on caffeates.

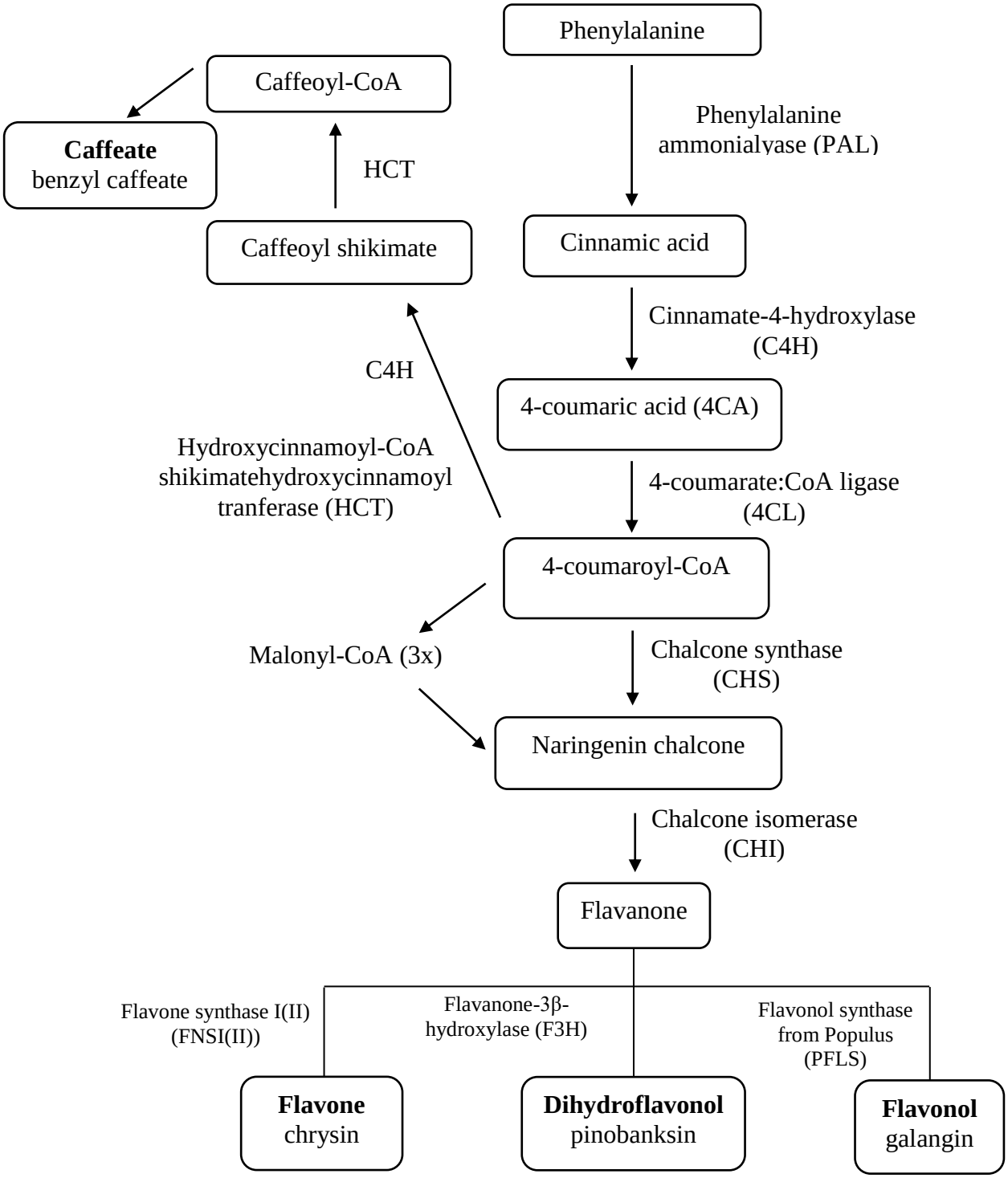

Fig. 4.39: Simplified diagram of general phenylpropanoid pathway (GPP) for the production of flavonoids such as chrysin, pinobanksin, galangin and benzyl caffeate, adapted from (Van Acker et al., 2017, Clark and Verwoerd, 2011, Song et al., 2014).

The U.S. Department of Agriculture database modified in 2014 has listed down several flavonoids subclasses commonly present in the human diet (Bhagwat et al., 2014). Flavonols that includes kaempferol, myricetin and quercetin can be found in onions, kale, broccoli, apples, cherries, fennel, sorrel, berries and tea. Flavones such as apigenin and luteolin are found in celery, parsley, thyme and red pepper. Flavanones including hesperedin and naringenin are found in citrus and prunes. Flavan-3-ols namely catechins and gallic esters of catechins, epicatechins, epigallocatechin, teaflavins and gallic esters of teaflavins are found in tea, apples and cocoa. Anthocyanidins such as cyanidin, delphinidin, malvidin, pelargonidin, peonidin and petunidin are found in cherries and grapes. In addition to that, isoflavones including genistein, daidzein, glycitein, formononetin and biochaninA are commonly found in soya beans and legumes. **Table 4.23** summarised the effect of dietary flavonoids on cancer risk.

Table 4.23: The meta-analysis of flavonoids on cancer risk.

Tumor	Outcome	Reference
prostate	protective effect of green tea, genistein and daidzein from soy food consumption in lowering the risk of prostate cancer	(Boehm et al., 2009) (Hwang et al., 2009) (Zheng et al., 2011b)
breast	soy isoflavones and green tea (≥ 5 cups/day) intake reduced the risk of breast cancer	(Dong and Qin, 2011) (Hooper et al., 2010) (Trock et al., 2006) (Wu et al., 2008) (Sun et al., 2005) (Seely et al., 2005)
lung	flavonoids and green tea (2 cups/day) intake reduced the risk of lung cancer	(Tang et al., 2009c) (Tang et al., 2009a)
ovarian	protective effects of green tea on ovarian and endometrial cancer	(Nagle et al., 2010) (Butler and Wu, 2011)
endometrial	tea consumption (2 cups/day) reduced endometrial cancer risk	(Tang et al., 2009b)
liver	protective effect of green tea against liver cancer	(Sing et al., 2011)
gastric	protective effect of green tea ((≥ 5 cups/day) against stomach cancer	(Kang et al., 2010)

Epidemiological studies of flavonoids and cancer risk have been widely investigated. A case control study in Italy covering 10,000 incidents of selected cancers and over 16,000 controls has proven the inverse effects of flavanols and flavanones to laryngeal and esophageal cancers, respectively (Rossi et al., 2010). Total flavonoids, flavanones, and flavonols were inversely related to oral and laryngeal cancers (Rossi et al., 2010). A reduced risk of colorectal cancer was found for anthocyanidins, flavonols, flavones and isoflavones intake (Rossi et al., 2010). The flavones and flavonols were also inversely related with breast cancer (Rossi et al., 2010). In the case of ovarian and renal cancer, flavonols and isoflavones were evident to prevent these cancers (Rossi et al., 2010). Whereas, inverse relations also were observed between proanthocyanidins and colorectal cancer (Rossi et al., 2010). A random sample of 10,054 participants from different region in Finland on their habitual food consumption was conducted to study the association of flavonoid intake and several chronic diseases (Knekt et al., 2002). High quercetin intake had lower mortality from ischemic heart disease, in addition with lowering lung cancer, asthma and diabetes. Meanwhile, high myricetin intake reduced the incident of prostate cancer and diabetes. Another study provided evidence of flavan-3-ols, anthocyanidins and total flavonoids against cholangiocarcinomas (CAC), whilst flavones may be inversely associated with hepatocellular carcinoma cells (HCC) risk (Lagiou et al., 2008). More human population studies on dietary flavonoid with inverse associations with common human cancers were presented in a review paper (Neuhouser, 2004).

4.4.1.2 Isolated flavonoids and its configuration-related biological activities

Galangin was first isolated from the aerial parts of *Helichrysum aureonitens* from which significant antiviral activity against herpes simplex virus type-1 (HSV-1) was shown at concentrations ranging from 12 to 47 µg/ml (Meyer et al., 1997). However, the complete NMR assignments of galangin was first reported in 2008 (Lee et al., 2008), which confirmed the structure of galangin as 5,7-dihydroxyflavonol. Recently, galangin was isolated from *Alpinia galangal* root. Galangin was utilised as a co-treatment for human lung cancer resistant to cisplatin (DDP). It was described to induce apoptosis in A549/DDP via STAT3/NF-κB/ and Bcl2/Bax signalling pathway (Yu et al., 2018). Furthermore, co-treatment with galangin and the conventional

drug, TRAIL at concentrations of 20 uM and 100 ng/ml was shown to reduce proliferation of breast cancer cell lines MCF-7 and T47D while being inactive on normal breast epithelial cell (MCF-10A) at the equal dose (Song et al., 2017). On top of that, the treatment using galangin only that was isolated from Chinese propolis collected by *A. mellifera L*. from *Populus sp*. at a concentration of 160 µM had a cytotoxic effect against MCF-7-ER(+), A549, and human colonic carcinoma (HeLa) cells. It was also effective against human breast cancer cell line MDA-MB-231- ER (-) at lower concentration of 80 µM (Xuan et al., 2016). Galangin also decreased cell viability in human ovarian cancer cell lines, A2780/CP70 and OVCAR-3 cells from 74.4% to 14.2% at a concentration of 40 µM and from 66.8% to 15.6% at a concentration of 160 µM, respectively. In addition, galangin at a concentration of 40 µM, significantly reduced the formation of blood vessels (angiogenesis) due to cancerous tumor release to<50% in chorioallantoic membrane (CAM)-induced OVCAR-3 in chicken embryo (Huang et al., 2015). In the present study, galangin exhibited potent cytotoxic effects on A2780 with IC_{50} of 21.3 µM, but weak IC_{50} of 64.79 and 80.49 µM against A549 and ZR75, respectively. These findings were supported by a previous study which gave IC_{50} 94 µM of galangin to inhibit TNF-α gene expression in A549 (Ludwiczuk et al., 2011).

Pinobanksin and chrysin were first isolated from the dried flowers and buds of *Populus nigra* in Hungary. Pinobanksin was obtained as colourless plates, $[\alpha]^{20}_{D}$+14.3º (c=0.5, MeOH) (Komoda, 1989). Later these compounds were identified and quantified in Brazilian propolis and commercial eucalyptus honey from Italy, Portugal and Spain (Marcucci et al., 2000, Martos et al., 2000). Furthermore, independent treatment using (*2R,3R*)-pinobanksin or chrysin isolated from Chinese propolis collected by *A. mellifera L*. from *Populus sp.* had cytotoxic effects on MDA-MB-231 at a concentration of 80 µM (Xuan et al., 2016). In addition, chrysin showed weak antiproliferative effects against A549 at 160 µM (Xuan et al., 2016). Co-treatment with chrysin at 25 µM and Docetaxel mitigates Docetaxel-induced oedema while increasing the therapeutic efficacy of lung cancer treatment in A549 (Lim et al., 2016). Based on an *In-vivo* experiment, the anticancer activity of chrysin was demonstrated at a dosage of 250 mg/kg via downregulating

the expression of PCNA, COX-2, and NF-kB proteins in maintaining cellular homeostasis in benzo(a)pyrene-induced lung carcinogenesis in Swiss albino mice (Kasala et al., 2016). In the present study, chrysin gave potent cytotoxicity effect at IC_{50} values of 23.74 μM on A549 compared to (2R, 3R)-pinobanksin at IC_{50} values of 36.65 μM. Moreover, chrysin and pinobanksin gave weak activity against A2780 at IC_{50} values of 89.72 and 66.57 μM, respectively. Interestingly, pinobanksin-3-acetate not only active on A549 at IC_{50} values of 30.07 μM, but also gave potent activity against A2780 at IC_{50} values of 1.22 μM.

Benzyl caffeate was first isolated from a balsam Beijing propolis as a white powder with the highest yield being 160 mg/g as compared with the yield obtained from Gifu, Nagano, Hokkaido, Hubei, and United States at 28, 17, 33, 128, and 7 mg/g , respectively. Benzyl caffeate was not detected in Brazilian samples of propolis (Yamauchi et al., 1992). Later in 2002, benzyl caffeate compound was described in Netherlands propolis, which showed strong cytotoxicity on murine melanoma B16-BL6, human fibrosarcoma (HT-1080), A549 and murine colon carcinoma 26-L5 with EC_{50} values of 2.03, 13.3, 18.9 and 0.288 μM, respectively (Banskota et al., 2002). It also gave equal strength of scavenging activity toward DPPH radical to that of α-tocopherol, a well-known antioxidant. The basic structure of caffeates was evidenced to give strong antiproliferative activity in comparison to other flavonoid constitutes such as flavanones and flavanols (Banskota et al., 2002). Benzyl caffeate isolated from Chinese propolis also showed potent antiproliferative activity towards B16-BL6, HT-1080, A549, human cervix adenocarcinoma (HeLa) and colon 26-L5 with EC_{50} values 9.78, 9.74, 35.0, 2.33 and 1.01 μM, respectively (Usia et al., 2002). In the present study, a potent cytotoxic effect of benzyl caffeate isolated from New Zealand propolis was demonstrated on A549 and A2780 at IC_{50} values of 15.81 and 15.38 μM. Eventhough, it was also found toxic on PNT2A normal cell line with slightly higher IC_{50} value of 20.2 μM. The antiproliferative effect of benzyl caffeate also can be related with its antioxidant and radical-scavenging properties, which further prevent oxidation-related diseases. The result obtained from the literature was comparable to or stronger than the positive control, Trolox, which exhibited amoderate antioxidant power at 1.39 mg/mg was consistent with its strong

bioactivity in DPPH and ABTS radical assays at 8.31 and 9.91 μg/ml, respectively (Yang et al., 2011a). It appears that phenolics having *ortho*-dihydroxyl substituents showed strong bioactivities. **Table 4.24** summarized the biological activities of isolated flavonoids from New Zealand propolis that have been reported in the literature.

Table 4.24: Biological activities of isolated compared as in the literature since 2010.

Chemical Name	Reported Activity/Literature	Source
galangin	1) Antioxidant identification by observation of yellow bands obtained from HPTLC chromatogram in DPPH solution (Guzelmeric et al., 2018)	Propolis from *Populus nigra*
	2) Attenuates the reduction activities of SOD, GPx, CAT and MDA levels relate to anti-ageing properties (Fu et al., 2012)	*Zingiber officinale* Roscoe
	3) 78.35% and 21.1% inhibition of Sarcoma 180 and Chinese hamster V79 cells at a dose of 10 µg/kg/day and 70 µg/ml, respectively (Singh et al., 2017)	*Heliotropium subulatum*
	4) Inhibit retinoblastoma cell proliferation, migration and induce apoptosis in vitro via activation of PTEN and Caspase-3 pathways, as well as In vivo via anti-proliferative and apoptogenic mechanisms (Zou and Xu, 2018)	*Alpiniao fficinarum*
	5) IC_{50} of 22.1 µM against human pancreatic cancer cells (PANC-1) (Li et al., 2010)	Mexico propolis
benzyl caffeate	1) 1µM increased H9c2 cellular antioxidant potential, decreased intracellular calcium ion ([Ca2+]i) level, and prevented cell apoptosis against acute oxidative stress induced by H_2O_2 in H9c2 cells (Sun et al., 2017)	Chinese propolis
	2) IC_{50} of 63.1 µM to inhibit angiotensin converting enzyme (ACE) that closely related in pathophysiology of hypertension (antihypertension) (Bhullar et al., 2014)	Synthetic
	3) MIC 31.25 µg/ml on *P. larvae* (ERIC I) and *P. larvae* (ERIC II) after 12 h of incubation in MYPGP medium (Bilikova et al., 2013)	Bulgaria propolis
	4) The use of human liver microsome to investigate the effect of cytochrome P450 1A2 (CYP1A2)-mediated chemical carcinogenesis via superoxide anion scavenging, nitric oxide radical scavenger, DPPH radical scavenging and phenacetin O-deethylation with IC_{50} 123.69, 52.64, 285.34 and 156.68 µg/ml, respectively (Jaikang et al., 2011)	Synthetic
	5) IC_{50} 45.8 and 39.0 µmol/L, respectively against A549 and colorectal adenocarcinoma (DLD-1), and also weak cytotoxicity effect on normal skin fibroblast (WS1) at IC_{50} 51.0 µmol/L (Pichette et al., 2010)	*Populus tremuloides* Michaux
(2*R*,3*R*)-pinobanksin	1) IC_{50} of 52.1 µM against murine-derived B-cell lymphoma (M12.C3.F6) (Alday et al., 2015)	Sonoran propolis
	2) 2.90 µM Trolox/µM.gave antioxidant activity by ORAC assay (Yan et al., 2011)	*Oroxylum indicum*
	3) 1 mM can exhibited 20% inhibition of free radical scavenging activity against 2,2'-azinobis(3-ethylbenzothiazoline-6-sulfonate) (ABTS) radical cation (Han et al., 2010)	Korea propolis
chrysin	1) Cholinesterase inhibitor in Alzheimer treatment (Hage and Morlock, 2017)	*Populus nigra*

	2) Anti neovascularisation at a concentration of 15 mg/kg to inhibit angiographic leakage in laser-induced animal models of Choroidal Neovascularization (CNV) in rats (Song et al., 2016)	Synthetic
	3) Antidiabetic ability at 60 mg/kg via a PPAR-g agonist improves myocardial injury in diabetic rats through inhibiting AGE-RAGE mediated oxidative stress and inflammation (Rani et al., 2016)	Synthetic
	4) The co-treatment of chrysin at 40 μM with 5 μg/ml of cisplatin can promote the apoptosis in human liver cancer cell (HepG2) by upregulating p53 (Li et al., 2015)	Synthetic
	5) Neuroprotective effects of chrysin at concentration of 12 μM chrysin and 1mM protocatechuic acid (PCA) to inhibit the activation of nuclear factor-kB and expression of inducible nitric oxide synthase on rat pheochromocytomacells (PC12), the Parkinson disease model (Zhang et al., 2015)	*Alpinia oxyphylla*
	6) Neuroprotective effect of chrysin at 1-300 mg/kg is effective in attenuating memory impairment, oxidative stress, acting as an antiaging agent (Souza et al., 2015)	Synthetic
	7) Antidepression of chrysin at 5 or 20 mg/kg culminated in the upregulation of brain-derived neurotrophic factor (BDNF) and nerve growth factor (NGF) levels in mice (Jesse et al., 2015)	Synthetic
	8) Anticancer effects of chrysin at 5, 10 and 20 μM to induce antimetastatic activity by regulating modulating matrix metalloproteinase-10 (MMP-10) and epithelial-mesenchymal transition (Yang et al., 2014)	*Passiflora caerulea*
	9) IC_{50} of chrysin at 49.1 μM against M12.C3.F6 (Alday et al., 2015)	Sonoran propolis
	10) Chrysin at 0.51 μM Trolox/μM.gave antioxidant activity via ORAC assay (Yan et al., 2011)	*Oroxylum indicum*
	11) The concentration of chrysin at 500 mM exhibited anti-Fenton induced DNA single strand breakage method through hydroxyl radical scavenging mode (Han et al., 2010)	Korea propolis
	12) IC_{50} of chrysin at 88.7uM against human pancreatic cancer cells (PANC-1) (Li et al., 2010)	Mexico propolis
pinobanksin-3-acetate	1) Antibacterial activity against strains of Gram-pos. methicillin-resistant (Biva et al., 2016)	*Eremophila alternifolia*
	2) Anti-oxidative effects on stress and protected cells from damage (Sun et al., 2016)	Chinese propolis
	3) Anticancer activity on colon cancer (SW480) cells at 25 ug/ml (Amet et al., 2015)	Chinese propolis
	4) Anti advanced glycation end-products (AGEs) associated with Alzheimer, diabetes, renal failure and atherosclerosis, IC_{50} at 0.06 mM (Boisard et al., 2014)	French Poplar type propolis
	5) Cytotoxicity at PC50 value of 36.6 uM on pancreas cancer cell (PANC-1) (Li et al., 2010)	Mexican propolis

Taken together, the bioactivity of flavonoids were closely related with their structure and configuration, such as the substitution of hydroxyl groups at *ortho*- or *meta*-dihydroxyl positions on the A ring. Additionally, the occurrence of a double bond between C-2 and C-3 of the C ring, as well as open structure C ring is evidenced to contribute to the strong cytotoxic effects of flavonoids on several cancer cell lines. Based on the present study, the strong cytotoxic effect was observed for benzyl caffeate against A549, followed by chrysin, pinobanksin-3-acetate, (*2R,3R*)-pinobanksin and galangin. For A2780 cytotoxicity assay, pinobanksin-3-acetate showed the strongest activity followed by benzyl caffeate, galangin, (*2R,3R*)-pinobanksin and chrysin. On the other hand, benzyl caffeate had a moderate cytotoxic effect on ZR75, whereas galangin and chrysin have shown weak activity; however, at equivalent concentrations, the compounds were also toxic to PNT2A. Thus, the anticancer effects of flavonoids from New Zealand propolis were only successful against A549 and A2780.

In conclusion, benzyl caffeate was very potent to cause the death of A549 and A2780 due to *ortho*-dihydroxyl substituents and open structure of C ring. It also can be concluded that the acetylation at C-3 of pinobanksin increased the potency of its cytotoxicity on A2780. Whereas, chrysin is more potent than galangin against A549, possibly due to the absence of hydroxyl group at C-3. In contrast, galangin is more potent than chrysin against A2780 possibly due to the presence *para*-dihydroxyl groups at C-5 and C-3 positions. In other word, the anticancer properties of flavonoids isolated from Manuka New Zealand propolis exhibited their bioactivities on specific cell lines were dependent on the functional group substituents. Above all, the pinobanksin congeners at equal concentrations were found not toxic to the normal cell line, PNT2A. In summary, the present study provides evidence that benzyl caffeate, chrysin and pinobanksin-3-acetate have the potential to modulate cell death in A549, while both benzyl caffeate and pinobanksin-3-acetate along with galangin were also found bioactive against A2780.

CHAPTER 5

5 HR-LCMS and NMR metabolite profiling of Malaysia and New Zealand honeys for anticancer activity

5.1 Introduction

Historically, honey has been used as food and cooking ingredient because of its sugars that serve as a source of energy (Wang et al., 2004). Nowadays, honey has a wider role in therapeutic applications. It has been investigated for a variety of medicinal uses including wound healing, cough, and skin allergies, as well as more advanced medicinal applications such as cancer (Alvarez-Suarez et al., 2010). Its anticancer activities were evidenced via *In vitro* and *In vivo* studies associated with breast, prostate, oral, renal, cervical cancer (Tsiapara et al., 2009, Ghashm et al., 2010, Samarghandian et al., 2011, Fauzi et al., 2011). A review published in 2009 summarized the anti-proliferative effect of honey and its polyphenol constituents, highlighting acacetin and kaempferol which gave promising outcomes in the inhibition of human lung cell lines, e.g A549 and H460 (Jaganathan and Mandal, 2009). Moreover, Hsu et al. (2004) provided evidence of the role of acacetin in enhancing the expression of p53 and Fas/FasL proteins in triggered apoptosis against human non-small lung cancer cell line (A549) (Hsu et al., 2004). Meanwhile, kaempferol has been demonstrated to induce biomarkers (caspase-3, apoptosis inducing factor and manganese superoxide dismutase) associated with apoptosis activation in human non-small lung carcinoma cell line (H460) (Leung et al., 2007). The use of crude honey at a dose of 2 g/kg (orally per day) for 10 consecutive days before tumour cells inoculation in mice also successfully prevented metastases in the lung (Oršolić et al., 2005).

There are several types of honey produced in Malaysia, famously known as Tualang, Gelam, Nanas and Acacia. These honeys were characterized based on the origin of their nectar. For example, Tualang honey was harvested and collected from the Tualang tree usually found in a Malaysian rainforest. Tualang honey has exhibited its effect as an anti-proliferative agent via the reduction of cell viability of oral

squamous cell carcinoma (OSCC) and human osteosarcoma (HOS) cell lines due to apoptosis machinery (Ghashm et al., 2010). A serial dilution of working concentration of honey with culture medium was used to determine the inhibitory effects of honey on both cell lines. Recorded cell viability was time and dose dependent. Inhibition of cell growth for both cell lines was greater than 80% at a concentration of 15% Tualang honey in solution. Concentration at 50% inhibition (IC_{50}) was found to be at 4% and 3.5% of dissolved honey for OSCC and HOS, respectively. Similarly, there were an increased percentage of apoptotic cells, detected by flow cytometry, according to time and dose in both cell lines. In addition, Gelam honey demonstrated to act as anti-proliferative agent against the liver cancer line (HepG2) while found to be relatively non-toxic to normal liver cell (WRL-68) (Jubri et al., 2012). Based on MTS assay findings, the IC_{50} values of Gelam honey on HepG2 and WRL-68 cells were at a concentration of 25% and 70% incorporated honey in the media, respectively. BrdU assay indicated that the proliferation of HepG2 was reduced by administration of Gelam honey at concentrations of 3% to 70% honey in solution. Jubri and colleagues concluded that Gelam honey potentially induced the anti-proliferative activity of cancer cell by triggering the apoptosis mechanism.

Several indigenous New Zealand honey were characterised by it floral sources such as *Leptospermum scoparium* (Manuka), *Kunzea ericoides* (Kanuka), *Trifolium* spp., (Clover), *Knightia excelsa* (Rewarewa), *Weinmannia racemosa* (Kamahi), *Ixerba brexioides* (Tawari), *Thymus vulgaris* (Thyme) as well as honey produced by the scale insects *Ultracoelostomaassimile* and *U. brittini* inhabiting the beech trees (Honeydew) *Nothofagus solandri* and *N. fusca* (Vanhanen et al., 2011). The Manuka and Rewarewa honeys were evident to suppress leukocyte infiltration via arachidonic acid-induced ear inflammation model in rat by decreased neutrophil level (Leong et al., 2012). Meanwhile the Kanuka honey showed high anti-inflammatory activity with the presence of different level of methylglyoxal (MGO), whereby the neutrophil superoxide production remained unaffected. It demonstrated that high MGO levels do not suppress anti-inflammatory activity of the honeys. Moreover, the Rewarewa honey not only can reduce inflammatory in leukocyte infiltration, but also in AA-

induced oedoma. This indicated that Rewarewa honey has the potential to revoke inflammation via several target including neutrophil respiratory burst, recruitment, and swelling. The Manuka and pasture honeys from New Zealand also showed significant increase in cytokine (TNF-α, IL-1β and IL-6) release from isolated human peripheral blood monocytes that can promote wound healing (Tonks et al., 2003). Taken together, even though the therapeutic properties of honey have been well described in the literature, in contrast there is a lack of information available on Malaysian and New Zealand honeys for potential anti-cancer application. Therefore, the present study has focused on metabolite profiling study of Malaysia and New Zealand honeys based on the HR-LCMS, ^{1}H NMR and their therapeutic effects on A549, A2780, ZR75, and PANC-1, as well as their toxicity on normal cell, HFL-1.

5.2 Materials and methods

5.2.1 Honey

Fresh Malaysian and New Zealand honeys were obtained from several beekeepers randomly from Malaysia and New Zealand (**Table 5.1**).

Table 5.1: Malaysian and New Zealand honey used in this study.

No.	ID	SOURCE OF NECTAR	TYPE OF BEE	GEOGRAPHICAL AREA	DISTRIBUTOR
MAS					
1	AH	*Hevea brasiliensis*	*Apis mellifera*	Rubber tree estate, Malaysia	Beeshop (Mrs Cathie)
2	BH	*Cinnamomum cassia*	*Apis cerana*	Hilly area, Malaysia	
3	CH	Acacia tree species	*Apis trigona*	Negeri Sembilan, Malaysia	
4	DH	*Melaleuca*	*Apis mellifera*	Melaka, Malaysia	
5	EH	Multifloral	*Apis cerana*	Malaysia	
6	FH	*Koompassia excels*	*Apis dorsata*	Malaysia	
7	GH	*Momordica charantia*	*Apis mellifera*	Pahang, Malaysia	
8	HH	*Melaleuca*		Hilly area, Malaysia	
9	IH	Multifloral	*Apis trigona*	Negeri Sembilan, Malaysia	
10	JH	*Asystasia gangetica*	*Apis mellifera*	Malaysia	
11	KH	Multifloral (fruity tree)	*Geniotrigona thoracica*	Negeri Sembilan, Malaysia	
12	LH	*Acacia mangium*	*Apis mellifera*	Negeri Sembilan, Malaysia	
13	MH	*Ananas comosus*		Johor, Malaysia	Mr. Ali
14	NH	*Acacia mangium*		Malacca, Malaysia	Pak long MaduTani
15	OH	Multifloral		Malacca, Malaysia	
16	PH	Multifloral	*Apis trigona*	Malacca, Malaysia	
17	QH	Multifloral	*Apis mellifera*	Malacca, Malaysia	Giant B (Mr.Ong)
18	RH	Multifloral	*Apis trigona*	Malacca, Malaysia	
19	SH	*Acacia mangium*	*Apis mellifera*	Sarawak, Malaysia	Summer Pacific (Mr.Esa)
NZ					
20	ANZ	Manuka (< Clover, Honey dew)	*Apis mellifera*	Wye Valley, New Zealand	The Honey Company Ltd (Natasha)
21	BNZ	Manuka (< Borage, Clover)		Upper Tanaka, New Zealand	
22	CNZ	Manuka (< Borage, Clover)		Upper Wairau, New Zealand	
23	DNZ	Manuka (< Borage, Clover)		Wairau, New Zealand	
24	ENZ	Manuka		Linkwater, New Zealand	
25	FNZ	Manuka		Keneperu, New Zealand	
26	GNZ	Manuka (< Borage, Clover, Matagouri)		Moutere	

27	HNZ	Manuka (< Borage, Clover, Kamahi)		Wairau Valley, New Zealand	
28	INZ	Manuka (< Clover)		Awatere Valley, New Zealand	
29	JNZ	Manuka (< Clover, Honey dew)		Awatere Valley, New Zealand	
30	KNZ	Manuka /Manuka blend		New Zealand	Honey New Zealand (International) Ltd (Dr. Young)
31	LNZ	*Knightia excels* (Rewarewa)		New Zealand	
32	MNZ	Manuka Manukablend		New Zealand	
33	NNZ	Manuka Manuka blend		New Zealand	
34	ONZ	Manuka Manuka blend		New Zealand	
35	PNZ	Manuka Manuka blend		New Zealand	
36	QNZ	Manuka Manuka blend		New Zealand	
37	RNZ	Manuka Manuka blend		New Zealand	
38	SNZ	Manuka Manuka blend		New Zealand	
39	TNZ	Manuka Manuka blend		New Zealand	
40	UNZ	Manuka Manuka blend		New Zealand	
41	VNZ	Manuka Manuka blend		New Zealand	
42	WNZ	Multifloral (Wild floral)		New Zealand	

5.2.2 Extraction of fresh Malaysia and New Zealand honeys

Samples of honey were weighed at 1g each and suspended in 25 ml of 1:1 water and methanol by stirring for a minimum duration of two hours. The supernatant was filtered and collected in a round bottom flask and concentrated *in vacuo* on a rotary evaporator, R-110 and R-3 (BŪCHI LabortechnikAG, Switzerland) at a standardised temperature of 40°C. When possible, the extraction with aqueous methanol was repeated three times. Once dry, all the samples were transferred to 5 ml tared vials by reconstituting the samples in an appropriate solvent such as acetone, methanol or distilled water or a combination of those solvents. Samples that were more difficult to reconstitute in solution were sonicated using Ultrawave sonicator (Scientific Laboratory Supplies, Ltd, Coatbridge, UK). The samples were then further concentrated on heating blocks (STUART Bibby Scientific Limited Stone, Staffordshire, United Kingdom) at 40°C under a stream of nitrogen gas. Water-

soluble extracts were lyophilized in the Christ Alpha 2 – 4 freeze dryer (Martin Christ Gefriertrocknungsanlangen GmbH, Germany) at -80°C. All the dried concentrated samples were weighed and stored in closed vials at room temperature until further analysis as described under Materials and Methods (*2.4.1*).

5.3 Results

5.3.1 Malaysia and New Zealand honey metabolomics profiling based on ^{1}H NMR experiment.

Proton signals at 3 to 6 ppm indicated the presence of a glucose moiety, as well as fructose within 3 and 4 ppm (Boffo et al., 2012). An olefinic group was also predicted for proton signals between 2 to 5 ppm. In addition, the proton signal at 2.31 and 4.81, ppm, respectively were assigned for methyl and alkyl protons in methylglyoxal were observed in honey from New Zealand (Donarski et al., 2010).Taken together, the proton spectra of Malaysia (MAS) and New Zealand (NZ) honey extracts were observed to have similar chemical finger print (**Fig. 5.1** and **5.2)**. The major compounds consisted of sugars and some of which were already converted to furfural then subsequently oxidized to its acid form (**Fig. 5.3)** (Lee et al., 2016), as shown by the doublet signals (Boffo et al., 2012) at 6.21 and 4.89 ppm, with coupling constants of 4.2 and 3.4 Hz, respectively (**Fig. 5.4A**). COSY NMR (**Fig. 5.4B**) indicated the presence of the glucose moiety and 5-(hydroxymethyl) furan-2-carboxylic acid. **Table 5.2** summarised a comparison of previous literature based on proton NMR signal of main constituents in honey with the present study.

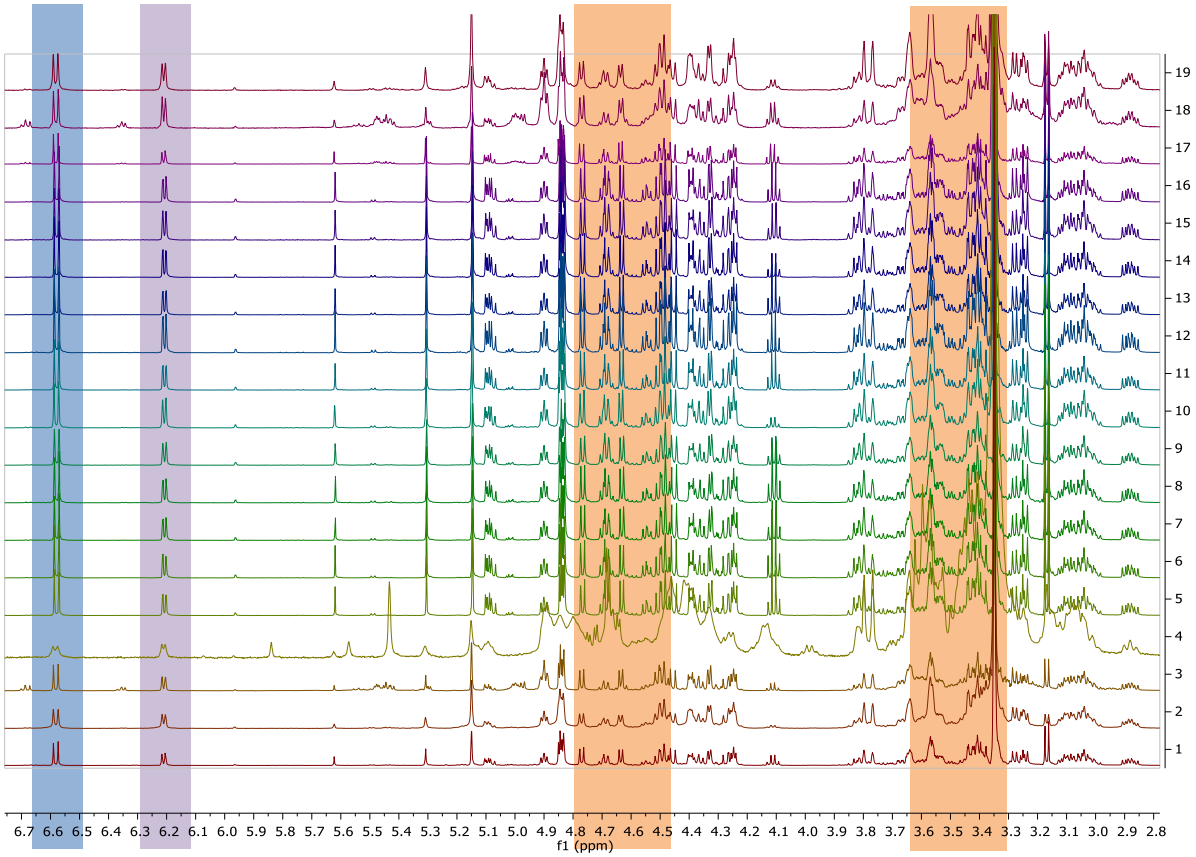

Fig. 5.1: The Malaysian honey extracts ^{1}H NMR spectra (400 Hz) in DMSO-d_6. The regions within 3.51 – 4.70 ppm were determined for fructose overlapping with glucose (highlighted in orange), the anomeric proton of glucose at 6.58 ppm (highlighted in blue), and 5-HMF, 5-hydroxymethyl-furan-2-carboxylic acid at 6.21 ppm (highlighted in purple). The spectra were labelled from 1 to 19 to represent sample codes MH, NH, OH, PH, AH, BH, CH, DH, EH, FH, GH, HH, IH, JH, KH, LH, QH, RH and SH, respectively.

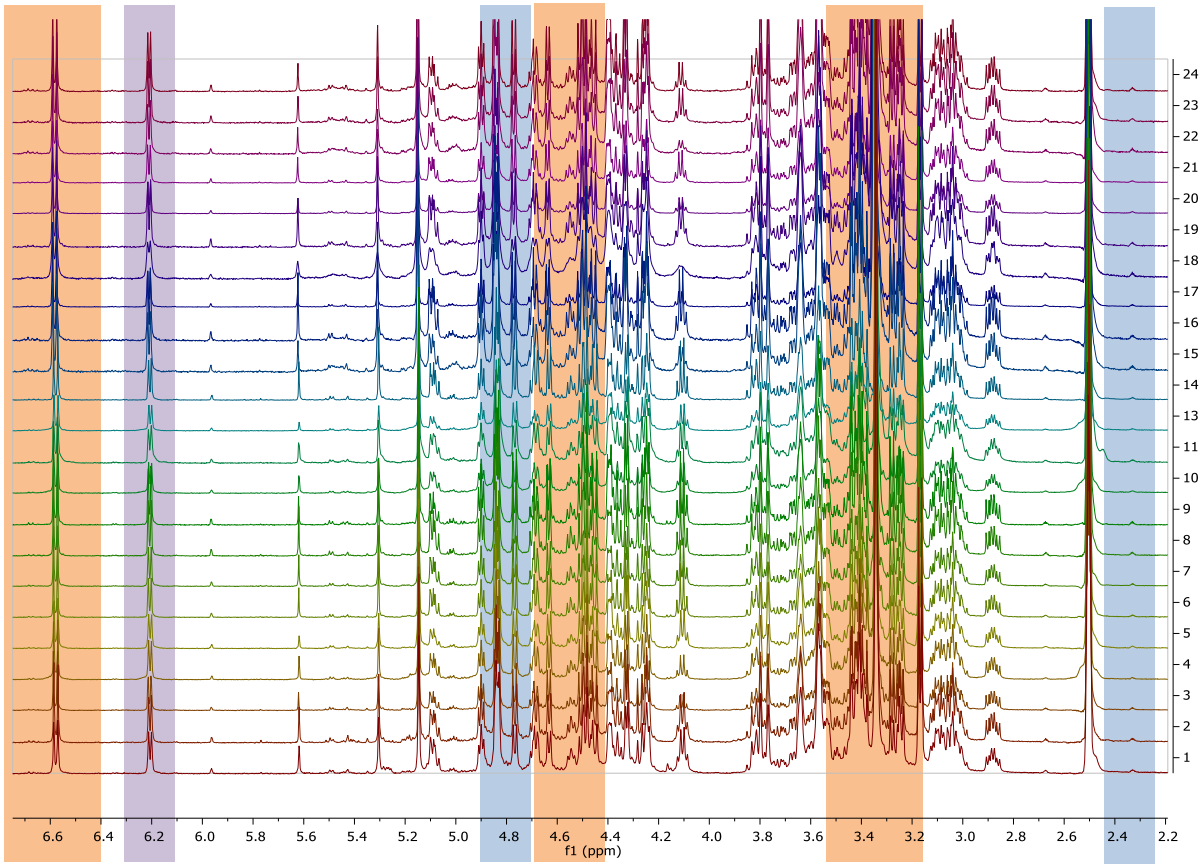

Fig. 5.2: The New Zealand honey extracts ^{1}H NMR spectra (400 Hz) in DMSO-d_6. The signal at 2.31 and 4.81 ppm was assigned respectively for methyl and alkyl proton in methylglyoxal (highlighted in blue).The spectrum within 3.51 – 6.58 ppm were determined for glucose and fructose (highlighted in orange) and the signal at 6.21 ppm is the prediction of 5-HMF (highlighted in purple). The spectra were labelled from 1 to 23 to represent sample codes KNZ, LNZ, MNZ, NNZ, ONZ, PNZ, QNZ, RNZ, SNZ, TNZ, UNZ, VNZ, WNZ, ANZ, BNZ, CNZ, DNZ, ENZ, FNZ, GNZ, HNZ, INZ and JNZ, respectively.

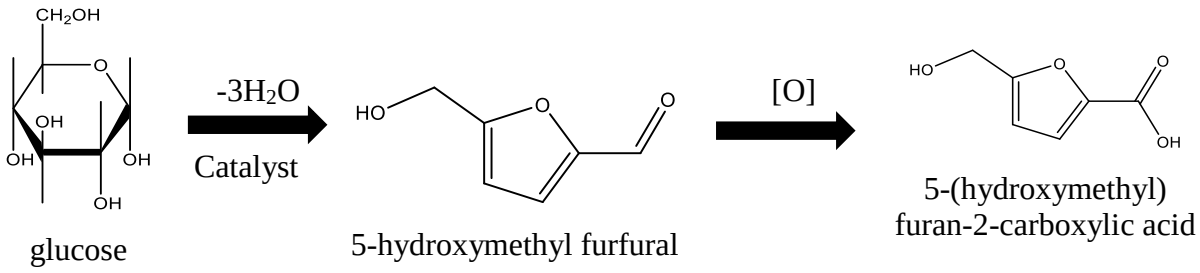

Fig. 5.3: Dehydration of glucose to 5-hydroxymethyl furfural then by oxidation to its acid form (Lee et al., 2016).

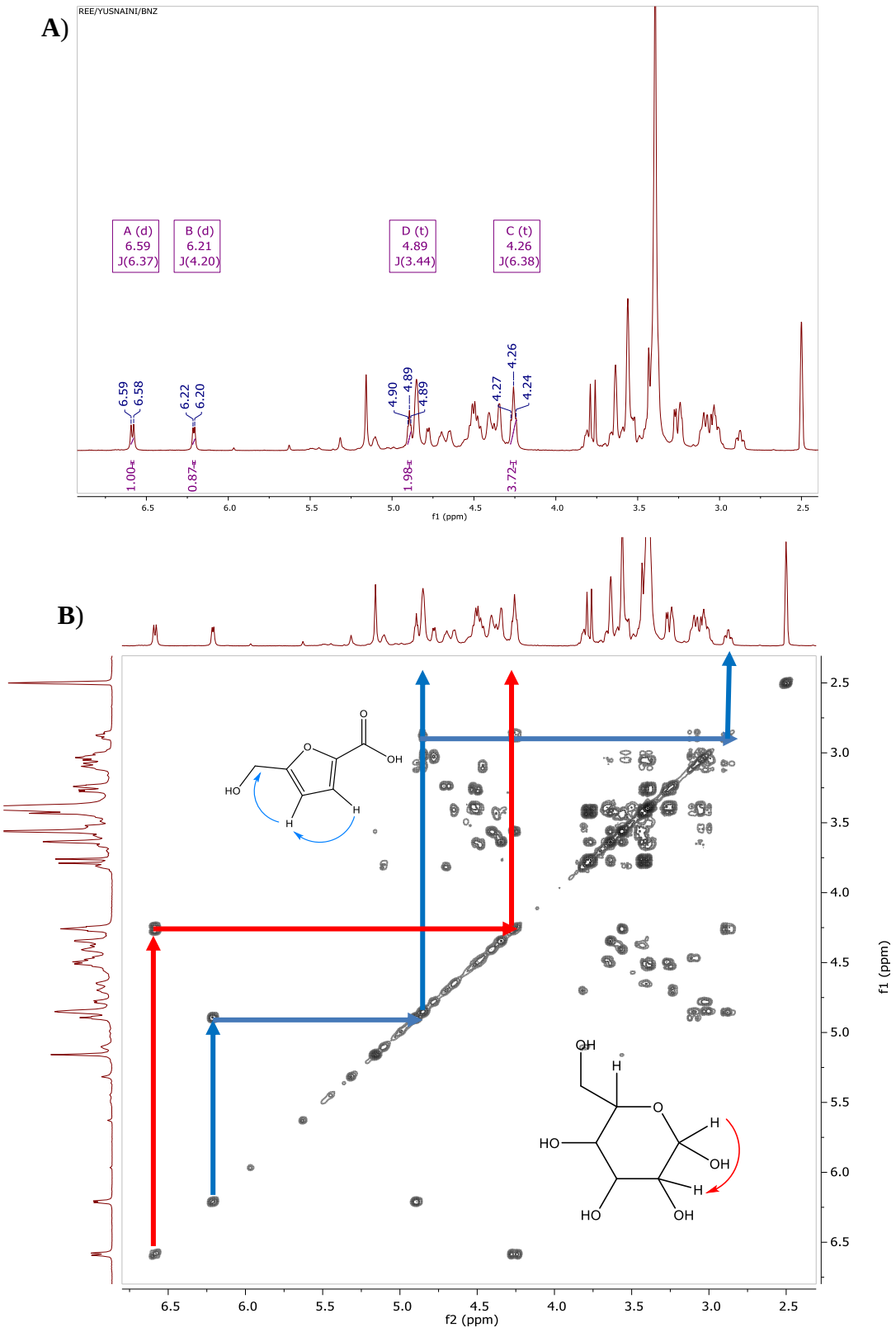

Fig. 5.4: **A)** ^{1}H and **B)** COSY NMR spectra of BNZ from New Zealand honey, indicating the presence of glucose moiety (red arrow) and 5-(hydroxymethyl)furan-2-carboxylic acid (blue arrow).

Table 5.2: ^{1}H NMR spectra of the main constituents found in honey.

Compound	^{1}H NMR found in Brazilian honey in D_2O (Boffo et al., 2012)	^{1}H NMR range (Ohmenhaeuser et al., 2013)*	^{1}H NMR used for identity check (Spiteri et al., 2015)*	Occurrence in the present study in DMSO-*d6*
HMF	-	9.43–9.47 (*s*)	7.54, 6.69	6.59
Formic acid	8.45 (s)	8.44–8.47 (*s*)	-	-
Phthalic acid	-	7.53–7.48 (*m*)	-	-
Fumaric acid	-	6.53–6.55 (*s*)	-	-
Pyruvic acid	-	6.42–6.45 (*s*)	-	-
L(+)-rhamnose	-	5.13–5.09 (*d*)	-	5.00-5.25
Glucose	3.23-5.22	4.63–4.65 (*s*)	4.65, 3.51	4.24-4.89
Arabinose	-	4.52–4.54 (*s*)	-	4.50-4.75
L(+)-tartaric acid	-	4.32–4.35 (*s*)	-	4.24-4.50
Fructose	3.52-4.10	4.14–4.08 (*d*)	4.04, 3.58	3.50-4.00
Sucrose	-	-	5.41, 4.20	4.24-5.50
Malic acid	-	2.73–2.70 (*s*)	-	2.75-3.00
Citric acid	2.79-2.94	2.69–2.68 (*s*)	-	-
Succinic acid	-	2.50–2.52 (*s*)	-	2.50
Methylglyoxal	-	-	1.38, 2.31	2.31

*NMR buffer (KH_2PO_4, NaN_3), distilled water, NMR lock solution (trimethylsilyl propionate, D_2O)

5.3.2 Biological activities of honey extracts

The 42 honey extracts from Malaysia and New Zealand demonstrated to give different bioactivities on various cancer and normal cell lines that included A549, A2780, ZR75, PANC-1 and HFL-1 at concentration of 100 µg/ml (**Table 5.3**). Overall, the maximum cytotoxicity effect of all honey extracts was observed to reduce the viability of the human lung fibroblast cell line HFL-1up to 71%. Therefore, the minimum cytotoxicity activity on cancer cell lines in this study was set to at least 70% of control viability. Meanwhile, several honey extracts including CH, FH, GH, HH, JH, KH, LH, NH, RH, SH showed mild cytotoxicity effect on ZR75, which reduced the cell growth respectively to 38, 41, 41, 39, 40, 41, 42, 39, 43 and 47 percent of control viability (in red). Whereas several honey extracts showed weak cytotoxicity effect on ZR75 which gave less than 71% of control viability, including MH, ANZ, BNZ, FNZ, JNZ, MNZ, ONZ, QNZ and WNZ, respectively at 70, 78, 66, 69, 68, 67, 68, 70 and 70 percentages (in green).

Table 5.3: Bioassay results of honey samples at 100 µg/ml on cell viability of A549, A2780, ZR75, PANC-1 and HFL-1as in percentage of the control, subjected to ≤70 % threshold (n=3**)**. Colour code represents mild (red) and weak (green) cytotoxicity effects of honey extracts.

No.	ID	A549	A2780	ZR75	PANC-1	HFL-1
1	AH	86	92	92	85	77
2	BH	88	92	94	84	79
3	CH	88	92	38	87	84
4	DH	88	92	90	86	79
5	EH	88	77	71	82	81
6	FH	83	92	41	85	78
7	GH	88	93	41	86	83
8	HH	83	91	39	90	80
9	IH	89	88	73	83	82
10	JH	87	93	40	85	81
11	KH	84	92	41	83	78
12	LH	85	92	42	85	80
13	MH	87	92	70	84	74
14	NH	87	93	39	89	84
15	OH	85	92	73	86	79
16	PH	90	91	72	86	81
17	QH	87	93	77	80	80
18	RH	89	83	43	89	83
19	SH	85	75	47	88	83
20	ANZ	90	79	68	89	87
21	BNZ	89	93	66	88	86
22	CNZ	83	90	93	86	78
23	DNZ	85	91	92	83	71
24	ENZ	86	86	92	88	82
25	FNZ	90	92	69	87	81
26	GNZ	84	92	92	88	82
27	HNZ	88	93	90	88	81
28	INZ	90	78	82	88	83
29	JNZ	91	92	68	88	83
30	KNZ	90	86	76	87	84
31	LNZ	88	92	71	88	82
32	MNZ	89	92	67	90	83
33	NNZ	89	92	72	88	78
34	ONZ	89	93	68	88	83
35	PNZ	87	92	72	84	73
36	QNZ	88	94	70	90	82
37	RNZ	89	90	91	89	81
38	SNZ	89	93	73	89	83
39	TNZ	88	91	71	88	77
40	UNZ	88	91	73	87	77
41	VNZ	88	92	73	89	84
42	WNZ	86	92	70	87	82

5.3.3 The chemical diversity of honey extracts from Malaysia and New Zealand based on HR-LCMS in both positive and negative modes

Base peak chromatograms of positive and negative ionization modes from nineteen bioactive honey extracts from Malaysia and New Zealand are shown in **Fig. 5.5** and **5.6**. Putative metabolites were identified from the Dictionary of Natural Product (DNP) database for compounds previously isolated and described from plant sources. The total number of features identified from the HR-LCMS data from respective bioactive Malaysian and New Zealand honey extracts were presented in **Table 5.4**. After the removal of variable features with peak areas >1 × 10^5 from the solvent blank, the Malaysian honey NH afforded the highest number of features, where 2743 and 2247 features were detected from the positive and negative ionization mode, respectively. Following dereplication, 27.8% (1383) of the combined features from both the positive and negative mode were putatively identified; whilst 72.2% (3593) remained unidentified indicating that, the sample may possibly contain novel compounds. Whereas, for the New Zealand honey samples, the highest number of features was yielded by the honey sample BNZ, where 2720 features were detected in the positive mode and 2079 features were revealed in the negative mode. By dereplication, 28.6% (1369) of the combined features from both positive and negative modes were putatively identified, whilst 71.4% (3415) were unidentified.

+Ve

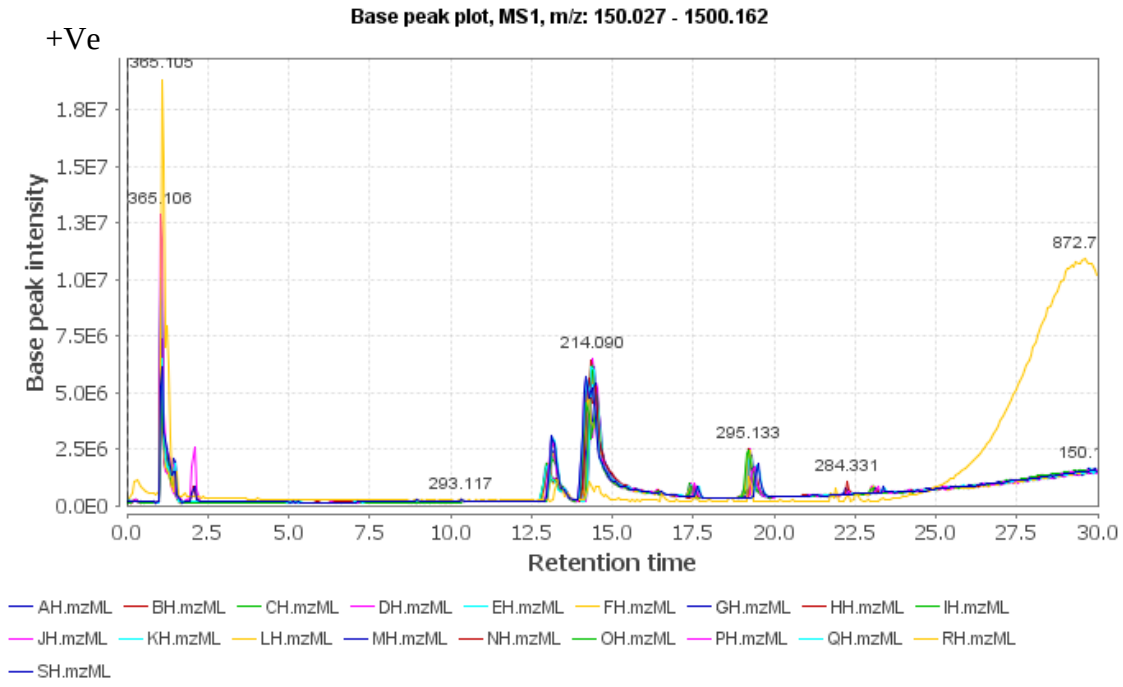

-Ve

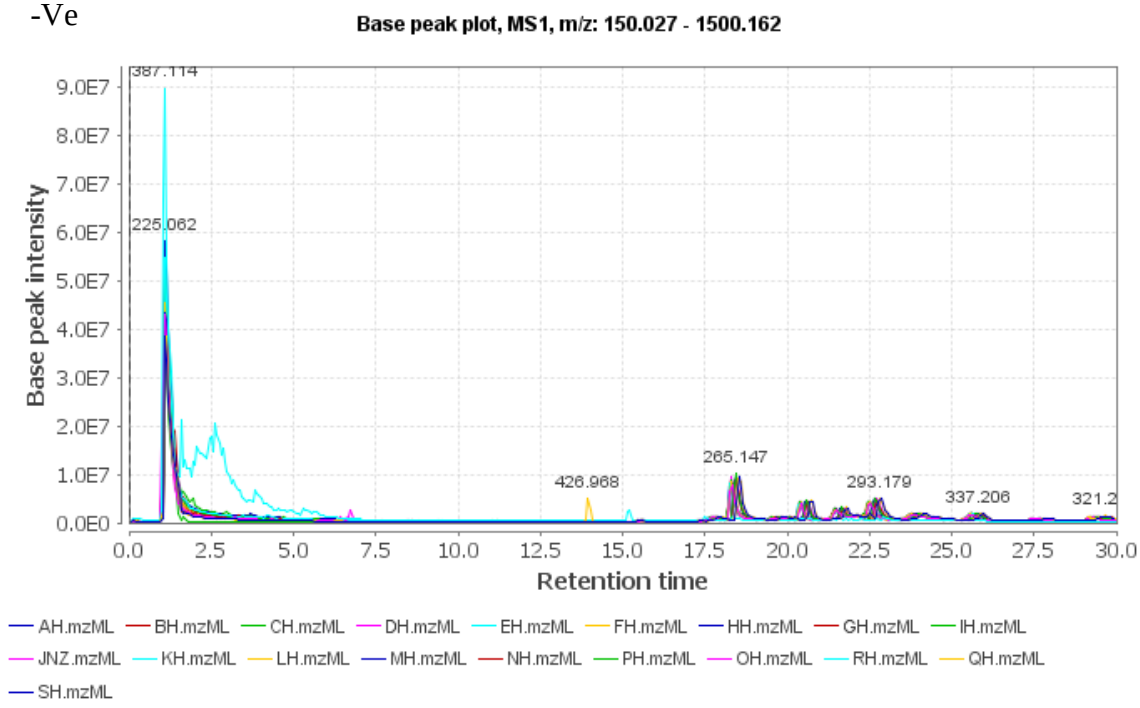

Fig. 5.5: The positive and negative modes base peak chromatograms showing metabolites from bioactive Malaysia honey extracts (CH, FH, GH, HH, JH, KH, LH, MH, NH, RH and SH).

+Ve

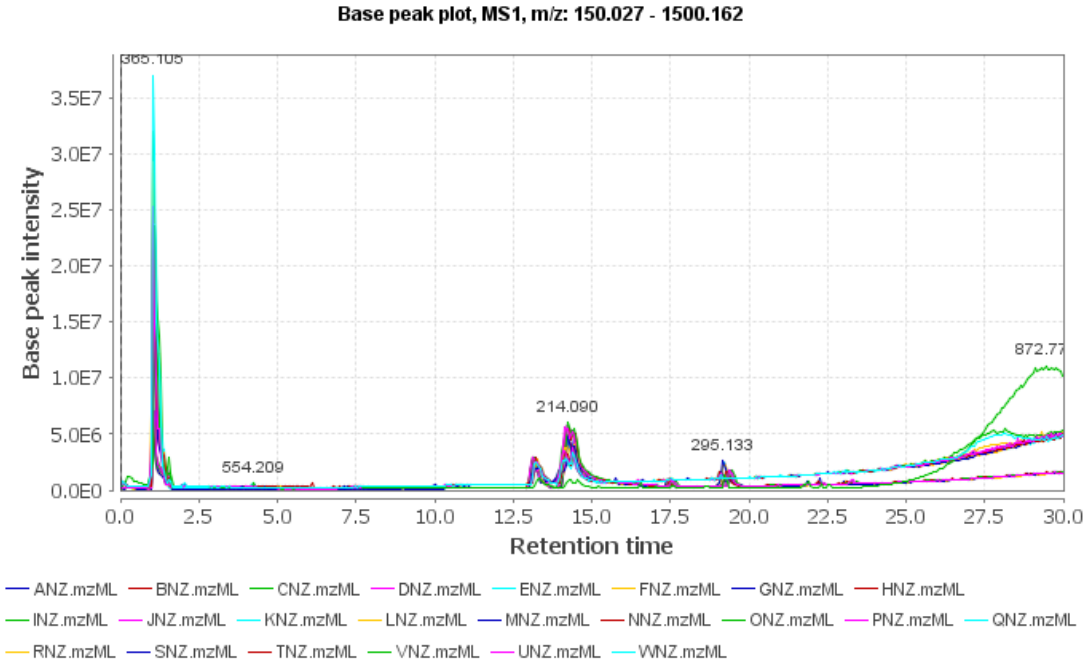

-Ve

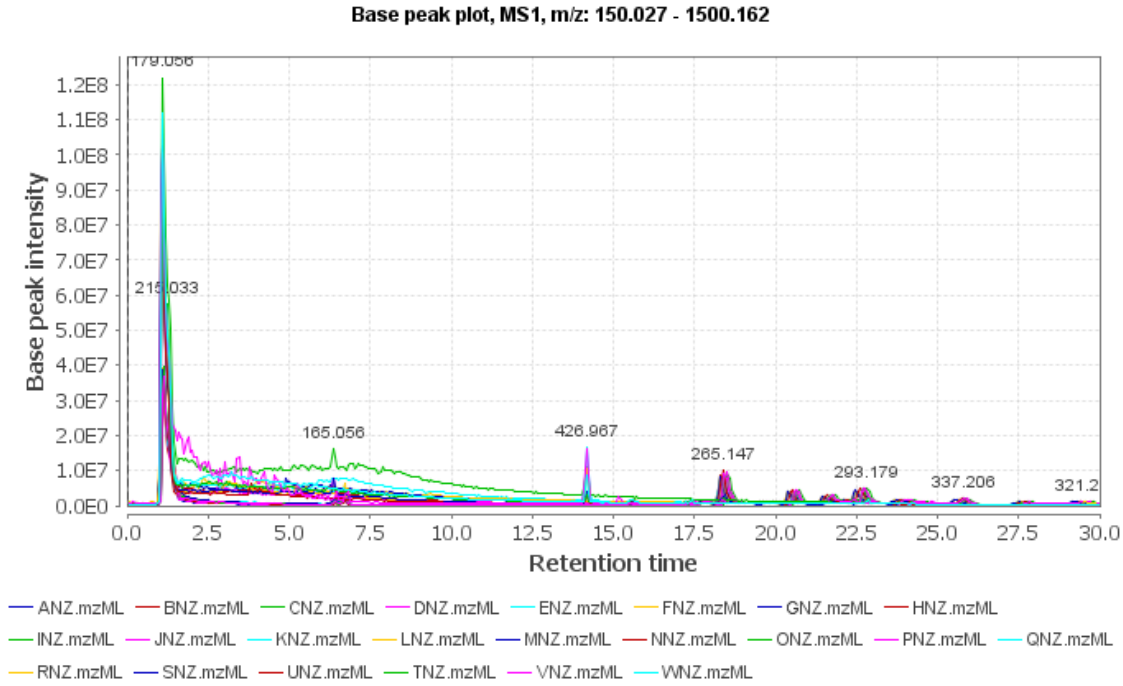

Fig. 5.6: The positive and negative modes base peak chromatograms showing metabolites from bioactive New Zealand honey extracts (ANZ, BNZ, FNZ, JNZ, MNZ, ONZ, QNZ and WNZ).

Table 5.4: Summary of the number of features detected in the bioactive honey extracts: (a) total number of features in positive and negative ionization modes (after the removal of features from solvent (blank) with intensity $>1 \times 10^5$; and (b) total number of features putatively identified by dereplication from the DNP database with number of unknowns.

Bioactive honey extracts	(a) Total number of features (*m/z*)		(b) Total number of features identified by dereplication with DNP	
	Positive ion mode	Negative ion mode	Putatively identified in positive and negative modes	Unidentified in positive and negative modes
CH	2638	2034	1354 (29%)	3303 (71%)
FH	2620	2009	1329 (28.8%)	3286 (71.2%)
GH	2587	2003	1317 (28.8%)	3258 (71.2%)
HH	2591	1999	1331 (29%)	3244 (71%)
JH	2585	1975	1315 (28.9%)	3231 (71.1%)
KH	2392	2038	1324 (30%)	3094 (70%)
LH	2646	2020	1330 (28.6%)	3321 (71.4%)
MH	2680	2114	1355 (28.3%)	3426 (71.7%)
NH	2743	2247	1383 (27.8%)	3593 (72.2%)
RH	2138	1870	1162 (29.1%)	2831 (70.9%)
SH	2656	1741	1317 (30%)	3068 (70%)
ANZ	2722	1953	1341 (28.8%)	3323 (71.2%)
BNZ	2720	2079	1369 (28.6%)	3415 (71.4%)
FNZ	2691	2093	1374 (28.8%)	3396 (71.2%)
JNZ	2595	2092	1372 (29.3%)	3303 (70.7%)
MNZ	2599	1929	1251 (27.7%)	3261 (72.3%)
ONZ	2709	1897	1260 (27.4%)	3331 (72.6%)
QNZ	2722	1938	1290 (27.8%)	3354 (72.2%)
WNZ	2712	1985	1259 (26.9%)	3422 (73.1%)

5.3.3.1. The principal component analysis (PCA) and hierarchical clustering analysis (HCA) using SIMCA 14.0

As mentioned above, the proton NMR spectra in both Malaysia (MAS) and New Zealand (NZ) were observed to have similar major compounds. However, only a few extracts exhibited cytotoxic effects on ZR75 cell line indicating a difference in chemical profiles of the honey samples. Therefore, an unsupervised multivariate analysis (MVA) was performed on the honey extracts using principal component (PCA) and hierarchical clustering analysis (HCA). There were 42 variables being analysed in unsupervised MVA. The objective of doing PCA and HCA analysis is to verify the differences and similarities between the honey samples being analysed. Based on two datasets, MVA was done by employing three approaches. The first approach utilised only proton NMR spectral data, the second approach applied only the HR-LCMS data while the third approach made used of the fused datasets of both HR-LCMS and ^{1}H NMR.

Clustering on the HCA was used in an attempt to characterize the bioassay results of mild (in red box) and weak (in green box) cytotoxicity to their chemical profile but the effect on ZR75 remained undifferentiated and unspecified into all groups. The clustering was performed on all variables where the ^{1}H NMR spectral dataset gave a relatively good model in terms of fitness and prediction ability (R^2=0.92 and Q^2=0.68, respectively). PCA (**Fig. 5.7A**) and HCA (**Fig. 5.7B**) of the samples based on the proton NMR spectral data distributed the bioactive extracts in two main groups, G2 and G3, while the presence of an outlier from the Malaysian sample set (PH) could be observed in G1. Although there was quite a variation observed between groups at 45% (R2X[1]) while within groups, it was only 18% (R2X[2]), it was still not possible to differentiate the samples according to their bioactivity and origin. Both NZ and MAS samples were dispersed in both G2 and G3. Since NMR could only detect the major metabolites in the respective samples, then it could be concluded that despite of the assigned groupings, it was not possible to differentiate the samples according to their origin as well as predict the metabolites affecting the cytotoxicity of the samples on ZR75.

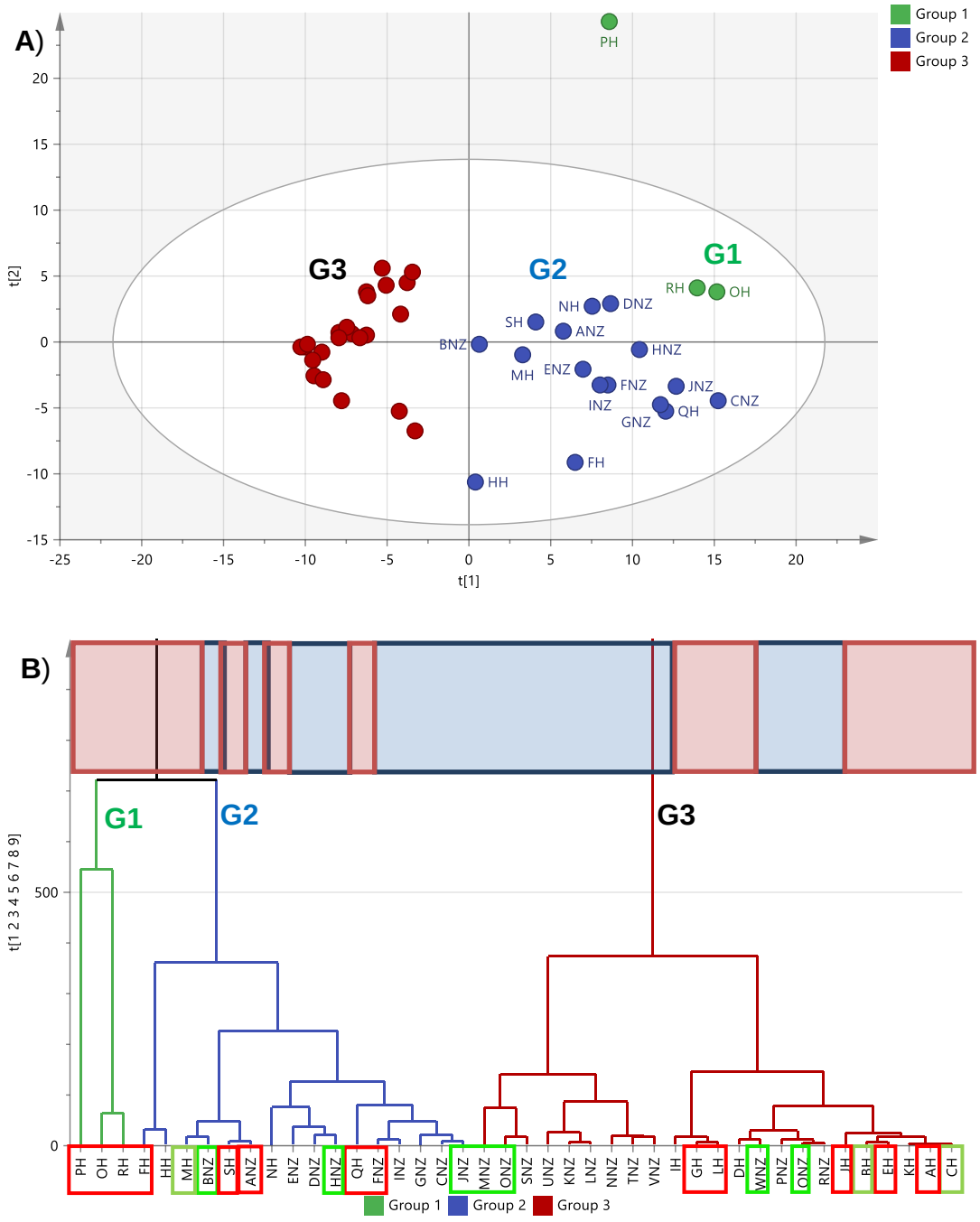

Fig. 5.7: **A**) The PCA and **B**) HCA on honey extracts based on ^{1}H NMR which gave a relatively good model and prediction (R^2=0.92 and Q^2=0.68). Mild samples were highlighted by a red box and weak bioactivity were highlighted by a green box. Highlighted boxes represents origin of honey samples where blue represents the New Zealand samples while the Malaysian samples are highlighted red. The removal of an outlier (PH) provides similar sample clustering for this model.

On the other hand, PCA and HCA (**Fig. 5.8A** and **5.8B**) of the HR-LCMS data set indicated a similar clustering pattern, which resulted in two big main groups, G2 and G3 along with an outlying group (G1) with one sample (ONZ) from New Zealand. Total 42 variables were dispersed into G1 (1), G2 (13) and G3 (28). The mass spectral dataset gave a relatively weaker model in terms of fitness and prediction ability (R^2=0.60 and Q^2=0.46) but was considered valid with a R^2 and Q^2 difference of 0.14, which is $\leq$ 0.3. Variation observed between groups increased to 49% (R2X[1]) while within groups, it decreased to 10% (R2X[2]). The bioactive samples were still dispersed in both G2 and G3. However, there was a better separation between the MAS and NZ samples. G2 clustered 56% of the NZ samples (highlighted in blue) while G3 had 94% of the MAS samples (highlighted in red), which were more tightly clustered as in the previous approach. Additionally, it can also be observed that the MAS samples possessed more of the mild active samples (enclosed in red boxes) while NZ samples had more weakly active samples (enclosed in green boxes). It could be said the mass spectral data indicated that the presence of low-concentration metabolites to be responsible in differentiating between MAS and NZ samples. As revealed by the PCA-loadings plot (**Fig. 5.8C**), the discriminating metabolites for NZ samples had low molecular weight metabolites ranging from 150 to 250, while the MAS samples had unique metabolites with higher molecular weights from 300 to 420. The discriminating metabolites for NZ and MAS samples were listed on **Table 5.5 and 5.6**, respectively.

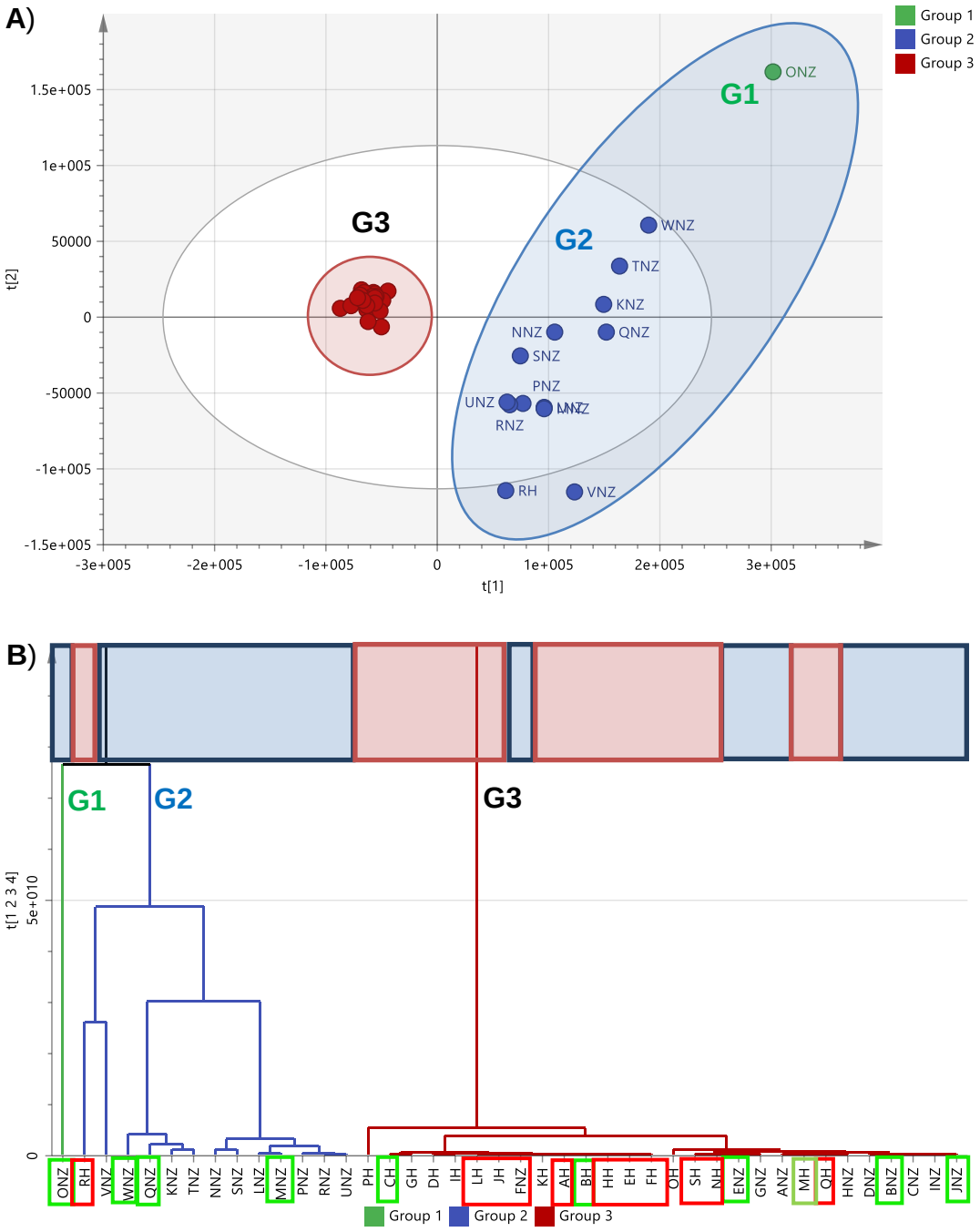

Fig. 5.8: **A**) PCA and **B**) HCA of honey extracts based on HR-LCMS (R^2=0.60 and Q^2=0.46). Mildly active samples were enclosed in a red box and weak bioactive samples in a green box. Highlighted boxes represents origin of honey samples where blue represents New Zealand (NZ) samples while the Malaysian (MAS) samples are highlighted red.

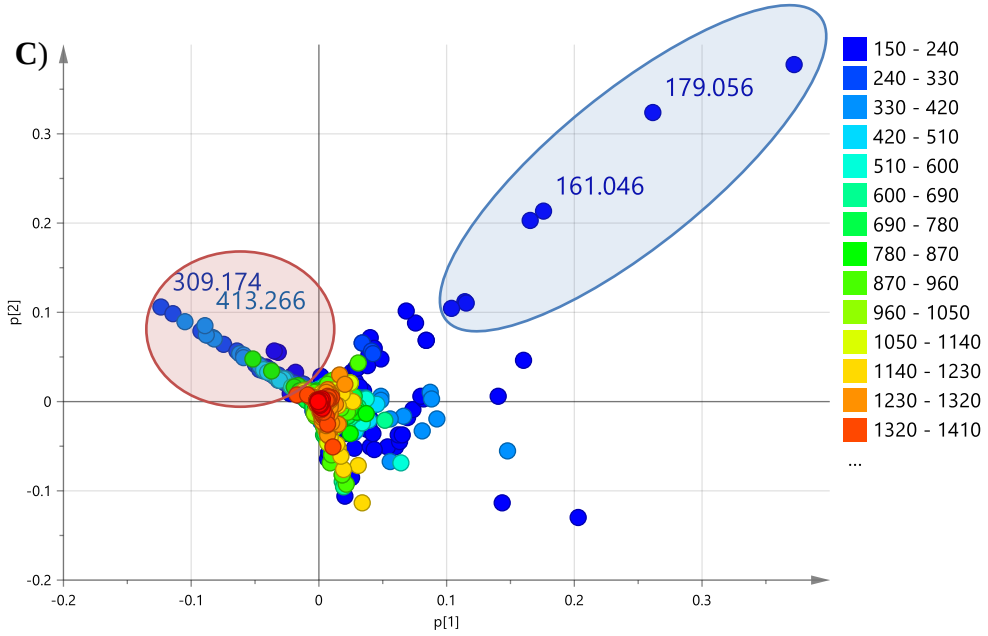

Fig. 5.8: **C**) PCA-loadings plot of honey extracts based on HR-LCMS. Highlighted circles represents origin of honey samples where blue represents New Zealand (NZ) samples while the Malaysian (MAS) samples were highlighted red.

Table 5.5: Discriminating metabolites for NZ samples from PCA loadings plot.

Var ID (Primary)	Var ID (m/z)	RT (min)	Predicted Molecular Formula	Exact Mass	Hits if any (with botanical source)
N_723	161.046	1.34	$C_6H_{10}O_5$	162.0528	1,5-anhydrofructose (*Pezizaechinospora*)
N_4692	179.056	1.33	$C_6H_{12}O_6$	180.0634	allose (*Protearubropilosa*)
N_30	207.051	1.58	$C_{14}H_6O_2$	206.0370	No hits
N_1011	225.062	1.34	$C_7H_{14}O_8$	226.0688	No hits
N_6	226.065	1.34			No hits

Table 5.6: Discriminating metabolites for MAS samples from PCA loadings plot.

Var ID (Primary)	Var ID (m/z)	RT (min)	Predicted Molecular Formula	Exact Mass	Hits if any (with botanical source)
P_3386	295.133	19.25	$C_{19}H_{18}O_3$	294.1255	3,7-dimethyl-1-octanol citrus fruits
N_1923	309.174	16.15	$C_{17}H_{26}O_5$	310.1776	No hits
N_4469	311.169	20.46	$C_{10}H_{20}N_{10}O_2$	312.1761	No hits
N_5114	325.184	21.55	$C_{11}H_{22}N_{10}O_2$	326.1916	No hits
N_1976	337.206	37.35	$C_9H_{26}N_{10}O_4$	338.2128	No hits
N_1925	353.200	37.39	$[C_{22}H_{28}NO_3]^+$	354.2228	2-methoxyatherosperminine
P_4751	413.266	32.33	$C_{22}H_{32}N_6O_2$	412.2590	No hits

The clustering observed in the PCA and HCA for the concatenated MS and NMR datasets (**Fig. 5.9A** and **B)** was comparable to employing the mass spectral dataset on its own. The fused datasets gave a fitness R^2 value of 0.71 and prediction ability (Q^2) of 0.413. The fitness of the model was improved but the prediction ability remained relatively the same while still considered valid with a R^2 and Q^2 difference of 0.30. The samples were grouped into three clusters, G1, G2, and G3, with approximately equal number of variables (13, 14 and 15, respectively) and disappearance of an outlying sample. G1 clustered 56% of the NZ samples (highlighted in blue) while G2 had 84% of the MAS samples (highlighted in red), which went down by 10% when compared to employing just the mass spectral dataset. G3 clustered together 40% of the entire number of observations. Both R2X[1] and R2X[2] variations were determined at 34% and 17%, respectively, indicating less variation between groups and increased in variation within groups when compared to the two latter approaches. Extraction of the NMR features from the concatenated datasets (**Fig. 5.9C)** revealed a higher density of highfield resonances between 1 to 3 ppm for the NZ samples (G1), which may indicate the presence of low molecular weight lipids. Alternatively, the MAS samples (G2) seems to be dominated by downfield signals between 3 to 5 ppm indicative for sugar compounds while G3 contained more signals from the 5 to 7 ppm region, which could belong to phenolic or other aromatic compounds.

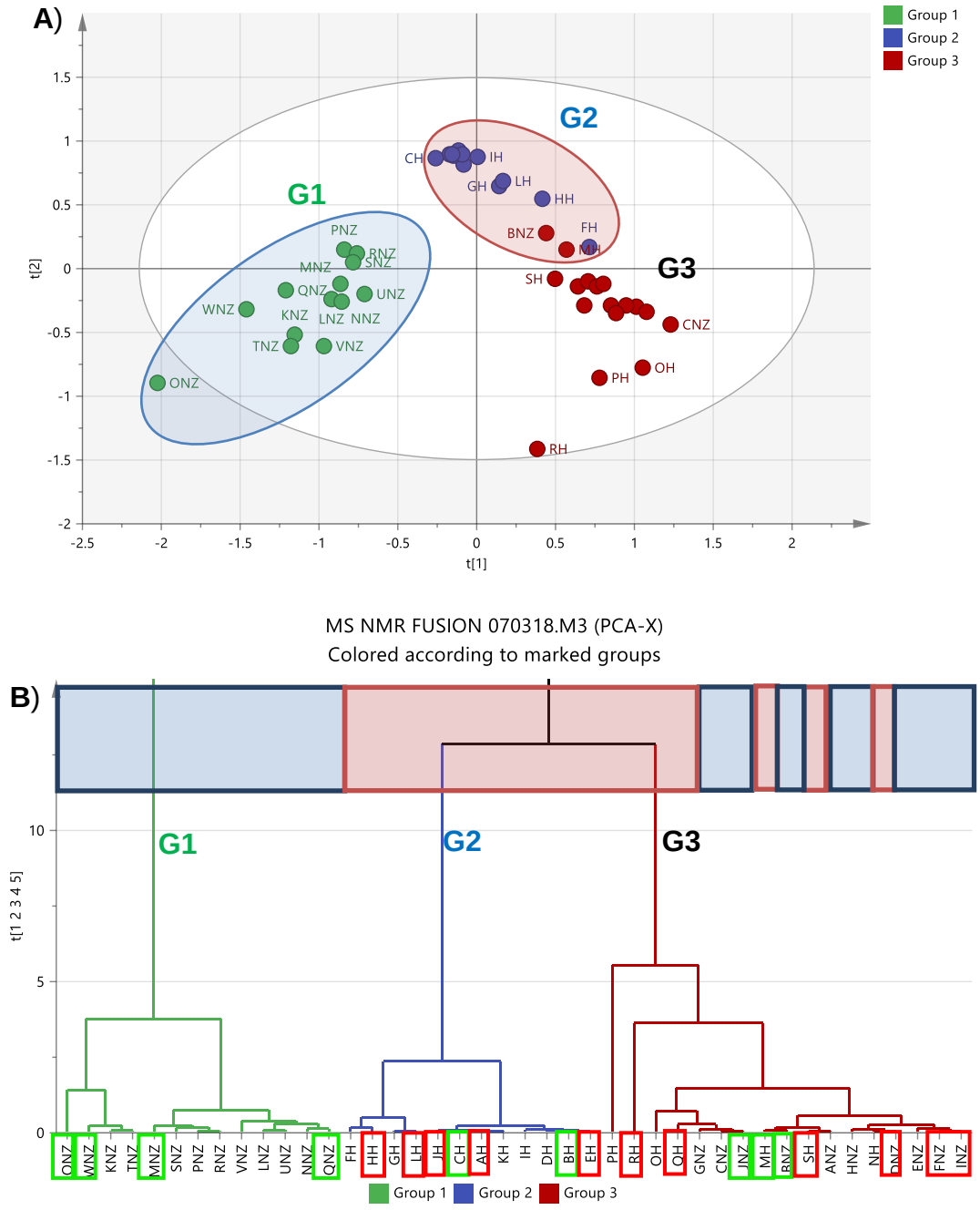

Fig. 5.9: **A**) PCA and **B**) HCA on honey extracts based on HR-LCMS and ^{1}H NMR fusion which gave a fitness R^2 value=0.715 and prediction ability Q^2=0.413. Mild samples were enclosed in red boxes and samples with weak bioactivity were in green boxes. Highlighted boxes represents origin of honey samples where blue represents New Zealand samples while the Malaysian samples were highlighted red.

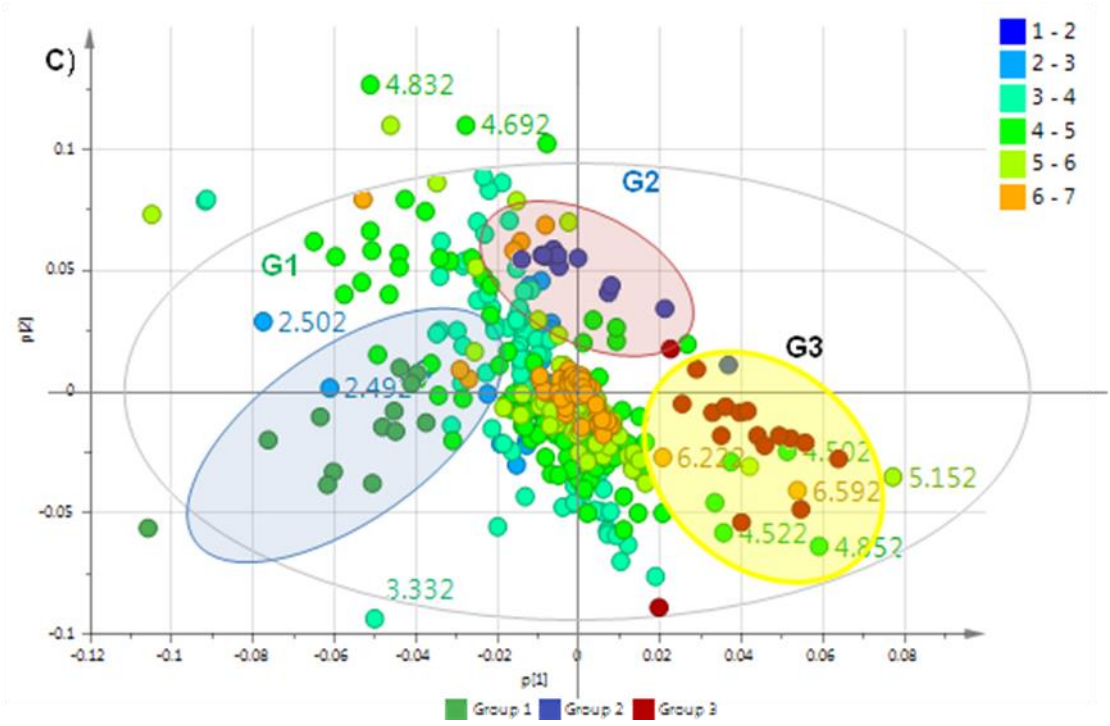

Fig. 5.9: **C**) PCA-biplot of the scores and extracted NMR loadings plot from the fused datasets. Highlighted in blue represents the New Zealand (NZ) samples and highlighted in red are the Malaysian (MAS) samples, while highlighted in yellow consisted of 40% of the total variables from MAS and NZ samples.

5.3.3.2. OPLS-DA based on geographical area

An OPLS-DA analysis (**Fig. 5.10 – 5.12)** was performed on MAS and NZ samples to confirm the discriminating metabolites found in PCA based on their geographical origins. Based on the proton NMR spectral data, the OPLS-DA scores plot (**Fig. 5.10A**) afforded a good model with R^2 of 0.84 for fitness, Q^2 of 0.59 for predictability, and R^2 and Q^2 difference of 0.25, which considered the model valid. Both R2X[1] and R2Xo[2] variations were determined at 6% and 43%, respectively, indicating a very small variation between the MAS and NZ samples while there was an increased in variation within the respective groups. The small variation between MAS and NZ samples could be deduced by two extracts, SH, and NNZ, belonging to MAS and NZ, respectively. SH and NNZ crossed over the quadrants of the respective groups as also shown on the HCA plot (**Fig. 5.10B**). The OPLS-DA coefficient plot (**Fig. 5.10C**) gave a clearer distribution of the resonances, which is comparable to the results obtained with the extracted NMR features from the PCA of the fused datasets (**Fig. 5.9C**). **Fig. 5.10C** demonstrated the occurrence of highfield resonances between 1 to 3 ppm for the presence of lipids in NZ samples. Alternatively, the MAS samples afforded an increase in number of signals in the downfield region between 5 and 7 ppm region, which could be evidenced for the occurrence of polyphenolic compounds in the samples. The presence of a hydroxyl substituent in a phenyl ring would shield protons to be resonating upfield from 7.25 ppm. Furthermore, between 3 to 5 ppm, the so-called sugar region, NZ samples seem to contain more intense signals than the MAS samples, indicating that the NZ honey extracts had higher sugar content than MAS honey.

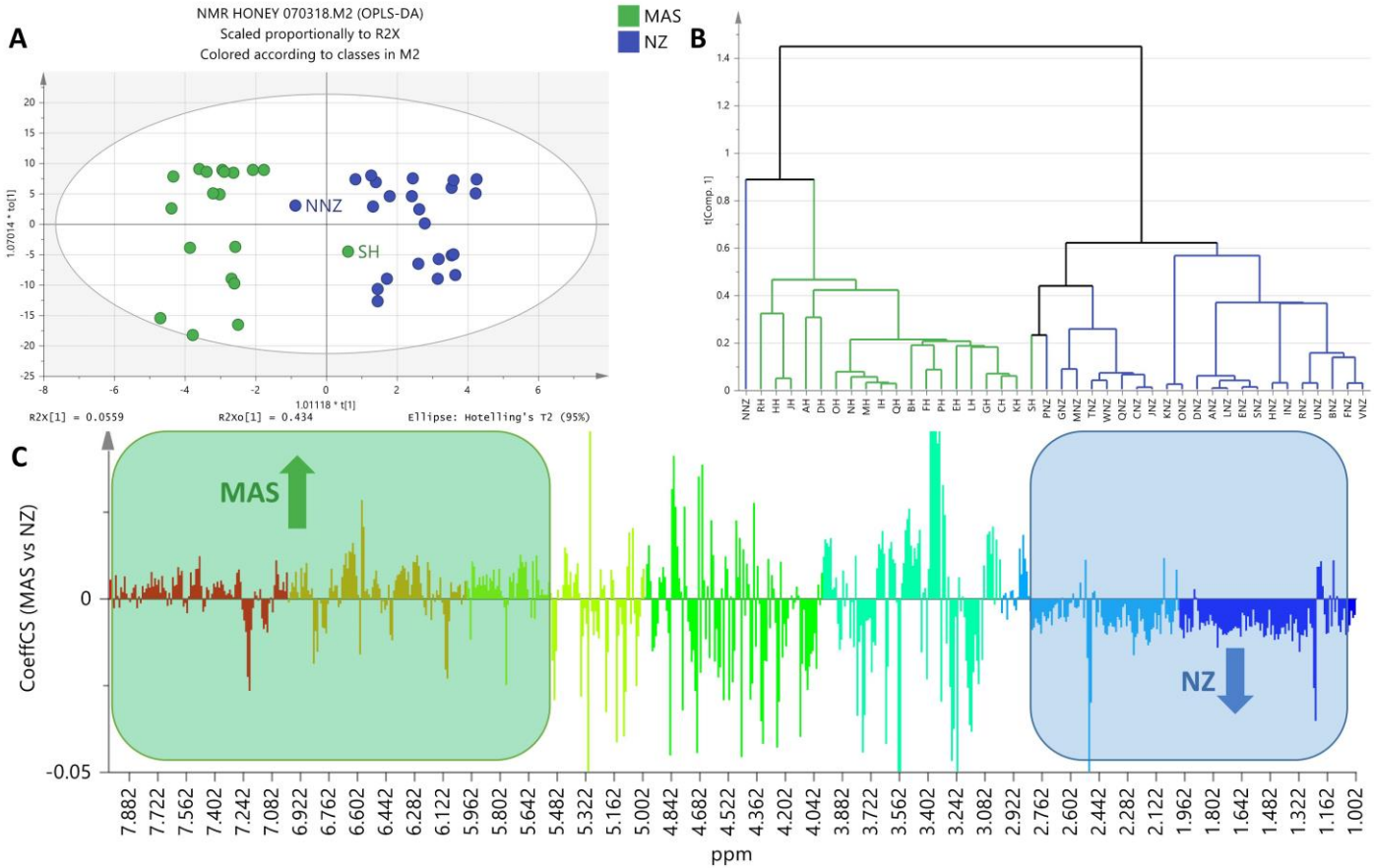

Fig. 5.10: **A**) OPLS-DA Scores plot, **B**) HCA by single linkage, and **C**) Coefficient plot of ^{1}H NMR spectral data of honey extracts. (R^2=0.84 and Q^2=0.59). Permutation test generated a Q2Y= -0.682 validated the model used.

Analysis of the mass spectral datasets by OPLS-DA (**Fig. 5.11A** and **B**) indicated a comparable clustering pattern as that obtained by PCA (**Fig. 5.8A**), which gave the same outliers, RH and ONZ from their respective groups. The loading plot showed dominant occurrences of compounds with the molecular weight between 280 and 420 g/mol for MAS samples observed on the lower left quadrant of the S-plot (**Fig. 5.11C**) and listed on **Table 5.7**. The higher molecular weight compounds could be predicted to be phenolic compounds as endorsed by their NMR spectral data as well (**Fig. 5.10C**). Whereas, the right upper quadrant had higher incidences of smaller molecular weight compounds ranging from 150 to 280 g/mol, which may indicate low molecular weight lipids and sugars (mono and disaccharides) in NZ honey that would be compatible with the NMR results. The discriminating metabolites generated by PCA and OPLS-DA were comparable but not identical to each other. The discriminating metabolites with $P < 0.05$ were listed according to their P values in **Table 5.7** and plotted on a bar graph in **Fig. 5.11D**. The list specified additional metabolites that differentiated MAS from NZ samples. The list also showed that there was a higher incidence of metabolites with even-numbered molecular weight and ionizing in the negative mode, which further indicated the presence of low molecular weight fatty acids and sugars (Hammad et al., 2009) for the NZ samples as well as phenolics in MAS samples. These set of metabolites differentiating the honey samples from MAS and NZ are very different to the type of compounds found in propolis as presented in chapters 3 and 4 of this dissertation. The chemical profile for honey is not necessarily identical with those found in propolis because bees would use them for different purposes. Honey is used by bees as long-term food supply, while propolis is used to protect the beehive, which would indicate the type of biological activity to be expected for these respective types of natural products.

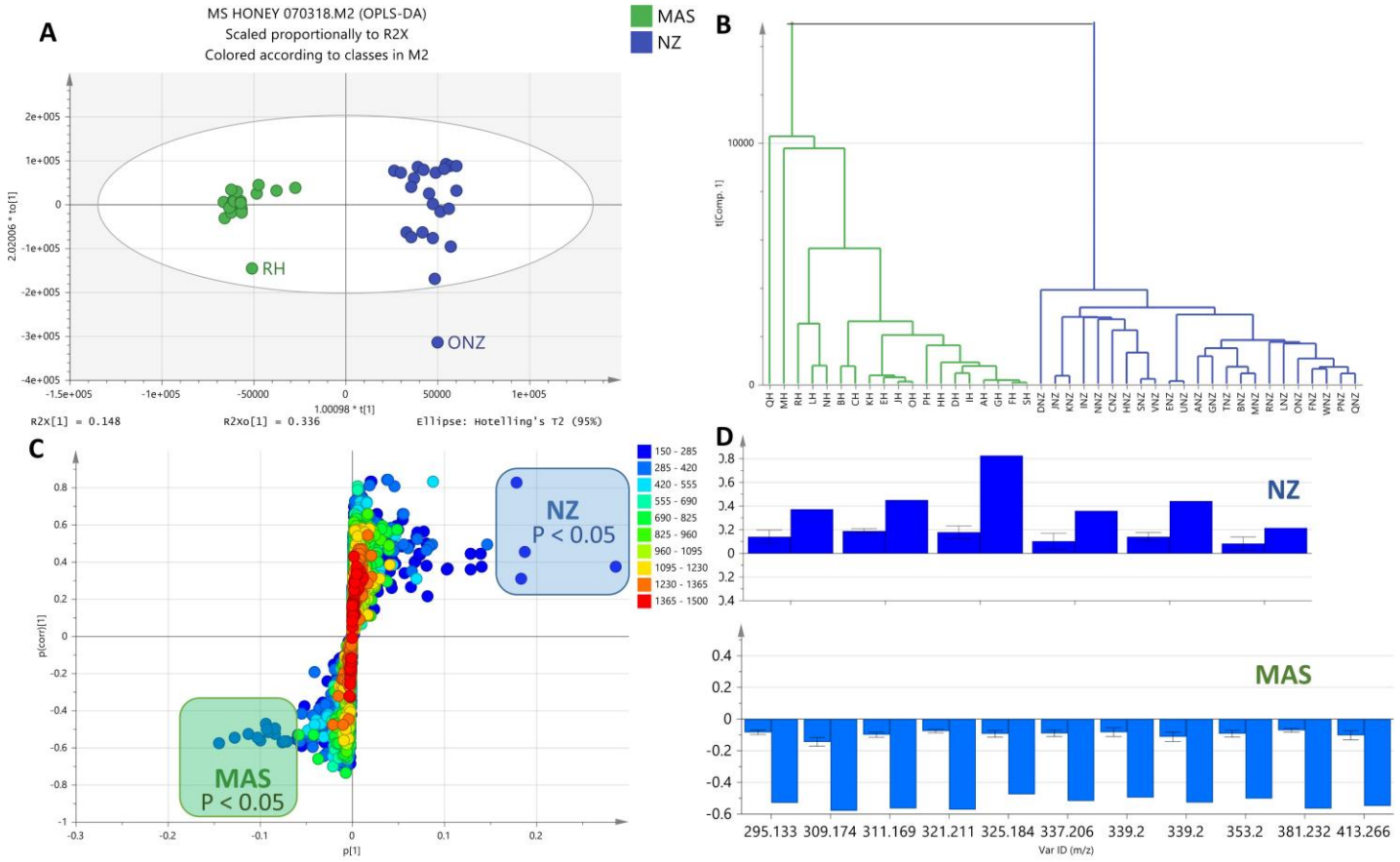

Fig. 5.11: **A**) OPLS-DA Scores plot, **B**) HCA by single linkage, **C**) S-loadings plot of mass spectral data of honey extracts, and **D**) Bar graph showing the discriminating metabolites with $P \leq 0.05$ as highlighted on the S-plot (R^2=0.91 and Q^2=0.64). Permutation test generated a Q2Y= -0.355 validated the model.

Table 5.7: Discriminating metabolites extracted from S-plot. Highlighted rows were the discriminating metabolites (P < 0.05) detected from the PCA-loadings plot. The list was arranged according to their P values as found by OPLS-DA.

Var ID	(*m/z*)	P values P ≤ 0.05	RT (min)	Molecular Formula	Exact Mass	Hits if any	Botanical Source
A. MAS samples							
N_1923	309.17	1.08E-04				see **Table 5.6**	
N_2025	321.21	1.41E-04	29.19	$C_{16}H_{34}O_4S$	322.2178	1-hexadecanol hydrogen sulfate	
N_2028	381.23	1.60E-04	27.52	$C_{24}H_{32}NO_3$	382.2392	No hits	
N_4469	311.17	1.77E-04				see **Table 5.6**	
P_3386	295.13	3.11E-04				see **Table 5.6**	
P_4751	413.27	3.86E-04				see **Table 5.6**	
N_4473	339.2	3.91E-04	26.88	$C_{23}H_{32}O_2$	340.2401	plastoquinone	*Spinacia oleracea*
N_1976	337.21	6.68E-04	37.35	$C_{22}H_{28}NO_2$	338.2128	No hits	
N_5130	339.20	8.66E-04				see **Table 5.6**	
N_1925	353.20	9.43E-04	21.38	$C_{24}H_{32}O_2$	352.2401	5-(12-Phenyl-8-dodecenyl)-1,3-benzenediol	*Knema laurina*
B. NZ samples							
N_7	195.05	2.39E-11	1.33	$C_6H_{12}O_7$	196.0582	gluconic acid	*Aureobasidium pullulans*
N_720	215.03	3.77E-03	1.28	$C_{16}H_6O$	214.0424	No hits	
N_1011	225.06	1.47E-02				see **Table 5.5**	
N_723	161.05	1.56E-02				see **Table 5.5**	
N_30	207.05	2.85E-02				see **Table 5.5**	
N_4692	179.06	5.49E-02				see **Table 5.5**	

On top of that, the best clustering was observed after spectral data fusion for MS and NMR as shown in **Fig. 5.12A** and **B**. In comparison to the latter two approaches, **t**he model was the best fit (R^2=0.96) and gave the best predictability (Q^2=0.74). At least three clustered groups were observed where all the MAS extracts were clustered in one group, whilst there were two independent groups detected for NZ extracts as shown on the right quadrant of the scores plot (**Fig. 5.12A**). However, the occurrence of two subgroups for the NZ samples was not properly reflected on the HCA (**Fig. 5.12B**) where samples between the two subgroups cross-linked each other. The occurrence of two subgroups for the NZ samples gave a high variation within groups at 31%, while between the two specified sample groups, MAS and NZ, the variation was only 9.9%. With no outliers, the percentage variation for the fused dataset was similar to the OPLS-DA model for the mass spectral data. Interestingly, both groups from NZ extracts were further clustered based on the two main islands of New Zealand, where the upper right quadrant covered the south island samples (**NZ-1**), particularly Awatere Valley, Wairau Valley, Linkwater and Moutere. Samples from the north island (**NZ-2**) of New Zealand clustered together in the lower right quadrant. However, the specific information about the geographical area was not provided by the supplier, therefore the result only relies on the trend observed from the OPLS-DA analysis. Furthermore, the S-plot (**Fig. 5.12C**) afforded similar results as indicated by the latter approaches used in this study.

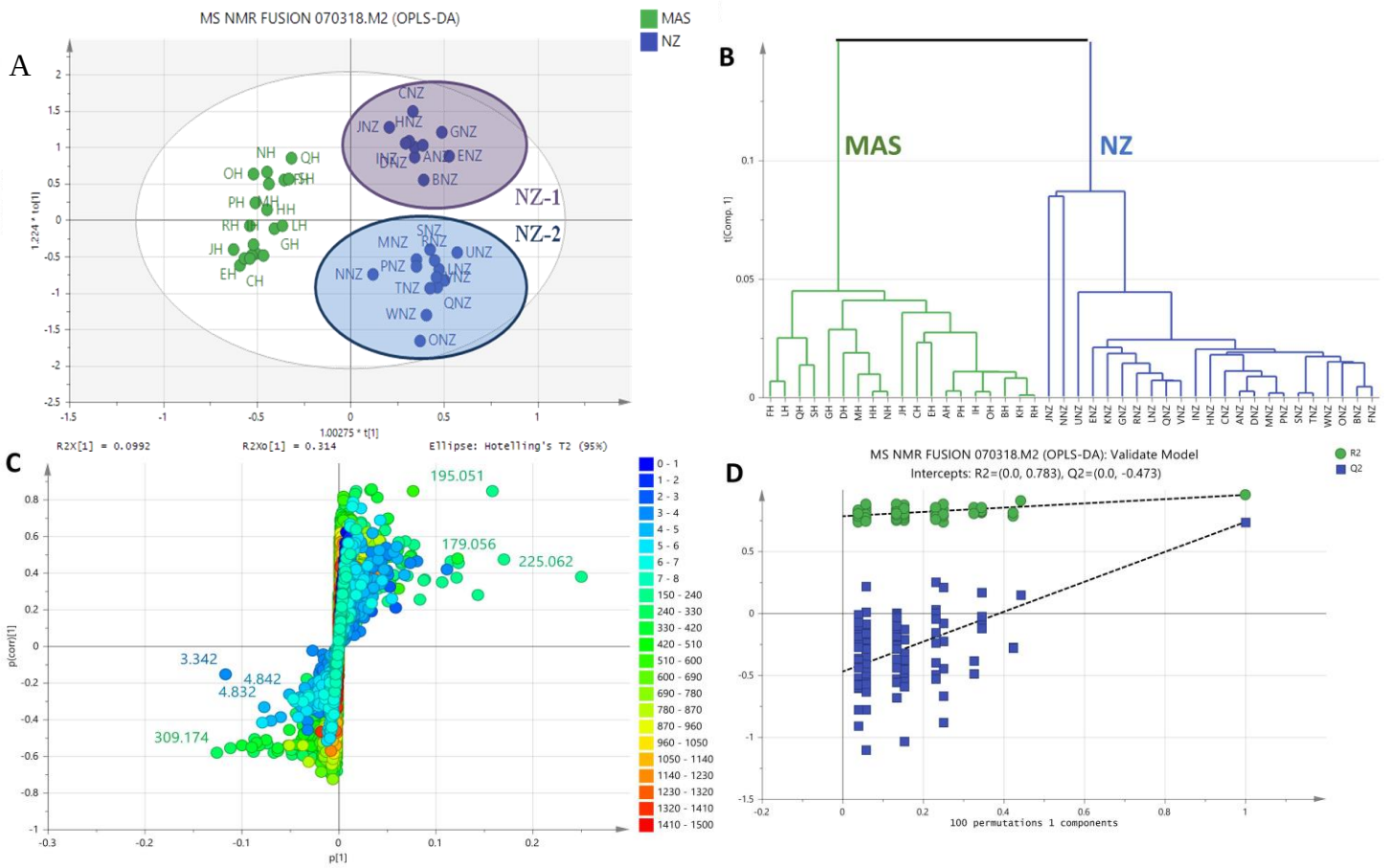

Fig. 5.12: **A**) OPLS-DA Scores plot, **B**) HCA by single linkage, and **C**) S-loadings plot of fused ^{1}H NMR and mass spectral data of honey extracts. (R^2=0.96 and Q^2=0.74). **D**) Permutation test generated a Q2Y= −0.473 validated the model.

To differentiate the samples collected from the South (**NZ-1**) and North (**NZ-2**) Islands in New Zealand, an OPLS-DA was performed on the fused NMR and mass spectral dataset of the NZ samples (**Fig. 5.13A**). A very good model was attained with R^2 of 0.997 and Q^2 of 0.974, while the permutation test afforded a Q2Y of −0.552. The samples collected from the south island were more tightly clustered. The occurrence of two distinct groups for the NZ samples increase the variation between groups at 47%, while within group variation was only 12%. The south island samples (**NZ-1**) were quite homogenous and were tightly clustered with each other. Whilst the north island samples (**NZ-2**) were loosely grouped and afforded ONZ as an outlier. The HCA (**Fig. 5.13B**) reflected the true distribution of the observations shown on the scores plot (**Fig. 5.13A**). The S-plot (**Fig. 5.13C**) revealed the features that differentiated **NZ-1** from **NZ-2**. The discriminating features, with P values < 0.05, were extracted and shown in a bar graph (**Fig. 5.13D**). The samples collected from the south island (**NZ-1**) gave higher molecular weight metabolites (*m/z* at 250 to 400 Da $[M-H]^-$) and indicated the presence of phenolic compounds with NMR resonances between 6 to 7 ppm. The northern island samples (**NZ-2**) were discriminated by low molecular weight compounds (*m/z* at 150 to 240 Da $[M-H]^-$) and NMR chemical shifts at 2 to 3 ppm, which could be evidenced by the presence of acetylated sugar or furfural molecules.

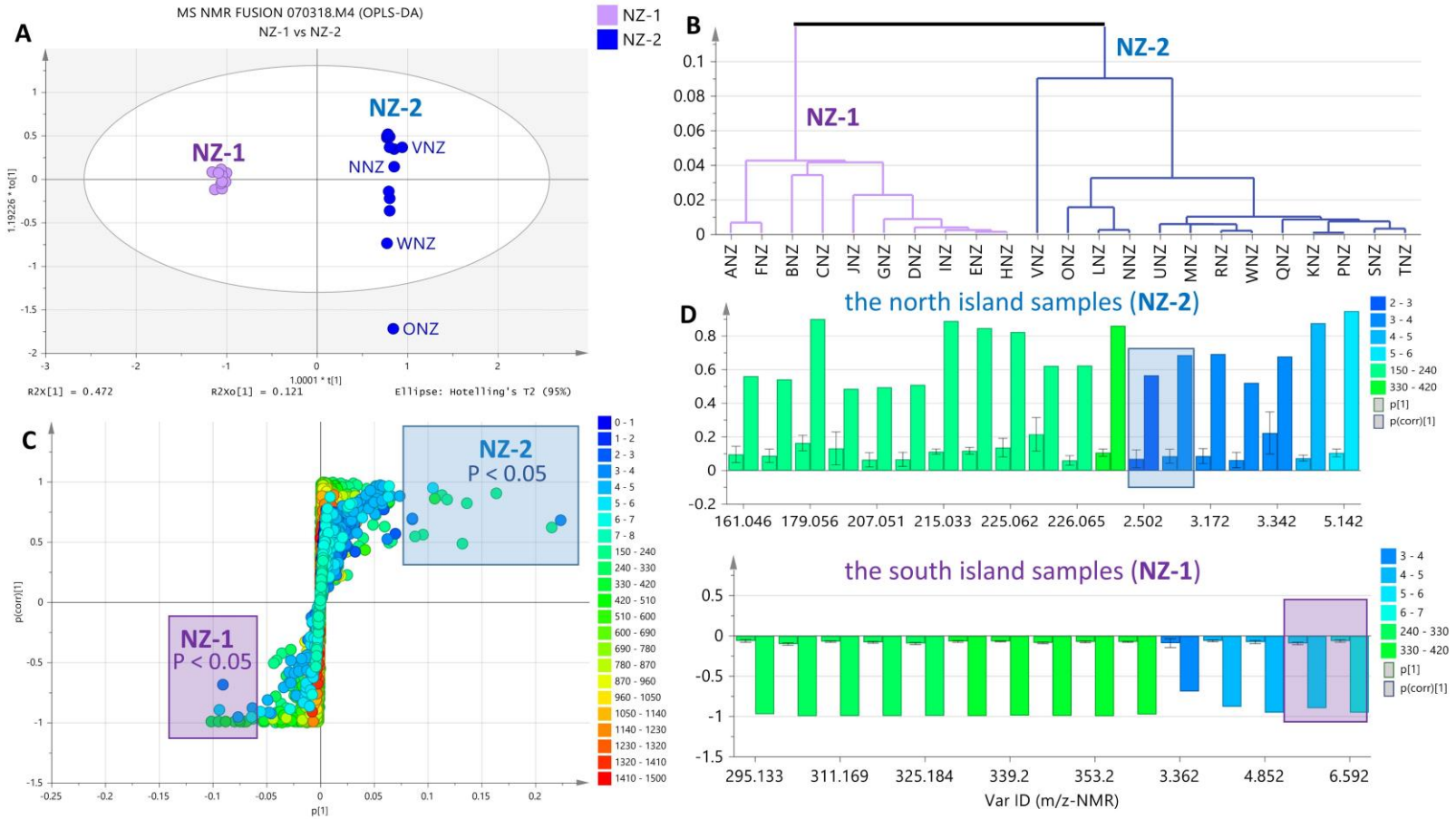

Fig. 5.13: **A**) OPLS-DA Scores plot, **B**) HCA by single linkage, **C**) S-loadings plot of mass spectral data of honey extracts, and **D**) Bar graph showing the discriminating metabolites as highlighted on the S-plot (R^2=0.997 and Q^2=0.974). Permutation test generated a Q2Y= -0.522 validated the model.

5.3.3.3. Heat maps generated from programme R version x64 3.0.3

As mentioned above, OPLS-DA based on geographical area gave better interpretation on the type of compounds found in MAS and NZ honey. Therefore, heat maps were generated to better visualise and compare the chemical diversity of each individual samples as well as further establish the similarities and differences according to their geographical origin and perhaps their bioactivity as well. The colour key from red to blue indicated increasing intensity of specific chemical constitutes in the extracts. The heat maps illustrated in **Fig. 5.14** and **5.15** were organized according to extracts showing differences in the chemical profiles at different intensity based on their ^{1}H NMR and HR-LCMS datasets, respectively.

Based on the proton NMR spectral data shown in **Fig. 5.14** the MAS honey extracts disclosed an interesting chemical profile (boxed in red), especially those from MH, OH, PH and RH, affording a denser set of signals between 5 and 6 ppm. From the NZ honey samples, the north island samples (**NZ-2**, boxed in green) yielded a more diverse chemical profile than the south island samples (**NZ-1**).

On the other hand, based on the mass spectral data displayed in **Fig. 5.15,** amongst the MAS samples (boxed in red); OH, PH and RH were observed to be the most diverse, where there is an increased in metabolites with molecular weights between 300 to 400 Da. For the NZ extracts, **NZ-2** samples were also found to have a more diverse chemical profile than **NZ-1**, which was a similar pattern, observed from the heat map of the NMR spectral data. **NZ-2** (boxed in green) samples afforded low molecular weight compounds ranging from 150 to 250 Da. These results were compatible to those achieved from the multivariate analysis of the samples.

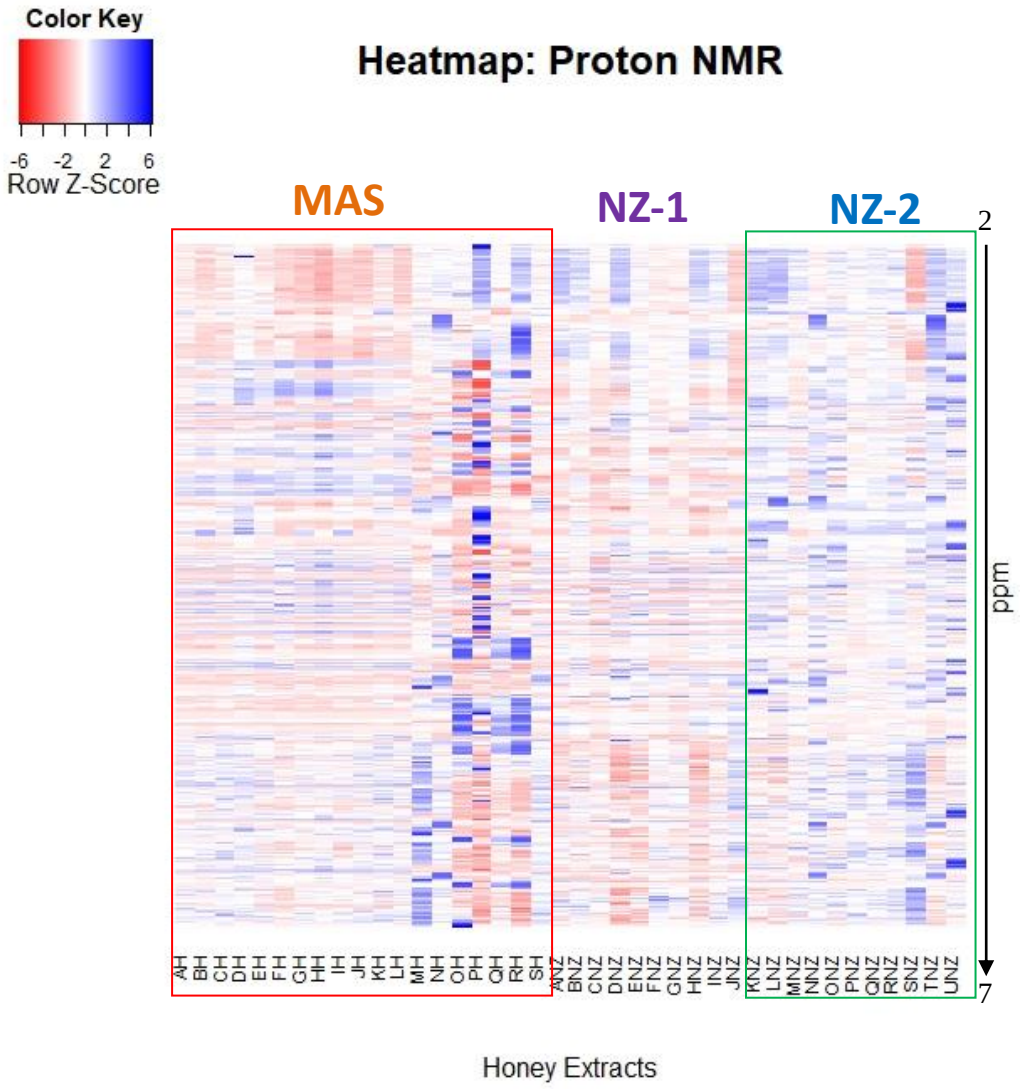

Fig. 5.14: The heat map based on ^{1}H NMR data displaying distinct metabolic profiles of 42 extracts, where the components highlighted in red box represents the metabolites from Malaysia honey. The components outside the red box are from New Zealand. Legend: **MAS** = Malaysian honey, **NZ-1** = south island New Zealand honey, **NZ-2** = north island New Zealand honey.

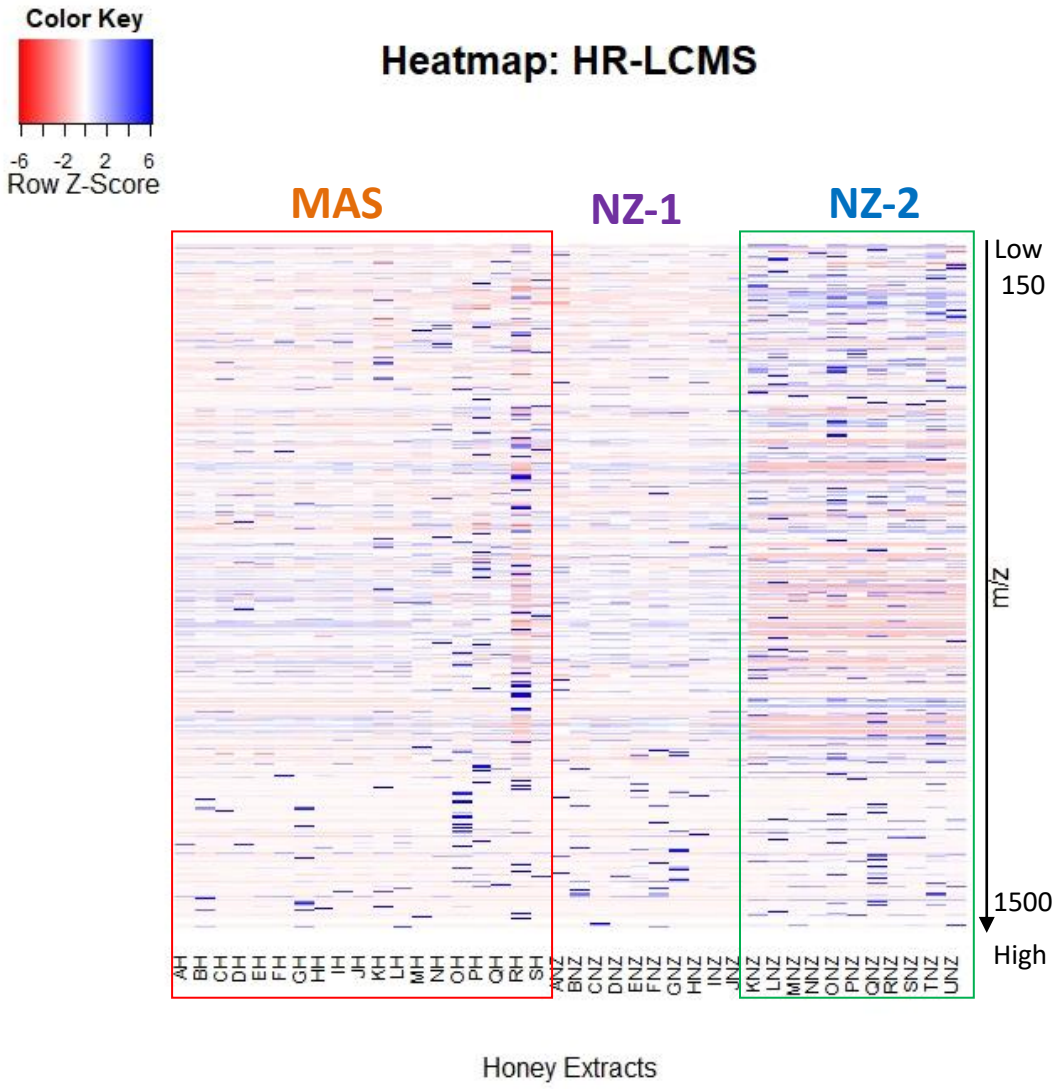

Fig. 5.15: The heatmap based on HR-LCMS data displaying distinct metabolic profiles of 42 extracts, where the components highlighted in red box represents the metabolites from Malaysia honey. The components outside the red box are from New Zealand. Legend: **MAS** = Malaysian honey, **NZ-1** = south island New Zealand honey, **NZ-2** = north island New Zealand honey.

5.3.4 Dereplication of bioactive Malaysian and New Zealand honey samples

Furthermore, the type of metabolites involved in the bioactive extracts against the breast cancer cell line were determined using an S-loadings plot, it was plausible to pinpoint the bioactive metabolite that maybe responsible for the bioactivity as shown in **Fig. 5.16** and **Fig. 5.17**.

For the Malaysian samples, the active and inactive extracts were compared using OPLS-DA method (**Fig. 5.16**). Both R^2 and Q^2 were observed at 0.91 and 0.14, respectively, showing good fitness but poor prediction ability. The permutation test afforded a Q^2 value of −0.299, which still supported the validity of this model. In addition, both R2X[1] and R2X[2] were determined at 0.073 and 0.39, respectively. This also indicated that the variation score between active and inactive was at only 7.3%, which was smaller than the variation score within group at 39%. This could be explained by the closeness of FH from the active group to EH belonging to the inactive samples. Meanwhile, the larger variation score within the group was due to the occurrence of an outlier sample (RH) amongst the active extracts shown in the score plot (**Fig. 5.16A**). S-loadings plot (**Fig. 5.16B**) was used to identify the putative bioactive metabolites that could have been responsible for the bioactivity of the samples. The dereplication database of the predicted bioactive metabolites was presented in **Table 5.8**.

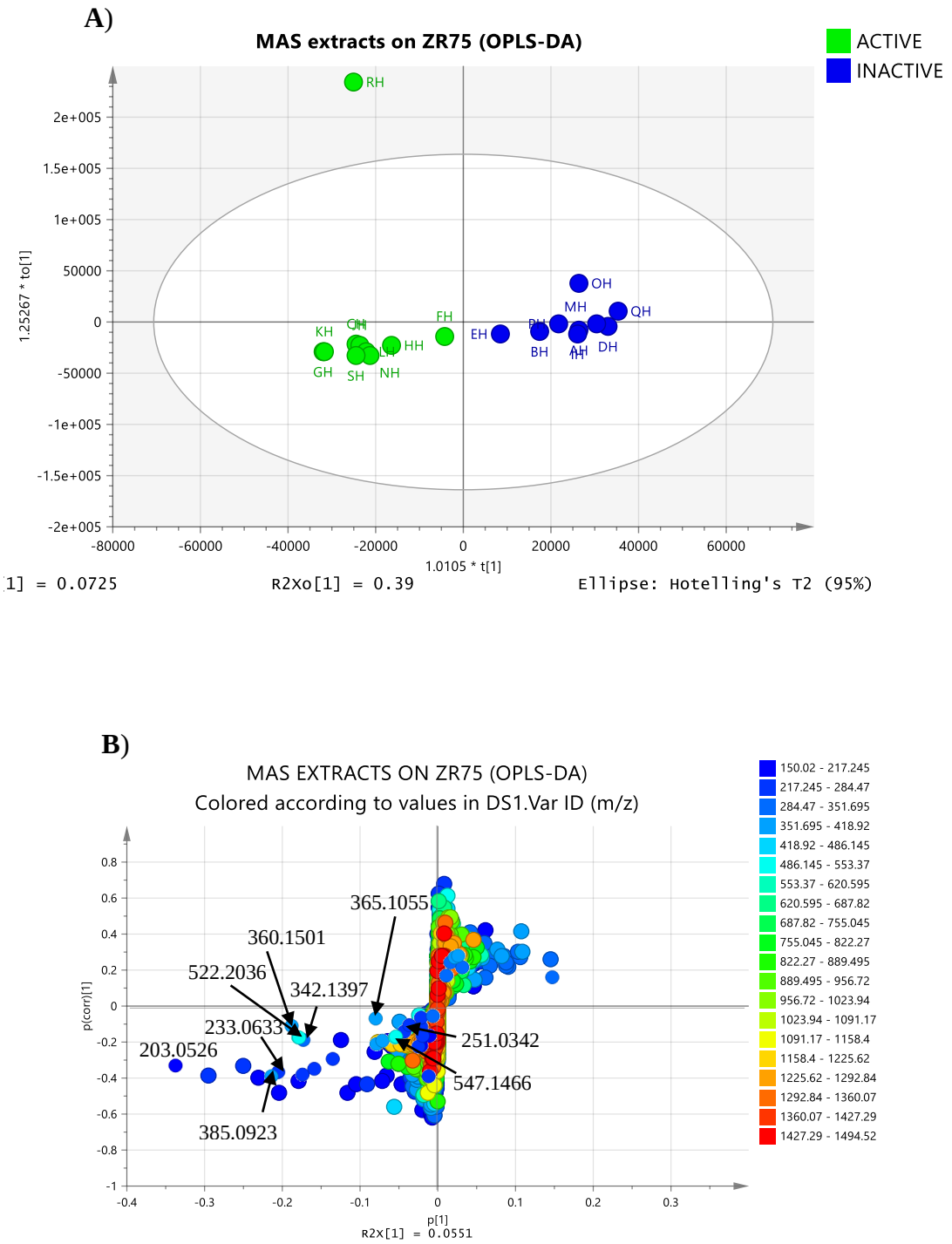

Fig. 5.16: A) OPLS-DA score plot of MAS samples and **B)** S-plot confirming the putative bioactive metabolites in Malaysia (MAS) extracts that responsible for its cytotoxicity effects on ZR75.

For the New Zealand samples, a comparison of the active and inactive extracts was done by using OPLS-DA as well (**Fig. 5.17**). R^2 and Q^2 were observed at 0.99 and 0.15, respectively, showing excellent fit but very poor prediction ability. The permutation test afforded a Q^2 value of −0.137, which was still considered to be a valid model. In addition, both R2X[1] and R2X[2] were determined at 0.036 and 0.51, respectively. The low variation of only 3.6%, between the active and inactive was reflected by the weak activities of the so-called "active" samples, averaging at 68% viability of control when the threshold for strong activity was set to 40% while the inactive NZ samples were averaging at 81%. The larger variation of 51.2% within the respective groups could be due to the formation of two distinct subgroups as shown in the score plot (**Fig. 5.17A**). S-loadings plot (**Fig. 5.17B**) was again used to identify the putative metabolites that could have been responsible for the bioactivity of the samples. The dereplication database of the predicted bioactive metabolites was presented in **Table 5.9**.

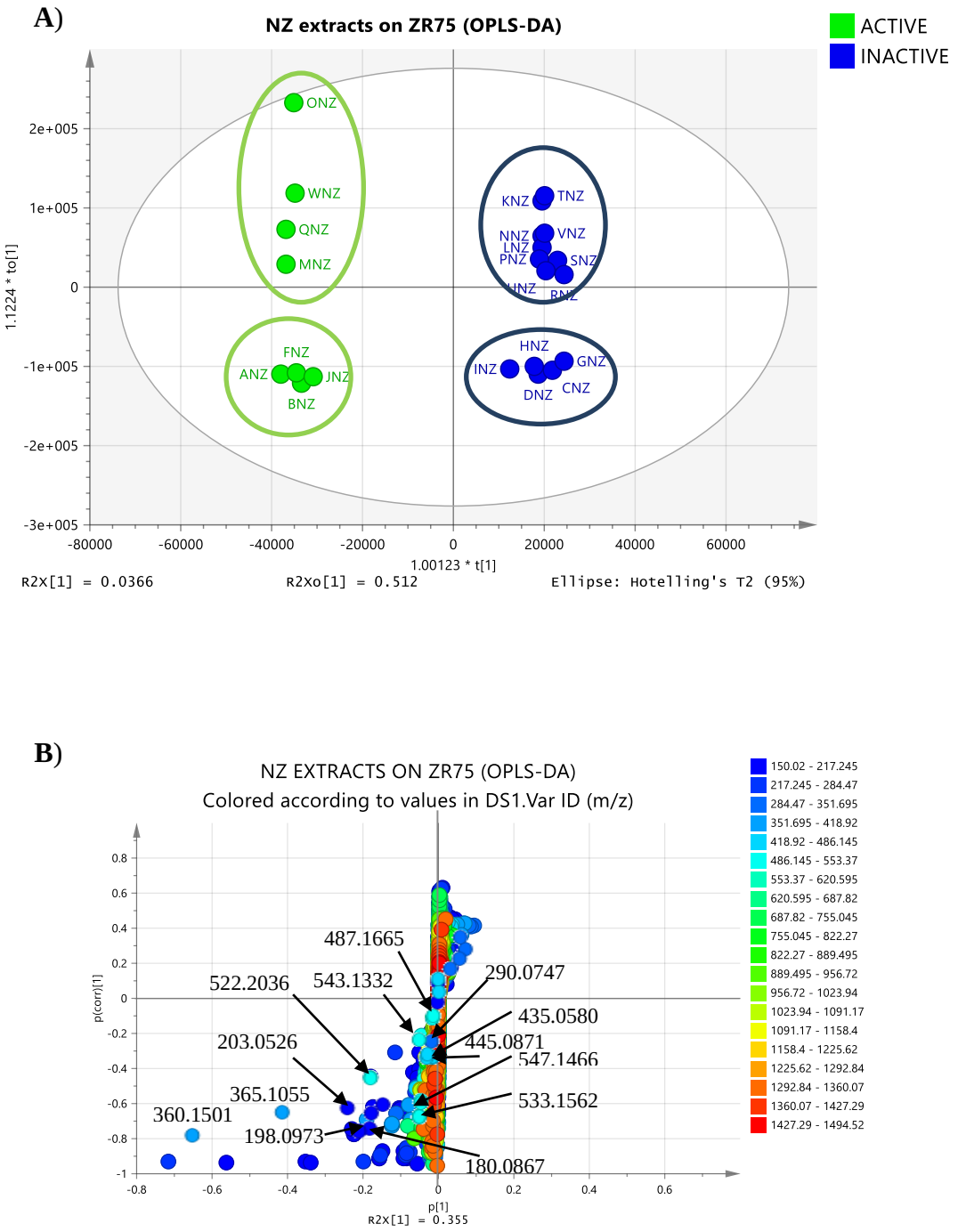

Fig. 5.17:**A**) OPLS-DA scores plot and **B**) S-plot displayed the putative bioactive metabolites in New Zealand (NZ) extracts that could be responsible for its cytotoxicity effects on ZR75.

Amongst the bioactive samples from both MAS and NZ, NH and BNZ had the highest numbers of features and were chosen as representative spectrum to identify the major ion peaks for the active samples. The aqueous methanol extracts of NH and BNZ were found active on the initial screening on the breast cancer cell line, ZR75. Through dereplication, furfural derivatives, previously isolated from *Chrysanthemum* sp., were amongst the metabolites putatively identified from both extracts (**Tables 5.8** and **5.9**). The furfural derivatives detected in both positive and negative ionization modes were eluted within the retention time range between 0.69 and 2.27 min, when the percentage of organic mobile phase (acetonitrile) was at only 10% (**Fig. 5.18** and **5.19**), and could be detected in both positive and negative ionization modes. Moreover, major compounds for the Malaysian samples consisted of sugars and benzylic-alcohol derivatives. On the other hand, glycosidic compounds earlier reported from *Hydrangea paniculata* and *Ficus ruficaulis* were observed from bioactive New Zealand samples. Alcoholic and carboxylic derivatives were also determined from the New Zealand samples; some of them previously described from the lichen *Lecanora jamesii*. All the putative bioactive metabolites from Malaysia and New Zealand extracts were observed in the S-plot in **Fig. 5.16** and **Fig. 5.17**, which were complemented by the dereplication hits from the DNP database. Labelled metabolites on the S-plots for both MAS and NZ samples represent the major compounds found in the respective sample extracts, which were listed in **Tables 5.8** and **5.9**, while shown in the mass spectra in **Fig. 5.18** and **5.19**. Interestingly, all major compounds found in both samples sets, MAS and NZ, were detected on the bioactive side of their respective S-plots.

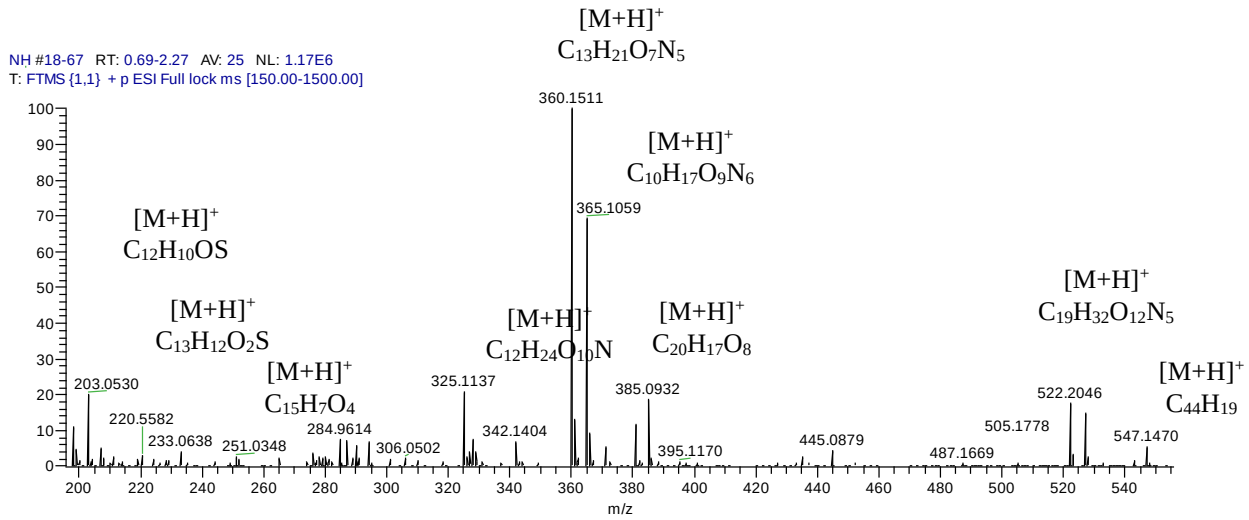

Fig. 5.18: Mass spectrum for NH in the positive ionization mode showing the presence of a cluster of features within the RT range of 0.69 – 2.27 min.

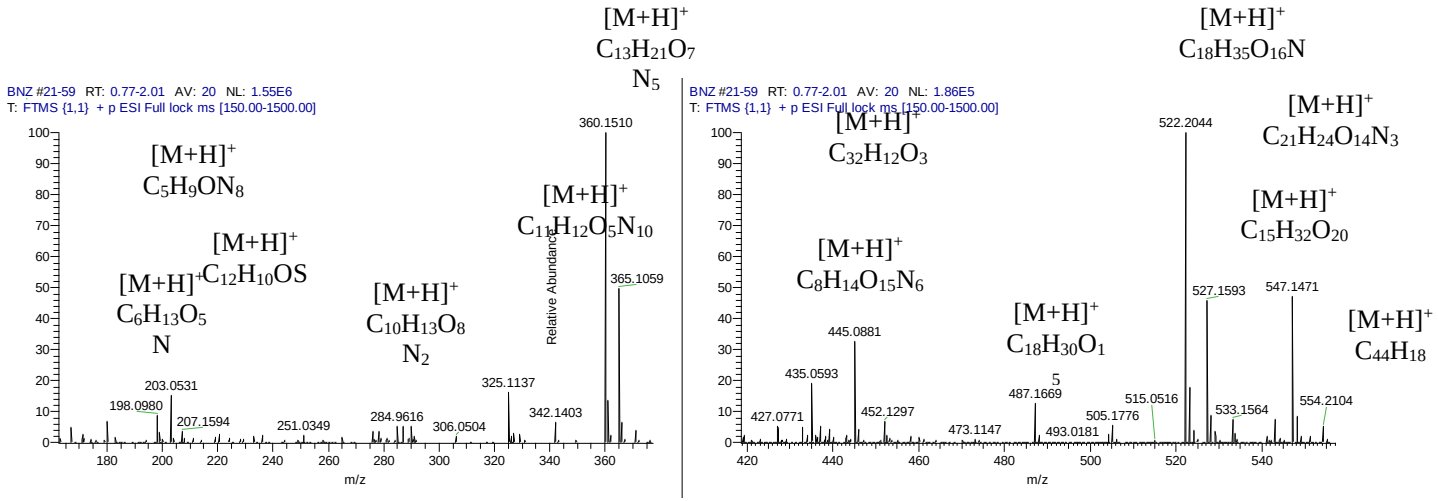

Fig. 5.19: Mass spectrum for BNZ in the positive ionization mode showing the presence of a cluster of features within the RT range of 0.77 – 2.01 min.

Table 5.8: Selected metabolites found in the bioactive Malaysian honey samples. All of these metabolites were also detected in negative ionization mode.

Polarity	*m/z*	Rt	MF	MW	Name	Source	NH
P	203.0526	1.07	$C_{12}H_{10}OS$	202.0453	1-(2,3-dihydro-2-furyl)-4-(thien-2-yl)but-1-en-3-yne	*Chrysanthemum macrotum*	4.03E+07
P	365.1055	1.07	$C_{10}H_{16}N_6O_9$	364.0982	No hits		7.93E+07
P	342.1397	1.10	ammonium adduct of $C_{12}H_{23}NO_{10}$	341.1325	2-amino-2-deoxy-3-glucopyranosylgalactose		2.71E+06
P	522.2036	1.10	$C_{19}H_{31}N_5O_{12}$	521.1963	No hits		4.18E+06
P	360.1501	1.11	$C_{13}H_{21}N_5O_7$	359.1428	No hits		2.55E+07
P	547.1466	1.19	$C_{44}H_{18}$	546.1393	No hits		2.51E+06
P	385.0923	1.28	$C_{20}H_{16}O_8$	384.0851	vitelignin A	*Vitex negundo*	1.36E+07
P	233.0633	1.34	$C_{13}H_{12}O_2S$	232.0560	5-[5-(methylthio)-4-penten-2-ynyl]-2-furanacrolein	*Chrysanthemum coronarium*	8.45E+06
P	251.0342	1.38	$C_{15}H_6O_4$	250.0269	No hits		2.61E+06

Table 5.9: Selected metabolites found in bioactive New Zealand samples.All of these metabolites were also detected in negative ionization mode.

Polarity	*m/z*	Rt	MF	MW	Name	Source	BNZ
P	543.1332	1.06	$C_{23}H_{26}O_{15}$	542.1260	5,6-diglucopyranosylangelicin	*Ficus ruficaulis* var. *antaoensis*	1.57E+06
P	203.0526	1.07	$C_{12}H_{10}OS$	202.0453	1-(2,3-dihydro-2-furyl)-4-(thien-2-yl)but-1-en-3-yne	*Chrysanthemum macrotum*	3.09E+07
P	365.1055	1.07	$C_{11}H_{12}N_{10}O_5$	364.0982	No hits		6.11E+07
P	487.1665	1.10	$C_{18}H_{30}O_{15}$	486.1592	galactopyranuronosyl-rhamnopyranosyl-rhamnose	*Hydrangea paniculata*	3.33E+06
P	522.2036	1.10	$C_{18}H_{35}NO_{16}$	521.1963	No hits		4.69E+06
P	360.1501	1.11	$C_{13}H_{21}N_5O_7$	359.1428	No hits		3.62E+07
P	533.1562	1.17	$C_{15}H_{32}O_{20}$	532.1489	No hits		2.75E+06
P	547.1466	1.19	$C_{44}H_{18}$	546.1393	No hits		2.45E+06
P	180.0867	1.26	$C_6H_{13}NO_5$	179.0794	6-amino-1,2,3,4,5-cyclohexanepentol		1.98E+06
P	290.0747	1.28	$C_{10}H_{13}N_2O_8$	289.0675	No hits		3.23E+07
P	445.0871	1.39	$C_{32}H_{12}O_3$	444.0798	No hits		1.85E+06
P	435.0580	1.40	$C_8H_{14}N_6O_{15}$	434.0507	No hits		2.81E+05
P	198.0973	1.51	$C_5H_9N_8O$	197.0901	No hits		2.40E+06

5.4 Discussion

5.4.1 Bioactive metabolites from Malaysian honey

Of the 19 honey samples from Malaysia analysed in this study, 11 of them exhibited bioactivity on ZR75. Furfural derivatives and sugar compounds were dereplicated with the DNP database from the honey samples through combined assessment of their proton NMR and HR-LCMS spectral data. The honey samples collected from different areas in Malaysia ascribed to uni-floral sources that included *Acacia* sp. (CH), *Koompassia excels* (FH), *Momordica charantia* (GH), *Melaleuca* sp. (HH), *Asystasia gangetica* (JH), *Acacia mangium* (LH, NH and SH), *Ananascomosus sp.* (MH) and also from multi-floral sources (KH and RH). Different geographical areas can provide both uni- and multi-floral forages opportunity to a variety of bee species such as *Apis trigona* sp. (CH, KH and RH), *Apis dorsata* sp. (FH) and *Apis mellifera* sp. (GH, HH, JH, LH, MH, NH and SH). By comparing the chromatograms of the different bioactive extracts, the putative bioactive metabolites were identified as 1-(2,3-dihydro-2-furyl)-4-(thien-2-yl)but-1-en-3-yne (Chen et al., 2005), 5-[5-(methylthio)-4-penten-2-ynyl]-2-furanacrolein (Bohlmann and Schuber, 1969), 2-amino-2-deoxy-3-glucopyranosylgalactose (Helferich and Müller, 1973) and vitelignin A (Zheng et al., 2011a) which previously have been isolated from Tonghaosu, *Chrysanthemum coronarium* L, synthetic and *Vitex negundo,* respectively (**Fig. 5.20**).

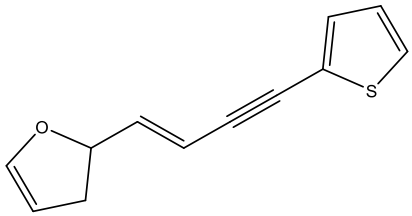

1-(2,3-dihydro-2-furyl)-4-(thien-2-yl)but-1-en-3-yne

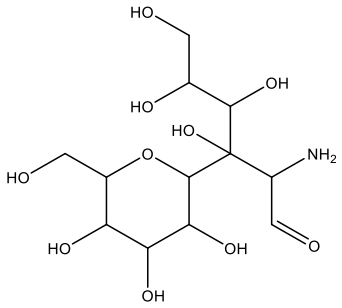

2-amino-2-deoxy-3-glucopyranosylgalactose

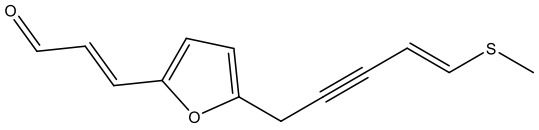

5-[5-(methylthio)-4-penten-2-ynyl]-2-furanacrolein

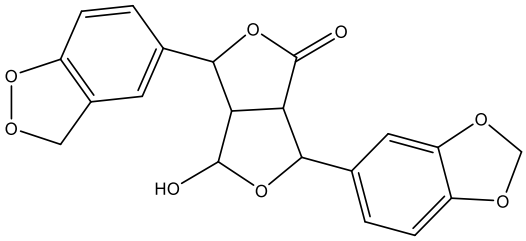

vitelignin A

Fig. 5.20: The putative major metabolites identified in bioactive Malaysia honey extracts.

5.4.2 Bioactive metabolites from New Zealand honey

From the 23 honey samples from New Zealand analysed in this study, eight of them exhibited biological activity against ZR75. Honey predominantly consists of sugars and other organic compounds. Meanwhile in this study, in addition to galactose and glucose, furfural and amino derivatives were also identified as major compounds in these extracts based on their high resolution mass spectral data. As reported in the literature, uni-floral honey samples represented a respective plant species if the predominant plant is abundant in more than 45% of the geographical area (Nayik and Nanda, 2016). The honey samples described to exhibit biological activity in this study were predominantly collected by the *Apis mellifera* bees from the Manuka tree (FNZ). Beside Manuka as its main source of nectar, other plant sources included clover (ANZ, BNZ and JNZ), honey dew (ANZ and JNZ) and borage (BNZ), as well as a mixture of other plants were also within the foraging area of the bees (MNZ, ONZ, QNZ and WNZ). By comparing the chromatograms of the various bioactive extracts, the putative bioactive metabolites were identified as 6-amino-1,2,3,4,5-cyclohexanepentol (Carter et al., 1948), galactopyranuronosyl-rhamnopyranosyl-rhamnose (Machida and Inano, 1955), 1-(2,3-dihydro-2-furyl)-4-(thien-2-yl)but-1-en-3-yne (Chen et al., 2005) and 5,6-diglucopyranosylangelicin (Chang et al., 2005), which previously have been isolated from *Hydrangea paniculata*, Tonghaosu and *Ficus ruficaulis*, respectively (**Fig. 5.21**).

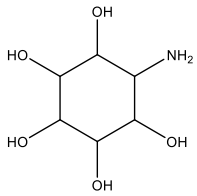

6-amino-1,2,3,4,5-cyclohexanepentol

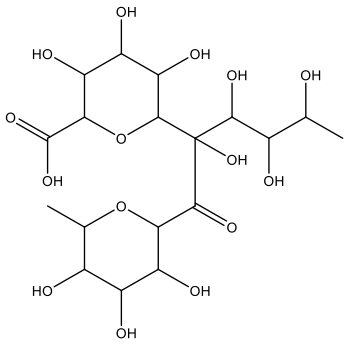

galactopyranuronosyl-rhamnopyranosyl-rhamnose

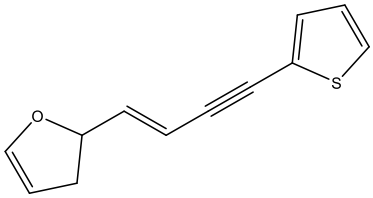

1-(2,3-dihydro-2-furyl)-4-(thien-2-yl)but-1-en-3-yne

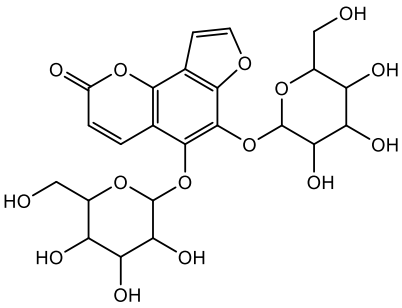

5,6-diglucopyranosylangelicin

Fig. 5.21: The putative major metabolites identified in bioactive New Zealand honey extract.

5.4.3 Vegetative diversity among samples in both countries contributed to cytotoxicity on ZR75 at different levels.

Based on the ZR75 assay, the honey extracts from Malaysia gave stronger cytotoxicity effects compared to New Zealand honey. Honey samples from both countries share one major compound which is 1-(2,3-dihydro-2-furyl)-4-(thien-2-yl)but-1-en-3-yne. It was suggested that the furfural derivative5-[5-(methylthio)-4-penten-2-ynyl]-2-furanacrolein along with 2-amino-2-deoxy-3-glucopyranosyl galactose and vitelignin A contributed to the mild cytotoxicity effects on ZR75 possibly through the induction of apoptosis (Fauzi et al., 2011) and the ability to control metastasis (Pashinskiĭ, 1990). For example, Tualang honey was evident to give strong antioxidant activity from ferric reducing ability of plasma (FRAP) assay (Mohamed et al., 2010). Several studies demonstrated the positive modulation effects of Tualang honey from Malaysia on breast cancer cell line, MCF-7 and DMBA/MNU-induced breast carcinogenesis in Sprague Dawley rats (Ahmed et al., 2017, Yaacob and Ismail, 2014, Ahmed and Othman, 2017, Kadir et al., 2013). The benefit of honey as an anti-cancer modulating agent has increased arguments, since honey highly contained carbohydrates, which exist in its concentrated form in honey. This could yield high levels of calories that could initiate cancer formation, especially in breast cancer (Welsch, 1994). However, it was evident that Tualang honey consumption in DMBA-induced breast cancer in rat did not cause major influence in their body weight (Kadir et al., 2013). In the present study, positive insight to enhance cytotoxicity effects against ZR75 was exemplified by several nectar sources of honey from Malaysia that included *Acacia* sp. (Acacia), *Koompassia excels* (Tualang), *Momordica charantia* (bitter gourd), *Melaleuca* sp. (paperbark), *Asystasia gangetica* (Chinese violet), *Acacia mangium* (black wattle), *Ananascomosus* sp. (pineapple) as well as from multifloral sources.

On the other hand, 6-amino-1,2,3,4,5-cyclohexanepentol, galactopyranuronosyl-rhamnopyranosyl-rhamnose and 5,6-diglucopyranosylangelicin were identified from New Zealand honey samples to be responsible for the cytotoxicity effect on ZR75 at 4% concentration (100µg/ml) after 48h treatment but at a weaker level that maybe due to the synergistic, time- or dose-dependent interaction. Maximum efficiency of Manuka honey at 0.6% concentration was demonstrated to inhibit atleast ≤ 90% of cell viability in breast cancer cell line (MCF-7) after 72h treatment (Fernandez-Cabezudo et al., 2013). Whereas, a co-treatment using Manuka honey and paclitaxel was evident to give better control of tumour growth and improved host survival in a melanoma mouse model (Fernandez-Cabezudo et al., 2013). Meanwhile, oral administration of Manuka honey at 1.0 g/kg body weight/day continuously for 120 days treatment was reported to alleviate breast cancer in rat increasing the expression of apoptotic proteins while suppressing expression of anti-apoptosis proteins (Ahmed et al., 2017). Overall, it is well said that the effectivity of Manuka honey against breast cancer is very specific, as the effect from previous studies do not represent the whole living organism. Furthermore, the existence of methylglyoxal (MGO) in New Zealand honey highly contributed to the Unique Manuka Factor (UMF) that was claimed to be responsible for potent antibacterial activity against *Staphylococcus aureus*, especially in wound healing (Speer et al., 2015, Hixon et al., 2017). In the present study, MGO was also observed in honey from New Zealand based on ^{1}H NMR spectra. In conclusion, the metabolite profiling of honey samples from Malaysia and New Zealand were best obtained employing both HR-LCMS and ^{1}H NMR as analytical tools. Mild cytotoxicity on ZR75 was determined for CH, FH, GH, HH, JH, KH, LH, NH, RH and SH. Meanwhile several honey extracts including MH, ANZ, BNZ, FNZ, JNZ, MNZ, ONZ, QNZ and WNZ inhibited the growth of ZR75 at weak level. Nonetheless, all the bioactive extracts were giving protective effect on normal cell lines like HFL-1. This is the first study comparing Malaysian and New Zealand honey as potential anti-cancer agents based on metabolomic approach.

CHAPTER 6

6 General Conclusions and Future Work

The primary aim of this project is to study the chemistry responsible for the therapeutic effects of Malaysia and New Zealand propolis and honey extracts by applying the tools of metabolomics. This chapter summarised the findings from every result chapters, which are chapters 3, 4 and 5. The objective was to determine cytotoxicity effects of propolis and honey samples from Malaysia and New Zealand on several cell lines; A2780, A549, ZR75, HFL-1, and PNT2A was achieved via the Alamar blue assay. In addition, the bioactive compounds in propolis and honey extracts from Malaysia and New Zealand were successfully pinpointed and identified through metabolomic tools cross-matched with dereplication based on the DNP database. Biologically active compounds were isolated successfully and the chemical structures of these compounds were elucidated by 1D and 2D NMR. Triterpenoids namely asiatic acid, hydroxydammarenone-II, oxodammaradienoic acid, dammarenolic acid, and nepetadiol were isolated from Malaysian propolis. Meanwhile, flavonoid compounds such as galangin, (*2R,3R*)-pinobanksin, pinobanksin-3-acetate, chrysin, and benzyl caffeate were isolated from New Zealand propolis. Metabolite profiling of the Malaysian honey based on high resolution liquid chromatography mass spectrometry (HR-LCMS) identified the presence of 1-(2,3-dihydro-2-furyl)-4-(thien-2-yl)but-1-en-3-yne, 5-[5-(methylthio)-4-penten-2-ynyl]-2-furanacrolein, 2-amino-2-deoxy-3-glucopyranosylgalactose and vitelignin A. Besides the 1-(2,3-dihydro-2-furyl)-4-(thien-2-yl)but-1-en-3-yne, other three metabolites includes 6-amino-1,2,3,4,5-cyclohexanepentol, galactopyranuronosyl-rhamnopyranosyl-rhamnose and 5,6-diglucopyranosylangelicinalso were identified from New Zealand honey extracts.

6.1 Therapeutic effects of compounds isolated from Malaysian propolis.

Triterpenes were the major bioactive compounds isolated from both Johor and Malacca propolis, which suggested a homogenous plant source from the southeast part of Peninsular Malaysia that was dominated by *Dipterocarpaceae* species. In the present study, *Trigona sp*. bees were responsible for the production of propolis from the same species of plants even though they were breeding at different area,

particularly Johor and Malacca. The cytotoxicity effects of dammarenolic acid, oxodammaradienoic acids, nepetadiol, and hydroxydammarenone-II against A2780 were determined with IC_{50} values of 41.97, 44.31, 50.75, 52.15 and 53.58 µM, respectively. On top of that, the dammarenolic acid was the only triterpenoid that can interfere Notch signalling in zebrafish assay at concentration of 10 and 20 µM, in addition of its cytotoxicity effects against ZR75 at IC_{50} of 45.53 µM. This is the first report of dammarenolic acid, oxodammaradienoic acids, nepetadiol, and hydroxydammarenone-II isolated from Malaysia propolis along with their cytotoxicity effects on A2780 and ZR75, as well as its phenotypic inteference on zebrafish assay, which were also found nontoxic at equivalent concentration on normal prostate epithelial cell, PNT2A.

6.2 Therapeutic effects of compounds isolated from New Zealand propolis.

Meanwhile, the present study showed that flavonoids were the major compounds isolated from New Zealand Manuka propolis. The cytotoxicity effects against A549 was observed in benzyl caffeate, chrysin, pinobanksin-3-acetate and (*2R,3R*)-pinobanksin with IC_{50} values of 15.81, 23.74, 30.07 and 36.65 µM, respectively. For A2780 cytotoxicity assay, pinobanksin-3-acetate, benzyl caffeate and galangin gave IC_{50} values of 1.22, 15.38 and 21.30 µM, respectively. Furthermore, the present study provided novel evidence that the isolated compounds from New Zealand propolis, which were benzyl caffeate, chrysin, pinobanksin-3-acetate, and (*2R,3R*)-pinobanksin have the potential to modulate cell death in A549. In addition, benzyl caffeate, galangin and pinobanksin-3-acetate exhibited anticancer activity against A2780. Interestingly, these bioactive compounds were found nontoxic on PNT2A at equivalent concentration.

6.3 Therapeutic effects of Malaysia and New Zealand honey extracts.

Metabolite profiling of Malaysian and New Zealand honey extracts were obtained via HR-LCMS and ^{1}H NMR experiments. The present study represented Malaysian honey that gave from several sources of honey including *Acacia* sp. (Acacia), *Koompassia excels* (Tualang), *Momordica charantia* (bitter gourd), *Melaleuca* sp. (paperbark), *Asystasia gangetica* (Chinese violet), *Acacia mangium* (black wattle),

Ananascomosus sp. (pineapple) and also from multifloral sources at concentration of 100 µg/ml. The collected Malaysian honey samples, 53% of which, exhibited mild cytotoxicity effects against ZR75. Based on the multivariate analysis by OPLS-DA of the metabolomic profile of Malaysian honey samples, the major compounds responsible for the cytotoxicity effects against ZR75 were identified as 1-(2,3-dihydro-2-furyl)-4-(thien-2-yl)but-1-en-3-yne, 5-[5-(methylthio)-4-penten-2-ynyl]-2-furanacrolein, 2-amino-2-deoxy-3-glucopyranosylgalactose and vitelignin A. On the other hand, there were four major metabolites being identified from New Zealand honey extracts that were predominantly produced from Manuka tree; 1-(2,3-dihydro-2-furyl)-4-(thien-2-yl)but-1-en-3-yne, 6-amino-1,2,3,4,5- cyclohexanepentol, galactopyranuronosyl- rhamnopyranosyl- rhamnose and 5,6-digluco pyranosylangelicin. Based on OPLS-DA, these compounds were responsible for the weak cytotoxicity effects against ZR75 at a sample concentration of 100 µg/ml. The nectar was predominantly obtained from Manuka tree with minor additional sources from clover and honey dew. This is the first report on the bioactivity of identified metabolites from Malaysia and New Zealand honey extracts against breast cancer cell line based on a metabolomics approach using HR-LCMS and NMR along with their fused datasets. The collected honey samples were also found nontoxic on normal human foetal lung fibroblast, HFL-1 at equivalent concentration.

6.4 Future work

Metabolomics is a powerful tool in providing concrete guideline for an isolation scheme based on HR-LCMS and NMR. Metabolomics tools such as Mzmine 2.10, In-house EXCEL Macro customised with the Dictionary of Natural Products (DNP) 2017, and SIMCA 14.0 assisted the prediction and interpretation of results. The multivariate analysis also provides significant outcomes for omic data analysis. Therefore it is necessary to have good knowledge on how to apply it in metabolomic study. Future metabolomics study can be further done on propolis from other parts of Malaysia, hence to have a well-documented metabolite profile to specify the value of honey samples in correlation to their bioactivity or prophylactic properties. Futhermore, a database consists of metabolomic profiling of honey and propolis can be generated which allow open access by public. Moreover a standard workflow can be built for the metabolomic processing, particularly on honey and propolis. A similar approach can be applied on honey from Malaysia with add-on of bioactive compounds isolation procedure. The discovery of bioactive compounds from propolis and honey from Malaysia indirectly will add value to commercialise Malaysia bee by-products globally as can be seen on New Zealand honey that is well known with their unique Manuka factor (UMF) honey product.

References

ABDEL-TAWAB, M., WERZ, O. & SCHUBERT-ZSILAVECZ, M. 2011. Boswellia serrata. *Clinical pharmacokinetics,* 50**,** 349-369.

ADAMS, C. J., MANLEY-HARRIS, M. & MOLAN, P. C. 2009. The origin of methylglyoxal in New Zealand manuka (Leptospermum scoparium) honey. *Carbohydrate research,* 344**,** 1050-1053.

AHMED, S. & OTHMAN, N. H. 2017. The anti-cancer effects of Tualang honey in modulating breast carcinogenesis: an experimental animal study. *BMC complementary and alternative medicine,* 17**,** 208.

AHMED, S., SULAIMAN, S. A. & OTHMAN, N. H. 2017. Oral Administration of Tualang and Manuka Honeys Modulates Breast Cancer Progression in Sprague-Dawley Rats Model. *Evidence-Based Complementary and Alternative Medicine,* 2017.

ALDAY, E., VALENCIA, D., CARREÑO, A. L., PICERNO, P., PICCINELLI, A. L., RASTRELLI, L., ROBLES-ZEPEDA, R., HERNANDEZ, J. & VELAZQUEZ, C. 2015. Apoptotic induction by pinobanksin and some of its ester derivatives from Sonoran propolis in a B-cell lymphoma cell line. *Chemico-biological interactions,* 242**,** 35-44.

ALI, M. M. 2011. *Holy Quran,* Ahmadiyya Anjuman Ishaat Islam Lahore USA.

ALTMAN, N. 2010. *The honey prescription: The amazing power of honey as medicine,* Inner Traditions/Bear & Co.

ALVAREZ-SUAREZ, J., TULIPANI, S., ROMANDINI, S., BERTOLI, E. & BATTINO, M. 2010. Contribution of honey in nutrition and human health: a review. *Mediterranean Journal of Nutrition and Metabolism,* 3**,** 15-23.

AMET, M., ABUDULA, A., AKELA, A., SHENG, L., ABABAIKERI, B., MAIMAITI, A., TAKIGCHI, Y., YAMAGUCHI, T. & RAHMAN, Y. 2015. Anticancer activity of propolis flavonoid pinobanksin**-** 3**-** acetate against human colon cancer in vitro. *Int J Biosci,* 7**,** 45.

ASAKAWA, J., KASAI, R., YAMASAKI, K. & TANAKA, O. 1977. 13 C NMR Study of ginseng sapogenins and their related dammarane type triterpenes. *Tetrahedron,* 33**,** 1935-1939.

BANKOVA, V. 2005. Recent trends and important developments in propolis research. *Evidence-based complementary and alternative medicine,* 2**,** 29-32.

BANKOVA, V. S., DE CASTRO, S. L. & MARCUCCI, M. C. 2000. Propolis: recent advances in chemistry and plant origin. *Apidologie,* 31**,** 3-15.

BANKOVA, V. S., POPOV, S. S. & MAREKOV, N. L. 1983. A Study on Flavonoids of Propolis. *Journal of Natural Products,* 46**,** 471-474.

BANSAL, V., MEDHI, B. & PANDHI, P. 2005. Honey--a remedy rediscovered and its therapeutic utility.

BANSKOTA, A. H., NAGAOKA, T., SUMIOKA, L. Y., TEZUKA, Y., AWALE, S., MIDORIKAWA, K., MATSUSHIGE, K. & KADOTA, S. 2002. Antiproliferative activity of the Netherlands propolis and its active principles in cancer cell lines. *Journal of ethnopharmacology,* 80**,** 67-73.

BANSKOTA, A. H., TEZUKA, Y. & KADOTA, S. 2001. Recent progress in pharmacological research of propolis. *Phytotherapy Research,* 15**,** 561-571.

BARAN, R., KOCHI, H., SAITO, N., SUEMATSU, M., SOGA, T., NISHIOKA, T., ROBERT, M. & TOMITA, M. 2006. MathDAMP: a package for differential analysis of metabolite profiles. *BMC bioinformatics,* 7**,** 530.

BHAGWAT, S., HAYTOWITZ, D. B. & WASSWA-KINTU, S. 2014. USDA's Expanded Flavonoid Database for the assessment of Dietary Intakes. U.S. Department of Agriculture, Agricultural Research Service.

BHULLAR, K. S., LASSALLE-CLAUX, G., TOUAIBIA, M. & RUPASINGHE, H. P. V. 2014. Antihypertensive effect of caffeic acid and its analogs through dual renin–angiotensin–aldosterone system inhibition. *European journal of pharmacology,* 730**,** 125-132.

BIDART-BOUZAT, M. G. & IMEH-NATHANIEL, A. 2008. Global change effects on plant chemical defenses against insect herbivores. *Journal of Integrative Plant Biology,* 50**,** 1339-1354.

BILIKOVA, K., POPOVA, M., TRUSHEVA, B. & BANKOVA, V. 2013. New anti-Paenibacillus larvae substances purified from propolis. *Apidologie,* 44**,** 278-285.

BIVA, I. J., NDI, C. P., GRIESSER, H. J. & SEMPLE, S. J. 2016. Antibacterial constituents of Eremophila alternifolia: An Australian aboriginal traditional medicinal plant. *Journal of ethnopharmacology,* 182**,** 1-9.

BOEHM, K., BORRELLI, F., ERNST, E., HABACHER, G., HUNG, S. K., MILAZZO, S. & HORNEBER, M. 2009. Green tea (Camellia sinensis) for the prevention of cancer. *The Cochrane Library*.

BOFFO, E. F., TAVARES, L. A., TOBIAS, A. C. T., FERREIRA, M. M. C. & FERREIRA, A. G. 2012. Identification of components of Brazilian honey by 1H NMR and classification of its botanical origin by chemometric methods. *LWT-Food Science and Technology,* 49**,** 55-63.

BOHLMANN, F. & SCHUBER, J. 1969. POLYACETYLENE COMPOUNDS. 171. SYNTHESIS OF THIOETHERS ISOLATED FROM CHRYSANTHEMUM CORONARIUM L. *CHEMISCHE BERICHTE-RECUEIL,* 102**,** 4209.

BOHLMANN, J. 2012. Pine terpenoid defences in the mountain pine beetle epidemic and in other conifer pest interactions: specialized enemies are eating holes into a diverse, dynamic and durable defence system. *Tree physiology,* 32**,** 943-945.

BOHNI, N., CORDERO-MALDONADO, M. L., MAES, J., SIVERIO-MOTA, D., MARCOURT, L., MUNCK, S., KAMUHABWA, A. R., MOSHI, M. J., ESGUERRA, C. V. & DE WITTE, P. A. M. 2013. Integration of microfractionation, qNMR and zebrafish screening for the in vivo bioassay-guided isolation and quantitative bioactivity analysis of natural products. *PLoS One,* 8**,** e64006.

BOISARD, S. V., LE RAY, A.-M., GATTO, J., AUMOND, M.-C., BLANCHARD, P., DERBRÉ, S. V., FLURIN, C. & RICHOMME, P. 2014. Chemical composition, antioxidant and anti-AGEs activities of a French poplar type propolis. *Journal of agricultural and food chemistry,* 62**,** 1344-1351.

BREWIS, S. & HALSALL, T. G. 1961. 130. The chemistry of triterpenes and related compounds. Part XXXVIII. The acidic constituents of dammar resin. *Journal of the Chemical Society (Resumed)***,** 646-650.

BRODOWSKA, K. M. 2017. Natural flavonoids: classification, potential role, and application of flavonoid analogues. *European Journal of Biological Research,* 7**,** 108-123.
BROWN, G. D. 2010. The biosynthesis of artemisinin (Qinghaosu) and the phytochemistry of Artemisia annua L.(Qinghao). *Molecules,* 15**,** 7603-7698.
BURDOCK, G. A. 1998. Review of the biological properties and toxicity of bee propolis (propolis). *Food and Chemical Toxicology,* 36**,** 347-363.
BUTLER, L. M. & WU, A. H. 2011. Green and black tea in relation to gynecologic cancers. *Molecular nutrition & food research,* 55**,** 931-940.
BUTZ HURYN, V. M. 1995. Use of native New Zealand plants by honey bees (Apis mellifera L.): a review. *New Zealand journal of botany,* 33**,** 497-512.
BYLKA, W., ZNAJDEK-AWIŻEŃ, P., STUDZIŃSKA-SROKA, E., DAŃCZAK-PAZDROWSKA, A. & BRZEZIŃSKA, M. 2014. Centella asiatica in dermatology: an overview. *Phytotherapy research,* 28**,** 1117-1124.
CAMPO FERNÁNDEZ, M., CUESTA-RUBIO, O., ROSADO PEREZ, A. S., MONTES DE OCA PORTO, R., MÁRQUEZ HERNÁNDEZ, I., PICCINELLI, A. L. & RASTRELLI, L. 2008. GC-MS determination of isoflavonoids in seven red Cuban propolis samples. *Journal of agricultural and food chemistry,* 56**,** 9927-9932.
CANTRELL, C. L., FRANZBLAU, S. G. & FISCHER, N. H. 2001. Antimycobacterial plant terpenoids. *Planta medica,* 67**,** 685-694.
CARTER, H. E., CLARK, R. K., LYTLE, B. & MCCASLAND, G. E. 1948. The synthesis of amino analogues of inositol (inosamines). *Journal of Biological Chemistry,* 175**,** 683-690.
CASATI, P. & WALBOT, V. 2005. Differential accumulation of maysin and rhamnosylisoorientin in leaves of high-altitude landraces of maize after UV-B exposure. *Plant, Cell & Environment,* 28**,** 788-799.
CASTRO-VÁZQUEZ, L., DÍAZ-MAROTO, M. C., DE TORRES, C. & PÉREZ-COELLO, M. S. 2010. Effect of geographical origin on the chemical and sensory characteristics of chestnut honeys. *Food Research International,* 43**,** 2335-2340.
CHAN, C. W., DEADMAN, B. J., MANLEY-HARRIS, M., WILKINS, A. L., ALBER, D. G. & HARRY, E. 2013. Analysis of the flavonoid component of bioactive New Zealand mānuka (Leptospermum scoparium) honey and the isolation, characterisation and synthesis of an unusual pyrrole. *Food chemistry,* 141**,** 1772-1781.
CHANG, M.-S., YANG, Y.-C., KUO, Y.-C., KUO, Y.-H., CHANG, C., CHEN, C.-M. & LEE, T.-H. 2005. Furocoumarin Glycosides from the Leaves of Ficus r uficaulis Merr. var. a ntaoensis. *Journal of natural products,* 68**,** 11-13.
CHEN, A. Y. & CHEN, Y. C. 2013. A review of the dietary flavonoid, kaempferol on human health and cancer chemoprevention. *Food chemistry,* 138**,** 2099-2107.
CHEN, L., XU, H. H., HU, T. S. & WU, Y. L. 2005. Synthesis of spiroketal enol ethers related to tonghaosu and their insecticidal activities. *Pest management science,* 61**,** 477-482.
CHEN, Y. W., WU, S. W., HO, K. K., LIN, S. B., HUANG, C. Y. & CHEN, C. N. 2008. Characterisation of Taiwanese propolis collected from different

locations and seasons. *Journal of the Science of Food and Agriculture,* 88**,** 412-419.
CHEUNG, H. T. & FENG, M. C. 1968. Constituents of dipterocarpaceae resins. Part I. Triterpene acids of Dryobalanops aromatica. *Journal of the Chemical Society C: Organic***,** 1047-1051.
CHOUDHARI, M. K., HAGHNIAZ, R., RAJWADE, J. M. & PAKNIKAR, K. M. 2013. Anticancer Activity of Indian Stingless Bee Propolis: An In Vitro Study. *Evidence-based Complementary and Alternative Medicine : eCAM,* 2013**,** 928280.
CLARK, S. T. & VERWOERD, W. S. 2011. A systems approach to identifying correlated gene targets for the loss of colour pigmentation in plants. *Bmc Bioinformatics,* 12**,** 343.
COTRIM, H. C., BARROSO, J. G., FIGUEIREDO, A. C., PAIS, M. S. S. & SCHEFFER, J. J. C. 1994. Composition of the essential oil from inflorescences of Nepeta tuberosa L. ssp. tuberosa. *Flavour and fragrance journal,* 9**,** 71-73.
CRANE, E. E. 2013. *The World History of Beekeeping and Honey Hunting*, Taylor & Francis.
CSUK, R. 2014. Betulinic acid and its derivatives: a patent review (2008–2013). *Expert opinion on therapeutic patents,* 24**,** 913-923.
CUESTA-RUBIO, O., FRONTANA-URIBE, B. A., RAMÍREZ-APAN, T. & CÁRDENAS, J. 2002. Polyisoprenylated Benzophenones In Cuban Propolis; Biological Activity Of Nemorosone §. *Zeitschrift für Naturforschung C,* 57**,** 372-378.
DAUGSCH, A., MORAES, C. S., FORT, P. & PARK, Y. K. 2008. Brazilian red propolis—chemical composition and botanical origin. *Evidence-Based Complementary and Alternative Medicine,* 5**,** 435-441.
DEMESTRE, M., MESSERLI, S. M., CELLI, N., SHAHHOSSINI, M., KLUWE, L., MAUTNER, V. & MARUTA, H. 2009. CAPE (caffeic acid phenethyl ester)-based propolis extract (Bio 30) suppresses the growth of human neurofibromatosis (NF) tumor xenografts in mice. *Phytotherapy research,* 23**,** 226-230.
DONARSKI, J. A., ROBERTS, D. P. T. & CHARLTON, A. J. 2010. Quantitative NMR spectroscopy for the rapid measurement of methylglyoxal in manuka honey. *Analytical Methods,* 2**,** 1479-1483.
DONG, J.-Y. & QIN, L.-Q. 2011. Soy isoflavones consumption and risk of breast cancer incidence or recurrence: a meta-analysis of prospective studies. *Breast cancer research and treatment,* 125**,** 315-323.
EDIRIWEERA, E. & PREMARATHNA, N. Y. S. 2012. Medicinal and cosmetic uses of bee's honey–A review. *Ayu,* 33**,** 178.
ESIMONE, C. O., ECK, G., DUONG, T. N., ÜBERLA, K., PROKSCH, P. & GRUNWALD, T. 2008. Potential anti-respiratory syncytial virus lead compounds from Aglaia species. *Die Pharmazie-An International Journal of Pharmaceutical Sciences,* 63**,** 768-773.
ESIMONE, C. O., ECK, G., NWORU, C. S., HOFFMANN, D., ÜBERLA, K. & PROKSCH, P. 2010. Dammarenolic acid, a secodammarane triterpenoid from Aglaia sp. shows potent anti-retroviral activity in vitro. *Phytomedicine,* 17**,** 540-547.

FADEL, H., SIFAOUI, I., LÓPEZ-ARENCIBIA, A., REYES-BATLLE, M., HAJAJI, S., CHIBOUB, O., JIMÉNEZ, I. A., BAZZOCCHI, I. L., LORENZO-MORALES, J. & BENAYACHE, S. 2018. Assessment of the antiprotozoal activity of Pulicaria inuloides extracts, an Algerian medicinal plant: leishmanicidal bioguided fractionation. *Parasitology Research***,** 1-7.

FAUZI, A. N., NORAZMI, M. N. & YAACOB, N. S. 2011. Tualang honey induces apoptosis and disrupts the mitochondrial membrane potential of human breast and cervical cancer cell lines. *Food and Chemical Toxicology,* 49**,** 871-878.

FERLAY, J., SOERJOMATARAM, I., DIKSHIT, R., ESER, S., MATHERS, C., REBELO, M., PARKIN, D. M., FORMAN, D. & BRAY, F. 2015. Cancer incidence and mortality worldwide: Sources, methods and major patterns in GLOBOCAN 2012. *International Journal of Cancer,* 136**,** E359-E386.

FERNANDEZ-CABEZUDO, M. J., EL-KHARRAG, R., TORAB, F., BASHIR, G., GEORGE, J. A., EL-TAJI, H. & AL-RAMADI, B. K. 2013. Intravenous administration of manuka honey inhibits tumor growth and improves host survival when used in combination with chemotherapy in a melanoma mouse model. *PLoS One,* 8**,** e55993.

FIUZA, S. M., GOMES, C., TEIXEIRA, L. J., DA CRUZ, M. T. G., CORDEIRO, M., MILHAZES, N., BORGES, F. & MARQUES, M. P. M. 2004. Phenolic acid derivatives with potential anticancer properties—a structure–activity relationship study. Part 1: Methyl, propyl and octyl esters of caffeic and gallic acids. *Bioorganic & medicinal chemistry,* 12**,** 3581-3589.

FLOTTUM, K. 2010. The backyard beekeeper an absolute beginner's guide to keeping bees in your yard and garden.

FU, L. Q., LI, X. Y. & YANG, C. X. 2012. Galangin attenuates cognitive impairment in senescent mice. *Herald of Medicine,* 7**,** 012.

FURUYA, T., ORIHARA, Y. & HAYASHI, C. 1987. Triterpenoids from Eucalyptus perriniana cultured cells. *Phytochemistry,* 26**,** 715-719.

GALATI, G. & O'BRIEN, P. J. 2004. Potential toxicity of flavonoids and other dietary phenolics: significance for their chemopreventive and anticancer properties. *Free Radical Biology and Medicine,* 37**,** 287-303.

GE, Y., WANG, Y., CHEN, P., WANG, Y., HOU, C., WU, Y., ZHANG, M., LI, L., HUO, C. & SHI, Q. 2016. Polyhydroxytriterpenoids and Phenolic Constituents from Forsythia suspensa (Thunb.) Vahl Leaves. *Journal of agricultural and food chemistry,* 64**,** 125-131.

GEMIARTO, A. T., NINYIO, N. N., LEE, S. W., LOGIS, J., FATIMA, A., CHAN, E. W. C. & LIM, C. S. Y. 2015. Isoprenyl caffeate, a major compound in manuka propolis, is a quorum-sensing inhibitor in Chromobacterium violaceum. *Antonie Van Leeuwenhoek,* 108**,** 491-504.

GHASHM, A., OTHMAN, N., KHATTAK, M., ISMAIL, N. & SAINI, R. 2010. Antiproliferative effect of Tualang honey on oral squamous cell carcinoma and osteosarcoma cell lines. *BMC Complementary and Alternative Medicine,* 10**,** 49.

GHOSH, S. 2016. Biosynthesis of structurally diverse triterpenes in plants: the role of oxidosqualene cyclases. *Proceedings of the Indian National Science Academy,* 82**,** 1189-1210.

GOHARSHENASAN, P., AMINI, S., ATRIA, A., ABTAHI, H. & KHORASANI, G. 2016. Topical application of honey on surgical wounds: a randomized clinical trial. *Complementary Medicine Research,* 23**,** 12-15.

GUZELMERIC, E., RISTIVOJEVIĆ, P., TRIFKOVIĆ, J., DASTAN, T., YILMAZ, O., CENGIZ, O. & YESILADA, E. 2018. Authentication of Turkish propolis through HPTLC fingerprints combined with multivariate analysis and palynological data and their comparative antioxidant activity. *LWT-Food Science and Technology,* 87**,** 23-32.

HAGE, S. & MORLOCK, G. E. 2017. Bioprofiling of Salicaceae bud extracts through high-performance thin-layer chromatography hyphenated to biochemical, microbiological and chemical detections. *Journal of Chromatography A,* 1490**,** 201-211.

HAJDU, S. I. 2011. A note from history: Landmarks in history of cancer, part 1. *Cancer,* 117**,** 1097-1102.

HAMMAD, L. A., SALEH, M. M., NOVOTNY, M. V. & MECHREF, Y. 2009. Multiple-reaction monitoring liquid chromatography mass spectrometry for monosaccharide compositional analysis of glycoproteins. *J Am Soc Mass Spectrom,* 20**,** 1224-34.

HAMZAH, N. & LEO, C. P. 2015. Microwave-assisted extraction of trigona propolis: the effects of processing parameters. *International journal of food engineering,* 11**,** 861-870.

HAN, M.-S., LEE, I.-K., KIM, Y.-S., KIM, J. T., CHOE, K.-R. & YUN, B.-S. 2010. Flavonoids from propolis inhibit DNA single strand breakage by the fenton reaction. *Journal of the Korean Society for Applied Biological Chemistry,* 53**,** 512-515.

HARVEY, A. L., EDRADA-EBEL, R. & QUINN, R. J. 2015. The re-emergence of natural products for drug discovery in the genomics era. *Nature Reviews Drug Discovery,* 14**,** 111-129.

HELFERICH, B. & MÜLLER, W. M. 1973. Zur Synthese von α-D-Glucopyranosyl-Derivaten. *European Journal of Inorganic Chemistry,* 106**,** 2508-2512.

HILL, R. A. & CONNOLLY, J. D. 2013. Triterpenoids. *Natural product reports,* 30**,** 1028-1065.

HIXON, K. R., LU, T., MCBRIDE-GAGYI, S. H., JANOWIAK, B. E. & SELL, S. A. 2017. A Comparison of Tissue Engineering Scaffolds Incorporated with Manuka Honey of Varying UMF. *BioMed research international,* 2017.

HOOPER, L., MADHAVAN, G., TICE, J. A., LEINSTER, S. J. & CASSIDY, A. 2010. Effects of isoflavones on breast density in pre-and post-menopausal women: a systematic review and meta-analysis of randomized controlled trials. *Human reproduction update,* 16**,** 745-760.

HORINAKA, M., YOSHIDA, T., SHIRAISHI, T., NAKATA, S., WAKADA, M. & SAKAI, T. 2006. The dietary flavonoid apigenin sensitizes malignant tumor cells to tumor necrosis factor–related apoptosis-inducing ligand. *Molecular Cancer Therapeutics,* 5**,** 945-951.

HSU, Y.-L., KUO, P.-L., LIU, C.-F. & LIN, C.-C. 2004. Acacetin-induced cell cycle arrest and apoptosis in human non-small cell lung cancer A549 cells. *Cancer Letters,* 212**,** 53-60.

HUANG, H., CHEN, A. Y., ROJANASAKUL, Y., YE, X., RANKIN, G. O. & CHEN, Y. C. 2015. Dietary compounds galangin and myricetin suppress ovarian cancer cell angiogenesis. *Journal of functional foods,* 15**,** 464-475.
HUANG, M., LU, J.-J., HUANG, M.-Q., BAO, J.-L., CHEN, X.-P. & WANG, Y.-T. 2012. Terpenoids: natural products for cancer therapy. *Expert opinion on investigational drugs,* 21**,** 1801-1818.
HUSSAIN, I., SHAH, S. N. H., BHUTTO, A. M., KHAN, B. A. & RASHID, A. 2015. NATURAL HERBAL VITILIGO TREATMENT, HONEY: AN APPLIED CASE STUDY. *Medical Channel,* 21.
HWANG, Y. W., KIM, S. Y., JEE, S. H., KIM, Y. N. & NAM, C. M. 2009. Soy food consumption and risk of prostate cancer: a meta-analysis of observational studies. *Nutrition and cancer,* 61**,** 598-606.
IBRAHIM, N., NIZA, N., RODI, M. M. M., ZAKARIA, A. J., ISMAIL, Z. & MOHD, K. S. 2016. Chemical and biological analyses of malaysian stingless bee propolis extracts. *Malaysian Journal of Analytical Sciences,* 20**,** 413-422.
JACOB, A., PAROLIA, A., PAU, A. & AMALRAJ, F. D. 2015. The effects of Malaysian propolis and Brazilian red propolis on connective tissue fibroblasts in the wound healing process. *BMC complementary and alternative medicine,* 15**,** 1.
JAGANATHAN, S. K. & MANDAL, M. 2009. Antiproliferative effects of honey and of its polyphenols: a review. *BioMed Research International,* 2009.
JAIKANG, C., NIWATANANUN, K., NARONGCHAI, P., NARONGCHAI, S. & CHAIYASUT, C. 2011. Inhibitory effect of caffeic acid and its derivatives on human liver cytochrome P450 3A4 activity. *Journal of Medicinal Plants Research,* 5**,** 3530-3536.
JESSE, C. R., DONATO, F., GIACOMELI, R., DEL FABBRO, L., DA SILVA ANTUNES, M., DE GOMES, M. G., GOES, A. T. R., BOEIRA, S. P., PRIGOL, M. & SOUZA, L. C. 2015. Chronic unpredictable mild stress decreases BDNF and NGF levels and Na+, K+-ATPase activity in the hippocampus and prefrontal cortex of mice: antidepressant effect of chrysin. *Neuroscience,* 289**,** 367-380.
JUBRI, Z., NARAYANAN, N. N. N., KARIM, N. A. & NGAH, W. Z. W. 2012. Antiproliferative activity and apoptosis induction by gelam honey on liver cancer cell line. *Int J Appl,* 2.
KADDURAH-DAOUK, R., KRISTAL, B. S. & WEINSHILBOUM, R. M. 2008. Metabolomics: a global biochemical approach to drug response and disease. *Annu. Rev. Pharmacol. Toxicol.,* 48**,** 653-683.
KADIR, E. A., SULAIMAN, S. A., YAHYA, N. K. & OTHMAN, N. H. 2013. Inhibitory effects of Tualang Honey on experimental breast cancer in rats: a preliminary study. *Asian Pacific Journal of Cancer Prevention,* 14**,** 2249-2254.
KAMARULZAIDI, M. A., YUSOFF, Z. M. & ADLI, D. S. H. 2014. Quranic Advocation of Honey Consumption and its Application Towards Memory Enhancement. *QURANICA-International Journal of Quranic Research,* 6**,** 17-32.
KANG, H., RHA, S. Y., OH, K. W. & NAM, C. M. 2010. Green tea consumption and stomach cancer risk: a meta-analysis. *Epidemiology and health,* 32.

KASALA, E. R., BODDULURU, L. N., BARUA, C. C., MADHANA, R. M., DAHIYA, V., BUDHANI, M. K., MALLUGARI, R. R., MARAMREDDY, S. R. & GOGOI, R. 2016. Chemopreventive effect of chrysin, a dietary flavone against benzo (a) pyrene induced lung carcinogenesis in Swiss albino mice. *Pharmacological Reports,* 68**,** 310-318.

KATAJAMAA, M., MIETTINEN, J. & OREŠIČ, M. 2006. MZmine: toolbox for processing and visualization of mass spectrometry based molecular profile data. *Bioinformatics,* 22**,** 634-636.

KAVITHA, C. V., AGARWAL, C., AGARWAL, R. & DEEP, G. 2011. Asiatic acid inhibits pro-angiogenic effects of VEGF and human gliomas in endothelial cell culture models. *PloS one,* 6**,** e22745.

KAŠKONIENĖ, V. & VENSKUTONIS, P. R. 2010. Floral Markers in Honey of Various Botanical and Geographic Origins: A Review. *Comprehensive Reviews in Food Science and Food Safety,* 9**,** 620-634.

KHAN, F. U., HUSSAIN, J., KHAN, I. U., ULLAH, R., ALI, I., MUHAMMAD, Z., HUSSAIN, H. & SHAH, M. R. 2011. Nepetadiol, a new triterpenediol from Nepeta suavis. *Chemistry of Natural Compounds,* 47**,** 234-236.

KIEW, R., CHUNG, R. C. K., SAW, L. G. & SOEPADMO, E. 2010. Seed plant families in Peninsular Malaysia. *Flora of Peninsular Malaysia Series II: Seed Plants,* 1**,** 3-20.

KIM, G.-S., JEONG, T.-S., KIM, Y. O., BAEK, N.-I., CHA, S. W., LEE, J.-W. & SONG, K.-S. 2010. Human acyl-CoA: cholesterol acyltransferase-inhibiting dammarane triterpenes from Rhus chinensis. *Journal of the Korean Society for Applied Biological Chemistry,* 53**,** 417-421.

KLIEBENSTEIN, D. J. 2004. Secondary metabolites and plant/environment interactions: a view through Arabidopsis thaliana tinged glasses. *Plant, Cell & Environment,* 27**,** 675-684.

KNEKT, P., KUMPULAINEN, J., JÄRVINEN, R., RISSANEN, H., HELIÖVAARA, M., REUNANEN, A., HAKULINEN, T. & AROMAA, A. 2002. Flavonoid intake and risk of chronic diseases. *The American journal of clinical nutrition,* 76**,** 560-568.

KOES, R. E., QUATTROCCHIO, F. & MOL, J. N. M. 1994. The flavonoid biosynthetic pathway in plants: function and evolution. *BioEssays,* 16**,** 123-132.

KOMODA, Y. 1989. Isolation of flavonoids from Populus nigra as Δ4-3-ketosteroid (5α) reductase inhibitors. *Chemical and pharmaceutical bulletin,* 37**,** 3128-3130.

KRELL, R. 1996. *Value added products from beekeeping,* Rome.

KUMAZAWA, S., NAKAMURA, J., MURASE, M., MIYAGAWA, M., AHN, M.-R. & FUKUMOTO, S. 2008. Plant origin of Okinawan propolis: honeybee behavior observation and phytochemical analysis. *Naturwissenschaften,* 95**,** 781.

KUROPATNICKI, A. K., KŁÓSEK, M. & KUCHARZEWSKI, M. 2018. Honey as medicine: historical perspectives. *Journal of Apicultural Research,* 57**,** 113-118.

KUROYANAGI, M., YAMAMOTO, Y., FUKUSHIMA, S., UENO, A., NORO, T. & MIYASE, T. 1982. Chemical studies on the constituents of Polygonum nodosum. *Chemical and Pharmaceutical Bulletin,* 30**,** 1602-1608.

KWON, Y. I., APOSTOLIDIS, E. & SHETTY, K. 2008. Inhibitory potential of wine and tea against α-Amylase and α-Glucosidase for management of hyperglycemia linked to type 2 diabetes. *Journal of Food Biochemistry,* 32**,** 15-31.

LAGIOU, P., ROSSI, M., LAGIOU, A., TZONOU, A., LA VECCHIA, C. & TRICHOPOULOS, D. 2008. Flavonoid intake and liver cancer: a case–control study in Greece. *Cancer Causes & Control,* 19**,** 813-818.

LANGSTROTH, L. L. 2004. *Langstroth's hive and the honey-bee : the classic beekeeper's manual,* Mineola, N.Y., Dover Publications.

LAO, L., XU, L. & XU, S. 2012. Traditional chinese medicine. *Integrative pediatric oncology.* Springer.

LAPIDOT, T., WALKER, M. D. & KANNER, J. 2002. Antioxidant and prooxidant effects of phenolics on pancreatic β-cells in vitro. *Journal of agricultural and food chemistry,* 50**,** 7220-7225.

LEE, R., HARRIS, J., CHAMPAGNE, P. & JESSOP, P. G. 2016. CO 2-Catalysed conversion of carbohydrates to 5-hydroxymethyl furfural. *Green Chemistry,* 18**,** 6305-6310.

LEE, S.-H., PARK, Y.-H., MOON, B.-H., LEE, E.-J., HONG, S.-W. & LIM, Y.-H. 2008. Substitution Effect of Hydroxyl Groups on the 1 H and 13 CC Chemical Shifts in Hydroxyflavonols. *Bulletin of the Korean Chemical Society,* 29**,** 1597-1600.

LEONG, A. G., HERST, P. M. & HARPER, J. L. 2012. Indigenous New Zealand honeys exhibit multiple anti-inflammatory activities. *Innate Immunity,* 18**,** 459-466.

LEUNG, H. W. C., LIN, C. J., HOUR, M. J., YANG, W. H., WANG, M. Y. & LEE, H. Z. 2007. Kaempferol induces apoptosis in human lung non-small carcinoma cells accompanied by an induction of antioxidant enzymes. *Food and Chemical Toxicology,* 45**,** 2005-2013.

LI, F., AWALE, S., TEZUKA, Y., ESUMI, H. & KADOTA, S. 2010. Study on the constituents of Mexican propolis and their cytotoxic activity against PANC-1 human pancreatic cancer cells. *Journal of natural products,* 73**,** 623-627.

LI, X., HUANG, J.-M., WANG, J.-N., XIONG, X.-K., YANG, X.-F. & ZOU, F. 2015. Combination of chrysin and cisplatin promotes the apoptosis of Hep G2 cells by up-regulating p53. *Chemico-biological interactions,* 232**,** 12-20.

LI, Y. & DING, Y. 2012. Minireview: Therapeutic potential of myricetin in diabetes mellitus. *Food Science and Human Wellness,* 1**,** 19-25.

LIM, H.-K., KIM, K. M., JEONG, S.-Y., CHOI, E. K. & JUNG, J. 2016. Chrysin increases the therapeutic efficacy of docetaxel and mitigates docetaxel-induced edema. *Integrative cancer therapies***,** 1534735416645184.

LIU, G., OETTEL, K., BAILEY, H., VAN UMMERSEN, L., TUTSCH, K., STAAB, M. J., HORVATH, D., ALBERTI, D., ARZOOMANIAN, R. & REZAZADEH, H. 2003. Phase II trial of perillyl alcohol (NSC 641066) administered daily in patients with metastatic androgen independent prostate cancer. *Investigational new drugs,* 21**,** 367-372.

LOMMEN, A. 2009. MetAlign: interface-driven, versatile metabolomics tool for hyphenated full-scan mass spectrometry data preprocessing. *Analytical chemistry,* 81**,** 3079-3086.

LOTTI, C., CAMPO FERNANDEZ, M., PICCINELLI, A. L., CUESTA-RUBIO, O., MÁRQUEZ HERNÁNDEZ, I. & RASTRELLI, L. 2010. Chemical constituents of red Mexican propolis. *Journal of Agricultural and Food Chemistry,* 58**,** 2209-2213.

LOUVEAUX, J., MAURIZIO, A. & VORWOHL, G. 1978. Methods of melissopalynology. *Bee world,* 59**,** 139-157.

LUDWICZUK, A., SAHA, A., KUZUHARA, T. & ASAKAWA, Y. 2011. Bioactivity guided isolation of anticancer constituents from leaves of Alnus sieboldiana (Betulaceae). *Phytomedicine,* 18**,** 491-498.

LUDWICZUK, A., SKALICKA-WOŹNIAK, K. & GEORGIEV, M. I. 2017. Chapter 11 - Terpenoids A2 - Badal, Simone. *In:* DELGODA, R. (ed.) *Pharmacognosy.* Boston: Academic Press.

MACHIDA, S. & INANO, M. 1955. Chemical Studies on Polyuronides. VI On the Mucilage of Nori-utsugi Plant, Hydrangea Paniculata, Sieb.(1). *Bulletin of the Chemical Society of Japan,* 28**,** 629-632.

MACINTYRE, L., ZHANG, T., VIEGELMANN, C., JUAREZ MARTINEZ, I., CHENG, C., DOWDELLS, C., ABDELMOHSEN, U. R., GERNERT, C., HENTSCHEL, U. & EDRADA-EBEL, R. 2014. Metabolomic Tools for Secondary Metabolite Discovery from Marine Microbial Symbionts. *Marine Drugs,* 12**,** 3416-3448.

MAI, H. L., GRELLIER, P., PROST, E., LEMOINE, P., POULLAIN, C., DUMONTET, V., DEGUIN, B., VO, T. B. H., MICHEL, S. & GROUGNET, R. 2016. Triterpenes from the exudate of Gardenia urvillei. *Phytochemistry,* 122**,** 193-202.

MAKRIS, D. P., KALLITHRAKA, S. & KEFALAS, P. 2006. Flavonols in grapes, grape products and wines: Burden, profile and influential parameters. *Journal of Food Composition and Analysis,* 19**,** 396-404.

MAQUART, F.-X., BELLON, G., GILLERY, P., WEGROWSKI, Y. & BOREL, J.-P. 1990. Stimulation of collagen synthesis in fibroblast cultures by a triterpene extracted from Centella asiatica. *Connective tissue research,* 24**,** 107-120.

MARCUCCI, M. C., FERRERES, F., CUSTÓDIO, A. R., FERREIRA, M., BANKOVA, V. S., GARCÍA-VIGUERA, C. & BRETZ, W. A. 2000. Evalution of phenolic compounds in Brazilian propolis from different geographic regions. *Zeitschrift für Naturforschung C,* 55**,** 76-81.

MARKHAM, K. R., MITCHELL, K. A., WILKINS, A. L., DALDY, J. A. & LU, Y. 1996. HPLC and GC-MS identification of the major organic constituents in New Zeland propolis. *Phytochemistry,* 42**,** 205-211.

MARTOS, I., FERRERES, F. & TOMÁS-BARBERÁN, F. A. 2000. Identification of flavonoid markers for the botanical origin of Eucalyptus honey. *Journal of Agricultural and Food Chemistry,* 48**,** 1498-1502.

MASSARO, F., BROOKS, P., WALLACE, H. & RUSSELL, F. 2011. Cerumen of Australian stingless bees (Tetragonula carbonaria): gas chromatography-mass spectrometry fingerprints and potential anti-inflammatory properties. *Naturwissenschaften,* 98**,** 329-337.

MAVRIC, E., WITTMANN, S., BARTH, G. & HENLE, T. 2008. Identification and quantification of methylglyoxal as the dominant antibacterial constituent of

Manuka (Leptospermum scoparium) honeys from New Zealand. *Molecular nutrition & food research,* 52**,** 483-489.
MELLIOU, E. & CHINOU, I. 2004. Chemical analysis and antimicrobial activity of Greek propolis. *Planta medica,* 70**,** 515-519.
MEYER, J. J. M., AFOLAYAN, A. J., TAYLOR, M. B. & ERASMUS, D. 1997. Antiviral activity of galangin isolated from the aerial parts of Helichrysum aureonitens. *Journal of ethnopharmacology,* 56**,** 165-169.
MILLS, J. S. 1956. 429. The constitution of the neutral, tetracyclic triterpenes of dammar resin. *Journal of the Chemical Society (Resumed)***,** 2196-2202.
MOHAMED, M., SIRAJUDEEN, K. N. S., SWAMY, M., YAACOB, M. & SULAIMAN, S. 2010. Studies on the antioxidant properties of Tualang honey of Malaysia. *African Journal of Traditional, Complementary and Alternative Medicines,* 7.
MOLAN, P. 2001. Why honey is effective as a medicine: 2. The scientific explanation of its effects. *Bee world,* 82**,** 22-40.
MOLAN, P. C. 1999. Why honey is effective as a medicine. 1. Its use in modern medicine. *Bee world,* 80**,** 80-92.
MURPHY, K. J., CHRONOPOULOS, A. K., SINGH, I., FRANCIS, M. A., MORIARTY, H., PIKE, M. J., TURNER, A. H., MANN, N. J. & SINCLAIR, A. J. 2003. Dietary flavanols and procyanidin oligomers from cocoa (Theobroma cacao) inhibit platelet function. *The American journal of clinical nutrition,* 77**,** 1466-1473.
NAGLE, C. M., OLSEN, C. M., BAIN, C. J., WHITEMAN, D. C., GREEN, A. C. & WEBB, P. M. 2010. Tea consumption and risk of ovarian cancer. *Cancer causes & control,* 21**,** 1485-1491.
NAYIK, G. A. & NANDA, V. 2016. A chemometric approach to evaluate the phenolic compounds, antioxidant activity and mineral content of different unifloral honey types from Kashmir, India. *LWT-Food Science and Technology,* 74**,** 504-513.
NEACSU, M., EKLUND, P. C., SJÖHOLM, R. E., PIETARINEN, S. P., AHOTUPA, M. O., HOLMBOM, B. R. & WILLFÖR, S. M. 2007. Antioxidant flavonoids from knotwood of Jack pine and European aspen. *Holz Roh Werkst* 65**,** 1-6.
NEUHOUSER, M. L. 2004. Dietary flavonoids and cancer risk: evidence from human population studies. *Nutrition and cancer,* 50**,** 1-7.
O'BRIEN, J., WILSON, I., ORTON, T. & POGNAN, F. 2000. Investigation of the Alamar Blue (resazurin) fluorescent dye for the assessment of mammalian cell cytotoxicity. *European Journal of Biochemistry,* 267**,** 5421-5426.
OELSCHLAEGEL, S., GRUNER, M., WANG, P.-N., BOETTCHER, A., KOELLING-SPEER, I. & SPEER, K. 2012. Classification and characterization of manuka honeys based on phenolic compounds and methylglyoxal. *Journal of agricultural and food chemistry,* 60**,** 7229-7237.
OHMENHAEUSER, M., MONAKHOVA, Y. B., KUBALLA, T. & LACHENMEIER, D. W. 2013. Qualitative and quantitative control of honeys using NMR spectroscopy and chemometrics. *ISRN Analytical Chemistry,* 2013.

OKUDA, K. S., LEE, H. M., VELAITHAN, V., NG, M. F. & PATEL, V. 2016. Utilizing zebrafish to identify anti-(lymph) angiogenic compounds for cancer treatment: promise and future challenges. *Microcirculation*.

ORSOLIC, N., SVER, L., TERZIC, S., TADIC, Z. & BASIC, I. 2003. Inhibitory effect of water-soluble derivative of propolis and its polyphenolic compounds on tumor growth and metastasizing ability: a possible mode of antitumor action. *Nutrition and cancer,* 47**,** 156-163.

ORŠOLIĆ, N. & BAŠIĆ, I. 2003. Immunomodulation by water-soluble derivative of propolis: a factor of antitumor reactivity. *Journal of Ethnopharmacology,* 84**,** 265-273.

ORŠOLIĆ, N., TERZIĆ, S., ŠVER, L. & BAŠIĆ, I. 2005. Honey-bee products in prevention and/or therapy of murine transplantable tumours. *Journal of the Science of Food and Agriculture,* 85**,** 363-370.

PANCHE, A. N., DIWAN, A. D. & CHANDRA, S. R. 2016. Flavonoids: an overview. *Journal of Nutritional Science,* 5.

PARK, Y., MOON, B. H., LEE, E., LEE, Y., YOON, Y., AHN, J. H. & LIM, Y. 2007. 1H and 13C-NMR data of hydroxyflavone derivatives. *Magnetic Resonance in Chemistry,* 45**,** 674-679.

PASHINSKIĬ, V. G. 1990. The antitumor properties of honey. *Voprosy Onkologii,* 36**,** 704-709.

PATEL, D., SHUKLA, S. & GUPTA, S. 2007. Apigenin and cancer chemoprevention: progress, potential and promise. *International journal of oncology,* 30**,** 233-245.

PHAN, M. G., TRUONG, T. T. C., PHAN, T. S., MATSUNAMI, K. & OTSUKA, H. 2011. A new diarylheptanoid and a rare dammarane triterpenoid from Alnus nepalensis. *Chemistry of Natural Compounds,* 47**,** 735-737.

PICHETTE, A., EFTEKHARI, A., GEORGES, P., LAVOIE, S., MSHVILDADZE, V. & LEGAULT, J. 2010. Cytotoxic phenolic compounds in leaf buds of Populus tremuloides. *Canadian journal of chemistry,* 88**,** 104-110.

POPOVA, M. P., GRAIKOU, K., CHINOU, I. & BANKOVA, V. S. 2010. GC-MS profiling of diterpene compounds in Mediterranean propolis from Greece. *Journal of agricultural and food chemistry,* 58**,** 3167-3176.

POPRAVKO, S. A. & SOKOLOV, I. V. 1980. Plant sources of propolis. *Pchelovodstvo***,** 28-29.

PRISIC, S., XU, M., WILDERMAN, P. R. & PETERS, R. J. 2004. Rice contains two disparate ent-copalyl diphosphate synthases with distinct metabolic functions. *Plant physiology,* 136**,** 4228-4236.

PUROW, B. W., HAQUE, R. M., NOEL, M. W., SU, Q., BURDICK, M. J., LEE, J., SUNDARESAN, T., PASTORINO, S., PARK, J. K. & MIKOLAENKO, I. 2005. Expression of Notch-1 and its ligands, Delta-like-1 and Jagged-1, is critical for glioma cell survival and proliferation. *Cancer research,* 65**,** 2353-2363.

RANI, N., BHARTI, S., BHATIA, J., NAG, T. C., RAY, R. & ARYA, D. S. 2016. Chrysin, a PPAR-γ agonist improves myocardial injury in diabetic rats through inhibiting AGE-RAGE mediated oxidative stress and inflammation. *Chemico-biological interactions,* 250**,** 59-67.

RASMUSSEN, C. & MICHENER, C. D. 2010. The identity and neotype of Trigona laeviceps Smith (Hymenoptera: Apidae). *Journal of the Kansas Entomological Society,* 83**,** 129-133.
REIN, D., PAGLIERONI, T. G., WUN, T., PEARSON, D. A., SCHMITZ, H. H., GOSSELIN, R. & KEEN, C. L. 2000. Cocoa inhibits platelet activation and function. *The American journal of clinical nutrition,* 72**,** 30-35.
ROSSI, M., BOSETTI, C., NEGRI, E., LAGIOU, P. & VECCHIA, C. L. 2010. Flavonoids, proanthocyanidins, and cancer risk: a network of case-control studies from Italy. *Nutrition and cancer,* 62**,** 871-877.
SALATINO, A., TEIXEIRA, É. W. & NEGRI, G. 2005. Origin and chemical variation of Brazilian propolis. *Evidence-Based Complementary and Alternative Medicine,* 2**,** 33-38.
SALIM, H. M. W., DZULKIPLY, A. D., HARRISON, R. D., FLETCHER, C., KASSIM, A. R. & POTTS, M. D. 2012. STINGLESS BEE (HYMENOPTERA: APIDAE: MELIPONINI) DIVERSITY IN DIPTEROCARP FOREST RESERVES IN PENINSULAR MALAYSIA. *Raffles Bulletin of Zoology,* 60.
SAMARGHANDIAN, S., AFSHARI, J. T. & DAVOODI, S. 2011. Honey induces apoptosis in renal cell carcinoma. *Pharmacognosy Magazine,* 7**,** 46-52.
SANZ, S., PEREZ, C., HERRERA, A., SANZ, M. & JUAN, T. 1995. Application of a statistical approach to the classification of honey by geographic origin. *Journal of the Science of Food and Agriculture,* 69**,** 135-140.
SAW, L. G. 2010. Vegetation of Peninsular Malaysia. *Flora of Peninsular Malaysia, Serie II. Seed plants,* 1**,** 21-45.
SEELY, D., MILLS, E. J., WU, P., VERMA, S. & GUYATT, G. H. 2005. The effects of green tea consumption on incidence of breast cancer and recurrence of breast cancer: a systematic review and meta-analysis. *Integrative cancer therapies,* 4**,** 144-155.
SFORCIN, J. M. & BANKOVA, V. 2011. Propolis: Is there a potential for the development of new drugs? *Journal of Ethnopharmacology,* 133**,** 253-260.
SHANMUGAM, M. K., ONG, T. H., KUMAR, A. P., LUN, C. K., HO, P. C., WONG, P. T. H., HUI, K. M. & SETHI, G. 2012. Ursolic acid inhibits the initiation, progression of prostate cancer and prolongs the survival of TRAMP mice by modulating pro-inflammatory pathways. *PLoS One,* 7**,** e32476.
SHIMADAD, K., YUSOFFC, M. N. B. M., CHOONCAJ, K. K. & WAN, L. E. E. T. 1987. Variation in Chemical Components with wood Age of Keruing mempelas (Dipterocarpus crinitus). *Bulletin of the Forestry and Forest Products Research Institute*.
SIMONE-FINSTROM, M. & SPIVAK, M. 2010. Propolis and bee health: the natural history and significance of resin use by honey bees. *Apidologie,* 41**,** 295-311.
SING, M. F., YANG, W.-S., GAO, S., GAO, J. & XIANG, Y.-B. 2011. Epidemiological studies of the association between tea drinking and primary liver cancer: a meta-analysis. *European Journal of Cancer Prevention,* 20**,** 157-165.

SINGH, B., SAHU, P. M. & SHARMA, R. A. 2017. Flavonoids from Heliotropium subulatum exudate and their evaluation for antioxidant, antineoplastic and cytotoxic activities II. *Cytotechnology,* 69**,** 103-115.
SINGH, B. & SHARMA, R. A. 2015. Plant terpenes: defense responses, phylogenetic analysis, regulation and clinical applications. *3 Biotech,* 5**,** 129-151.
SJÖLUND, J., JOHANSSON, M., MANNA, S., NORIN, C., PIETRAS, A., BECKMAN, S., NILSSON, E., LJUNGBERG, B. & AXELSON, H. 2008. Suppression of renal cell carcinoma growth by inhibition of Notch signaling in vitro and in vivo. *The Journal of clinical investigation,* 118**,** 217.
SMITH, C. A., WANT, E. J., O'MAILLE, G., ABAGYAN, R. & SIUZDAK, G. 2006. XCMS: processing mass spectrometry data for metabolite profiling using nonlinear peak alignment, matching, and identification. *Analytical chemistry,* 78**,** 779-787.
SOLFRIZZI, V. & PANZA, F. 2015. Plant-based nutraceutical interventions against cognitive impairment and dementia: meta-analytic evidence of efficacy of a standardized Gingko biloba extract. *Journal of Alzheimer's Disease,* 43**,** 605-611.
SONG, J. H., KIM, Y. H., LEE, S. C., KIM, M. H. & LEE, J. H. 2016. Inhibitory Effect of Chrysin (5, 7-Dihydroxyflavone) on Experimental Choroidal Neovascularization in Rats. *Ophthalmic research,* 56**,** 49-55.
SONG, M. C., KIM, E. J., KIM, E., RATHWELL, K., NAM, S.-J. & YOON, Y. J. 2014. Microbial biosynthesis of medicinally important plant secondary metabolites. *Natural product reports,* 31**,** 1497-1509.
SONG, W., YAN, C.-Y., ZHOU, Q.-Q. & ZHEN, L.-L. 2017. Galangin potentiates human breast cancer to apoptosis induced by TRAIL through activating AMPK. *Biomedicine & Pharmacotherapy,* 89**,** 845-856.
SOUZA, L. C., ANTUNES, M. S., BORGES FILHO, C., DEL FABBRO, L., DE GOMES, M. G., GOES, A. T. R., DONATO, F., PRIGOL, M., BOEIRA, S. P. & JESSE, C. R. 2015. Flavonoid Chrysin prevents age-related cognitive decline via attenuation of oxidative stress and modulation of BDNF levels in aged mouse brain. *Pharmacology Biochemistry and Behavior,* 134**,** 22-30.
SPEER, S. L., SCHREYACK, G. E. & BOWLIN, G. L. 2015. Manuka honey: a tissue engineering essential ingredient. *Journal of Tissue Science & Engineering,* 6**,** 1.
SPITERI, M., JAMIN, E., THOMAS, F., REBOURS, A., LEES, M., ROGERS, K. M. & RUTLEDGE, D. N. 2015. Fast and global authenticity screening of honey using 1H-NMR profiling. *Food chemistry,* 189**,** 60-66.
STILL, W. C., KAHN, M. & MITRA, A. 1978. Rapid chromatographic technique for preparative separations with moderate resolution. *The Journal of Organic Chemistry,* 43**,** 2923-2925.
SUBRAHMANYAM, M. 2007. Topical Application of Honey for Burn Wound Treatment - an Overview. *Annals of Burns and Fire Disasters,* 20**,** 137-139.
SUN, C.-L., YUAN, J.-M., KOH, W.-P. & YU, M. C. 2005. Green tea, black tea and breast cancer risk: a meta-analysis of epidemiological studies. *Carcinogenesis,* 27**,** 1310-1315.
SUN, L., WANG, K., XU, X., GE, M., CHEN, Y. & HU, F. 2017. Potential Protective Effects of Bioactive Constituents from Chinese Propolis against

Acute Oxidative Stress Induced by Hydrogen Peroxide in Cardiac H9c2 Cells. *Evidence-Based Complementary and Alternative Medicine,* 2017.
SUN, L.-P., XU, X., HWANG, H.-H., WANG, X., SU, K.-Y. & CHEN, Y.-L. S. 2016. Dichloromethane extracts of propolis protect cell from oxygen-glucose deprivation-induced oxidative stress via reducing apoptosis. *Food & nutrition research,* 60**,** 30081.
SUN, W., GAYKALOVA, D. A., OCHS, M. F., MAMBO, E., ARNAOUTAKIS, D., LIU, Y., LOYO, M., AGRAWAL, N., HOWARD, J. & LI, R. 2014. Activation of the NOTCH pathway in head and neck cancer. *Cancer research,* 74**,** 1091-1104.
SUNG, T. V., LAVAUD, C., PORZEL, A., STEGLICH, W. & ADAM, G. 1992. Triterpenoids and their glycosides from the bark ofSchefflera octophylla. *Phytochemistry,* 31**,** 227-231.
SVENDSEN, A. B. & VERPOORTE, R. 2011. *Chromatography of alkaloids, part A: thin-layer chromatography*, Elsevier.
TAKAISHI, M., FUJITA, F., UCHIDA, K., YAMAMOTO, S., SAWADA, M., HATAI, C., SHIMIZU, M. & TOMINAGA, M. 2012. 1, 8-cineole, a TRPM8 agonist, is a novel natural antagonist of human TRPA1. *Molecular pain,* 8**,** 86.
TANG, L.-X., HE, R.-H., YANG, G., TAN, J.-J., ZHOU, L., MENG, X.-M., HUANG, X. R. & LAN, H. Y. 2012. Asiatic acid inhibits liver fibrosis by blocking TGF-beta/Smad signaling in vivo and in vitro. *PloS one,* 7**,** e31350.
TANG, N., WU, Y., ZHOU, B., WANG, B. & YU, R. 2009a. Green tea, black tea consumption and risk of lung cancer: a meta-analysis. *Lung cancer,* 65**,** 274-283.
TANG, N.-P., LI, H., QIU, Y.-L., ZHOU, G.-M. & MA, J. 2009b. Tea consumption and risk of endometrial cancer: a metaanalysis. *American journal of obstetrics and gynecology,* 201**,** 605-e1.
TANG, N.-P., ZHOU, B., WANG, B., YU, R.-B. & MA, J. 2009c. Flavonoids intake and risk of lung cancer: a meta-analysis. *Japanese journal of clinical oncology*, 39**,** 352-359.
TAWFIKE, A. F., VIEGELMANN, C. & EDRADA-EBEL, R. 2013. Metabolomics and dereplication strategies in natural products. *Metabolomics Tools for Natural Product Discovery: Methods and Protocols***,** 227-244.
TONKS, A. J., COOPER, R. A., JONES, K. P., BLAIR, S., PARTON, J. & TONKS, A. 2003. Honey stimulates inflammatory cytokine production from monocytes. *Cytokine,* 21**,** 242-247.
TORPOCCO, V., CHÁVEZ, H., ESTÉVEZ-BRAUN, A. & RAVELO, Á. G. 2007. New dammarane triterpenes from Maytenus macrocarpa. *Chemical and pharmaceutical bulletin,* 55**,** 812-814.
TRAN, V. H., DUKE, R. K., ABU-MELLAL, A. & DUKE, C. C. 2012. Propolis with high flavonoid content collected by honey bees from Acacia paradoxa. *Phytochemistry,* 81**,** 126-32.
TROCK, B. J., HILAKIVI-CLARKE, L. & CLARKE, R. 2006. Meta-analysis of soy intake and breast cancer risk. *Journal of the National Cancer Institute,* 98**,** 459-471.
TRUJILLO, E. B., ROSS, S. A. & DAVIS, C. D. 2017. Diet, Physical Activity, and Cancer Prevention. *In:* TEMPLE, N. J., WILSON, T. & BRAY, G. A. (eds.)

Nutrition Guide for Physicians and Related Healthcare Professionals. Cham: Springer International Publishing.
TRUSHEVA, B., POPOVA, M., BANKOVA, V., TSVETKOVA, I., NAYDENSKI, C. & SABATINI, A. G. 2003. A new type of European propolis, containing bioactive labdanes. *Rivista Italiana EPPOS,* 13**,** 3-8.
TRUSHEVA, B., POPOVA, M., KOENDHORI, E. B., TSVETKOVA, I., NAYDENSKI, C. & BANKOVA, V. 2011. Indonesian propolis: chemical composition, biological activity and botanical origin. *Natural Product Research,* 25**,** 606-613.
TRUSHEVA, B., POPOVA, M., NAYDENSKI, H., TSVETKOVA, I., RODRIGUEZ, J. G. & BANKOVA, V. 2004. New polyisoprenylated benzophenones from Venezuelan propolis. *Fitoterapia,* 75**,** 683-689.
TSIAPARA, A. V., JAAKKOLA, M., CHINOU, I., GRAIKOU, K., TOLONEN, T., VIRTANEN, V. & MOUTSATSOU, P. 2009. Bioactivity of Greek honey extracts on breast cancer (MCF-7), prostate cancer (PC-3) and endometrial cancer (Ishikawa) cells: Profile analysis of extracts. *Food Chemistry,* 116**,** 702-708.
UKIYA, M., KIKUCHI, T., TOKUDA, H., TABATA, K., KIMURA, Y., ARAI, T., EZAKI, Y., OSETO, O., SUZUKI, T. & AKIHISA, T. 2010. Antitumor-Promoting Effects and Cytotoxic Activities of Dammar Resin Triterpenoids and Their Derivatives. *Chemistry & biodiversity,* 7**,** 1871-1884.
USIA, T., BANSKOTA, A. H., TEZUKA, Y., MIDORIKAWA, K., MATSUSHIGE, K. & KADOTA, S. 2002. Constituents of Chinese propolis and their antiproliferative activities. *Journal of natural products,* 65**,** 673-676.
USMAN, U. Z. & MOHAMED, M. 2015. Analysis of phytochemical compounds in water and ethanol extracts of Malaysian propolis. *International Journal of Pharma and Bio Sciences,* 6**,** P374-P380.
VAN ACKER, R., DÉJARDIN, A., DESMET, S., HOENGENAERT, L., VANHOLME, R., MORREEL, K., LAURANS, F., KIM, H., SANTORO, N., FOSTER, C., GOEMINNE, G., LÉGÉE, F., LAPIERRE, C., PILATE, G., RALPH, J. & BOERJAN, W. 2017. Different Routes for Conifer- and Sinapaldehyde and Higher Saccharification upon Deficiency in the Dehydrogenase CAD1. *Plant Physiology,* 175**,** 1018.
VAN DER MEER, I. M., STAM, M. E., VAN TUNEN, A. J., MOL, J. N. & STUITJE, A. R. 1992. Antisense inhibition of flavonoid biosynthesis in petunia anthers results in male sterility. *The Plant Cell,* 4**,** 253-262.
VANHANEN, L. P., EMMERTZ, A. & SAVAGE, G. P. 2011. Mineral analysis of mono-floral New Zealand honey. *Food chemistry,* 128**,** 236-240.
VASAS, A., RÉDEI, D., CSUPOR, D., MOLNÁR, J. & HOHMANN, J. 2012. Diterpenes from European Euphorbia Species Serving as Prototypes for Natural-Product-Based Drug Discovery. *European journal of organic chemistry,* 2012**,** 5115-5130.
VELAITHAN, V., OKUDA, K. S., NG, M. F., SAMAT, N., LEONG, S. W., FAUDZI, S. M. M., ABAS, F., SHAARI, K., CHEONG, S. C. & TAN, P. J. 2017. Zebrafish phenotypic screen identifies novel Notch antagonists. *Investigational new drugs,* 35**,** 166-179.
WALL, P. E. 2007. *Thin-layer chromatography: a modern practical approach*, Royal Society of Chemistry.

WANG, F. & LIU, J.-K. 2008. Highly oxygenated lanostane triterpenoids from the fungus Ganoderma applanatum. *Chemical and Pharmaceutical Bulletin,* 56**,** 1035-1037.
WANG, G., TANG, W. & BIDIGARE, R. R. 2005. Terpenoids as therapeutic drugs and pharmaceutical agents. *Natural products.* Springer.
WANG, J.-L., LI, X.-C., XIONG, J., DING, J.-K. & YANG, C.-R. 1991. CHEMICAL CONSTITUENTS OF THE RESIN FROM DIPTEROCARPUS TUBINATUS IN YUNNAN [J]. *Acta Botanica Yunnanica,* 3**,** 020.
WANG, T.-H., POPP, D. M., WANG, H.-S., SAITOH, M., MURAL, J. G., HENLEY, D. C., ICHIJO, H. & WIMALASENA, J. 1999. Microtubule dysfunction induced by paclitaxel initiates apoptosis through both c-Jun N-terminal kinase (JNK)-dependent and-independent pathways in ovarian cancer cells. *Journal of Biological Chemistry,* 274**,** 8208-8216.
WANG, X. H., GHELDOF, N. & ENGESETH, N. J. 2004. Effect of Processing and Storage on Antioxidant Capacity of Honey. *Journal of Food Science,* 69**,** fct96-fct101.
WARDLE, P. 1964. Facets of the distribution of forest vegetation in New Zealand. *New Zealand journal of botany,* 2**,** 352-366.
WASSON, A. P., PELLERONE, F. I. & MATHESIUS, U. 2006. Silencing the flavonoid pathway in Medicago truncatula inhibits root nodule formation and prevents auxin transport regulation by rhizobia. *The Plant Cell,* 18**,** 1617-1629.
WATANABE, M. A. E., AMARANTE, M. K., CONTI, B. J. & SFORCIN, J. M. 2011. Cytotoxic constituents of propolis inducing anticancer effects: a review. *Journal of Pharmacy and Pharmacology,* 63**,** 1378-1386.
WELSCH, C. W. 1994. Interrelationship between dietary lipids and calories and experimental mammary gland tumorigenesis. *Cancer,* 74**,** 1055-1062.
WEN, C., WANG, D., LI, X., HUANG, T., HUANG, C. & HU, K. 2018. Targeted isolation and identification of bioactive compounds lowering cholesterol in the crude extracts of crabapples using UPLC-DAD-MS-SPE/NMR based on pharmacology-guided PLS-DA. *Journal of pharmaceutical and biomedical analysis,* 150**,** 144-151.
WENG, A. P., FERRANDO, A. A., LEE, W., MORRIS, J. P., SILVERMAN, L. B., SANCHEZ-IRIZARRY, C., BLACKLOW, S. C., LOOK, A. T. & ASTER, J. C. 2004. Activating mutations of NOTCH1 in human T cell acute lymphoblastic leukemia. *Science,* 306**,** 269-271.
WINSTON, M. L. 1991. *The biology of the honey bee,* Cambridge, Mass., Harvard University Press.
WISHART, D. S. 2016. Emerging applications of metabolomics in drug discovery and precision medicine. *Nature Reviews Drug Discovery,* 15**,** 473-484.
WU, A. H., YU, M. C., TSENG, C. C. & PIKE, M. C. 2008. Epidemiology of soy exposures and breast cancer risk. *British journal of cancer,* 98**,** 9-14.
WU, S., SCHALK, M., CLARK, A., MILES, R. B., COATES, R. & CHAPPELL, J. 2006. Redirection of cytosolic or plastidic isoprenoid precursors elevates terpene production in plants. *Nature biotechnology,* 24**,** 1441-1447.
WYATT-SMITH, J. 1963. Manual of Malayan silviculture for inland forest.
XUAN, H., WANG, Y., LI, A., FU, C., WANG, Y. & PENG, W. 2016. Bioactive components of Chinese propolis water extract on antitumor activity and

quality control. *Evidence-Based Complementary and Alternative Medicine,* 2016.
YAACOB, N. S. & ISMAIL, N. F. 2014. Comparison of cytotoxicity and genotoxicity of 4-hydroxytamoxifen in combination with Tualang honey in MCF-7 and MCF-10A cells. *BMC complementary and alternative medicine,* 14**,** 106.
YAMASHITA, H., MASUDA, K., KOBAYASHI, T., AGETA, H. & SHIOJIMA, K. 1998. Dammarane triterpenoids from rhizomes of Pyrrosia lingua. *Phytochemistry,* 49**,** 2461-2466.
YAMAUCHI, R., KATO, K., OIDA, S., KANAEDA, J. & UENO, Y. 1992. Benzyl caffeate, an antioxidative compound isolated from propolis. *Bioscience, biotechnology, and biochemistry,* 56**,** 1321-1322.
YAN, R.-Y., CAO, Y.-Y., CHEN, C.-Y., DAI, H.-Q., YU, S.-X., WEI, J.-L., LI, H. & YANG, B. 2011. Antioxidant flavonoids from the seed of Oroxylum indicum. *Fitoterapia,* 82**,** 841-848.
YANG, B., HUANG, J., XIANG, T., YIN, X., LUO, X., HUANG, J., LUO, F., LI, H., LI, H. & REN, G. 2014. Chrysin inhibits metastatic potential of human triple-negative breast cancer cells by modulating matrix metalloproteinase-10, epithelial to mesenchymal transition, and PI3K/Akt signaling pathway. *Journal of Applied Toxicology,* 34**,** 105-112.
YANG, H., DONG, Y., DU, H., SHI, H., PENG, Y. & LI, X. 2011a. Antioxidant compounds from propolis collected in Anhui, China. *Molecules,* 16**,** 3444-3455.
YANG, H., JEONG, E. J., KIM, J., SUNG, S. H. & KIM, Y. C. 2011b. Antiproliferative triterpenes from the leaves and twigs of Juglans sinensis on HSC-T6 cells. *Journal of natural products,* 74**,** 751-756.
YU, S., GONG, L.-S., LI, N.-F., PAN, Y.-F. & ZHANG, L. 2018. Galangin (GG) combined with cisplatin (DDP) to suppress human lung cancer by inhibition of STAT3-regulated NF-κB and Bcl-2/Bax signaling pathways. *Biomedicine & Pharmacotherapy,* 97**,** 213-224.
ZHANG, L., FOURCHES, D., SEDYKH, A., ZHU, H., GOLBRAIKH, A., EKINS, S., CLARK, J., CONNELLY, M. C., SIGAL, M. & HODGES, D. 2013. Discovery of novel antimalarial compounds enabled by QSAR-based virtual screening. *Journal of chemical information and modeling,* 53**,** 475-492.
ZHANG, Y., JIANG, P., YE, M., KIM, S.-H., JIANG, C. & LÜ, J. 2012. Tanshinones: sources, pharmacokinetics and anti-cancer activities. *International journal of molecular sciences,* 13**,** 13621-13666.
ZHANG, Z., LI, G., SZETO, S. S. W., CHONG, C. M., QUAN, Q., HUANG, C., CUI, W., GUO, B., WANG, Y. & HAN, Y. 2015. Examining the neuroprotective effects of protocatechuic acid and chrysin on in vitro and in vivo models of Parkinson disease. *Free Radical Biology and Medicine,* 84**,** 331-343.
ZHENG, C.-J., LAN, X.-P., CHENG, R.-B., HUANG, B.-K., HAN, T., ZHANG, Q.-Y., ZHANG, H., RAHMAN, K. & QIN, L.-P. 2011a. Furanofuran lignans from Vitex negundo seeds. *Phytochemistry Letters,* 4**,** 298-300.
ZHENG, J., YANG, B., HUANG, T., YU, Y., YANG, J. & LI, D. 2011b. Green tea and black tea consumption and prostate cancer risk: an exploratory meta-analysis of observational studies. *Nutrition and cancer,* 63**,** 663-672.

ZOU, W.-W. & XU, S.-P. 2018. Galangin inhibits the cell progression and induces cell apoptosis through activating PTEN and Caspase-3 pathways in retinoblastoma. *Biomedicine & Pharmacotherapy,* 97**,** 851-863.